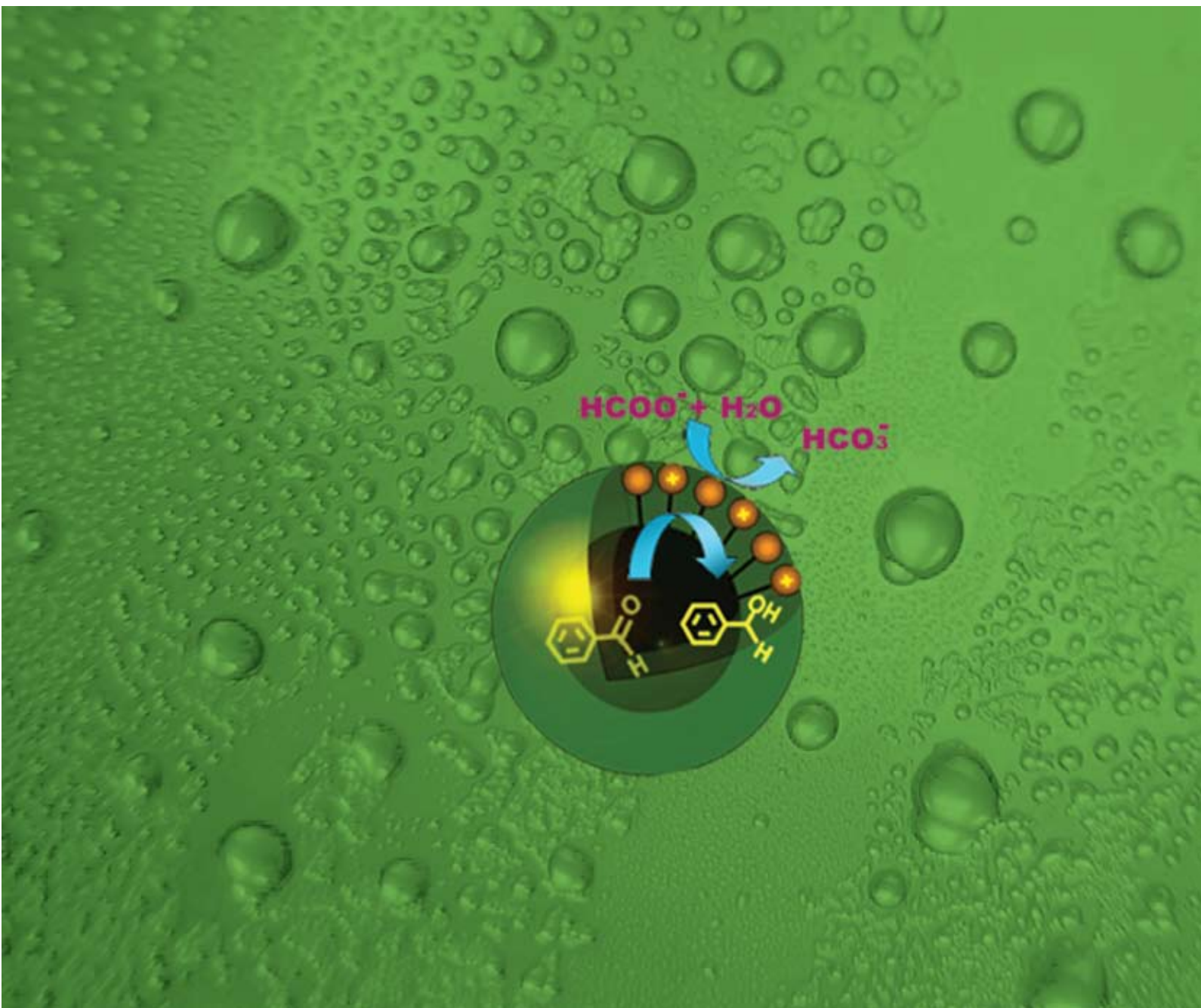


Green Chemistry

Cutting-edge research for a greener sustainable future

www.rsc.org/greenchem

Volume 10 | Number 6 | June 2008 | Pages 597–720



ISSN 1463-9262

Li *et al.*
Transfer hydrogenation of aldehydes
on amphiphilic catalysts

Jin *et al.*
Hydrothermal conversion of
carbohydrate biomass



RSC Publishing

1463-9262(2008)10:6;1-C

GORDON RESEARCH CONFERENCES



Gordon Research Conference on Green Chemistry

August 3-8, 2008
Bates College, Lewiston, ME

Chairs:
James E. Hutchison & Janet L. Scott

<http://www.grc.org/programs.aspx?year=2008&program=green>

Green chemistry: applying innovation to the design and realisation of chemical products and processes with reduced environmental impact, maximum energy-efficiency and the least possible intrinsic hazard. This focus includes design for inherent safety for human health and the environment.



SESSION TOPICS & SPEAKERS

- **Design of Greener Chemicals and Nanoparticles**
(Paul Anastas / Robert Tanguay)
- **Bio-Based and Bio-Inspired Products**
(Richard Wool / Angela Belcher / Yonas C. Gebre)
- **Using Technology in Greener Routes to Complex Molecular Targets**
(Steven Ley)
- **Additive Processing & sc-Fluids for High Performance Materials**
(Douglas Keszler / Steven Howdle)
- **Catalysis for Activation of Small Molecules and in Organic Synthesis**
(Shu Kobayashi / Karen Goldberg / Walter Leitner)
- **Bio-Based Processing and Catalysis**
(Laura Babcock / Roger Sheldon)
- **Future Fuels - Some Possibilities**
(Jeremy Tomkinson / Arno de Klerk)
- **Green Chemistry Advances in Organic Chemistry**
(Paul Wender / Michael Krische)
- **Clean Stereoselective Chemical Transformations**
(Miguel Garcia-Garibay)

Visit the frontiers of science... attend a GRC! www.grc.org

Green Chemistry

Cutting-edge research for a greener sustainable future

www.rsc.org/greenchem

RSC Publishing is a not-for-profit publisher and a division of the Royal Society of Chemistry. Any surplus made is used to support charitable activities aimed at advancing the chemical sciences. Full details are available from www.rsc.org

IN THIS ISSUE

ISSN 1463-9262 CODEN GRCHFJ 10(6) 597–720 (2008)



Cover

See Li *et al.*, pp. 608–611.
The approach that amphiphilic catalysts are assembled at the interface of emulsions (O/W) provides a generally green procedure for organic synthesis in water.

Image reproduced with permission from Can Li, from *Green Chem.*, 2008, **10**, 608.

CHEMICAL TECHNOLOGY

T41

Drawing together research highlights and news from all RSC publications, *Chemical Technology* provides a 'snapshot' of the latest applications and technological aspects of research across the chemical sciences, showcasing newsworthy articles and significant scientific advances.

Chemical Technology

June 2008/Volume 5/Issue 6

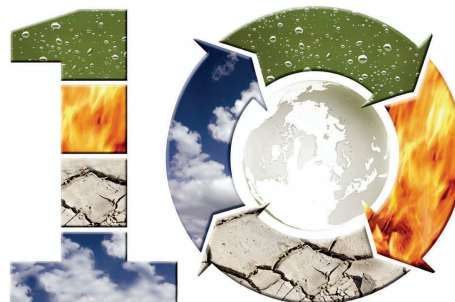
www.rsc.org/chemicaltechnology

EDITORIAL

607

Fusing green chemistry and green engineering: DesignBuild at the molecular level

Paul Anastas discusses the importance of the fusion of green chemistry and green engineering for the generation of sustainable science and technology.



EDITORIAL STAFF

Editor

Sarah Ruthven

Assistant editor

Sarah Dixon

Publishing assistant

Ruth Bircham

Team leader, serials production

Stephen Wilkes

Technical editor

Edward Morgan

Production administration coordinator

Sonya Spring

Administration assistantsClare Davies, Donna Fordham, Kirsty Lunnon,
Julie Thompson**Publisher**

Emma Wilson

Green Chemistry (print: ISSN 1463-9262; electronic: ISSN 1463-9270) is published 12 times a year by the Royal Society of Chemistry, Thomas Graham House, Science Park, Milton Road, Cambridge, UK CB4 0WF.

All orders, with cheques made payable to the Royal Society of Chemistry, should be sent to RSC Distribution Services, c/o Portland Customer Services, Commerce Way, Colchester, Essex, UK CO2 8HP. Tel +44 (0) 1206 226050; E-mail sales@rscdistribution.org

2008 Annual (print + electronic) subscription price: £947; US\$1799. 2008 Annual (electronic) subscription price: £852; US\$1695. Customers in Canada will be subject to a surcharge to cover GST. Customers in the EU subscribing to the electronic version only will be charged VAT.

If you take an institutional subscription to any RSC journal you are entitled to free, site-wide web access to that journal. You can arrange access via Internet Protocol (IP) address at www.rsc.org/ip. Customers should make payments by cheque in sterling payable on a UK clearing bank or in US dollars payable on a US clearing bank. Periodicals postage paid at Rahway, NJ, USA and at additional mailing offices. Airfreight and mailing in the USA by Mercury Airfreight International Ltd., 365 Blair Road, Avenel, NJ 07001, USA.

US Postmaster: send address changes to Green Chemistry, c/o Mercury Airfreight International Ltd., 365 Blair Road, Avenel, NJ 07001. All despatches outside the UK by Consolidated Airfreight.

PRINTED IN THE UK

Advertisement sales: Tel +44 (0) 1223 432246; Fax +44 (0) 1223 426017; E-mail advertising@rsc.org

Green Chemistry

Cutting-edge research for a greener sustainable future

www.rsc.org/greenchem

Green Chemistry focuses on cutting-edge research that attempts to reduce the environmental impact of the chemical enterprise by developing a technology base that is inherently non-toxic to living things and the environment.

EDITORIAL BOARD

Chair

Professor Martyn Poliakoff
Nottingham, UK

Scientific Editor

Professor Walter Leitner
RWTH-Aachen, Germany

Associate Editors

Professor C. J. Li
McGill University, Canada

Members

Professor Paul Anastas
Yale University, USA
Professor Joan Brennecke
University of Notre Dame, USA
Professor Mike Green
Sasol, South Africa
Professor Buxing Han
Chinese Academy of Sciences,
China

Dr Alexei Lapkin
Bath University, UK
Professor Steven Ley
Cambridge, UK
Dr Janet Scott
Unilever, UK
Professor Tom Welton
Imperial College, UK

ADVISORY BOARD

James Clark, York, UK
Avelino Corma, Universidad
Politécnica de Valencia, Spain
Mark Harmer, DuPont Central
R&D, USA
Herbert Hugl, Lanxess Fine
Chemicals, Germany
Roshan Jachuck,
Clarkson University, USA
Makato Misono, nite,
Japan

Colin Raston,
University of Western Australia,
Australia
Robin D. Rogers, Centre for Green
Manufacturing, USA
Kenneth Seddon, Queen's
University, Belfast, UK
Roger Sheldon, Delft University of
Technology, The Netherlands
Gary Sheldrake, Queen's
University, Belfast, UK

Pietro Tundo, Università ca
Foscari di Venezia, Italy

INFORMATION FOR AUTHORS

Full details of how to submit material for publication in Green Chemistry are given in the Instructions for Authors (available from <http://www.rsc.org/authors>). Submissions should be sent via ReSource: <http://www.rsc.org/resource>.

Authors may reproduce/republish portions of their published contribution without seeking permission from the RSC, provided that any such republication is accompanied by an acknowledgement in the form: (Original citation) – Reproduced by permission of the Royal Society of Chemistry.

© The Royal Society of Chemistry 2008. Apart from fair dealing for the purposes of research or private study for non-commercial purposes, or criticism or review, as permitted under the Copyright, Designs and Patents Act 1988 and the Copyright and Related Rights Regulations 2003, this publication may only be reproduced, stored or transmitted, in any form or by any means, with the prior permission in writing of the Publishers or in the case of reprographic reproduction in accordance with the terms of licences issued by the Copyright Licensing Agency in the UK. US copyright law is applicable to users in the USA.

The Royal Society of Chemistry takes reasonable care in the preparation of this publication but does not accept liability for the consequences of any errors or omissions.

The paper used in this publication meets the requirements of ANSI/NISO Z39.48-1992 (Permanence of Paper).

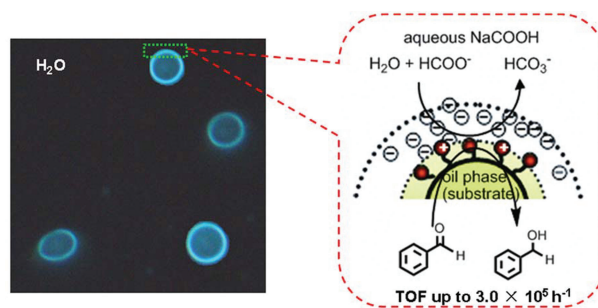
Royal Society of Chemistry: Registered Charity No. 207890

608

Transfer hydrogenation of aldehydes on amphiphilic catalyst assembled at the interface of emulsion droplets

Jun Li, Yanmei Zhang, Difei Han, Guoqing Jia, Jinbo Gao, Lin Zhong and Can Li*

An amphiphilic polymer-based iridium catalyst assembled at the interface of emulsion droplets shows a remarkable rate acceleration for the transfer hydrogenation of aldehydes in water.

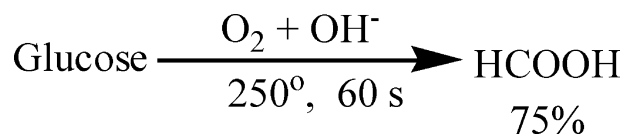


612

Hydrothermal conversion of carbohydrate biomass into formic acid at mild temperatures

Fangming Jin,* Jun Yun, Guangming Li, Ashushi Kishita, Kazuyuki Tohji and Heiji Enomoto

Glucose, a model compound of carbohydrate biomass, was converted into formate salt in an excellent yield by low-temperature alkaline hydrothermal oxidation.

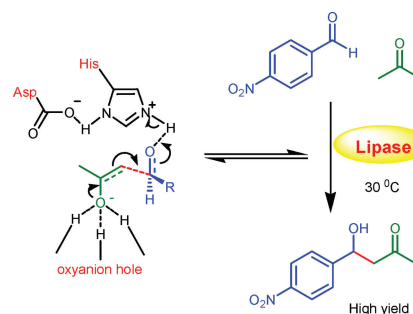


616

Biocatalytic promiscuity: the first lipase-catalysed asymmetric aldol reaction

Chao Li, Xing-Wen Feng, Na Wang,* Yu-Jie Zhou and Xiao-Qi Yu*

It was first observed that PPL, lipase from porcine pancreas, and several other lipases have a promiscuous ability to catalyse asymmetric aldol reactions between acetones and aldehydes in the presence of water.

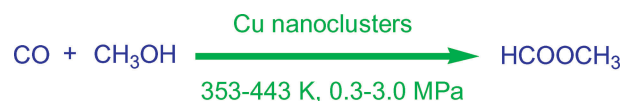


619

Liquid-phase synthesis of methyl formate *via* heterogeneous carbonylation of methanol over a soluble copper nanocluster catalyst

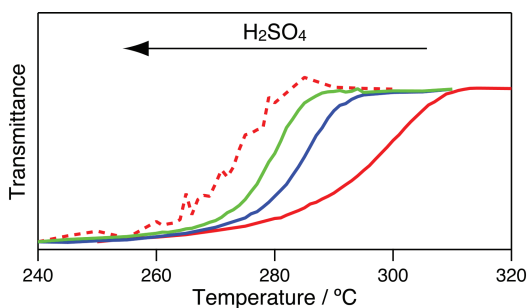
Ling He, Haichao Liu, Chao-xian Xiao and Yuan Kou*

Liquid-phase synthesis of methyl formate (MF) was achieved by green carbonylation of methanol with CO on a soluble copper nanocluster catalyst with high activities and 100% MF selectivities under mild reaction conditions



COMMUNICATIONS

623

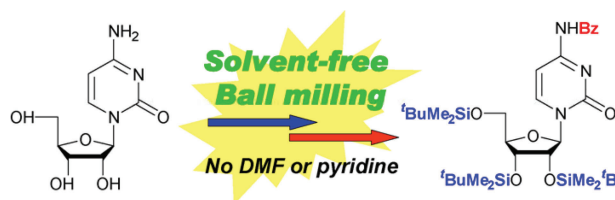


Effect of acid catalyst on structural transformation and hydrolysis of cellulose in hydrothermal conditions

Shigeru Deguchi,* Kaoru Tsujii and Koki Horikoshi

The effect of H₂SO₄ on the structure and hydrolysis of cellulose in hydrothermal conditions was revealed for the first time by *in situ* high-resolution optical microscopy.

627



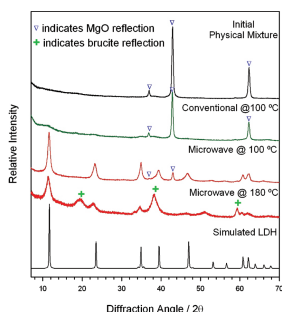
Fast, quantitative nucleoside protection under solvent-free conditions

Nicola Giri, Caroline Bowen, Joseph S. Vyle* and Stuart L. James*

Undesirable solvents such as DMF and pyridine are avoided by using solvent-free ball milling. Reactions are fast, quantitative and potentially applicable to many other biological molecules with difficult solubility profiles.

PAPERS

629

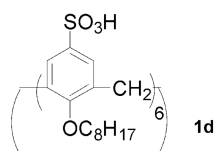
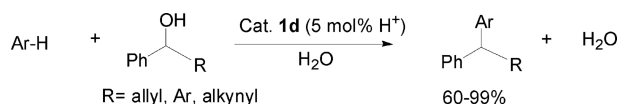


The application of focused microwave irradiation coupled with freeze drying to investigate the reaction of MgO and Al₂O₃ slurries in the formation of layered double hydroxides

Sharon Mitchell, Ian R. Baxendale and William Jones*

The hydrothermal reaction of Al₂O₃–MgO–H₂O systems has been studied using focused microwave irradiation and freeze drying techniques. Results are compared with those of conventional synthesis. These techniques provide a useful method for studying reaction kinetics and phase selectivity.

635



Calix[n]arene sulfonic acids bearing pendant aliphatic chains as recyclable surfactant-type Brønsted acid catalysts for allylic alkylation with allyl alcohols in water

Yu-Liang Liu, Li Liu,* Yi-Lin Wang, Yu-Chun Han, Dong Wang* and Yong-Jun Chen

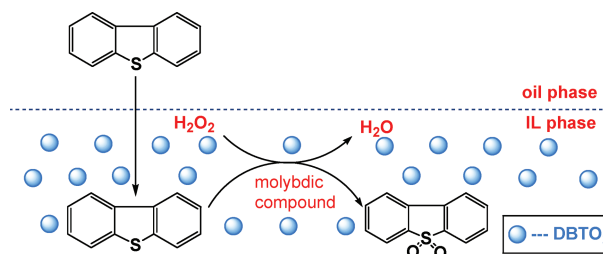
Calix[n]arene sulfonic acids bearing pendant aliphatic chains can be used as efficient and recyclable surfactant-type Brønsted acid catalysts for the nucleophilic substitution reaction of aromatic compounds with alcohols in water.

641

Commercially available molybdc compound-catalyzed ultra-deep desulfurization of fuels in ionic liquids

Wenshuai Zhu, Huaming Li,* Xue Jiang, Yongsheng Yan, Jidong Lu, Lining He and Jiexiang Xia

Ionic liquids play an important role in extraction and catalytic oxidative desulfurization, not only serving as extractant and reaction media but also stabilizing hydrogen peroxide in the reaction.

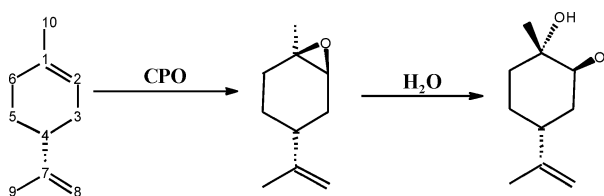


647

Stereoselective oxidation of *R*-(+)-limonene by chloroperoxidase from *Caldariomyces fumago*

Sergio Águila, Rafael Vazquez-Duhalt,* Raunel Tinoco, Manuel Rivera, Gina Pecchi and Joel B. Alderete

Stereoselective oxidation of *R*-(+)-limonene by chloroperoxidase from *Caldariomyces fumago* to form (1*S*,2*S*)-4*R*-limonene-1,2-diol with a diastereomeric excess >99.0%.

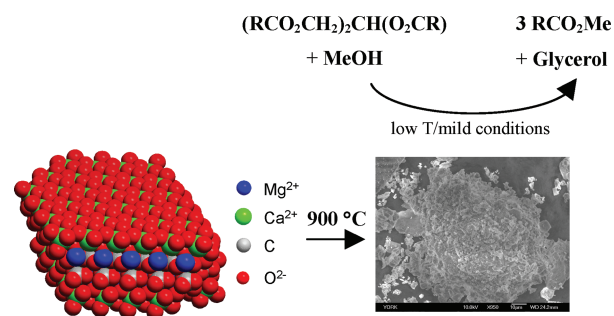


654

The application of calcined natural dolomitic rock as a solid base catalyst in triglyceride transesterification for biodiesel synthesis

Karen Wilson,* Chris Hardacre, Adam F. Lee,* Janine M. Montero and Lee Shellard

Calcined dolomitic rock exhibits high activity towards the liquid phase transesterification of glyceryl tributyrate and trioctanoate, and even olive oil, with methanol for biodiesel production.



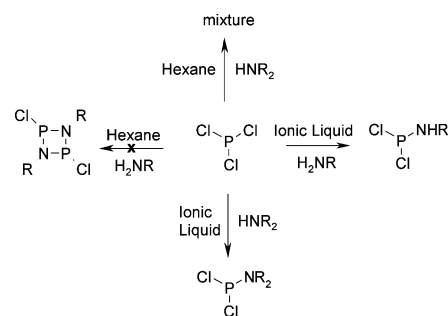
660



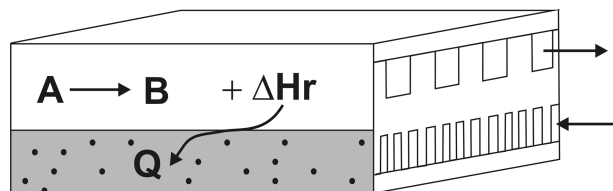
Solvent-modulated reactivity of PCl_3 with amines

Eric Jean Amigues, Christopher Hardacre,* Gillian Keane and Marie Eugenie Migaud*

The reactivity of phosphorus trichloride towards amines in ionic liquids has been investigated and compared with that in conventional organic solvents.



670

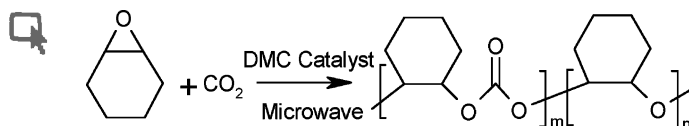


Potential of 'nanofluids' to further intensify microreactors

Xiaolei Fan, Haisheng Chen, Yulong Ding, Pawel K. Plucinski and Alexei A. Lapkin*

A nanofluid based on TiO₂ material dispersed in ethylene glycol has been studied in an integrated reactor–heat exchanger.

678

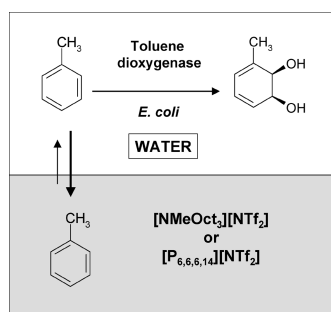


Moderate route for the utilization of CO₂-microwave induced copolymerization with cyclohexene oxide using highly efficient double metal cyanide complex catalysts based on Zn₃[Co(CN)₆]

Manju Mamparambath Dharman, Ji-Yeon Ahn, Mi-Kyung Lee, Hye-Lim Shim, Kyung-Hoon Kim, Il Kim and Dae-Won Park*

A double metal cyanide complex catalyzed rapid process for the effective utilization of CO₂ by the copolymerization with cyclohexene oxide is established through microwave irradiation.

685



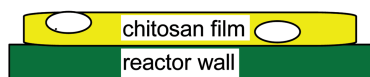
Using a biphasic ionic liquid/water reaction system to improve oxygenase-catalysed biotransformation with whole cells

Robert J. Cornmell, Catherine L. Winder, Stephanie Schuler, Royston Goodacre and Gill Stephens*

Ionic liquids can be used to increase product yields in oxygenase-catalysed reactions.

692

Aqueous – peptide hydrolysis
Organic – peptide synthesis



○ = subtilisin

Efficient subtilisin immobilization in chitosan, and peptide synthesis using chitosan–subtilisin biocatalytic films

Duncan J. Macquarrie* and Anna Bacheva*

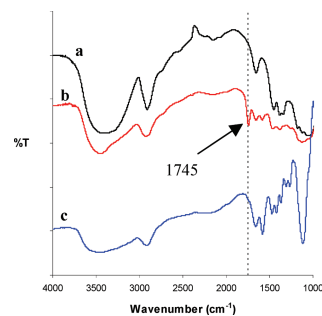
Chitosan films containing subtilisin are capable of peptide hydrolysis in aqueous conditions and peptide synthesis in non-aqueous media.

696

Designing enzyme-compatible ionic liquids that can dissolve carbohydrates

Hua Zhao,* Gary A. Baker, Zhiyan Song, Olarongbe Olubajo, Tanisha Crittle and Darkeysha Peters

The enzymatic transesterification of cellulose and methyl methacrylate (both dissolved in an ionic liquid) was catalyzed by the immobilized lipase B from *Candida antarctica*.

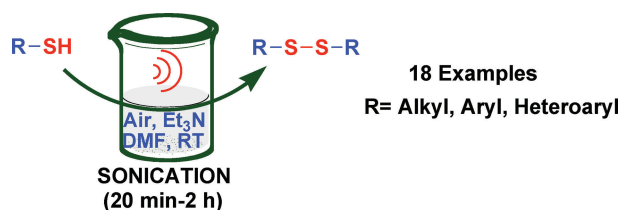


706

Efficient synthesis of disulfides by air oxidation of thiols under sonication

José Luis García Ruano,* Alejandro Parra and José Alemán

Alkyl, aryl and heteroaryl symmetrical disulfides can be easily obtained from the corresponding thiols with atmospheric oxygen under thermal or sonication conditions.

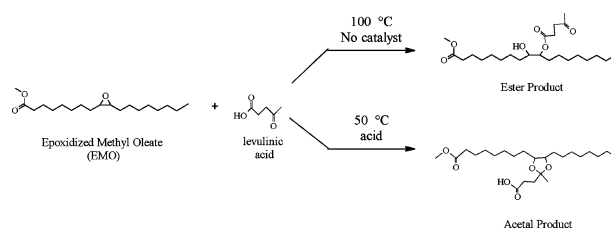


712

Synthesis of cyclic acetals (ketals) from oleochemicals using a solvent free method

Kenneth M. Doll* and Sevim Z. Erhan

Selective production of ketal or ester type surfactant precursors starting from soybean based methyl oleate.




AUTHOR INDEX

- Águila, Sergio, 647
 Ahn, Ji-Yeon, 678
 Alderete, Joel B., 647
 Alemán, José, 706
 Amigues, Eric Jean, 660
 Bacheva, Anna, 692
 Baker, Gary A., 696
 Baxendale, Ian R., 629
 Bowen, Caroline, 627
 Chen, Haisheng, 670
 Chen, Yong-Jun, 635
 Cornmell, Robert J., 685
 Crittle, Tanisha, 696
 Deguchi, Shigeru, 623
 Dharman, Manju
 Mamparabath, 678
 Ding, Yulong, 670
 Doll, Kenneth M., 712
 Enomoto, Heiji, 612
 Erhan, Sevim Z., 712
 Fan, Xiaolei, 670
 Feng, Xing-Wen, 616
 Gao, Jinbo, 608
- García Ruano, José Luis, 706
 Giri, Nicola, 627
 Goodacre, Royston, 685
 Han, Difei, 608
 Han, Yu-Chun, 635
 Hardacre, Chris, 654
 Hardacre, Christopher, 660
 He, Ling, 619
 He, Lining, 641
 Horikoshi, Koki, 623
 James, Stuart L., 627
 Jia, Guoqing, 608
 Jiang, Xue, 641
 Jin, Fangming, 612
 Jones, William, 629
 Keane, Gillian, 660
 Kim, Il, 678
 Kim, Kyung-Hoon, 678
 Kishita, Ashushi, 612
 Kou, Yuan, 619
 Lapkin, Alexei A., 670
 Lee, Adam F., 654
 Lee, Mi-Kyung, 678
- Li, Can, 608
 Li, Chao, 616
 Li, Guangming, 612
 Li, Huaming, 641
 Li, Jun, 608
 Liu, Haichao, 619
 Liu, Li, 635
 Liu, Yu-Liang, 635
 Lu, Jidong, 641
 Macquarrie, Duncan J., 692
 Migaud, Marie Eugenie, 660
 Mitchell, Sharon, 629
 Montero, Janine M., 654
 Olubajo, Olarongbe, 696
 Park, Dae-Won, 678
 Parra, Alejandro, 706
 Pecchi, Gina, 647
 Peters, Darkeysha, 696
 Plucinski, Pawel K., 670
 Rivera, Manuel, 647
 Schuler, Stephanie, 685
 Shellard, Lee, 654
 Shim, Hye-Lim, 678
- Song, Zhiyan, 696
 Stephens, Gill, 685
 Tinoco, Raunel, 647
 Tohji, Kazuyuki, 612
 Tsujii, Kaoru, 623
 Vazquez-Duhalt, Rafael, 647
 Vyle, Joseph S., 627
 Wang, Dong, 635
 Wang, Na, 616
 Wang, Yi-Lin, 635
 Wilson, Karen, 654
 Winder, Catherine L., 685
 Xia, Jiexiang, 641
 Xiao, Chao-xian, 619
 Yan, Yongsheng, 641
 Yu, Xiao-Qi, 616
 Yun, Jun, 612
 Zhang, Yanmei, 608
 Zhao, Hua, 696
 Zhong, Lin, 608
 Zhou, Yu-Jie, 616
 Zhu, Wenshuai, 641

FREE E-MAIL ALERTS AND RSS FEEDS


Contents lists in advance of publication are available on the web *via* www.rsc.org/greenchem – or take advantage of our free e-mail alerting service (www.rsc.org/ej_alert) to receive notification each time a new list becomes available.

 Try our RSS feeds for up-to-the-minute news of the latest research. By setting up RSS feeds, preferably using feed reader software, you can be alerted to the latest Advance Articles published on the RSC web site. Visit www.rsc.org/publishing/technology/rss.asp for details.

ADVANCE ARTICLES AND ELECTRONIC JOURNAL

Free site-wide access to Advance Articles and the electronic form of this journal is provided with a full-rate institutional subscription. See www.rsc.org/ejs for more information.

* Indicates the author for correspondence: see article for details.

 Electronic supplementary information (ESI) is available *via* the online article (see <http://www.rsc.org/esi> for general information about ESI).

RSC online shop

Simple, secure, fast!

24/7 access: The RSC online shop gives you continuous access to class leading products and services, expertly tailored to cater for your training and educational needs.

Browse and buy: Visit our shop to browse over 750 book titles, subscribe or purchase an individual article in one of our journals, join or renew your RSC membership, or register to attend a conference or training event.

Gift ideas: If you're looking for gift ideas, look no further. In our online shop you'll find everything from popular science books like *The Age of the Molecule* and the inspirational *Elegant Solutions* from award winning writer, Philip Ball, to our stunning Visual Elements wall chart and jigsaw.

With secure online payment you can shop online with confidence.

The RSC has so much to offer... **why not go online today?**

19120654b

RSCPublishing

www.rsc.org/shop

Registered Charity Number 207890



Chemical Technology

On-chip suction stops worm wriggling during medical research

The worm doesn't turn

Scientists in the US have developed a microfluidic method for immobilising worms in fractions of a second, allowing them to be used in high throughput studies of disease.¹

Caenorhabditis elegans is a tiny, semi-transparent worm. Its properties make it useful for studying a wide variety of diseases and biological processes, including Parkinson's disease, Alzheimer's disease and aging. But to be able to study the worm, scientists have to stop it wriggling.

Mehmet Fatih Yanik and colleagues at the Massachusetts Institute of Technology, Cambridge, put the worm inside a microfluidic channel. They lowered the pressure inside the channel, causing the worm to be sucked up against the side. A flexible membrane then sealed the worm to the side, restricting its movement completely.

Previously, scientists used anaesthesia or cooling to immobilise worms but this affected their biological functioning. Using the new method, Yanik's group can



immobilise worms for longer than with previous methods, allowing more detailed studies to be performed, and without any negative effects.

'We improved on our previous landmark study² so that we can immobilise awake animals on the chip for several minutes, instead of a few seconds,' says Yanik. 'This

Low pressure and a flexible membrane seal the worm to the side of the channel

allows us to take three-dimensional movies of single cells in the animals and represents a significant leap in high throughput studies of multi-cellular organisms.'

Aaron Wheeler, an expert in microfluidics at the University of Toronto, Canada, states that this work shows that 'microfluidics has emerged as a powerful tool for basic biology studies in whole animal models, facilitating experiments that would be impossible by conventional means.'

Yanik says he believes that this new technology could dramatically accelerate large scale studies on disease models. 'We are currently using large scale genetic and drug libraries to discover factors that affect neural regeneration *in vivo* using femtosecond laser nanosurgery,' he says.
Ziva Whitelock

References

- 1 F Zeng, C R Rohde and M F Yanik, *Lab Chip*, 2008, **8**, 653 (DOI: 10.1039/b804808h)
- 2 C B Rohde et al, *Proc. Natl. Acad. Sci. USA*, 2007, **104**, 13891 (DOI: 10.1073/pnas.0706513104)

In this issue

10 minute diagnosis on the microscale

New device uses surface plasmon resonance to speed up disease detection

Hydrogel helps the medicine go down

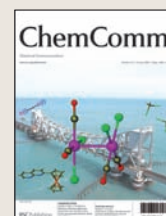
Microdevice could provide better treatment for cancer patients

Instant insight: Making sense of DNazymes

Itamar Willner and colleagues discuss the applications of DNA-based enzymes

Interview: People power

Duncan Graham tells Nina Notman just how important people are for the future of science



The latest applications and technological aspects of research across the chemical sciences

Application highlights

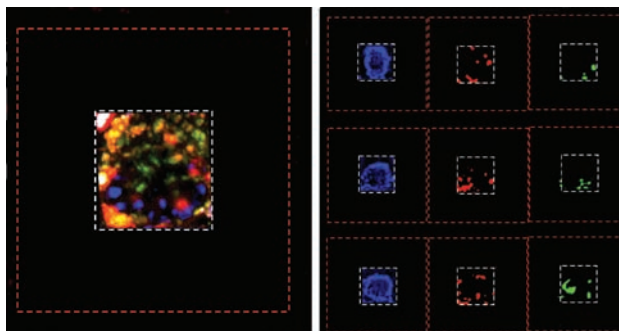
Microdevice could provide better treatment for cancer patients

Hydrogel helps the medicine go down

US scientists have made an easy-to-swallow device to controllably deliver cancer drugs into the body. After treatment, the device passes safely out of the body through digestive tract, they claim.

Many cancer drugs must be injected into the bloodstream because they cannot pass easily into the blood through the stomach and intestine walls. To overcome this barrier to oral delivery, Tejal Desai and colleagues at the University of California, San Francisco, made a polymer-based microdevice with a tiny reservoir in the centre. They filled the reservoir with a polymer-derived gel known as a hydrogel, which can store drugs and release them in a controlled way.

Desai loaded the hydrogel with a drug and tested the device on a model that mimics cell absorption. He found that the device seemed



to concentrate release of the drug at the cell interface, increasing permeability through the cells. Also, because the device limits the amount of free drug by releasing it slowly, it prevents damage to surrounding tissues.

'The devices can be used to deliver a variety of cancer drugs,' says Kristy Ainslie, who works on the project. 'This creates a broad range of

Fluorescence imaging can be used to view drugs in the microdevice

treatment options for cancer patients so they are treated more effectively and with fewer side effects.'

'This is an innovative application of microfabrication technology, which is already used to cost-effectively mass-produce sophisticated computer chips and miniature air-bag deployment sensors,' enthuses Shuvo Roy, a biomedical engineer from the Cleveland Clinic Lerner Research Institute, US.

Desai's group plan additional studies with the microdevice, using models that more closely mimic the digestive tract. They are considering using hydrogels with triggered release options, to turn the release of drugs on and off on demand.

Rachel Cooper

Reference

K M Ainslie, C M Kraning and T A Desai, *Lab Chip*, 2008, DOI:10.1039/b800604k

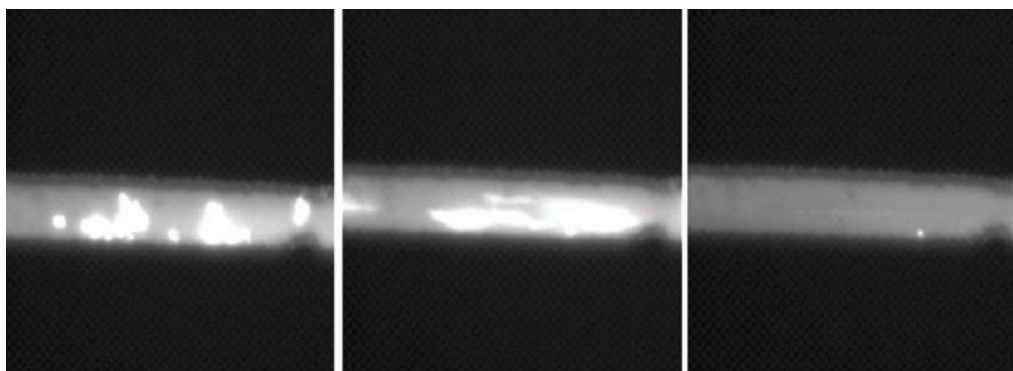
Simple method for monitoring reaction rates in microfluidic devices

Keeping track of particles-in-a-chip

How does trapping a nanoparticle in a microdevice affect its reactions? US scientists are answering this question thanks to a straightforward method using fluorescent tags.

Meghan Caulum and Charles Henry at Colorado State University in Fort Collins have developed what they say is 'a simple, inexpensive way to monitor reactions at the surface of magnetic particles within a microfluidic device.' The researchers used their method to look at reaction rates in the system.

Using small magnetic particles in microfluidic systems has great potential in chemical synthesis and biological techniques such as immunoassays, declare Caulum and Henry. But few researchers so far have studied how reaction rates at the particle surfaces differ in microfluidic devices from those in solution. Caulum and Henry say that understanding the processes involved is important when trying to optimise previously solution-based assays on-chip.



The duo's technique is based on following a bond-breaking reaction inside a microfluidic device. A reducing agent is made to flow over fluorescently tagged particles captured inside the device by magnets. This breaks disulfide bonds that link the tags to the particle surfaces, reducing the fluorescence. By monitoring the loss of fluorescence with time, the researchers can measure the reaction's kinetics.

Capture and release of magnetic particles in a microchip

Reference

M M Caulum and C S Henry, *Lab Chip*, 2008, **8**, 865 (DOI: 10.1039/b714822d)

Sabeth Verpoorte, head of the pharmaceutical analysis group at the University of Groningen in the Netherlands, says 'There is no doubt that combining micro- and nanoparticles with microfluidics will lead to powerful new approaches for chemical and biochemical processing and analysis. This work represents a significant step forward in this area, as it yields new information on particle-based reactions and handling.' *Katherine Davies*

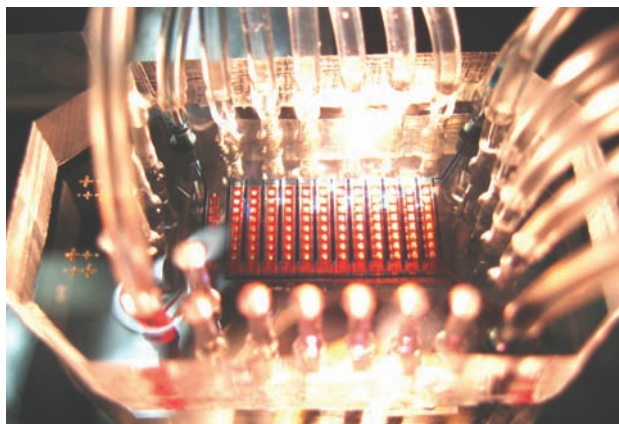
New device uses surface plasmon resonance to speed up disease detection

10 minute diagnosis on the microscale

Scientists in the US have taken a step towards faster and more efficient immunoassays for diagnosing HIV and other diseases.

Richard Zare and colleagues from Stanford University have designed and constructed a new microfluidic device that can monitor immunoreactions – the reaction between an antigen and its antibody – in real time. Using a combination of an immunoassay and surface plasmon resonance imaging (SPR), the device provides a diagnosis in approximately 10 minutes, compared with an hour or more using traditional methods.

Zare's device has several other advantages over other immunoassay methods, including specially designed nanolitre-scale channels that mean a smaller volume of sample is needed. The



channels also allow the reagents to be delivered by the device in just one step. The speed comes from the SPR detection method, which can monitor antibody-antigen interactions in real

The microfluidic device can monitor interactions between an antigen and its antibody in real time

time. SPR measures a refractive change caused by antibodies binding to the antigens on the surface of the array of thin gold spots in the device. Microfluidic devices can potentially be fully automated, meaning samples can be manipulated precisely and efficiently.

Zare believes that, with some further improvements, this combination of immunoassays and SPR in microfluidic devices will have many future applications to real-world problems. 'The results are quite encouraging – so much so that we feel that the prospects for the use of this type of device are quite promising.' *May Copsey*

Reference

Y Luo, F Yu and R N Zare, *Lab Chip*, 2008, **8**, 694 (DOI:10.1039/b800606g)

Organometallic complex turns natural gas into alcohol

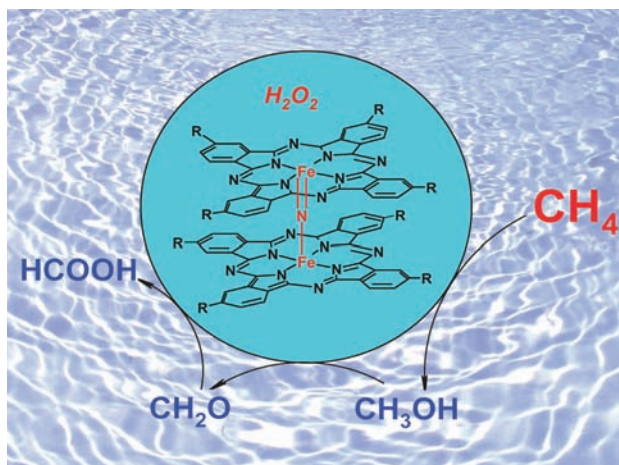
Catalyst mimics nature's methane oxidation

Scientists in France have developed the first mild, enzyme-inspired method to convert methane to industrially valuable products.

Alexander Sorokin and colleagues at the University of Lyon made an organometallic complex that oxidises methane to methanol at low temperatures using hydrogen peroxide.

Methane is the main component of natural gas but also the least reactive. In certain types of bacteria, the enzyme methane monooxygenase converts methane to methanol under very mild conditions. Essential for its activity is its diiron centre, which forms a reactive oxygen-bridged species that can oxidise C–H bonds. Chemists have tried to mimic this catalytic process but until now have not succeeded.

Using porphyrin-like ligands known as phthalocyanines, Sorokin made a diiron complex in which the two irons are bridged with a nitrogen atom. He



found that the complex activated hydrogen peroxide, forming a very strong species that oxidised methane in water at temperatures as low as 25 degrees Celsius. Depending on the reaction conditions, the resulting methanol could be oxidised further to formaldehyde and formic acid.

'Dimeric structures are often

The N-bridged complex oxidises methane in water

considered as inactive in catalysis,' explains Sorokin. 'However, we hypothesised that diiron porphyrin-like complexes could stabilise high oxidation state species due to delocalisation of charge at the two irons and the ligands. The key point is the stability of the binuclear core during catalysis.'

Robert Crabtree, professor of inorganic chemistry at Yale University, New Haven, US, is impressed by the results. 'This is a significant step in advancing one of the great problems: the direct partial oxidation of methane to methanol,' he says.

Sorokin says he believes that this novel catalyst presents great potential for further development. 'This finding should initiate studies directed towards optimising its structure to tune its catalytic properties and increase its scope towards the clean oxidation of other difficult-to-oxidise substrates to useful products,' he says.

Roxane Owen

Reference

A B Sorokin, E V Kudrik and D Bouchu, *Chem. Commun.*, 2008, DOI: 10.1039/b804405h

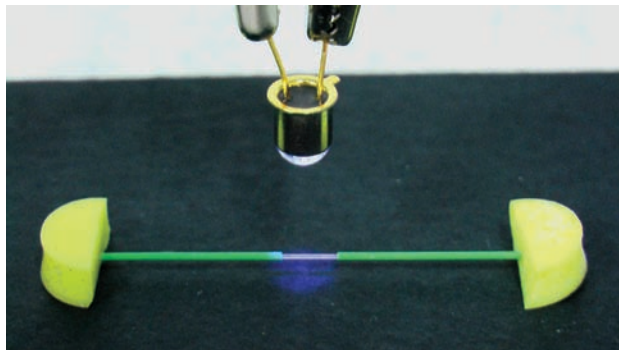
Solid-state light source offers low energy route to polymer structures

LED triggers on-chip construction

For the first time, scientists have used ultra violet light emitting diodes (UV-LEDs) to make polymer columns in lab-on-a-chip devices. The columns could be used as micropumps to move solutions through the devices, claim Mirek Macka at Dublin City University, Ireland, and colleagues in Ireland and the Czech Republic.

The team used the light from UV-LEDs to start a polymerisation reaction between methacrylate units inside the channels of a microfluidic chip. They found that channels containing the resulting polymer columns were better at pumping solutions than bare channels when they applied an electric field to the chip.

LEDs are solid-state light sources,



where electrical energy is converted to light in a semiconductor material. Although conventional UV light sources, such as xenon arc lamps, can be used in photopolymerisation reactions, UV-LEDs offer a number of advantages: they are

The UV light sets off a photopolymerisation reaction

much smaller and can be used in miniature devices; they use less energy; and they are cheaper.

At present, commercially available UV-LEDs have poor electric energy-to-light conversion, which in turn can generate a lot of heat. 'Further development and improvement of the technical parameters is needed for UV-LEDs to become really attractive for mainstream chemistry,' says Macka. He plans to use UV-LEDs to photocatalyse other reactions to investigate their versatility, compared with classical UV sources. *Michael Brown*

Reference

S Abele *et al*, *Analyst*, 2008, DOI:10.1039/b802693a

Layered structure substantially boosts performance

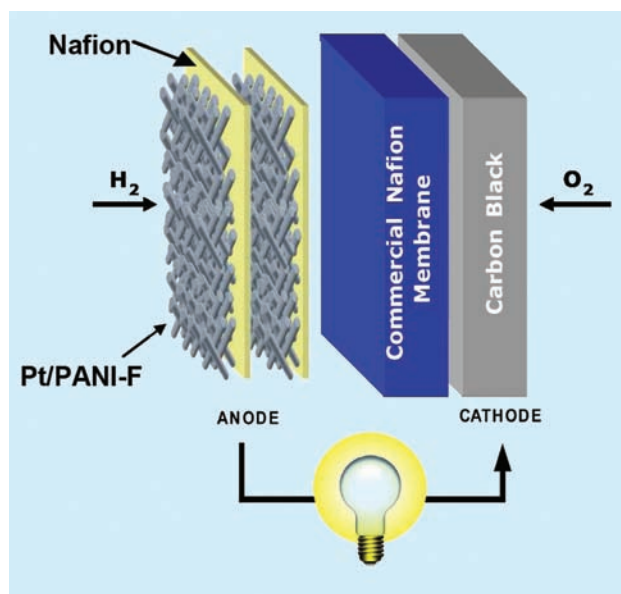
Spray-on electrodes

Scientists have developed a quicker method to make multilayered electrodes for fuel cells.

Led by Marc Michel, a team based at Darmstadt University, Germany, used a sprayed layer-by-layer method to assemble the electrodes for proton exchange membrane (PEM) fuel cells.

PEM fuel cells split hydrogen into protons and electrons at the anode using a platinum catalyst. The protons travel through a polyelectrolyte membrane to the cathode, where they react with oxygen to form water. For high performance, the polyelectrolyte must be permeable to protons but not electrons and the catalyst's structure must allow the hydrogen and protons to diffuse easily through it.

Scientists achieve this by building up the components of the cells in layers. Conventionally, they alternately dip Nafion, the most commonly used polyelectrolyte membrane, into two solutions of oppositely charged polyelectrolytes. Instead, Michel sequentially sprayed the solutions on to



Platinum-functionalised polyaniline fibres accelerate charge and ion transport

Nafion, which he claims can boost performance.

Michel used a mixture of platinum catalyst and polyaniline, a highly conductive polymer, as the positive solution and Nafion as the negative one. He found that polyaniline's high conductivity and

fibrous structure improved charge and ion transport through the fuel cell.

Michel says the spraying technique is much faster and doesn't affect the quality of the films produced. '20 layers can be obtained in less than five minutes compared to about two and a half hours for the conventional layer-by-layer dipping method,' he says. Moreover, the amount of platinum used in this method is almost half of that used for conventional carbon-supported platinum catalysts used in fuel cells, making the cells cheaper and less toxic.

Michel says he hopes that the reduced cost and preparation time will make the spraying technique attractive to industries, but first more work has to be done. 'We have to do long term stability investigations to check whether polyaniline is a good candidate for fuel cells,' he says. *Ian Gray*

Reference

M. Michel *et al*, *Phys. Chem. Chem. Phys.*, 2006, DOI:10.1039/b802813n

Interview

People power

Duncan Graham tells Nina Notman just how important people are for the future of science



Duncan Graham

Professor Duncan Graham is director of the Centre for Molecular Nanometrology at the University of Strathclyde, UK, which is focused on creating new methods of bioanalysis based on nanoparticle based sensors and optical spectroscopy, and in particular surface enhanced Raman scattering. Duncan is on the editorial board for *The Analyst*.

Who or what inspired you to become a scientist?

It was the DNA double helix that inspired me to become a scientist. First I heard about DNA and the story involved in it, and then I was shown the film 'Race for the Double Helix' by my biology teacher in fifth year at school, and I thought 'I want to do science.'

What is the secret to running a successful research group?

What I try to do is allow students and postdocs to do their own decision making and empower them in terms of their research direction as opposed to dictating to them. I don't think that dictation works. If you give students and postdocs responsibility and enthuse them about what they are doing then they contribute a lot more than they would otherwise and they really get into it.

You are the director of the Centre for Molecular Nanometrology at the University of Strathclyde. Can you explain what nanometrology is?

It is the measurement of very small things on a very small scale. It is using molecules and chemistry to develop new methods of measurement on the nanoscale, preferably in living systems.

What is the most exciting project that your group is working on at the moment?

We are trying to do *in vivo* detection of different disease states using surface enhanced Raman scattering (SERS), nanoparticles and some bio-interactions. This involves functionalising nanoparticles that respond to a specific biological molecule or interaction and that response is indicated by the SERS spectra. The challenging part of this is trying to take the chemistry of detection that we are doing on the bench into a living environment.

What do you think will be the next breakthrough for SERS?

It is likely to be combining the exquisite selectivity

and sensitivity of the technique to make a biological measurement which relates to some human health issue, for example detection of a specific protein marker or biomarker relating to a disease state that can't be detected by other techniques.

What is the most rewarding aspect of your work?

The people, especially seeing my colleagues' faces light up when they get a scientific breakthrough. Another rewarding aspect is the ability to come up with an idea, discuss it with other scientists, colleagues and collaborators, and work it through to a natural experiment that generates data that is new and exciting.

How do you see the future of analytical science in the UK?

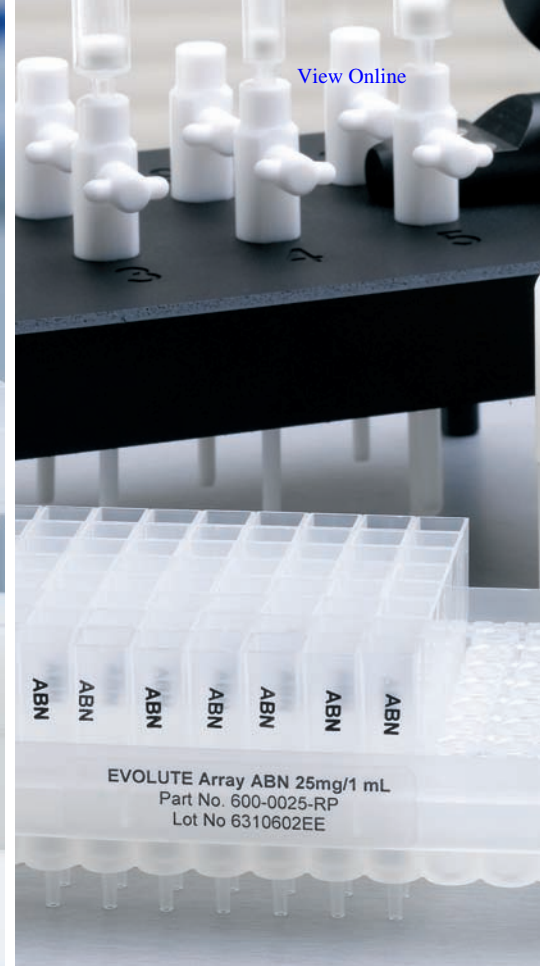
That will depend on a number of different factors. There is a good body of new scientists being trained in analytical chemistry and they are being trained to have a multidisciplinary outlook on the subject. Analytical science shouldn't pigeon hole itself, it needs to become more expansive and encompassing than it is. This is starting to happen, but funding councils and the people who promote the subject need to realise it. They need to support the subject more adequately than they have done already, otherwise it is not going to deliver on the same scale as some of our counterparts in the US have. People who are having massive breakthroughs in what we would consider analytical science are not necessarily traditional analytical chemists.

What piece of lab equipment would you most like to be?

A cork! It is the first thing that came into my head.

If you weren't a scientist, what would you be?

I think I would be a deep sea diver. Or maybe a bus driver, or a labourer? Or a butcher – I have always fancied being a butcher.



IST Sample Preparation • Bioanalysis • Clinical • Environmental • Forensic • Agrochemical • Food • Doping Control

EVOLUTE® CX **NEW!**

Mixed-mode selectivity, generic methodology and efficient extraction

EVOLUTE® CX mixed-mode resin-based SPE sorbent extracts a wide range of **basic drugs** from biological fluid samples. EVOLUTE CX removes matrix components such as proteins, salts, non-ionizable interferences and phospholipids, delivering cleaner extracts with reproducible recoveries for accurate quantitation.

EVOLUTE® ABN

Minimize matrix effects, reduce ion suppression and concentrate analytes of interest

EVOLUTE® ABN (Acid, Base, Neutral) is a water-wettable polymeric sorbent optimized for fast generic reversed phase SPE. Available in 30 μm columns and 96-well plates for bioanalysis and **NEW 50 μm columns** – ideally suited for environmental, food/agrochemical and industrial analysis as well as forensic and doping control applications.

Contact your local Biotage representative or visit www.biotage.com to request a **FREE** sample.

Instant insight

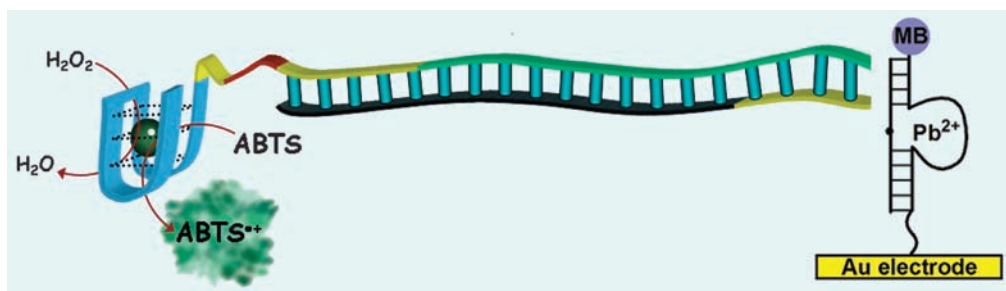
Making sense of DNAzymes

Itamar Willner and colleagues from the Hebrew University of Jerusalem, Israel, discuss the applications of DNA-based enzymes

RNA and DNA molecules, like proteins, have complex three-dimensional structures that depend on the sequence of their building blocks – though whereas proteins have twenty amino acids, RNA or DNA molecules have only four types of nucleotide to play with. Still, this variety, together with single-stranded and double-stranded domains, can give complex structures that, much like enzymes, can selectively bind substrates and catalyse useful chemical reactions. Such nucleic acid based catalysts are called DNAzymes and ribozymes and hold great promise as chemical sensors; tools to construct nanostructures; and molecular machines and computing systems.

The idea of designing structures that selectively bind substrates (aptamers), or act as catalytic enzyme-like DNA strands, became practical in the 1990s, following the development of the Systematic Evolution of Ligands by Exponential Enrichment (SELEX) process. Here, nucleic acids with specific binding properties, or affinities towards a particular transition-state analogue, are fished out of a library of 10^{15} nucleic acids and amplified by the polymerase chain reaction (PCR). The aptamers and catalytic nucleic acids made this way are, in effect, man-made analogues of protein-based antibodies and enzymes, respectively. But the nucleic acid enzymes have advantages over their protein analogues: DNA is chemically very stable; the enzymes can be efficiently machine-synthesised by PCR; and one can even couple aptamers with DNAzymes, yielding hybrids which not only bind to specific substrates, but also have enzyme-like catalytic activity.

Some of the broadest applications of DNAzymes have been in the development of biosensors. For example, among the many DNAzymes and ribozymes prepared in recent years is a sequence of



nucleic acids that mimics the action of the enzyme horseradish peroxidase. Together with hydrogen peroxide and an appropriate substrate, this DNAzyme generates a colour change, which can be used to detect nucleic acids or as a marker for cancer cells.

Similarly, metal ions such as lead or copper can be detected by nucleic acid strands that become catalytic when they bind around metals. Once catalytically active, these metal-dependent DNAzymes cleave a specific part of a DNA sequence, which acts as a fluorescent signal advertising the metal's presence.

DNAzyme-based systems have even been suggested as potential substitutes for the PCR protocol as a way to detect small amounts of DNA. Nucleic acids have been designed that, upon recognising a required piece of DNA, stimulate self-assembling syntheses of DNAzyme units. The accumulation of the DNAzyme provides a catalytic label, amplifying the original sensing event.

DNAzymes can also be used as tools for shaping and correcting nanostructures. Gold nanoparticles, for instance, can be forced into a blue-coloured crosslinked assembly when nucleic acid strands attached to each particle hybridise. A DNAzyme can cleave these nucleic acid crosslinks, turning the blue assembly into red-coloured individual nanoparticles: a sensitive read-out signal. In this way, DNAzymes have been used as proof-reading units that check through mixtures

A DNAzyme mimics the action of horseradish peroxidase

of nanoparticles and remove any erroneous crosslinking.

Some ingenious molecular machines based on DNA are driven by DNAzymes. DNAzyme-containing nucleic acid structures have duplicated the mechanical functions of a scissor, while DNAzymes have also been used to cleave nucleic acid strands, allowing them to 'walk' along a DNA or RNA track. At first glance, these concepts seem only to satisfy scientific curiosity, but the emerging systems highlight some extremely valuable and promising applications of DNA-based machines.

One further application of DNAzymes relates to their use as 'smart' biomolecules that perform logic operations for computing systems. Nucleic acids of pre-designed sequences have been used as templates that activate, in the presence of appropriate nucleic acids as inputs, logic gate operations. These logic functions have been used, most famously, to make molecular calculators and a system that can play noughts and crosses (tic-tac-toe). Such DNA-based computing systems are not aimed to substitute man-made computers but to complement computer science and could eventually furnish new perspectives for drug design and nanomedicine in the future.

Read more in 'DNAzymes for Sensing, Nanobiotechnology and Logic Gate Applications' in issue 6 of Chemical Society Reviews.

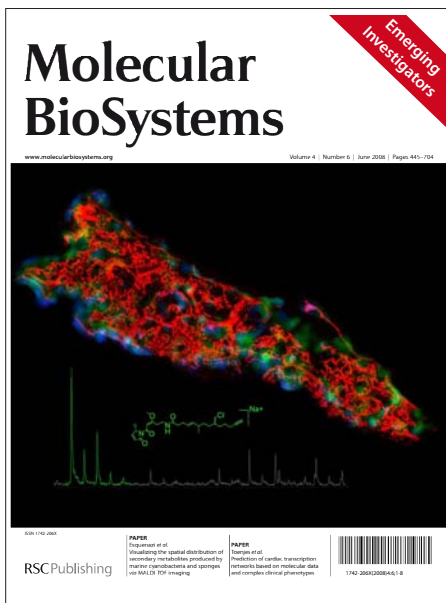
Reference
I Willner et al. *Chem. Soc. Rev.*, 2008, DOI: 10.1039/b718428j

Essential elements

Emerging Investigators

Highlighting the brightest new researchers in the field, issue 6 of *Molecular BioSystems* (MBS) is not to be missed. The 20 full research papers, seven communications and two reviews are written by outstanding young scientists at the chemical- and systems-biology interfaces. The issue features novel methods to visualise and manipulate protein function in living cells, the development of chemical techniques to monitor specific protein post-translational modifications, new insights into metabolomics and much, much more.

All the contributors were personally recommended by MBS editorial or advisory board members as young scientists whose work has the potential to



influence the future directions of these fields. All submissions were subjected to full peer review and the result is an issue showcasing

work in some of the most fascinating and important areas of biology.

We intend to run future issues of this kind so watch this space. Finally, MBS extends a big thank-you to all the Emerging Investigators themselves for making this such an excellent collection of papers. We wish them every success in their future careers and – in the words of Tom Kodadek, the MBS editorial board chair – ‘Clearly the future of this exciting area of biology is in good hands!’

Find out more at www.molecularbiosystems.org

And watch out for a related theme issue from *ChemSocRev* (www.rsc.org/chemsocrev) in July; issue 7 will be a thematic issue examining the interface of chemistry with biology.

Listen up



Building on the success of their monthly podcast – which has been drawing listeners since launch in October 2006 – *Chemistry World* has now launched a weekly mini-podcast. With a leading scientist or author as your guide to bring you the story behind the science, ‘Chemistry in its element’ allows you to work your way through the periodic table as each episode pays a five-minute visit to an element. And – just like the monthly podcast – it’s completely free! Make a start with episodes on iron, gold, silver, bromine, zirconium and oxygen.

In addition, join the thousands of listeners who enjoy the *Chemistry World* monthly podcast and you could be the lucky winner of an iPod. It’s simple: listen to the latest episode of the monthly podcast, answer our short feedback survey and we’ll enter you into our prize draw.

For further information about the *Chemistry World* podcasts, and your chance to win, visit www.chemistryworld.org/podcast

Pioneers in Miniaturisation Prize

Leading the way in miniaturisation, *Lab on a Chip* has teamed up with Corning Incorporated to again host the Pioneers in Miniaturisation Prize. Spanning a variety of disciplines, this prize recognises outstanding achievements and significant contributions by a younger scientist to the understanding and advancement of micro- and nanoscale science.

As a leading-edge science and technology organisation, Corning Incorporated is keen to reward, recognise and encourage the development of miniaturisation in the chemical and biological sciences and promotes interdisciplinary research required for the most significant innovations in this area.

The recipient of the award will receive a US\$5000 bursary

to support their continued contribution to the field. A deadline for applications has been set for 31st August 2008. Following the final decision, which will be made by committee, a winner will be announced at the μ TAS 2008 conference, in San Diego, CA, US.

For more information visit www.rsc.org/loc

Chemical Technology (ISSN:1744-1560) is published monthly by the Royal Society of Chemistry, Thomas Graham House, Science Park, Milton Road, Cambridge UK CB4 0WF. It is distributed free with *Chemical Communications*, *Journal of Materials Chemistry*, *The Analyst*, *Lab on a Chip*, *Journal of Atomic Absorption Spectrometry*, *Green Chemistry*, *CrystEngComm*, *Physical Chemistry Chemical Physics* and *Analytical Abstracts*. *Chemical Technology* can also be purchased separately. 2008 annual subscription rate: £199; US \$396. All orders accompanied by payment should be sent to Sales and Customer Services, RSC (address above). Tel +44 (0) 1223 432360, Fax +44 (0) 1223 426017 Email: sales@rsc.org

Editor: Joanne Thomson
Deputy editor: Michael Spence
Associate editors: Celia Clarke, Nina Notman
Interviews editor: Elinor Richards
Web editors: Nicola Convine, Michael Townsend, Debora Giovannelli
Essential elements: Daniel Bradnam and Kathryn Lees
Publishing assistant: Ruth Bircham
Publisher: Graham McCann

Apart from fair dealing for the purposes of research or private study for non-commercial purposes, or criticism or review, as permitted under the Copyright, Designs and Patents Act 1988 and the copyright and Related Rights Regulations 2003, this publication may not be reproduced, stored or transmitted, in any form or by any means, with the prior permission of the Publisher or in the case of reprographic reproduction in accordance with the terms of licences issued by the Copyright Licensing Agency in the UK. US copyright law is applicable to users in the USA.

The Royal Society of Chemistry takes reasonable care in the preparation of this publication but does not accept liability for the consequences of any errors or omissions.

Royal Society of Chemistry: Registered Charity No. 207890.

RSC Publishing

Fusing green chemistry and green engineering: DesignBuild at the molecular level

DOI: 10.1039/b808091g

At the end of June, 2008, our journal, *Green Chemistry*, will be holding a reception to celebrate the tenth anniversary of the first issue of the journal. It is notable because the reception will be held at the annual Green Chemistry and Engineering Conference in Washington, D.C. For those who have not attended the conference previously (I encourage you to do so this year and stop by the reception), I would note that it regularly receives an outstanding review by its attendees because of the interdisciplinarity that is ingrained even in the conference title. The importance of the inclusion and fusion of the various talents needed for the generation of science and technology for sustainability cannot be overstated.

It is said that the concept of a Master Builder can be traced back to the Code of Hammurabi in Mesopotamia in 1800 B.C. Since the inception of this model, the Master Builder has been responsible for the erection of everything from temples, to bridges, to municipal building, to castles, to skyscrapers throughout millennia. It was the case that the role of Master Builder was almost always filled by an architect or some close equivalent of an architect, and the construction experts were only brought in to implement the design plans of the Master Builder. In recent decades, the concept of DesignBuild has been increasingly used as an alternative to the Master Builder model. DesignBuild brings together the designer (architect) and the builder (construction experts) in an integrated manner. The advantages of this new approach have been compelling enough to result in the DesignBuild approach being adopted in the majority of the projects in the E.U. and North America.

This architectural analogy can be particularly instructive for what needs to happen in the field of green chemistry. Since the field of chemistry emerged in its modern form, the molecular architects, the chemists, have designed chemicals to have the properties, the performance

and the capabilities that they desire them to possess. The chemist Master Builder would then engage the expertise, such as chemical engineers, needed to bring the new chemicals to scale. This model has been effective in producing molecules that can cure disease, provide energy and be the basis of new materials. It is also important to recognize that this process has been in place during the time in which many concerns have arisen about the effects of chemicals on the environment and human health. In order to fully understand these issues, and more importantly address these issues, requires the full integration of other essential disciplines such as engineering, exposure and fate, and toxicology.¹ In other words, the DesignBuild model needs to be incorporated as a central approach in the field of green chemistry.

It has often been said that the field of green chemistry is inherently interdisciplinary.² While there is some truth to this statement because green chemistry deals with performance criteria beyond those typical physical/chemical properties and narrow measures of efficiency historically used to evaluate the quality of our chemistry, there is still much room for improvement in the implementation of DesignBuild in the practice of chemistry. Green chemistry is well poised to lead the way in this important evolution in the molecules that we make and the way we make them.

There have been important developments in recent years that demonstrate how the field of green chemistry is moving toward this integrated interdisciplinary model. Several years ago, the University of Nottingham launched a program that illustrated how chemistry, engineering and important communication disciplines could work together on issues of sustainability. The DICE model, Driving Innovation in Chemistry and Chemical Engineering, has served to show the importance and the productivity of interdisciplinary integration. No longer would it be acceptable that a new molecule be designed

or a new synthetic process be discovered and then tossed over the transom to the chemical engineers to scale-up. The inefficiencies, the rework and the unforeseen consequences of that approach were too numerous and too well-documented to continue with that process. The DICE model is one for others to look at, emulate, and hopefully improve upon as we seek to implement DesignBuild for chemistry.

A little over a year ago, Yale University launched the Center for Green Chemistry and Green Engineering in the Department of Chemistry, the Department of Chemical Engineering and the School of Forestry and Environment. The Center also has on its Board representatives from the Schools of Medicine, Law, Management, Architecture and Divinity. While we are moving toward a more complete integration of the chemical design process, there is a long way to go. We need to have the molecular designers, process designers, product designers, and expertise on all life-cycle stages present at the design table—if not in person then at least their knowledge base needs to be represented.

DesignBuild for chemistry may very well show the type of efficiencies, performance benefits and innovations for our field as it has in the building and infrastructure trades. At a minimum, it should be valuable in avoiding the unforeseen and undesirable consequences of our chemistry that is an important mission of green chemistry.

Paul Anastas

Director, Center for Green Chemistry and Green Engineering, Yale University, USA.

References

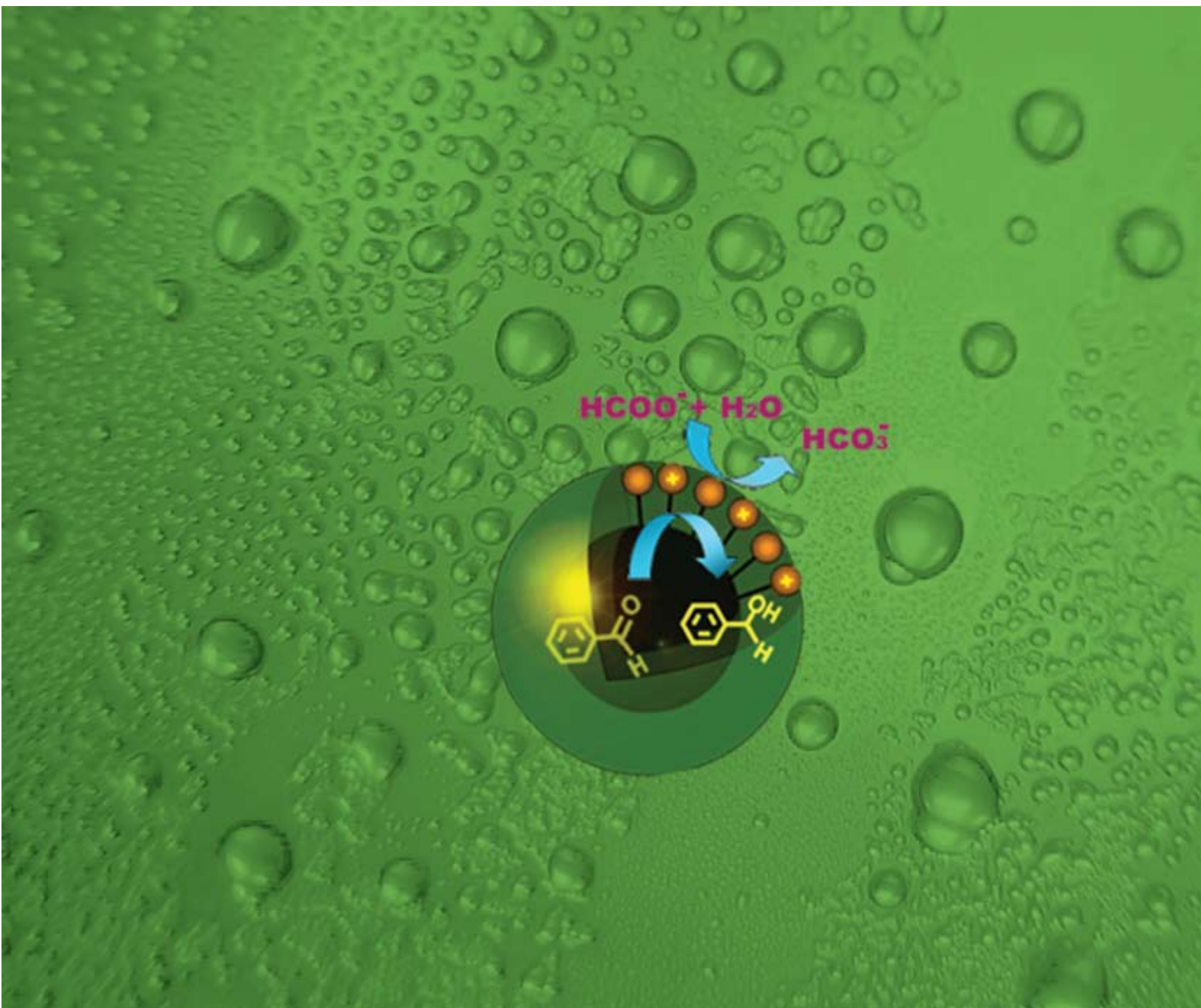
- 1 William McDonough, Michael Braungart, Paul T. Anastas and Julie B. Zimmerman, *Environ. Sci. Technol.*, 2003, **37**(23), 434A–441A.
- 2 Rebecca L. Lankey and Paul T. Anastas, *Ind. Eng. Chem. Res.*, 2002, **41**(18), 4498–4502.

Green Chemistry

Cutting-edge research for a greener sustainable future

www.rsc.org/greenchem

Volume 10 | Number 6 | June 2008 | Pages 597–720



ISSN 1463-9262

Li *et al.*
Transfer hydrogenation of aldehydes
on amphiphilic catalysts

Jin *et al.*
Hydrothermal conversion of
carbohydrate biomass



RSC Publishing

1463-9262(2008)10:6;1-C

Transfer hydrogenation of aldehydes on amphiphilic catalyst assembled at the interface of emulsion droplets†

Jun Li, Yanmei Zhang, Difei Han, Guoqing Jia, Jinbo Gao, Lin Zhong and Can Li*

Received 25th February 2008, Accepted 15th April 2008

First published as an Advance Article on the web 24th April 2008

DOI: 10.1039/b803209b

An amphiphilic polymer-based iridium catalyst assembled at the interface of emulsion droplets shows a remarkable rate acceleration for the transfer hydrogenation of aldehydes in water, which may result from the high surface area of the emulsion droplets and the high local concentrations of reactants around the active sites.

Catalytic transfer hydrogenation has severer as a powerful, practical and versatile protocol for selective reduction of aldehydes. Therefore, many efforts have been devoted to the development of new catalysts and catalytic systems for transfer hydrogenation.¹ To date, the most efficient catalytic system is likely the transfer hydrogenation aldehydes using HCOONa as a reductant based on iridium–diamine complexes in neat water, providing a simple, excellently selective and green pathway for alcohol production, as reported by Xiao.² These iridium complex catalysts are partitioned in the substrate (aldehydes) and aqueous phase, being more soluble in the former. The distribution of catalysts in the reaction favors the high concentration of substrate around catalytic active sites and diminishes the mass-diffusion limitation of the hydrophobic substrate, which is often a major problem using water-soluble catalysts in aqueous biphasic systems. However, most of catalysts sequestered in the droplets of substrates are difficult to meet with the reductant HCOO⁻, resulting in the insufficient utilization of catalyst.

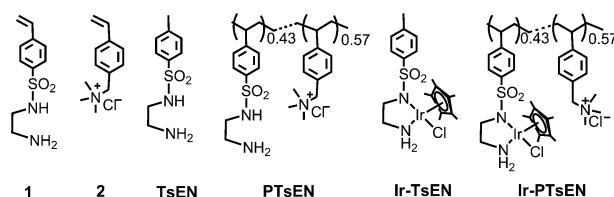
The utilization of surfactants to form micelles is the most often employed strategy to overcome the reagent incompatibility, involving hydrophobic substrates and inorganic salts. Indeed, a significant acceleration of rate has been occasionally observed in micellar medium (e.g. hydrolysis).³ In organometallic catalysis, however, catalyst and reactants often reside in different locations within micelles due to the polarity difference, thus exhibiting somewhat low acceleration of rate, even an inhibiting effect in some cases.⁴ Another appealing alternative is to use amphiphilic catalysts with surfactant structure and amphiphilic polymer-supported catalysts.⁵ These amphiphilic catalysts can form supramolecular assemblies ranging from the nanoscale to microscale in aqueous solution that could possibly afford high local concentrations of reactants near the catalysts. This strategy has mainly been applied to overcome the limitation of the solubility of hydrophobic substrates in water, such as in

hydroformylation,^{5a,5f} hydrogenation,^{5c} and C–C bond-forming reactions.^{5b,5e}

In our previous work, we developed the emulsion catalysis system, where amphiphilic quaternary ammonium polyoxometalates, acting as both catalysts and surfactants, can be assembled at the interface of emulsion droplets.⁶ This emulsion catalysis system shows remarkably high activities in the selective oxidation of alcohols to ketones, using H₂O₂ as oxidant. The emulsion reaction medium is favorable for the improvement of the mass-diffusion limitation in liquid multiphase systems caused by reactants being located in the different phases. The challenge to develop a more general and highly active emulsion catalytic system in water is to design and synthesize the amphiphilic catalysts, which can be readily assembled at the interface of the emulsion (O/W or W/O) droplets.

Herein, we present a novel amphiphilic copolymer-based iridium catalyst for transfer hydrogenation of aldehydes. Beyond simple catalyst immobilisation on a polymer, these copolymer-based catalysts, at a microscopic level, are assembled at the interface of emulsion droplets and consequently act as microreactors, exhibiting a remarkable rate acceleration for the reduction of aldehydes in water.

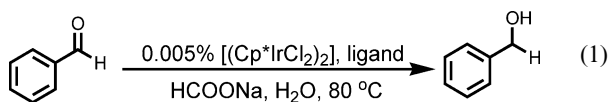
A TsEN-derived (TsEN = *N*-(*p*-toluenesulfonyl)-ethylenediamine) polymeric ligand **1** was synthesized according to the literature (Scheme 1).⁷ An amphiphilic polymer-based ligand PTsEN was synthesized by radical polymerization of monomers **1** and **2**. This amphiphilic ligand PTsEN with a hydrophobic backbone of polystyrene and strongly hydrophilic ammonium units could simultaneously provide a suitable microenvironment for hydrophobic substrates and HCOO⁻. To investigate the efficiency of ligand PTsEN, the iridium-catalyzed transfer hydrogenation of benzaldehyde in water was chosen as a model reaction [eqn (1)].² The catalyst was generated *in situ* by a reaction of the ligand PTsEN (1.2 mM)⁸ with precursor complex [(Cp*IrCl₂)₂] (Cp* = C₅Me₅) in water at 80 °C for 1 h, and the solution of resultant catalyst Ir-PTsEN remained pellucid. A stable emulsion can be formed upon the addition of benzaldehyde (2.7 M) to the above solution with stirring or ultrasonication (see ESI).†



Scheme 1 Structures of monomers, ligands and catalysts.

State Key Laboratory of Catalysis, Dalian Institute of Chemical Physics, Chinese Academy of Sciences, 457 Zhongshan Road, Dalian, 116023, China. E-mail: canli@dicp.ac.cn; Web: <http://www.canli.dicp.ac.cn/>; Fax: 86-411-84694447; Tel: 86-411-84379070

† Electronic supplementary information (ESI) available: Full experimental details and some characterizations. See DOI: 10.1039/b803209b



As shown in Fig. 1, the catalyst Ir-PTsEN shows a considerably high activity for the reduction of benzaldehyde, and a quantitative conversion is achieved at substrate/Ir (S/Ir) ratio of $1 \times 10^4 : 1$ in only 6 min using 2.5 equiv HCOONa (6.7 M) as the reductant. Most of the previous studies show that excess HCOO^- is indispensable to drive the reaction to completion in biphasic system.⁹ However, the current emulsion system gives a 93% conversion in 10 min even with a stoichiometric amount of HCOONa (2.7 M), while the parent catalyst Ir-TsEN only gives an 8% conversion under identical conditions.¹⁰ These results suggest that the significant rate acceleration is most likely due to the formation of emulsions resulting from the unique structure of the ligand PTsEN.

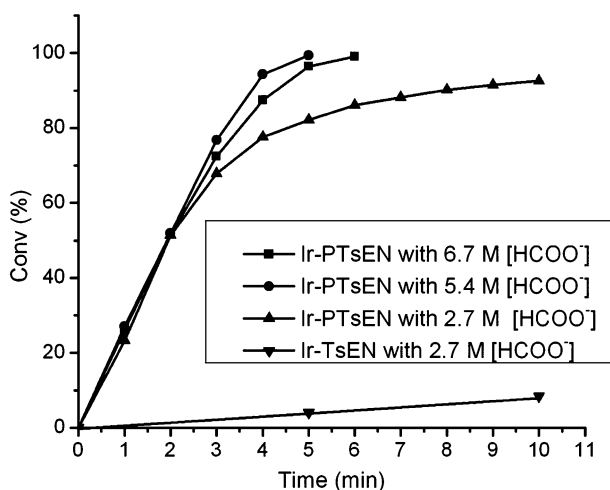


Fig. 1 Reduction of benzaldehyde (2.7 M) at different $[\text{HCOO}^-]$ in water (15 mL) using Ir-PTsEN and Ir-TsEN catalysts at 80 °C. The concentration of ligand PTsEN is 1.2 mM and S/Ir is 1.0×10^4 .

Interestingly, the initial rate of Ir-PTsEN in the emulsions is almost constant at the different $[\text{HCOO}^-]$. For instance, about 25% conversion is achieved in 1 min for Ir-PTsEN with $[\text{HCOO}^-]$ varying from 2.7 M to 6.7 M. Correspondingly, the initial rate is up to $1.5 \times 10^5 \text{ h}^{-1}$, which is found to be 30 times higher than that of Ir-TsEN (4800 h^{-1}) with a stoichiometric amount of HCOONa. These results suggest that the presence of the ammonium salt and its neighbouring effect on active sites can efficiently entrap HCOO^- , and enhance the local concentration of HCOO^- . This is one of the important factors for the acceleration of reaction. The initial rate independence on $[\text{HCOO}^-]$ suggests that the activation of HCOO^- to generate hydride is not the rate-determining step for the transfer hydrogenation reaction in the emulsion system.

Light microscopic observations confirm the formation of the emulsion droplets (Fig. 2a). The emulsion droplets are spherical particles with a narrow size distribution, and the multilayers of emulsion droplets with an average size below $1 \mu\text{m}$ are also observed. Fortunately, Ir-PTsEN exhibits a fluorescence emission in the range of 400–600 nm in the emulsion system, which allows us to observe the location of Ir-PTsEN in the

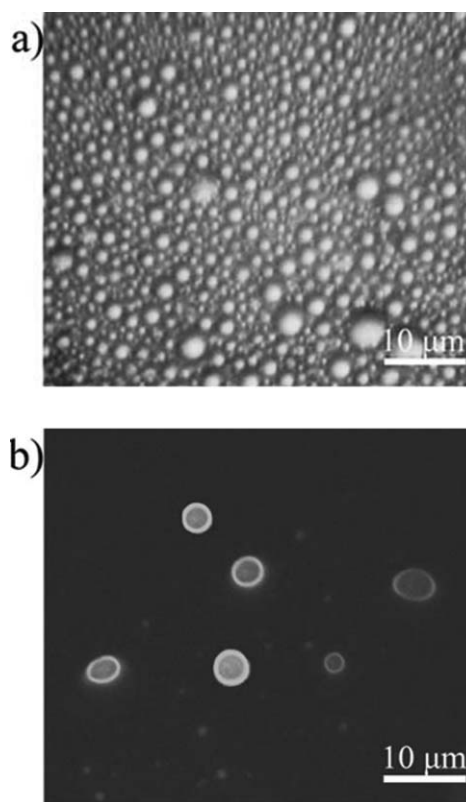


Fig. 2 Microscope images of emulsion system formed with Ir-PTsEN, benzaldehyde (2.7 M) and water (15 mL). The concentration of ligand PTsEN is 1.2 mM. (a) Optical micrograph. (b) Fluorescence micrograph ($\lambda_{\text{exc}} = 340 \text{ nm}$). Scale bar = $10 \mu\text{m}$.

emulsion droplets by fluorescence microscopy. As shown in Fig. 2b, bright blue circular-shaped fluorescent domains, emitted from Ir-PTsEN, are clearly observed, indicating that the catalyst Ir-PTsEN is mainly distributed at the interface of emulsion droplets.

Fig. 3 shows the dependence of reaction rate on the concentration of PTsEN. The initial rate shows an increased trend as

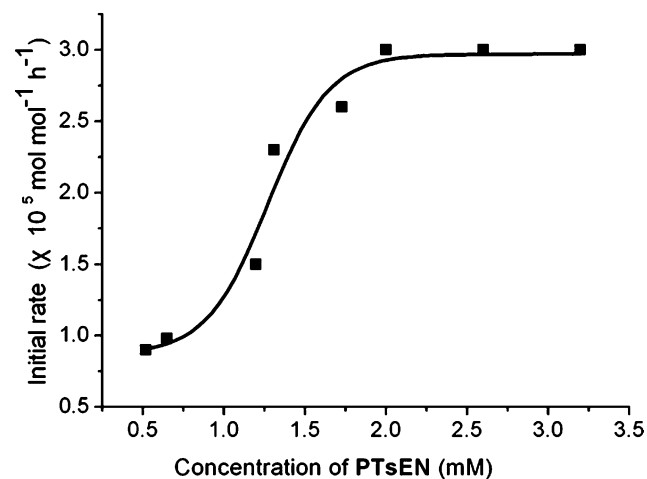


Fig. 3 Initial rate vs. the concentration of ligand PTsEN in the reduction of benzaldehyde (2.7 M) in water (15 mL) using Ir-PTsEN catalyst and HCOONa (2 equiv.) at 80 °C. The initial rate is based on the conversion after 1 min at S/Ir 1.0×10^4 .

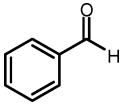
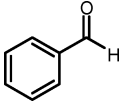
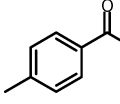
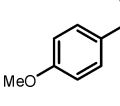
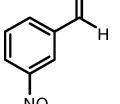
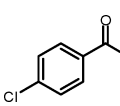
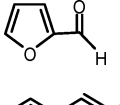
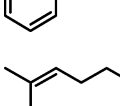
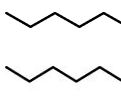
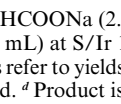
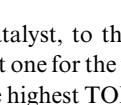
the concentration of ligand PTsEN is increased. A plateau of reaction rate appears when the concentration of PTsEN exceeds 2.0 mM. An analogue is observed for bimolecular reactions in micellar catalysis.¹¹ The phase separation is observed at 0.5 mM PTsEN, indicating that part of benzaldehyde is not trapped into the emulsions, where the initial rate is 9000 h⁻¹. However, the mixture of reaction gradually becomes stable with the enhancement of the concentration of PTsEN. Concomitantly, the initial rate increases from 9000 h⁻¹ to 300 000 h⁻¹. The average sizes of these emulsion droplets formed at 0.5, 1.2 and 2.0 mM ligand PTsEN were proved to be 476, 189 and 123 nm in diameter, respectively, by dynamic light scattering. The change of the reaction rate with the concentration of ligand PTsEN maybe attributed to the different solubilization effect in the emulsion droplets. More ligand favors the formation of the more emulsion droplets with smaller size, which can efficiently disperse the substrate in the emulsion droplets.

In order to demonstrate the possibility for a general application of this emulsion catalysis system, a wide range of aldehyde substrates were tested with Ir-PTsEN, and the results are summarized in Table 1. To our delight, Ir-PTsEN shows a much higher activity compared with the parent catalyst Ir-TsEN for most aromatic aldehydes.² Particularly, the catalyst Ir-PTsEN shows a superior catalytic activity for the selective reduction of long chain α,β -unsaturated aldehydes, more lipophilic substrates, possibly due to the product, long chain alcohol, as a co-surfactant.¹² The quantitative α,β -unsaturated alcohol is obtained at S/Ir 1000 : 1 in 5 min for the reduction of *trans*-2-nonenal, and the initial reaction rate is 16 600 h⁻¹ (entry 10). Though the aldol by-product of nonanal can inhibit the catalytic activity,² a 53% conversion is obtained in 15 min (entry 11). An exception is observed for the reduction of furfural, giving a low conversion because furfural is soluble in water and the O/W emulsion droplets are difficult to form with furfural as the interior oil phase (entry 7).

An attractive feature of the present emulsion catalytic system lies in the easy separation of product by an extraction due to the low solubility of Ir-PTsEN in diethyl ether. After three extractions, the isolated yield of benzaldehyde is up to 94% and ICP analysis of the solution phase shows that less than 0.9% of iridium leaches into the ether phase. Water-soluble catalysts in aqueous biphasic system, though exhibiting low efficiency, can be easily reused.¹³ So, attempts have been made to recycle the catalyst Ir-PTsEN with benzaldehyde. The catalyst shows an excellent activity in the first cycle, and the activity drops dramatically thereafter (see ESI).[†] In the second cycle, 67% activity is retained compared with the first cycle. An observation might partly account for the loss of activity as well as the possible deactivation of catalyst during the recycling procedure. In the mixture of benzaldehyde and Et₂O (v/v 4 : 1), the catalyst Ir-PTsEN only exhibits about 40% activity at room temperature, and 85% activity even at 80 °C in aqueous solution compared with that in the absence of diethyl ether. These results indicate that the residual diethyl ether in the emulsions possibly affects the assembling behavior of polymer-based catalysts, resulting in negative effects for the reduction of substrates.

In summary, we have demonstrated that a novel O/W emulsion catalytic system is formed by the assembly of amphiphilic polymer-based catalyst Ir-PTsEN at the water–oil interphase.

Table 1 Transfer hydrogenation of aldehydes with Ir-PTsEN catalyst in emulsion system.^a

Entry	Substrates	S/Ir	Time/min	Conv (%) ^b
1		10 000	6	99 (94)
2		10 000	60 ^c	58
3		10 000	8	99 (95)
4		10 000	9	99 (96)
5		10 000	10	99 (94)
6		10 000	21	99 (96)
7		10 000	13	20
8		1000	60 ^d	99 (95)
9		1000	15 ^d	>99 (96)
10		1000	5 ^d	99 (96)
11		1000	15	53

^a 80 °C, HCOONa (2.0 equiv.) in water (15 mL) at S/Ir 1 × 10⁴ : 1 or in water (5 mL) at S/Ir 1000 : 1. ^b Determined by GC and numbers in the brackets refer to yields of isolated products. ^c With Ir-TsEN, no emulsion is formed. ^d Product is the corresponding α,β -unsaturated alcohol.

This catalyst, to the best of our knowledge, is likely the most efficient one for the transfer hydrogenation of aldehydes in water, and the highest TOF is up to 3.0 × 10⁵ h⁻¹. The excellent performance can be ascribed to the assembly of catalyst at the interface of emulsions, resulting in a large reaction area. Furthermore, the cooperative effects of both the hydrophobic and hydrophilic parts of the catalyst ensure the high concentrations of reactants, both organic substrates and HCOO⁻, around active sites. This study demonstrates that emulsion catalysis provides a promising and general strategy to develop organic synthesis in water.

This work was supported by the National Natural Science Foundation of China (No. 20621063 and 20423004), the

Program for Strategic Scientific Alliances between China and Netherlands (No. 2004CB720607 and 20520130214).

Notes and references

- (a) F. Joo, *Acc. Chem. Res.*, 2002, **35**, 738–745; (b) T. Dwars and G. Oehme, *Adv. Synth. Catal.*, 2002, **344**, 239–260; (c) B. Chen, U. Dingerdissen, J. G. E. Krauter, H. G. J. L. Rotgerink, K. Mobus, D. J. Ostgard, P. Panster, T. H. Riermeier, S. Seebald, T. Tacke and H. Trauthwein, *Appl. Catal., A*, 2005, **280**, 17–46, and references therein; (d) M. Kidwai, V. Bansal, A. Saxena, R. Shankar and S. Mozumdar, *Tetrahedron Lett.*, 2006, **47**, 4161–4165, and references therein.
- X. F. Wu, J. K. Liu, X. H. Li, A. Zanotti-Gerosa, F. Hancock, D. Vinci, J. W. Ruan and J. L. Xiao, *Angew. Chem., Int. Ed.*, 2006, **45**, 6718–6722.
- T. Dwars, E. Paetzold and G. Oehme, *Angew. Chem., Int. Ed.*, 2005, **44**, 7174–7199.
- (a) F. Wang, H. Liu, L. F. Cun, J. Zhu, J. G. Deng and Y. Z. Jiang, *J. Org. Chem.*, 2005, **70**, 9424–9429; (b) T. Rispens and J. B. F. N. Engberts, *J. Org. Chem.*, 2002, **67**, 7369–7377.
- (a) M. S. Goedheijt, B. E. Hanson, J. N. H. Reek, P. C. J. Kamer and P. W. N. M. van Leeuwen, *J. Am. Chem. Soc.*, 2000, **122**, 1650–1657; (b) K. Manabe, Y. Mori, T. Wakabayashi, S. Nagayama and S. Kobayashi, *J. Am. Chem. Soc.*, 2000, **122**, 7202–7207; (c) Q. H. Fan, G. J. Deng, X. M. Chen, W. C. Xie, D. Z. Jiang, D. S. Liu and A. S. C. Chan, *J. Mol. Catal. A: Chem.*, 2000, **159**, 37–43; (d) D. M. Vriezema, M. C. Aragonés, J. A. A. W. Elemans, J. J. L. M. Cornelissen, A. E. Rowan and R. J. M. Nolte, *Chem. Rev.*, 2005, **105**, 1445–1489; and references therein; (e) S. Z. Luo, X. L. Mi, S. Liu, H. Xu and J. P. Cheng, *Chem. Commun.*, 2006, 3687–3689; (f) M. Bortenschlager, N. Schollhorn, A. Wittmann and R. Weberskirch, *Chem.–Eur. J.*, 2007, **13**, 520–528.
- J. B. Gao, Y. N. Zhang, G. Q. Jia, Z. X. Jiang, S. G. Wang, H. Y. Lu, B. Song and C. Li, *Chem. Commun.*, 2008, 332–334.
- K. Polborn and K. Severin, *Chem.–Eur. J.*, 2000, **6**, 4604–4611.
- The concentration of ligand PTsEN based on the amount of monomer **1**.
- X. G. Li, X. F. Wu, W. P. Chen, F. E. Hancock, F. King and J. L. Xiao, *Org. Lett.*, 2004, **6**, 3321–3324.
- The catalyst Ir-TsEN gives 9% conversion in the addition of monomer **2** and gives 27% conversion in the addition of CTAB (cetyltrimethylammonium bromide) under identical reaction conditions.
- J. E. Klijn and J. B. F. N. Engberts, *Org. Biomol. Chem.*, 2004, **2**, 1789–1799.
- K. Holmberg, *Eur. J. Org. Chem.*, 2007, 731–742.
- J. M. Gosselin, C. Mercier, G. Allmang and F. Grass, *Organometallics*, 1991, **10**, 2126–2133.

Hydrothermal conversion of carbohydrate biomass into formic acid at mild temperatures

Fangming Jin,^{*a} Jun Yun,^a Guangming Li,^a Ashushi Kishita,^b Kazuyuki Tohji^b and Heiji Enomoto^b

Received 6th February 2008, Accepted 9th April 2008

First published as an Advance Article on the web 21st April 2008

DOI: 10.1039/b802076k

The production of formic acid or formate salts by hydrothermal oxidation of glucose, a model compound of carbohydrate biomass, was investigated in the presence and absence of alkali using a batch reactor with H₂O₂ oxidant. Results showed that glucose was converted into formate salts with an excellent yield of 75% at a mild temperature of 250 °C in the presence of alkali. The results should be helpful to facilitate studies for developing a new green process for the conversion of carbohydrate biomass into formic acid, which can be a potential intermediate for fuels, as well as other value-added products.

Although biomasses have been used as fuels and resources, there is still increasing interest in converting them into more convenient and valuable fuels and other value-added products. The remarkable properties of high temperature water has proven their ability to convert a wide range of biomass materials into fuels and other value-added products.^{1,2} Also, it is an environmentally benign solvent that is preferable to less desirable organic solvents or alternative reaction media. Although some researchers have demonstrated hydrothermal conversion of carbohydrate biomass into value-added products, few studies have shown targeted high yields for conversion of carbohydrate biomass into commodity chemicals such as formic acid.

As described in our previous study,^{3,4} formic acid is a basic reaction product in the hydrothermal oxidation of carbohydrates. According to the proposed oxidation mechanism,³ it can be expected that 1 mol of glucose produces 6 moles of formic acid, as shown in eqn (1).



Formic acid is an important organic chemical. For example, calcium formate has been used as a leather tanning agent, as a concrete cure accelerator, and also in the animal feed industry. Formic acid in its Na/Ca form has been proposed as an environmentally-friendly road de-icer.^{5,6} Moreover, formic acid might be expected to be used as a raw material for hydrogen production, because formic acid is easily dissolved in water, particularly in high temperature water, where the decarboxylation pathway strongly predominates.^{7,8} More importantly, recent research has demonstrated that formic acid has the potential to

power fuel cells for electricity generation and automobiles.^{9–11} Thus, if carbohydrate biomass could be converted readily into formic acid efficiently at mild temperatures, this should provide the basis for new green processes.

In this study, experiments for the production of formic acid by hydrothermal oxidation of glucose, a model compound of carbohydrate biomass, were carried out to investigate the optimum conditions to obtain high yields of formic acid.

Reagent-grade glucose (>99%) was used as a test material. H₂O₂ (30% water solution, special class) was used as an oxidant for experimental convenience in respect to simplified handling (in an industry practice air or oxygen will be used). All chemicals and H₂O₂ were purchased from Wako Pure Chemicals. The stoichiometric demand for complete oxidation of glucose to formic acid and water was defined as 100% H₂O₂ supply according to eqn (2), assuming 1 mol of H₂O₂ gives 1/2 mol of O₂.



The present experiments were performed using a batch reactor consisting of SUS 316 tubing. Experimental procedures and techniques have been described in detail elsewhere.^{3,4} Briefly, 0.07 g of glucose and 1.7 cm³ of H₂O₂–water mixture were introduced into the reactor to occupy 30% of the total reactor volume. Then, the reactor was immersed in a salt bath preheated to the desired temperature for reaction. The reactor was shaken during the reaction in order to mix the contents. After the desired reaction time (defined as the elapsed time for which the reactor was kept in the salt bath), the reactor was removed from the salt bath and immersed into a cold water bath. After the reaction, liquid samples were collected for GC/MS and HPLC analyses. In cases where alkali was added, after filtration, the pH of the solution was adjusted to 3 with HCl for analysis. GC/MS analyses were performed with a HP 5890 Series II GC equipped with a HP-INNOWAX capillary column (30 m × 0.25 mm ID, 0.25 μm film thickness) and 5898 B mass spectrometer. HPLC analyses were performed on an RSpak KC-811 (SHODEX) column with a UV detector (210 nm). Quantitative estimation of formic acid was based on average values obtained from the HPLC analysis of three samples.

First, the effect of the reaction temperature and time on the yield of formic acid from the oxidation of glucose was investigated using an excess amount of H₂O₂ than the stoichiometric requirement. The excess amount of H₂O₂ is necessary to prevent the dehydration of glucose, which yields intermediate products such as 5-hydroxymethyl-2-furaldehyde that easily produces acetic acid through oxidation.³ Fig. 1 shows the variation in

^aState Key Laboratory of Pollution Control and Resources Reuse, College of Environmental Science and Engineering, Tongji University, Shanghai, 200092, China. E-mail: fmjin@mail.tongji.edu.cn

^bGraduate School of Environmental Studies, Tohoku University, Sendai, 980-8579, Japan

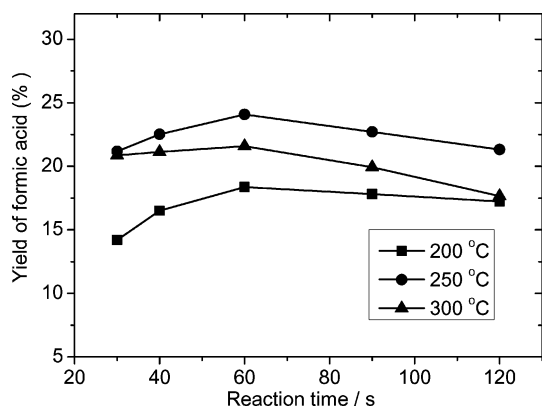


Fig. 1 Variation in yields of formic acid with reaction time at 200 °C, 250 °C and 300 °C in the oxidation of glucose (240% H₂O₂ supply).

the yield of formic acid with reaction time at 200 °C, 250 °C and 300 °C. The formic acid yield is defined as the percentage of formic acid to initial glucose on the carbon basis. At all temperatures, the formic acid yield initially increased up until 60 s and then decreased for any further increase in reaction time. The formic acid yield at 250 °C was higher than the yields at 200 °C and 300 °C throughout the reaction time. Consequently, the highest formic acid yield of 24% occurred at a reaction temperature and time of 250 °C and 60 s, respectively. These results show that a considerable yield of formic acid can be obtained by hydrothermal oxidation of glucose.

Subsequently, the effect of H₂O₂ supply on formic acid production was examined at 250 °C. As shown in Fig. 2, there was no significant effect on the yield of formic acid for the H₂O₂ supply in the range from 200 to 280%. However, the yield at 240% H₂O₂ was slightly higher than the yields at either 200 or 280%, except for the reaction time of 30 s. With 280% H₂O₂, a decrease in the yield of formic acid was observed for a reaction time of 90 s. When the H₂O₂ supply was lower than 200%, the yield of formic acid decreased with the decrease of H₂O₂ supply and other products became more dominant. The yield of formic acid was less than 1% for the H₂O₂ free case.

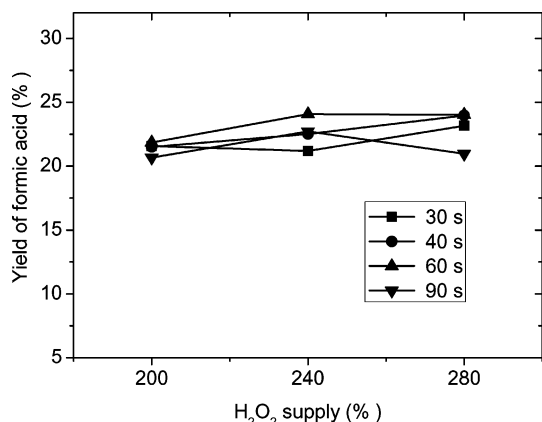


Fig. 2 Effect of H₂O₂ supply on yields of formic acid in the oxidation of glucose at 250 °C.

Based on the oxidation mechanism of glucose,³ formic acid yield very much higher than 24% is expected. Low yield was

probably due to either further decomposition of the formed formic acid through oxidation or by decarboxylation and/or dehydration. However, the possibility of decarboxylation and dehydration of formic acid was eliminated by analysing gas samples, which showed that most of the gaseous product was carbon dioxide with a small amount of CO, and no hydrogen was detected. Hydrogen gas is not so highly active under hydrothermal conditions and if formed it should remain in the system.

As shown in Fig. 3, results of decomposition experiments of formic acid indicate that formic acid is very stable in the absence of H₂O₂, and that the decomposition of formic acid increased with increasing H₂O₂. When the H₂O₂ supply was increased to 240%, about 60% of formic acid decomposed. When H₂O₂ was added, the gas composition was almost the same as that after the oxidation of glucose; that is, the predominant gaseous product was carbon dioxide, and no hydrogen was detected. These results further indicate that the oxidative decomposition of formic acid limited the yield to about 24%. Thus, preventing the oxidative decomposition is very important in order to improve the formic acid yield.

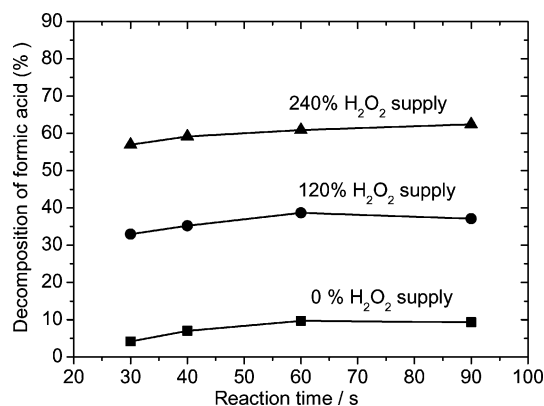


Fig. 3 Effect of H₂O₂ supply on the decomposition of formic acid (temp.: 250 °C).

The addition of an alkali may be an effective way to prevent oxidative decomposition of formic acid. Though many reports claim that alkali can accelerate the decomposition of organic compounds,^{12–16} our previous studies, as well as some other studies, have demonstrated that alkali can prevent organic compounds from being oxidized.^{17–20} As expected (see Fig. 4), an increase of NaOH above 0.1 M in concentration led to a significant decrease in the decomposition of formic acid even when there was an excess H₂O₂ supply. These results suggested that a higher yield of formic acid could be realized if the oxidative decomposition of formic acid is inhibited by adding an alkali.

Fig. 5 shows the influence of alkali on the yield of formic acid in the oxidation of glucose. Note that in the above case the real product is formate, rather than formic acid. But, for simplicity, we use the same terminology. From Fig. 5, it can be seen that an increase in alkali concentration beyond 0.2 M led to a significant increase in yield of formic acid. When the alkali concentration increased to 1.25 M, the formic acid yield increased to about 70 and 75% for NaOH and KOH, respectively.

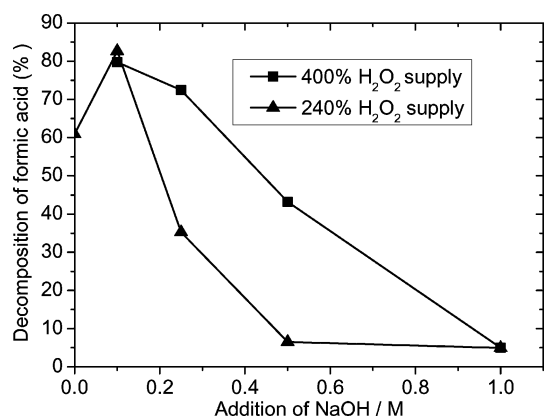


Fig. 4 Effect of NaOH on the decomposition of formic acid. (temp.: 250 °C; reaction time: 60 s).

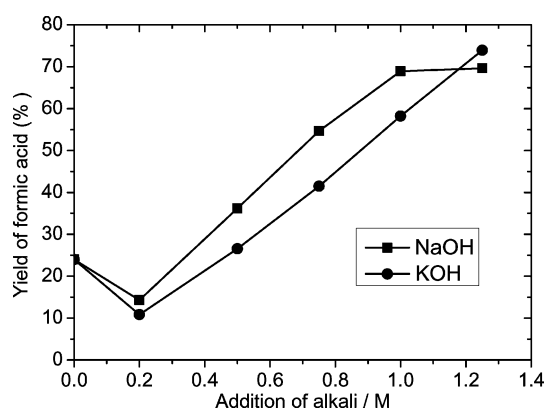


Fig. 5 Effect of NaOH and KOH concentration on the yield of formic acid (temp.: 250 °C; reaction time: 60 s; H₂O₂ supply 240%).

We examined the purity of formic acid for the highest yield sample and found it to be as high as 95%. The purity of formic acid is defined as the percentage of carbon in a liquid sample of formic acid against the TOC of the liquid sample after the reaction. As indicated in Fig. 6, in addition to formic acid, only a few low molecular weight carboxylic acids, such as lactic acid and acetic acid, were identified. Quantitative analyses for lactic and acetic acids showed that their concentrations were only about 100 ppm. Oxidation pathways for formic acid formation

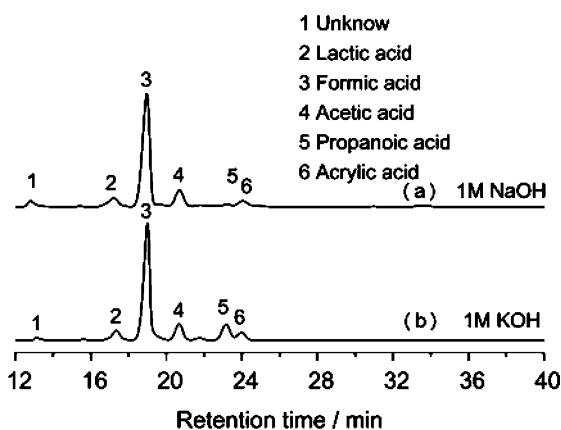


Fig. 6 HPLC chromatograms for samples after hydrothermal oxidation of glucose with the addition of NaOH and KOH (temp.: 250 °C; reaction time: 60 s; H₂O₂ supply 240%).

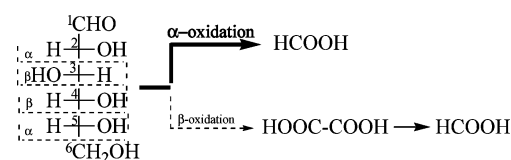
Table 1 Decomposition of oxalic acid^a

Run no.	Condition	Decomposition (%)
1.	0% H ₂ O ₂ supply	72.3
2.	240% H ₂ O ₂ supply	95.0
3.	0% H ₂ O ₂ supply, 0.2 M NaOH	0.0
4.	240% H ₂ O ₂ supply, 0.2 M NaOH	17.5

^a Reaction condition: 5000 ppm oxalic acid, temp. 250 °C, reaction time 40 s.

from glucose were investigated. As reported by Jin *et al.*, formic acid is probably formed in the oxidation of glucose by the rupture of C1–C2 or C5–C6 (α -scission) and/or the rupture of C2–C3 or C4–C5 (β -scission). The former directly yields formic acid, but the latter yields it *via* oxalic acid. Oxidation experiments were done for oxalic acid at 250 °C for 40 s with an H₂O₂ concentration of 240%, both with and without alkali. Results showed that no formic acid was detected when no NaOH was added. Furthermore, the yield of formic acid yield was only about 14% even in the case where alkali (0.20 M NaOH) was added. This result is clear evidence that if the rupture of C2–C3 or C4–C5 (β -scission) is predominant, the yield could not be as high as 75%.

On the other hand, in the analysis of the intermediates, oxalic acid was not identified irrespective of the presence or absence of alkali in the reaction medium. The absence of oxalic acid in the system due to its decomposition can be ruled out. As shown in Table 1, the decomposition rate of oxalic acid was low in the case where alkali was added, even under excess H₂O₂ concentration. Therefore, formic acid is probably formed mainly from the direct oxidation of glucose by α -scission, rather than *via* oxalic acid by β -scission, as shown in Scheme 1.



Scheme 1

In conclusion, the highest yield of formic acid through hydrothermal oxidation of glucose in the absence of alkali was about 24%. The reaction temperature, time and H₂O₂ concentrations were 250 °C, 60 s and 240%, respectively. However, when alkali was added at the above experimental conditions, the yield and purity of formic acid rose to about 75% and 95%, respectively. These results show that it is possible to develop a process for conversion of carbohydrate biomass into formic acid with high yields. Methods to separate formic acid from formate are still needed to fulfil the requirements of a green chemical process. Work along these line is now in progress.

References

- 1 N. Akiya and P. E. Savage, *Chem. Rev.*, 2002, **102**, 2725.
- 2 M. Watanabe, T. Sato, H. Inomata, R. L. Smith, K. Arai, A. Kruse and E. Dinjus, *Chem. Rev.*, 2004, **104**, 5803.
- 3 F. Jin, Z. Zhou, T. Moriya, H. Kishida, H. Higashijima and H. Enomoto, *Environ. Sci. Technol.*, 2005, **39**, 1893.

- 4 F. Jin, Z. Zhou, A. Kishita and H. Enomoto, *J. Mater. Sci.*, 2006, **41**, 1495.
- 5 D. A. Palmer, *Transport. Res. Rec.*, 1987, **1127**, 34.
- 6 S. S. Bang and D. Johnston, *Arch. Environ. Contam. Toxicol.*, 1998, **35**, 580.
- 7 N. Akiya and P. E. Savage, *AIChE J.*, 1998, **44**, 405.
- 8 J. Yu and P. E. Savage, *Ind. Eng. Chem. Res.*, 1998, **37**, 2.
- 9 C. Rice, S. Ha, R. I. Masel, P. Waszczuk, A. Wieckowski and T. Barnard, *J. Power Sources*, 2002, **111**, 83.
- 10 S. Uhm, S. T. Chung and J. Lee, *J. Power Sources*, 2008, **178**, 34.
- 11 M. Weber, J. T. Wang, S. Wasmus and R. F. Savinell, *J. Electrochem. Soc.*, 1996, **143**, 158.
- 12 J. Tardio, S. Bhargava, J. Prasad and D. B. Akolekar, *Top. Catal.*, 2005, **33**, 193.
- 13 R. Keen and C. R. Baillod, *Water Res.*, 1985, **19**, 767.
- 14 C. J. Chang, S.-S. Li and C.-M. Ko, *J. Chem. Technol. Biotechnol.*, 1995, **64**, 245.
- 15 A. B. Thomsen, *Water Res.*, 1998, **32**, 136.
- 16 Y. Kojima, T. Fukuta, T. Yamada, M. S. Onyango, E. C. Bernardo, H. Matsuda and K. Yagishita, *Water Res.*, 2005, **39**, 29.
- 17 F. Jin, A. Kishita, T. Moriya, H. Enomoto and N. Sato, *Shigen to sozai (in Japanese)*, 2000, **116**, 265.
- 18 T. M. Mccollom and J. S. Seewald, *Geochim. Cosmochim. Acta*, 2003, **67**, 3625.
- 19 P. J. Oefner, A. H. Lanziner, G. Bonn and O. Bobleter, *Monatsh. Chem.*, 1992, **123**, 547.
- 20 L. Calvo and D. Vallejo, *Ind. Eng. Chem. Res.*, 2002, **41**, 6503.

Biocatalytic promiscuity: the first lipase-catalysed asymmetric aldol reaction

Chao Li, Xing-Wen Feng, Na Wang,* Yu-Jie Zhou and Xiao-Qi Yu*

Received 27th February 2008, Accepted 9th April 2008

First published as an Advance Article on the web 1st May 2008

DOI: 10.1039/b803406k

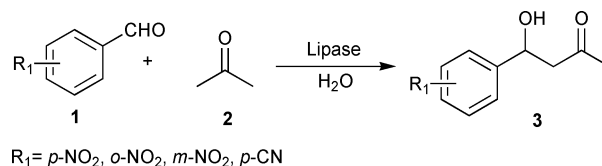
It was first observed that PPL, lipase from porcine pancreas, and several other lipases have a promiscuous ability to catalyse asymmetric aldol reactions between acetones and aldehydes in the presence of water.

Biocatalytic promiscuity, a new frontier extending the use of enzymes in organic synthesis, has attracted much attention and expanded rapidly in recent years.¹ It focuses on the enzyme catalytic activities with unnatural substrates and alternative chemical transformations, such as the side ability harbored by decarboxylase to catalyse acyloin condensation.² Exploiting enzyme catalytic promiscuity might lead to improvements in existing catalysts and provide novel synthesis pathways that are currently not available. Some elegant works have been done in the last decades.³

Among the promiscuous enzymes, hydrolases (such as lipase, protease and esterase) undoubtedly play an important role due to their high stability, wide sources and broad range of substrates.⁴ Recently, several promiscuous hydrolase-catalysed reactions have been reported.⁵ For instance, Wu *et al.* demonstrated that penicillin G acylase, a hydrolase which is widely used as a biocatalyst in the enzymatic synthesis of β -lactam antibiotics, can catalyse Markovnikov addition of allopurinol to vinyl ester.⁶ A further example is reported by the group of Gotor.⁷ They found an unprecedented lipase catalysed Michael addition of secondary amines to acrylonitrile. These cases and other relevant reports encouraged us to believe that the catalytic activities for addition reaction rather than the well-known hydrolytic function may also have a natural role in hydrolase evolution.

Aldol addition is one of the most useful methods for carbon-carbon bond formation in organic synthesis.⁸ Berglund and co-workers once used mutant CAL-B (lipase from *Candida antarctica*) to catalyse aldol addition in 2003.⁹ Although the Ser105Ala mutant CAL-B exhibited an increased reaction rate as compared with the wide type in their experiments, both of them showed quite low activities (reaction time more than 50 days). Besides, the enzymatic process is not enantioselective and only simple aliphatic aldehydes, such as propanal and hexanal, had been used. Generally, practical lipase-catalysed aldol reactions hadn't been developed in organic synthesis. To the best of our knowledge, other lipase-catalysed aldol additions, especially asymmetric aldol reactions have never been reported.

Herein, we surprisingly found that several lipases display observable activities and enantioselectivities for aldol addition in a "wet" reaction condition, where lipase always presents a hydrolytic function (Scheme 1). During our continued work on the new catalytic promiscuity, lipase from porcine pancreas (PPL, EC 3.1.1.3), which is triacylglycerol acylhydrolase and was already commercially available long before, showed a special promiscuous catalytic activity, such as considerable reaction activity and higher enantioselectivity. To clarify the enzymatic process, we performed some experiments to tentatively hypothesize the mechanism of this new biocatalytic promiscuity. Since this novel catalytic promiscuity is enantioselective and can especially tolerate a wide range of substrates, it not only could extend the enzymatic reaction specificity, but might be practically utilised in organic synthesis.



Scheme 1 Aldol reaction catalyzed by lipase in the presence of water.

In order to confirm the catalytic activity of the lipases, we performed some experiments to focus on the specific catalytic effect of enzymes. As shown in Table 1, several lipases had been screened in our experiments. In the case of PPL, the yield increased with time progress, up to 96.4% after 144 h (entries 2, 3, 4 and 5). Two lipases from *Mucor* (MJL and MML) also showed the ability to catalyse the asymmetric aldol reaction, while their catalytic activities were less efficient (entries 8 and 12). CAL-B showed very low but detectable activity in the same condition (entry 11). Other lipases (CRL, PCL, PSL) displayed no activity for aldol reaction in the reaction conditions (entries 10, 14 and 15). The control experiment was carried out in the absence of any biocatalyst (entry 1). No product had been detected, even after 72 h. When the reaction was incubated with denatured PPL, denatured MJL, denatured MML or bovine serum albumin (BSA), respectively, the reaction rate was nearly equal to the control reaction, suggesting that the specific structure of lipase was necessary to carry out the aldol addition (entries 7, 9, 13 and 16). Interestingly, when the water concentration was controlled to 1%, the degree of enantioselectivity rose up to 43.6% (entry 6). All the results suggest that the special spatial conformation of these lipases is responsible for the aldol reaction.

To improve the activity of the enzyme, we carried out some experiments focusing on the influence of water concentration,

Department of Chemistry, Key Laboratory of Green Chemistry and Technology (Ministry of Education), Sichuan University, Chengdu, 610064, People's Republic of China. E-mail: xqyu@tfol.com; Fax: + 86 28 85415886; Tel: +86 28 85460576

Table 1 The catalytic activities and stereoselectivities of the aldol reaction between 4-nitrobenzaldehyde and acetone^a

Entry	Catalyst	Reaction time/h	Yield (%)	E.e (%)
1	No enzyme	72	< 0.5	— ^b
2	PPL	24	25.6	17.7
3	PPL	48	32.2	18.5
4	PPL	72	55.7	15.8
5	PPL	144	96.4	14.7
6	PPL	72	11.7	43.6 ^c
7	Denatured PPL ^d	48	< 0.5	—
8	MJL	24	14.5	12.9
9	Denatured MJL ^d	48	< 0.5	—
10	CRL	24	< 0.5	—
11	CAL-B	24	2.3	9.4
12	MML	24	9.8	9.6
13	Denatured MML ^d	48	< 0.5	—
14	PCL	24	< 0.5	—
15	PSL	24	< 0.5	—
16	BSA	24	< 0.5	—

^a Reaction conditions: lipase 20 mg, 4-nitrobenzaldehyde 0.12 mmol, acetone 1 ml, deionized water 0.25 ml, 30 °C. ^b Not determined. ^c Reaction conditions: lipase 20 mg, 4-nitrobenzaldehyde 0.12 mmol, acetone 1 ml, deionized water 0.01 ml, 30 °C. ^d Pretreated with urea at 100 °C for 8 h.

which commonly exhibits special promotion for many addition reactions.¹⁰ The range of water concentration from 0% to 55% was screened for the lipase-catalysed aldol reaction and the results are shown in Fig. 1. The three hill-shaped curves show that water concentration can greatly influence the reaction rate. The parts of larger percentages are not shown here, as excessive water lead to a serious decrease of the solubility of aldehyde and could change the special conformation of the active site. The optimal water concentration for the PPL-catalysed aldol reaction was about 20%. The results suggest that the special spatial conformation corresponding to the catalytic site of PPL can be mediated by water. A wider range of substrates, such as butanone, cyclohexanone, 4-nitrobenzaldehyde, had been expanded in the wet reaction condition.

Some further experiments were performed to get more information about the catalytic mechanism. It was observed that the reaction rate could be changed by altering the order of the addition of the reactants in our experiments. Firstly, acetone was added into the mixture containing PPL and a proper amount of water, then the mixture was stirred for 12 h. Finally, aldehyde was added into the mixture to initiate the reaction. An observable increase of the initial reaction rate was observed as compared with the typical process (data not shown). Another important observation was that the lipase-catalysed aldol reaction seemed

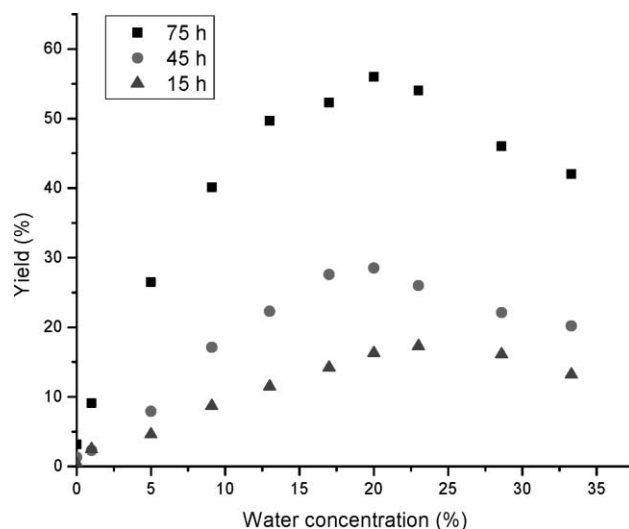
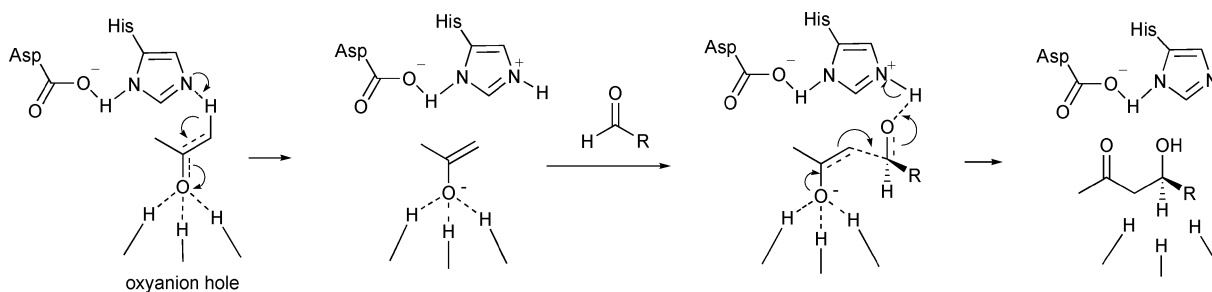


Fig. 1 The influence of water concentration on PPL-catalysed aldol reaction under conditions: lipase 20 mg, 4-nitrobenzaldehyde 0.12 mmol, acetone 1 ml, deionized water from 0% to 35% (water/[water + acetone], v/v), 30 °C.

to prefer acetone than any other ketone (such as butanone and cyclohexanone), as other ones lead to the decrease of the reaction rate. These cases indicate that acetone might at first be captured by the specific catalytic site to initiate this lipase-catalysed aldol reaction.[†]

A generally accepted catalytic mechanism for hydrolase is that the active site for hydrolysis also contributed to the promiscuous catalysis.¹¹ Combining that viewpoint with our observations described above, we hypothesized the mechanism of the lipase-catalysed aldol reaction and summarized them in Scheme 2. Firstly, the substrate acetone was stabilized by the Asp-His dyad and the oxyanion. Then, a proton was transferred from the acetone to the His residue and enolate ion was formed. Thirdly, another substrate aldehyde accepted the proton and simultaneously connected the acetone with the forming of a carbon-carbon bond. Finally, the aldol adduct was released from the oxyanion hole. This proposed catalytic process is similar with type II aldolase (belongs to lyase), but no metal ion exists.¹²

In conclusion, we described several lipase catalysed asymmetric aldol reactions. Lipase PPL can efficiently catalyse the aldol reaction and presents asymmetric catalytic activity, while another three lipases (MML, MJL, CAL-B) show lower catalytic activities. Interestingly, these lipase-catalysed addition reactions



Scheme 2 Proposed mechanism of lipase-catalysed aldol reaction.

can be greatly promoted by water, which is seldom mentioned in other lipase catalysed promiscuous reactions. The lipase-catalysed asymmetric aldol reaction provides a novel case of catalytic promiscuity and might be a potential synthetic method for organic chemistry.

Acknowledgements

Authors gratefully acknowledge the National Natural Science Foundation of China (Nos. 20702034, 20725206 and 20732004) for financial support.

Notes and references

† A typical enzymatic procedure of aldol reaction: the reaction was initiated by adding 200 mg PPL and 1.2 mmol (181.2 mg) aldehyde to a mixture of 5 ml anhydrous ketone and 1.25 ml water. The suspension was maintained at 30 °C and shaken at 200 rpm for 144 h (formation of products was detected by TLC). The residue was then filtered off and the solvent was evaporated. A single product was prepared by silica gel chromatography with an eluent consisting of petroleum/ethyl acetate (2 : 1, v/v).

- 1 U. T. Bornscheuer and R. J. Kazlauskas, *Angew. Chem., Int. Ed.*, 2004, **43**, 6032; R. J. Kazlauskas, *Curr. Opin. Chem. Biol.*, 2005, **9**, 195; P. Berglund and S. Park, *Curr. Org. Chem.*, 2005, **9**, 325.
- 2 O. P. Ward and A. Singh, *Curr. Opin. Biotechnol.*, 2000, **11**, 520.
- 3 D. M. Z. Schmidt, E. C. Mundorff, M. Dojka, E. Bermudez, J. E. Ness, S. Govindarajan, P. C. Babbitt, J. Minshull and J. A. Gerlt, *Biochemistry*, 2003, **42**, 8387; O. Khersonsky, C. Roodveldt and D. S. Tawfik, *Curr. Opin. Chem. Biol.*, 2006, **10**, 498.
- 4 K. Hult and P. Berglund, *Trends Biotechnol.*, 2007, **25**, 231.
- 5 M. Svedendahl, K. Hult and P. Berglund, *J. Am. Chem. Soc.*, 2005, **127**, 17988; W. B. Wu, J. M. Xu, Q. Wu, D. S. Lv and X. F. Lin, *Adv. Synth. Catal.*, 2006, **348**, 487; Y. Cai, S. P. Yao, Q. Wu and X. F. Lin, *Biotechnol. Lett.*, 2004, **26**, 525; J. M. Xu, F. Zhang, B. K. Liu, Q. Wu and X. F. Lin, *Chem. Commun.*, 2007, 2078.
- 6 W. B. Wu, N. Wang, J. M. Xu, Q. Wu and X. F. Lin, *Chem. Commun.*, 2005, 2348.
- 7 O. Torre, I. Alfonso and V. Gotor, *Chem. Commun.*, 2004, 1724.
- 8 T. D. Machajewski and C. H. Wong, *Angew. Chem., Int. Ed.*, 2000, **39**, 1352.
- 9 C. Branneby, P. Carlqvist, A. Magnusson, K. Hult, T. Brinck and P. Berglund, *J. Am. Chem. Soc.*, 2003, **125**, 874.
- 10 Y. Hayashi, *Angew. Chem., Int. Ed.*, 2007, **45**, 8103.
- 11 C. Branneby, P. Carlqvist, K. Hult, T. Brinck and P. Berglund, *J. Mol. Catal. B: Enzym.*, 2004, **31**, 123.
- 12 S. M. Dean, W. A. Greenberg and C. H. Wong, *Adv. Synth. Catal.*, 2007, **349**, 1308.

Liquid-phase synthesis of methyl formate *via* heterogeneous carbonylation of methanol over a soluble copper nanocluster catalyst†

Ling He, Haichao Liu, Chao-xian Xiao and Yuan Kou*

Received 17th March 2008, Accepted 29th April 2008

First published as an Advance Article on the web 8th May 2008

DOI: 10.1039/b804459g

Liquid-phase synthesis of methyl formate (MF) was achieved by green carbonylation of methanol with CO on a soluble copper nanocluster catalyst with high activities (*e.g.* 2.7–6.1 mol_{MF} mol_{Cu}⁻¹ h⁻¹) and 100% MF selectivities under mild reaction conditions (353–443 K, 0.3–3.0 MPa CO), showing that the Cu nanoclusters can potentially replace the caustic catalysts of alkaline metal alkoxides (*e.g.* CH₃ONa), required for the current carbonylation process in industry.

Many chemical processes in use today are not green, and frequently utilize corrosive liquid acids and bases, or hazardous solvents.¹ Some examples include alkylation of isobutane with C₃–C₅ alkenes (to form fuel alkylate) catalyzed by H₂SO₄ or HF, and carbonylation of methanol with CO (to form methyl formate) catalyzed by CH₃ONa. In accordance with the formalized principles of green chemistry,² numerous efforts have been made during the last decade to study green alternatives to these important processes, consequently reducing and eliminating use and generation of any non-green chemicals. In this work, we aim to develop a greener methanol carbonylation process for the synthesis of methyl formate (MF) in the absence of any base.

MF is a versatile chemical precursor to a wide range of other chemicals such as formic acid, acetic acid, acetaldehyde, methyl acetate, ethylene glycol and formamide.³ MF can be synthesized *via* carbonylation of methanol with CO,^{4–6} dehydrogenation of methanol,⁷ or oxidation of methanol.^{8,9} Among these routes to MF, the carbonylation of methanol is more advantageous in terms of energy-efficiency and atom-economy, which is currently performed homogeneously using alkaline metal alkoxide catalysts, *e.g.* CH₃ONa, with high CO conversions (*e.g.* 95%) and MF selectivities (*e.g.* 99%). However, the use of strong bases in this effective industrial process is clearly not green and leads to inevitable problems such as corrosion and waste byproducts and, in particular, deactivation by CO₂ and H₂O impurities. Therefore, there is an urgent need to develop environmentally benign processes without using any base.

Soluble metal nanocluster catalysts have aroused increasing interest in recent years. The major reason is that in contrast with the traditional supported metal clusters generally restricted on support surfaces, the soluble metal

nanoclusters with controllable sizes and morphologies are freely rotational and three-dimensional in reaction systems, leading to their superior catalytic performances.^{10–15} Examples of these catalysts include rhodium nanoclusters for hydrogenation of arenes,¹¹ platinum nanoclusters for selective hydrogenation of *o*-chloronitrobenzene¹² and aerobic oxidation of alcohols,^{13,14} and ruthenium nanoclusters for low-temperature, aqueous-phase F–T synthesis.¹⁵ Here, we report the discovery of heterogeneous liquid-phase carbonylation of methanol to synthesize MF on a soluble copper nanocluster catalyst; this catalyst in methanol behaves like homogeneous catalysts, but with ease of operation, separation and scale-up as a result of its heterogeneous nature.

Soluble nanocluster catalysts of Cu, Ru, Pt, Pd, Rh, Ir and Au with similar mean diameters (*ca.* 2–3 nm, see TEM results of Fig. 1 and S1 in ESI†) were examined for the carbonylation of methanol with CO. As shown in Table 1, all of these metal nanoclusters catalyzed the carbonylation of methanol with CO to exclusively form MF. A CO conversion as high as 32.7% was achieved on Cu at 373 K and 1.0 MPa CO in 2 h, corresponding to an activity of 2.7 mol_{MF} mol_{Cu}⁻¹ h⁻¹ (Table 1, entry 1). The activity decreased to 1.3, 0.8 and 0.7 mol_{MF} mol_{metal}⁻¹ h⁻¹ on Ru, Pt and Rh, respectively. In contrast to these metals, Ir, Au and Pd were not active and gave negligible activities (~0.1 mol_{MF} mol_{metal}⁻¹ h⁻¹, see Table 1, entries 2–7). For

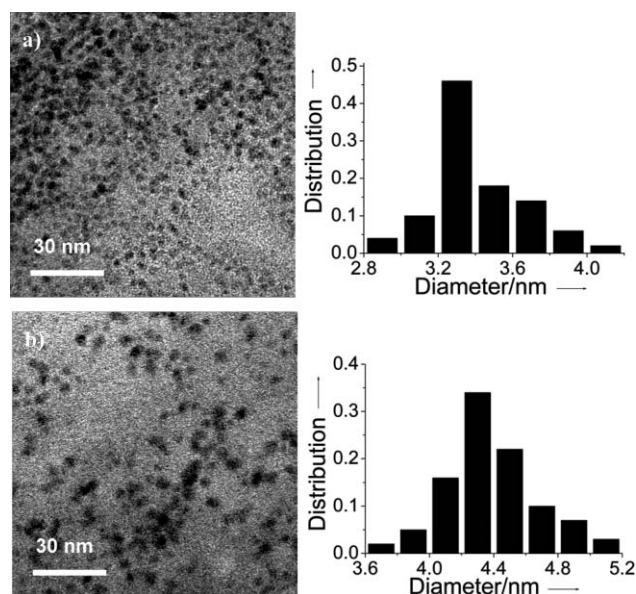


Fig. 1 TEM images and histograms of particle size distribution of polymer-stabilized copper nanoclusters (a) before and (b) after carbonylation of methanol at 373 K and 1.0 MPa CO for 48 h.

PKU Green Chemistry Center, Beijing National Laboratory for Molecular Sciences, College of Chemistry and Molecular Engineering, Peking University, Beijing, 100871, China.
E-mail: yuankou@pku.edu.cn; Fax: +86-10-62751708;
Tel: +86-10-62757792

† Electronic supplementary information (ESI) available: TEM images of polymer-stabilized metal nanoclusters. See DOI: 10.1039/b804459g

Table 1 Catalytic performance of different soluble metal nanocluster catalysts in the carbonylation of methanol^a

Entry	Catalyst	CO conversion (%)	Activity/mol _{MF} mol _{metal} ⁻¹ h ⁻¹	MF Selectivity (%)
1	Cu	32.7	2.7	100
2	Ru	15.2	1.3	100
3	Pt	10.2	0.8	100
4	Rh	8.2	0.7	100
5	Ir	1.6	0.1	100
6	Au	1.3	0.1	100
7	Pd	1.1	0.1	100
8 ^b	Cu	0	0	—
9 ^c	Non	0	0	—

^a Reaction conditions: 2 h reaction time, 373 K, 1.0 MPa CO, 1.0 mmol metal, 1/10 metal to polymer molar ratio, 20.0 mL methanol. ^b In the absence of CO. ^c In the absence of any metal nanocluster catalyst.

comparison, blank experiments were also performed under the same conditions. It was noted that there were no detectable methanol reactions in the absence of CO or in the absence of the nanocluster catalysts (Table 1, entries 8 and 9). Taken together, these results clearly show that the soluble Cu nanoclusters are efficient and highly selective for catalyzing the carbonylation of methanol with CO to form MF.

Such exclusive formation of MF can be realized under a wide range of reaction conditions. As shown in Table 2, increasing the amount of the Cu nanoclusters in methanol from 0.1 to 1.0 mmol led to a gradual increase in the CO conversions from 20.5 to 32.7% (Table 2, entries 1–3, and Table 1, entry 1), showing that higher Cu concentrations favour methanol carbonylation to MF. However, the activities conversely decreased from 16.8 to 2.7 mol_{MF} mol_{Cu}⁻¹ h⁻¹. TEM characterization showed that the size of the Cu nanoclusters, independent of their concentration in this range examined, is essentially the same. Thus, the decrease in the activities with increasing Cu concentrations is not due to the decrease in the number of the Cu sites accessible to the reactants, but maybe due to the limited CO concentrations, *i.e.* the solubility of CO, in largely excess methanol under the given conditions. Such a proposition is confirmed by the effects of CO pressure and reaction temperature. The activities increased from 1.0 to 6.1 mol_{MF} mol_{Cu}⁻¹ h⁻¹ with increasing the CO pressure in the range of 0.3–3.0 MPa (Table 1, entry 1, and

Table 2, entries 4–6), indicating nearly a first-order dependence on the CO pressure. For the temperature effects, it was found that the carbonylation of methanol occurred even at a low temperature of 353 K (Table 2, entry 7), where the activity was 2.0 mol_{MF} mol_{Cu}⁻¹ h⁻¹ (*i.e.* a 27.2% CO conversion). This activity increased to 2.7 mol_{MF} mol_{Cu}⁻¹ h⁻¹ as the temperature increased to 373 K, and then more gradually to 2.8, 2.9 and 3.2 mol_{MF} mol_{Cu}⁻¹ h⁻¹ at 403, 423 and 443 K, respectively (Table 2, entries 8–10). Such behavior appears to reflect the general temperature effects on both the reaction rate and the CO solubility in methanol. Clearly, these preliminary results offer directions to optimize the reaction conditions and catalytic activities.

In order to examine the stability of the Cu nanocluster catalyst, the carbonylation of methanol was performed at 373 K for 48 h in a semi-batch mode, which was conducted by repeatedly pressurizing the reactor with CO back to 1.0 MPa every two hours. As shown in Fig. 2, the activities decreased gradually from 2.7 mol_{MF} mol_{Cu}⁻¹ h⁻¹ (32.7% CO conversion) after the first 2 h to 1.8 mol_{MF} mol_{Cu}⁻¹ h⁻¹ (21.2% CO conversion) at 16 h, and then remained constant in the next 32 h, demonstrating a relatively good stability of the catalyst. No leaching of Cu into the solution was detected by ICP. TEM characterization results showed the growth of Cu nanoclusters (from 3.3 nm to 4.3 nm) for the used catalyst (Fig. 1b), which

Table 2 Catalytic performance of soluble Cu nanocluster catalysts in the carbonylation of methanol under different reaction conditions^a

Entry	Cu/mmol	Catalyst T/K	CO pressure/MPa	CO conversion (%)	Activity/mol _{MF} mol _{Cu} ⁻¹ h ⁻¹	MF Selectivity (%)
1	0.1	373	1.0	20.5	16.8	100
2	0.2	373	1.0	24.9	10.2	100
3	0.5	373	1.0	29.1	4.8	100
4	1.0	373	0.3	33.9	1.0	100
5	1.0	373	2.0	28.7	4.7	100
6	1.0	373	3.0	24.6	6.1	100
7	1.0	353	1.0	27.2	2.0	100
8	1.0	403	1.0	34.1	2.8	100
9	1.0	423	1.0	35.4	2.9	100
10	1.0	443	1.0	38.1	3.2	100
11 ^b	1.0	373	0.9	30.4	2.5	100
12 ^c	1.0	373	1.0	31.6	2.6	97.9
13 ^d	1.0	373	1.0	21.2	1.7	93.2

^a Reaction conditions: 2 h reaction time, 1/10 Cu to polymer molar ratio, 20.0 mL methanol. ^b With 0.1 MPa CO₂. ^c With 1 mol% H₂O. ^d With 10 mol% H₂O.

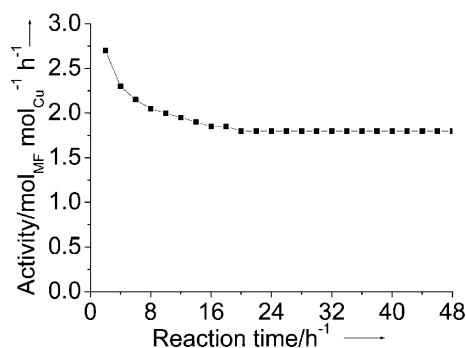


Fig. 2 Catalytic activities of Cu nanocluster catalysts as a function of reaction time at 373 K within 48 h (1.0 mmol Cu, 1.0 MPa CO).

thus likely correlates with the observed decline in the catalytic activities. Such correlation indicates that Cu nanoclusters with smaller sizes favour the carbonylation of methanol, as found prevalently with nanocluster catalysts in many other reactions. It also tempted us to improve the stability of the soluble Cu nanocluster catalyst, which was indeed realized, for example, by simply increasing the molar ratios of polymer stabilizer to Cu (e.g. from 10 to 20, 50 and 100), on the basis of our preliminary results.

As discussed above, the current industrial carbonylation process, because of the use of strong bases such as CH₃ONa, is extremely sensitive to minor contaminants of CO₂ and H₂O in the reactants. In direct comparison to this process, poisoning effects of CO₂ and H₂O were also examined in our reaction system. It was noted that CO₂ essentially did not affect the carbonylation of methanol on the soluble Cu nanoclusters in the presence of even as large as 0.1 MPa CO₂ (10 mol% of the total gas pressure; Table 2, entry 11). The effects of H₂O depend on its amounts present in the methanol solutions. No significant change in the activity and MF selectivity was observed at lower H₂O concentrations, e.g. 1 mol% in methanol, and notably the presence of 10 mol% H₂O still led to a reasonably high activity of 1.7 mol_{MF} mol_{Cu}⁻¹ h⁻¹ (vs. 2.7 mol_{MF} mol_{Cu}⁻¹ h⁻¹) with a 93.2% MF selectivity (Table 2, entries 12 and 13). The only byproduct in the presence of H₂O was CO₂, apparently formed from the known water–gas shift reaction. The negative H₂O effects on the activity may be caused by the competitive adsorption of H₂O and CH₃OH on the Cu sites, which appears to be dictated by the mechanism of the methanol carbonylation on the Cu catalyst. The mechanism is still not clear at this stage, but it may involve CH₃OH adsorption and its oxidative addition to Cu sites to form Cu–OCH₃ and Cu–H species, and CO adsorption and its insertion into the Cu–O bond (in Cu–OCH₃ species) to give a CH₃OC=O intermediate, followed by reductive elimination of this intermediate to form MF. These tentative mechanistic steps are being examined using spectroscopic, isotopic and transient techniques.

In conclusion, green synthesis of MF in liquid phase *via* heterogeneous carbonylation of methanol with CO has been efficiently achieved for the first time on a soluble Cu nanocluster catalyst under mild conditions. This new process exhibits high resistance to CO₂ and H₂O contaminants. Further advances in understanding this new process and in improving its MF productivity will potentially lead to a green substitute for the

current industrial process that requires strong liquid bases of alkaline metal alkoxides as catalysts.

Experimental

Cu nanoclusters were synthesized under N₂ (>99.9995%) by reduction of Cu(NO₃)₂·3H₂O with NaBH₄ in the presence of a polymer, poly[(*N*-vinyl-2-pyrrolidone)-co-(1-vinyl-3-alkylimidazolium halide)] (poly(NVP-*co*-VBIM⁺Cl⁻)), as the stabilizer that was prepared according to the reported method.¹¹ Briefly, a methanolic solution of NaBH₄ (10.0 mL, 2.0 mmol) was added dropwise into a methanolic solution of Cu(NO₃)₂·3H₂O (10.0 mL, 1.0 mmol) and the polymer stabilizer in a Schlenk-bottle with vigorous stirring for 10–30 min. The molar ratio of Cu to the polymer stabilizer was varied in the range of 1/100–1/10. The resulting solutions of Cu nanoclusters were a deep-red color, and were stored under nitrogen for use. In a similar way, other metal nanoclusters of Ru, Pt, Rh, Ir, Pd and Au were synthesized at a molar ratio of metal to the polymer stabilizer of 1/10. All solvents used here were anhydrous.

Transmission electron microscopy (TEM) images for metal nanoclusters were taken with a Hitachi H-9000 equipped with a NAR electron microscope. Samples were prepared in a glove box under nitrogen by placing a droplet of the dispersed methanol solution onto a carbon-coated Ni grid. The size distribution of the metal nanoclusters was determined by measuring about 200 random particles on the images.

Carbonylation of methanol was carried out in a batch mode. The as-synthesized solution of Cu nanoclusters (1.0 mmol of Cu in 20.0 mL of anhydrous methanol) and anhydrous cyclohexane (0.05 mL) as internal standard were added under N₂ into a stainless-steel autoclave. The autoclave was purged several times with CO (99.9%, purified with 5 Å molecular sieves), pressurized to the desired CO pressure (0.3–3.0 MPa) at room temperature, and then heated to the desired temperature (353–443 K) with vigorous stirring at a speed of *ca.* 1000 rpm. After the reaction, the composition of the liquid products was measured by a GC (Agilent 6820) equipped with a FID detector and a capillary column (Innowax, 30 m × 0.25 mm), while the composition of the gas phase in the autoclave was measured by a GC with a TCD detector and two packed columns of Porapak and molecular sieves.

Acknowledgements

This work was supported by the National Natural Science Foundation of China (20533010, 20573004, and 20473002).

Notes and references

- J. H. Clark, *Green Chem.*, 1999, **1**, 1.
- P. T. Anastas and M. M. Kirchhoff, *Acc. Chem. Res.*, 2002, **35**, 686.
- J. S. Lee, J. C. Kim and Y. G. Kim, *Appl. Catal.*, 1990, **57**, 1.
- E. Gérard, H. Götz, S. Pellegrini, Y. Castanet and A. Mortreux, *Appl. Catal., A*, 1998, **170**, 297.
- I. Y. Guzman-Jimenez, J. W. van Hal and K. H. Whitmire, *Organometallics*, 2003, **22**, 1914.
- S. J. Choi, J. S. Lee and Y. G. Kim, *J. Mol. Catal.*, 1993, **85**, L109.
- A. Y. Rozovskii, *Kinet. Catal.*, 2003, **3**, 360.
- W. Li, H. Liu and E. Iglesia, *J. Phys. Chem. B*, 2006, **110**, 23337.
- J. M. Tatibouët, *Appl. Catal., A*, 1997, **148**, 213.

-
- 10 D. Astruc, F. Lu and J. R. Aranzaes, *Angew. Chem., Int. Ed.*, 2005, **44**, 7852.
- 11 X. D. Mu, J. Q. Meng, Z. C. Li and Y. Kou, *J. Am. Chem. Soc.*, 2005, **127**, 9694.
- 12 C. X. Xiao, H. Z. Wang, X. D. Mu and Y. Kou, *J. Catal.*, 2007, **250**, 25.
- 13 T. Wang, C. X. Xiao, L. Yan, L. Xu, J. Luo, H. Shou, Y. Kou and H. C. Liu, *Chem. Commun.*, 2007, 4375.
- 14 H. Miyamura, R. Matsubara, Y. Miyazaki and S. Kobayashi, *Angew. Chem., Int. Ed.*, 2007, **46**, 4151.
- 15 C. X. Xiao, Z. P. Cai, T. Wang, Y. Kou and N. Yan, *Angew. Chem., Int. Ed.*, 2008, **47**, 746.

Effect of acid catalyst on structural transformation and hydrolysis of cellulose in hydrothermal conditions†

Shigeru Deguchi,^{*a} Kaoru Tsujii^b and Koki Horikoshi^a

Received 27th February 2008, Accepted 14th April 2008

First published as an Advance Article on the web 22nd April 2008

DOI: 10.1039/b803384f

The effect of H₂SO₄ on the crystalline-to-amorphous transformation and hydrolysis of cellulose in water at high temperatures and high pressures was revealed for the first time by using *in situ* high-resolution optical microscopy.

With annual production of approximately 1.5×10^{12} tons, cellulose is by far the most abundant renewable biomass.¹ Establishing efficient conversion of cellulose to its constituting unit, glucose, is one of the most important challenges chemistry faces today. Such a process is deemed crucial to make possible large-scale use of bioethanol.² However, hydrolysis of cellulose is hampered by its resistance, and current bioethanol production is obliged to rely on starch as the starting material, bringing about bizarre competition between fuel and food demands.³

The preliminary process necessary for conversion of starch is gelatinisation, in which semi-crystalline starch is transformed to an easily-hydrolysable amorphous form by heating in water at 60–70 °C.⁴ As the resistance of cellulose against hydrolysis also arises from its robust crystalline structure where the cellulose chains are bound tightly by extensive hydrogen bonding networks,⁵ it is plain to see that any changes in the crystalline structure of cellulose should have similar impacts on its reaction behaviour. It has been demonstrated recently that crystalline cellulose is also transformed to an amorphous state when it is heated in water to temperatures around 300 °C at 25 MPa.^{6,7} The transformation has a very striking impact on the hydrolysis of cellulose in hydrothermal conditions, such as nearly instantaneous hydrolysis of cellulose (99.0% conversion within 0.01 s) in supercritical water ($T_c = 374$ °C, $P_c = 22.1$ MPa).^{8–11}

In practice, hydrolysis of cellulose is performed with the aid of catalysts.^{8,10–12} Especially, the acid-catalysed hydrolysis has been used for saccharification of cellulosic biomass for more than a century.¹³ To avoid issues associated with the acid-catalysed hydrolysis, such as wastewater treatment and corrosion of the reactor, a dilute acid process is favoured.¹⁴ In this method, hydrolysis is performed at high temperatures (170–240 °C) in the presence of dilute acids.¹⁴ At such high reaction temperatures, the acid catalyst may affect the structural characteristics of

cellulose, thereby accelerating the hydrolysis.^{8,10,15} Indeed, Mok *et al.* reported that the hydrolysis rate of cellulose in dilute sulfuric acid changed suddenly when the reaction temperature was raised from 212 °C to 215 °C, and speculated that physical changes in the structure of cellulose were responsible for the change.⁸ However, nothing is known as to how acid catalyst affects the behaviour of cellulose in hydrothermal conditions.

We performed *in situ* optical microscopic observation of crystalline cellulose in water at high temperatures and high pressures in the presence of various concentrations of H₂SO₄ (Fig. 1). In the presence of 10 mol dm⁻³ and 20 mol dm⁻³ H₂SO₄, significant formation of particulate objects was observed at temperatures above 200 °C (see ESI†). Such objects appeared even when 10 mol dm⁻³ H₂SO₄ was heated without cellulose, indicating that dilute sulfuric acid became so corrosive at such high temperatures that even a Ni-based corrosion-resistant superalloy that comprises the cell body¹⁶ was corroded.

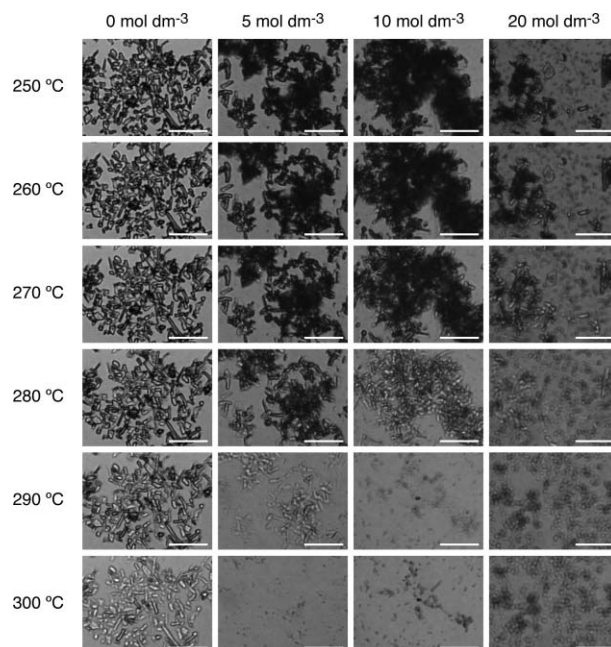


Fig. 1 A series of *in situ* optical microscopic images showing crystalline cellulose in the presence of various amounts of H₂SO₄. Each bar represents 100 μm. Particles that appeared in the presence of 10 and 20 mol dm⁻³ H₂SO₄ at high temperatures are due to corrosion of the cell. Movies showing the behaviour of cellulose in 10 and 20 mol dm⁻³ H₂SO₄ are available as ESI.† Some images in pure water are taken from ref. 7.

^aExtremobiosphere Research Center, Japan Agency for Marine-Earth Science and Technology, 2-15 Natsushima-cho, Yokosuka, 237-0061, Japan. E-mail: shigeru.deguchi@jamstec.go.jp; Fax: +81-46-867-9715; Tel: +81-46-867-9679

^bNanotechnology Research Center, Research Institute for Electronic Science, Hokkaido University, N21, W10, Kita-ku, Sapporo, 001-0021, Japan

† Electronic supplementary information (ESI) available: Movies showing behaviour of cellulose in the presence of 10 and 20 mol dm⁻³ of H₂SO₄ at high temperatures and high pressures. See DOI: 10.1039/b803384f

Despite the harsh solution atmosphere, crystalline cellulose remained essentially unchanged in water well over 200 °C, even in the presence of H₂SO₄ up to 20 mol dm⁻³. We did not observe any significant changes between 212 and 215 °C, where the sudden change in the reaction behaviour was reported previously.⁸ Transformation of crystalline cellulose to an amorphous state, which is characterised typically by the cellulose crystals becoming transparent with temperature,⁷ was observed only at temperatures above 260 °C (Fig. 1). The transformation was immediately followed by complete dissolution, because amorphous cellulose is hydrolysed promptly in hydrothermal conditions.⁷ Thus, no precipitate appeared when the specimen was cooled to room temperature.

It appears in Fig. 1 that complete dissolution of cellulose occurred at lower temperatures as the H₂SO₄ concentration was increased. This trend was quantified by a computer-based image analysis, in which change of relative brightness of the images was measured as a function of temperature (Fig. 2). The analysis parallels a turbidity measurement. In all the cases, the relative brightness was almost constant up to about 260 °C, and started to increase gradually with temperature, due to increasing transparency of cellulose associated with the crystalline-to-amorphous transformation. It then increased sharply, which was mainly ascribed to dissolution of cellulose due to rapid hydrolysis.⁷ Finally, the brightness became constant again after the complete dissolution. The analysis revealed that the slope at which the relative brightness increased sharply with temperature became steeper as the H₂SO₄ concentration was increased, while the temperature at which the sharp increase started was not affected very much. As a result, the temperature at which cellulose dissolved completely decreased with the H₂SO₄ concentration.

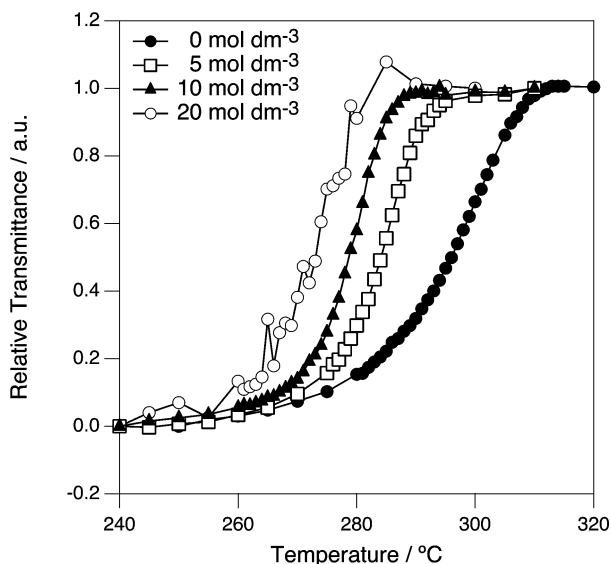


Fig. 2 Comparison of dissolution behaviour of crystalline cellulose in the presence of various amounts of H₂SO₄. The figure shows the change of relative brightness of the optical microscopic images. The data obtained in the presence of 20 mol dm⁻³ H₂SO₄ are noisy due to significant formation of particulate objects resulting from corrosion of the cell. The data in pure water are taken from ref. 7.

To further pursue the effect of the H₂SO₄ concentration, the dissolution temperature, $T_{\text{dissolution}}$, was defined as the temperature at which the relative brightness reached 0.5 in Fig. 2. Dependence of $T_{\text{dissolution}}$ on the added H₂SO₄ concentration is shown in Fig. 3. Addition of 5 mol dm⁻³ of H₂SO₄ decreased the dissolution temperature by approximately 10 °C, but the decrease became less pronounced upon further addition of H₂SO₄. By fitting the data with an exponentially decaying function, we obtained

$$T_{\text{dissolution}} = 271.0 + 24.8 \exp(-0.1[\text{H}_2\text{SO}_4]) \quad (1)$$

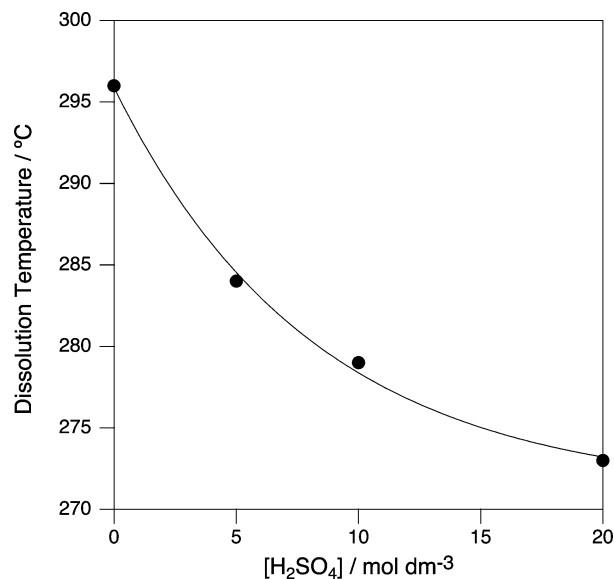


Fig. 3 Change of dissolution temperature ($T_{\text{dissolution}}$) of crystalline cellulose as a function of the concentration of added H₂SO₄.

The result shows that $T_{\text{dissolution}}$ reaches a limiting value of 271 °C at high H₂SO₄ concentrations, and cannot be lowered further no matter how high the H₂SO₄ concentration is made.

Transformation of crystalline cellulose to an amorphous form in water at high temperatures and high pressures is not simple thermal melting, but water plays an important role because no such transformation is observed in ethanol.⁶ It is suggested that the transformation is rather elicited by changes in the solid properties of cellulose,⁷ such as glass transition,¹⁷ transformation of cellulose crystals,¹⁸ and a drastic change in the hydrogen-bond structure,¹⁹ all of which occur above 200 °C. Such changes affect cellulose–water interactions, leading eventually to the transformation to an amorphous state.⁷ Interestingly enough, the limiting temperature agrees well with the temperature at which the steep increase of the relative brightness starts regardless of the concentration of H₂SO₄ (Fig. 2). This may suggest that such changes in the solid properties occur at the limiting temperature. The crystalline structure of cellulose is so robust that it is not affected by H₂SO₄ at low temperatures. However, once cellulose is transformed to an amorphous state, the cellulose chains become easily accessible and their hydrolysis is catalysed by H₂SO₄.

Acceleration of cellulose hydrolysis by H₂SO₄ was reported even though the reaction was performed at temperatures far below the limiting temperature.^{8,10} For example, complete

hydrolysis of cellulose was achieved after 1 h of reaction in water at 215 °C and 34.5 MPa in the presence of 20 mol dm⁻³ H₂SO₄, while the reaction was not completed even after 7.5 h without H₂SO₄.⁸ Although the temperature at which crystalline cellulose is transformed to an amorphous state is affected by various structural characteristics, such as crystallinity,⁷ it seems safe to assume that cellulose remains crystalline at such low temperatures. In such a case, the acceleration of hydrolysis should be ascribed purely to the added acids catalysing the hydrolysis of the cellulose chains on the solid surface.^{8,10,15}

In the present study, we did not observe a noticeable change of the size of the cellulose crystals below the limiting temperature, probably because the observation was made while heating the specimens rapidly (15 °C min⁻¹). However, the observation suggested that H₂SO₄ indeed affected the surface properties of the cellulose crystals. In our previous study, rather large cellulose crystals (1–10 µm in size) moved around on the surface of the optical window in water at high temperatures, but the movements ceased completely at around 260–270 °C, which was followed by crystalline-to-amorphous transformation.⁷ It was concluded that the transformation was preceded by change of surface properties of cellulose crystals, which made the crystals stick on the surface of the optical window.⁷ The situation was completely different in the presence of H₂SO₄, and no such movement was observed at all (see ESI†). The difference suggests that similar physical changes of the surface properties of the cellulose crystals take place at significantly lower temperatures in the presence of H₂SO₄, leading to faster hydrolysis.

In summary, the effect of H₂SO₄ on the behaviour of crystalline cellulose in hydrothermal conditions was studied for the first time by *in situ* high-resolution optical microscopy. Crystalline cellulose is transformed to an amorphous form in dilute H₂SO₄ at high temperatures and high pressures, just like it is in pure water. However, unlike the expectations from the reaction behaviour, the temperature at which such transformation occurs is not affected by H₂SO₄. The robust crystalline structure of cellulose plays an essential role in determining its reactivity in hydrothermal conditions even in the presence of H₂SO₄.

Once crystalline cellulose is transformed to an amorphous state and the cellulose chains become accessible, added H₂SO₄ facilitates the hydrolysis. Interestingly, the effect becomes less significant with increasing the H₂SO₄ concentration. This means that rapid hydrolysis of cellulose could be achieved with low acid concentrations by conducting the reaction at high enough temperatures where cellulose is in an amorphous state. At low temperatures where cellulose remains crystalline, added H₂SO₄ affects the surface properties of the cellulose crystals, leading to higher hydrolysis rate. This is in marked contrast to the hydrolysis in pure water, in which the surface effect is negligible.⁷

Experimental

Materials

Cellulose used in this work was Funacel SF for thin-layer chromatography (derived from wood, Funakoshi, Tokyo, Japan), and used as received. The degree of polymerization was found to be 220 by viscometry.²⁰ The crystallinity index was found by X-ray

diffraction to be 58.2%, showing highly crystalline nature of the sample.²⁰

In situ high-resolution optical microscopy

The behaviour of crystalline cellulose was examined by using an optical microscope equipped with a high-temperature and high-pressure sample chamber.¹⁶ The instrument allows *in situ* direct observation of specimen in water at temperatures and pressures up to 400 °C and 35 MPa with an unprecedented optical resolution of 2 µm.¹⁶ The instrument was used successfully to study the chemical stability of polystyrene and silica,²¹ and the Brownian motion of colloids,²² all in water at high temperatures and high pressures up to a supercritical state. A detailed description of the instrument can be found elsewhere.¹⁶

Crystalline cellulose was dispersed in dilute sulfuric acid, and introduced into the cell. The specimen in the cell was pressurized to 25 MPa at room temperature, and then heated while keeping the pressure constant at 25 MPa. The instrument was able to heat the sample to 350 °C within 25 min.⁷ At temperatures above 50 °C, the heating rate was nearly constant at around 15 °C min⁻¹.⁷ Due to the flow type design of the cell, it was not possible to recover the specimen after observation, and end products of the specimen after observation were not analyzed in this study. Under the present experimental conditions, high thermal energy prevents clustering of the water molecules, leading to properties that are significantly different from those of ambient water.²³ For example, the dielectric constant, which is 78 at 25 °C and 0.1 MPa, decreases to 21 at 300 °C and 25 MPa. However, the difference does not affect properties of H₂SO₄.²⁴

Image analysis

The observation was quantified by computer-based image analysis.^{6,7} The analysis is based on measuring brightness of images, and parallels turbidity measurements. The same analysis was used successfully to quantify the crystalline-to-amorphous transformation or comparing the behaviour of cellulose samples having different structural characteristics.^{6,7} The values were normalized so that the brightness at 240 °C became 0 and the brightness at the highest measurement temperature became unity.

Acknowledgements

We thank Dr Sada-atsu Mukai, Kyushu University, for a critical reading of the manuscript. Financial support from the Ministry of Education, Culture, Sports, Science and Technology (Grant-in-Aid for Young Scientists (B) No. 15750109) is acknowledged.

Notes and references

- 1 D. Klemm, B. Heublein, H.-P. Fink and A. Bohn, *Angew. Chem., Int. Ed.*, 2005, **44**, 3558–3393.
- 2 A. E. Farrell, R. J. Plevin, B. T. Turner, A. D. Jones, M. O'Hare and D. M. Kammen, *Science*, 2006, **311**, 506–508; J. Hill, E. Nelson, D. Tilman, S. Polasky and D. Tiffany, *Proc. Natl. Acad. Sci. U. S. A.*, 2006, **103**, 11206–11210.
- 3 M. R. Schmer, K. P. Vogel, R. B. Mitchell and R. K. Perrin, *Proc. Natl. Acad. Sci. U. S. A.*, 2008, **105**, 464–469.
- 4 W. A. Atwell, L. F. Hood, D. R. Lineback, E. Varriano-Marston and H. F. Zobel, *Cereal Foods World*, 1988, **33**, 306–311.

- 5 P. Langan, Y. Nishiyama and H. Chanzy, *Biomacromolecules*, 2001, **2**, 410–416; Y. Nishiyama, P. Langan and H. Chanzy, *J. Am. Chem. Soc.*, 2002, **124**, 9074–9082; Y. Nishiyama, J. Sugiyama, H. Chanzy and P. Langan, *J. Am. Chem. Soc.*, 2003, **125**, 14300–14306.
- 6 S. Deguchi, K. Tsujii and K. Horikoshi, *Chem. Commun.*, 2006, 3293–3295.
- 7 S. Deguchi, K. Tsujii and K. Horikoshi, *Green Chem.*, 2008, **10**, 191–196.
- 8 W. S.-L. Mok, M. J. Antal, Jr. and G. Varhegyi, *Ind. Eng. Chem. Res.*, 1992, **31**, 94–100.
- 9 T. Adschiri, S. Hirose, R. Malaluan and K. Arai, *J. Chem. Eng. Jpn.*, 1993, **26**, 676–680; M. Sasaki, B. Kabyemela, R. Malaluan, S. Hirose, N. Takeda, T. Adschiri and K. Arai, *J. Supercrit. Fluids*, 1998, **13**, 261–268; S. Saka and T. Ueno, *Cellulose*, 1999, **6**, 177–191; M. Sasaki, Z. Fang, Y. Fukushima, T. Adschiri and K. Arai, *Ind. Eng. Chem. Res.*, 2000, **39**, 2883–2890; K. Ehara and S. Saka, *Cellulose*, 2002, **9**, 301–311; M. Sasaki, T. Adschiri and K. Arai, *AIChE J.*, 2004, **50**, 192–202.
- 10 O. Bobleter, *Prog. Polym. Sci.*, 1994, **19**, 797–841.
- 11 T. Minowa, F. Zhen and T. Ogi, *J. Supercrit. Fluids*, 1998, **13**, 253–259.
- 12 A. Fukuoka and P. L. Dhepe, *Angew. Chem., Int. Ed.*, 2006, **45**, 5161–5163.
- 13 E. E. Harris, *Adv. Carbohydr. Chem.*, 1949, **4**, 153–188.
- 14 B. Girisuta, L. P. B. M. Janssen and H. J. Heeres, *Ind. Eng. Chem. Res.*, 2007, **46**, 1696–1708.
- 15 H. Zhao, J. H. Kwak, Y. Wang, J. A. Franz, J. M. White and J. E. Holladay, *Energy Fuels*, 2006, **20**, 807–811.
- 16 S. Deguchi and K. Tsujii, *Rev. Sci. Instrum.*, 2002, **73**, 3938–3941.
- 17 K. Kamide and M. Saito, *Polym. J.*, 1985, **17**, 919–928; Y. Nishio, S. K. Roy and R. S. J. Manley, *Polymer*, 1987, **28**, 1385–1390.
- 18 F. Horii, H. Yamamoto, R. Kitamaru, M. Tanahashi and T. Higuchi, *Macromolecules*, 1987, **20**, 2946–2949.
- 19 A. Watanabe, S. Morita and Y. Ozaki, *Biomacromolecules*, 2006, **7**, 3164–3170; A. Watanabe, S. Morita and Y. Ozaki, *Biomacromolecules*, 2007, **8**, 2969–2975.
- 20 S. Deguchi, M. Tsudome, Y. Shen, S. Konishi, K. Tsujii, S. Ito and K. Horikoshi, *Soft Matter*, 2007, **3**, 1170–1175.
- 21 S. Deguchi, S. K. Ghosh, R. G. Alargova and K. Tsujii, *J. Phys. Chem. B*, 2006, **110**, 18358–18362.
- 22 S. Mukai, S. Deguchi and K. Tsujii, *Colloids Surf., A*, 2006, **282–283**, 483–488.
- 23 S. Deguchi and K. Tsujii, *Soft Matter*, 2007, **3**, 797–803.
- 24 T. Xiang, K. P. Johnston, W. T. Wofford and E. F. Gloyna, *Ind. Eng. Chem. Res.*, 1996, **35**, 4788–4795.

Fast, quantitative nucleoside protection under solvent-free conditions

Nicola Giri, Caroline Bowen, Joseph S. Vyle* and Stuart L. James*

Received 25th January 2008, Accepted 16th April 2008

First published as an Advance Article on the web 30th April 2008

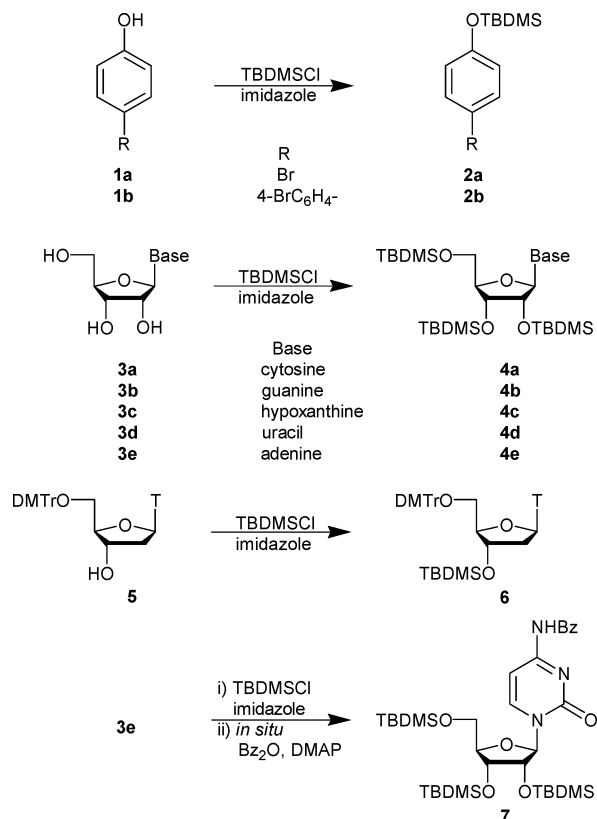
DOI: 10.1039/b801455h

Persilylation of nucleoside hydroxyls was effected in quantitative yields under solvent-free conditions using a ball mill. In addition, one-pot persilylation and acylation of cytidine was performed as an exemplar reaction demonstrating the utility of solvent-free approaches to nucleoside chemistry.

Solvent-free synthesis is increasingly attractive for its potential to provide both convenient and greener routes to chemical products.^{1,2} The mechanical ball milling technique has been broadly applied for industrial materials processing and for producing inorganic materials.¹ Under solvent-free conditions, this technique has recently been used for organic and metal-organic reactions, offering the benefits of lower toxic waste, low cost and ease of processing and handling.² Nucleoside chemistry is particularly interesting in this regard because the solubility profiles of these compounds often require solvents such as DMF and pyridine, which are carcinogenic or highly toxic.³ In addition, solvent predrying over calcium hydride or phosphorus pentoxide and distillation is required for reactions with moisture sensitive reagents such as chlorosilanes. Recently, solvent-free protection of nucleoside amino groups has been reported, as well as transient hydroxyl protection.⁴ This has prompted us to report our complementary findings in the permanent protection of ribo- and deoxyribonucleoside hydroxyls under solvent-free Corey conditions.⁵ Fast, quantitative persilylation is achieved using a small commercial ball mill, which circumvents the drawbacks associated with DMF or pyridine.

We observed that simple phenols **1a–b** reacted readily with 1.1 equivalents of *t*-butyldimethylsilylchloride (TBDMSCl) in the ball mill in the presence of 2 equivalents of imidazole (Scheme 1) within 45 min at 25 Hz (Table 1) to give the corresponding silyl ethers (**2a–b**).⁴ Yields were quantitative and by-products readily removed by extraction, after washing the mixture from the reactor with a small amount of methanol. The effectiveness and convenience of this procedure prompted us to investigate related protection of nucleosides which would normally involve DMF or pyridine as solvents.³

Grinding commercially available ribonucleosides **3a–d** in the ball mill with 4 equivalents of TBDMSCl and 8 equivalents of imidazole at a frequency of 30 Hz gives within 1–3 h the persilylated ribonucleosides **4a–d** in quantitative yield (Table 1).[†] This is remarkably faster than the solution-based processes



Scheme 1 Solvent-free derivatisation of phenols and nucleosides (T = thymine). Reagents and conditions: (i) TBDMSCl, imidazole, ball milling (for equivalents and times see table); (ii) *in situ* Bz₂O (2 eq.), DMAP (0.2 eq.), ball milling (30 Hz), 120 min.

which are typically performed overnight.⁵ Although the temperatures of the reactions did not exceed 60 °C (significantly lower than the melting points of either starting materials or products),⁶ the reaction mixtures were found to become pastes. This suggests that these reactions are effectively liquid-state due to the formation of low-melting eutectics.⁷ It is also notable that inosine (**3d**) which is only sparingly soluble even in DMF could be efficiently derivatised in this fashion.

Despite the presence of exocyclic amino groups in cytidine (**3a**) and guanosine (**3b**), no silylation was observed at these sites. Only with adenosine (**3e**), using elevated reagent excesses, was *N*-silylation observed and the slightly lower recovery of **4e** (87%) reflected this. However, decreasing the equivalents of the silylating agent or the frequency (to 25 Hz) lead to an incomplete reaction (even with prolonged grinding), resulting in a mixture of the di- and tri-*O*-silylated nucleoside. The grinding frequency, which is related to the mechanical energy provided to the system,

Innovative Molecular Materials (IMM) Group and Centre for the Theory and Application of Catalysis (CentTACat), School of Chemistry and Chemical Engineering, Queen's University Belfast, David Keir Building, Stranmillis Road, Belfast, Northern Ireland, UK BT9 5AG. E-mail: j.vyle@qub.ac.uk, s.james@qub.ac.uk; Fax: +44 (0)28 90972117; Tel: +44 (0)28 90975419

Table 1 Solvent-free persilylation and *N*-benzoylation in the ball mill

Substrate	TBDMSCl equiv	Imidazole equiv	Frequency/Hz	Time/min	Product (yield%)
1a	1.1	2	25	45	2a (98)
1b	1.1	2	25	45	2b (95)
3a	4	8	30	60	4a (95)
3b	4	8	30	180	4b (99)
3c	4	8	30	180	4c (94)
3d	4	8	30	180	4d (96)
3e	5	10	30	90	4e (87)
5	1.3	8	30	90	6 (99)
3a	4	8	30	60/120	7 (90) ^a

^a One-pot persilylation-*N*⁴-benzoylation (60 min persilylation followed by 120 min with 2 equiv Bz₂O/0.2 equiv DMAP).

was found to be an important parameter in obtaining complete derivatisation of all nucleosides, even in the presence of excess TBDMSCl.

Importantly, the trityl protecting group is also compatible with these reaction conditions in the ball mill, despite its thermal- and acid-sensitivity. In particular, reaction of the trityl-protected 5'-DMTr-thymidine (**5**) with TBDMSCl at a frequency of 30 Hz gave the corresponding 2'-silylated derivative (**6**) quantitatively in 90 min. To explore further the versatility of the solvent free-approach, we successfully performed a one-pot persilylation and *N*⁴-benzoylation of cytidine (**3a**) to yield **7** in quantitative yield. The reaction was conducted simply by adding the benzoic anhydride and a catalytic amount of DMAP directly to the crude persilylated material in the ball mill. Under typical solvent-based conditions two steps are used, both involving dry DMF or pyridine as solvent.^{3,8} This alternative, solventless procedure avoids the use of such solvents and the intermediate work-up, providing a more efficient method to consecutively protect two different functional groups.

In summary, persilylation of phenols, ribonucleosides and protected nucleosides under solvent-free conditions using a ball mill has been demonstrated. Quantitative one-pot silylation-*N*-benzoylation of cytidine has also been effected. The solvent-free ball mill approach simplifies the synthesis and avoids undesirable solvents, offering significant advantages in the preparation of protected nucleosides. Given the similar solubility profiles of amino acids, sugars and free nucleobases, we suggest there is great scope for solvent-free ball milling in synthesis involving other biological molecules.

Notes and references

† Typical nucleoside protection procedure: a 20 cm³ steel vessel was charged with the ribonucleoside (0.6 mmol), TBDMSCl (2.4 mmol) and imidazole (4.8 mmol) and a steel ball bearing and shaken with a Retsch MM200 mixer mill for 90–180 min at 30 Hz. The crude material was washed from the reactor with a small amount of MeOH. The solvent was evaporated and the residue applied to a short pad of silica gel, eluting using hexane/ethyl acetate = 7 : 3.

- R. Janot and D. Guérard, *Prog. Mater. Sci.*, 2005, **50**, 1; D. L. Zhang, *Prog. Mater. Sci.*, 2004, **49**, 537; L. Takacs, *Prog. Mater. Sci.*, 2002, **47**, 355; C. Suryanarayana, *Prog. Mater. Sci.*, 2001, **46**, 1.
- A. Lazuen Garay, A. Pichon and S. L. James, *Chem. Soc. Rev.*, 2007, **36**, 846; G. Kaupp, *CrystEngComm*, 2006, **8**, 794; B. Rodriguez, A. Bruckmann, T. Rantanen and C. Bolm, *Adv. Synth. Catal.*, 2007, **349**, 2213; G. Kaupp, *CrystEngComm*, 2003, **5**, 117; K. Tanaka and F. Toda, *Chem. Rev.*, 2000, **100**, 1025; G. W. V. Cave, C. L. Raston and J. L. Scott, *Chem. Commun.*, 2001, 2159; K. Tanaka, *Solvent-free organic synthesis*, Wiley-VHC, Weinheim, 2003.
- G. H. Hakimelahi, Z. A. Proba and K. K. Ogilvie, *Can. J. Chem.*, 1982, **60**, 1106 and references cited therein; M. D. Erlacher, K. Lang, B. Wotzel, R. Rieder, R. Micura and N. Polacek, *J. Am. Chem. Soc.*, 2007, **128**, 4453.
- S. A. Sikchi and P. G. Hultin, *J. Org. Chem.*, 2006, **71**, 5888.
- E. J. Corey and A. Venkates, *J. Am. Chem. Soc.*, 1972, **94**, 6190.
- Reported melting points for both starting materials and products (except TBDMS₃rU) are greater than 85 °C: TBDMSCl (86–88 °C); imidazole (88–91 °C); ribonucleosides (rN – range from 163 to 250 °C); imidazole.HCl (158–161 °C); TBDMS₃rN (103–288 °C).
- G. Rothenburg, A. P. Downie, C. L. Raston and J. L. Scott, *J. Am. Chem. Soc.*, 2001, **123**, 8701.
- K. K. Ogilvie, M. J. Nemer, J. Mona, G. H. Hakimelahi, Z. A. Zbigniew and M. Lucas, *Tetrahedron Lett.*, 1982, **26**, 2615.

The application of focused microwave irradiation coupled with freeze drying to investigate the reaction of MgO and Al₂O₃ slurries in the formation of layered double hydroxides

Sharon Mitchell, Ian R. Baxendale and William Jones*

Received 24th January 2008, Accepted 25th March 2008

First published as an Advance Article on the web 25th April 2008

DOI: 10.1039/b801365a

Focused microwave irradiation (MI) and freeze drying (FD) techniques have been used to study the generation of layered double hydroxides prepared from MgO–Al₂O₃–H₂O systems. Reactions were undertaken at temperatures of between 100 and 180 °C in order to study the formation of the 3R₁ and 3R₂ polytypes, respectively. MI was found to enhance the rate of formation of both polytypes. FD provided an effective means of quenching the reaction, enabling effective *ex situ* analysis at intermediate stages. The phase selectivity of the reaction was shown to vary with temperature, promoting the formation of an impurity Mg(OH)₂ at elevated temperatures.

Introduction

Layered double hydroxides (LDHs) are a class of important inorganic lamellar materials which have found applications in many areas, such as catalysis,¹ pharmaceuticals,² and absorbents.³ They have a layered structure similar to that of the mineral brucite (Mg(OH)₂) and have the general formula [M²⁺_{1-n}M³⁺_n(OH)₂]ⁿ⁺(Aⁿ⁻_{x/n})_x·mH₂O.³ Numerous metal (M) and anion (A) combinations have been reported, with the number of potential compositions extremely large.⁴

The performance of an LDH in any given application is dependent both on its composition and chemical structure, properties determined during synthesis. There are several methods of LDH preparation.⁵ The simplest and most commonly used is that of coprecipitation of soluble metal salts. Other routes include hydrothermal synthesis, the sol-gel method and dehydration and reconstruction of a precursor LDH. Additionally, the properties of the LDH are also dependent on the synthesis conditions, including for example pH, temperature, M(II) : M(III) stoichiometry, source of anions and length of reaction.^{6,7} Understanding the influence of these parameters is, therefore, becoming increasingly important in order to control and/or tailor the specific properties of the resulting LDH.

Microwave irradiation (MI) is known to enhance the rate of nucleation and growth of crystals in many inorganic reactions, reducing the required synthesis time and resulting in environmental and economic benefits.⁸ The use of MI for LDH synthesis has primarily focused on modifying and improving nucleation and growth properties, when concerned with the precipitation of soluble metal salts.⁹ In this way, crystalline materials with relatively high specific surface area values have been reported. Metals which have been studied include M(II) = Mg, Co, Ni,

Cu, Zn, M(III) = Al, Fe, Co, Ga.¹⁰ Carbonate is the most commonly studied anionic species due to its high abundance (from CO₂ uptake) and strong interaction with the surrounding layer. Other anionic species which have been intercalated using MI include chlorides, Evans Blue dye,¹¹ α -naphthaleneacetate,¹² and anthraquinone-2,6-disulfate.¹³ Additionally, MI has been used to prepare PO₄³⁻, P₂O₇⁴⁻,¹⁴ and heteropolyoxometalate pillared Mg–Al LDHs.¹⁵

In this investigation, we have studied the influence of MI on the reaction of slurries of the MgO–Al₂O₃–H₂O system in the formation of LDHs. This reaction has previously been reported under standard thermal conditions, receiving commercial interest for the preparation of synthetic meixnerite.¹⁶ It also is of interest in the field of green chemistry as water may be used as the solvent and it allows accurate control of the reacting species, thereby reducing waste products.¹⁷ Of particular preparative significance is the dependence of the resulting LDH structure on the synthesis temperature.¹⁸ In this respect, two polytypes, designated by Bookin and Drits as 3R₁ and 3R₂, are known to form depending on the stacking of consecutive layers. The two polytypes may be identified by small shifts in the mid 2 theta range (35–55°) of the PXRD pattern.¹⁹ The occurrence of polytypism is important since polytypes may have different physical properties. Anion exchange, for example, may change since the LDH layer–anion interaction strength varies between polytypes due to the change in symmetry of the interlayer sites.²⁰

As most methods of preparation involve water, a drying procedure is required. It is not atypical to read in the literature that samples have been dried in a conventional oven at 70 °C for prolonged periods of time. This will clearly affect the products of the reaction if the reaction has not already reached completion. In this study we report on the use of freeze drying (FD) as a convenient method to quench the reacting slurries, effectively preventing further transformations. The use of FD has enabled *ex situ* phase analysis at intermediate stages of reaction which is beneficial as the resolution of *ex situ* analysis is improved

Department of Chemistry, University of Cambridge, Lensfield Road, Cambridge, Cambridgeshire, UK. E-mail: wj10@cam.ac.uk; Fax: +44 (0)1223 336017; Tel: +44 (0)1223 336468

compared to the *in situ* approaches such as energy dispersive X-ray diffraction that have previously been applied.²¹

Experimental details

Slurries of reagent grade MgO (Aldrich) and Cp3 Al₂O₃ (ALCOA), were prepared with distilled water at the desired stoichiometry ($R = [\text{Mg}]/[\text{Al}] = 2, 5 \text{ wt\% solids}$). The Cp3 Al₂O₃ is an amorphous, γ alumina, prepared by the flash calcination of gibbsite (an amorphous form of alumina was chosen as crystalline Al₂O₃ is known to be slower to react).²² The resulting slurries were loaded into 5 ml microwave reaction vials made from borosilicate glass, designed to withstand operating pressures up to 20 bars (300 psi).²³ The reactions were then heated at 100 °C either conventionally (C) in a Carbolite furnace or with MI using an Emrys Synthesizer Optimiser from Biotage. During MI the power level (W) was kept constant. Reactions were also undertaken using MI at 180 °C but it was not possible to achieve the equivalent conventional experiment at this temperature with these reaction vessels. All reactions were undertaken at autogeneous pressure.

After heating for the specified period of time (min) the reaction vessels were cooled within one minute to room temperature under a gas flow. The resultant slurries were then filtered to remove excess water and were then either freeze dried (FD) using a VirTis AdVantage bench top freeze-dryer, or conventionally dried (CD) in a furnace at 70 °C. During the freeze drying process the product was cooled to -40 °C, and held at this temperature under reduced pressure for 2 hours. The shelf temperature was then gradually raised to room temperature over a further 4 hour period.

Powder X-ray diffraction (PXRD) patterns of the resultant materials were then recorded using a Philips PW3710 diffractometer in reflection geometry using graphite monochromated Cu K α radiation. Data were collected from finely ground samples pressed on a flat plate, glass sample holder. Phase identification was achieved by comparison with PXRD patterns simulated, using the X'Pert Plus software, from single crystal structural information data obtained from the International Crystal Structure Database (Numbers: brucite No. 95475, boehmite No. 59608, MgO periclase No. 95468).

Fourier transform infra-red (FTIR) spectra were recorded on a ThermoNicolet Nexus Spectrometer using the Smart Golden Gate single reflection stage attenuated total reflection. A background spectrum was recorded before the sample was placed on the sample stage, pressure applied and data acquired. Data were recorded in the range $\nu = 550\text{--}3800 \text{ cm}^{-1}$.

Scanning electron microscopy (SEM) was undertaken using a JEOL 5800LV instrument. Samples were dispersed from ethanol onto a freshly cleaved mica surface. A thin platinum coating was applied to reduce the effects of sample charging.

Results

Nomenclature

The following nomenclature is used in the remainder of this paper; X_t@T_Y, where X = heating method MI or C, t =

reaction time (minutes), T = reaction temperature (°C) and Y = drying method FD or CD.

Capturing intermediate stages of reaction

Fig. 1 compares the PXRD patterns of the FD products obtained by conventional and MI heating after 10 minutes of reaction at 100 and 180 °C. The pattern of the initial physical mixture and a simulated pattern of an Mg–Al LDH²⁴ are shown for comparison.

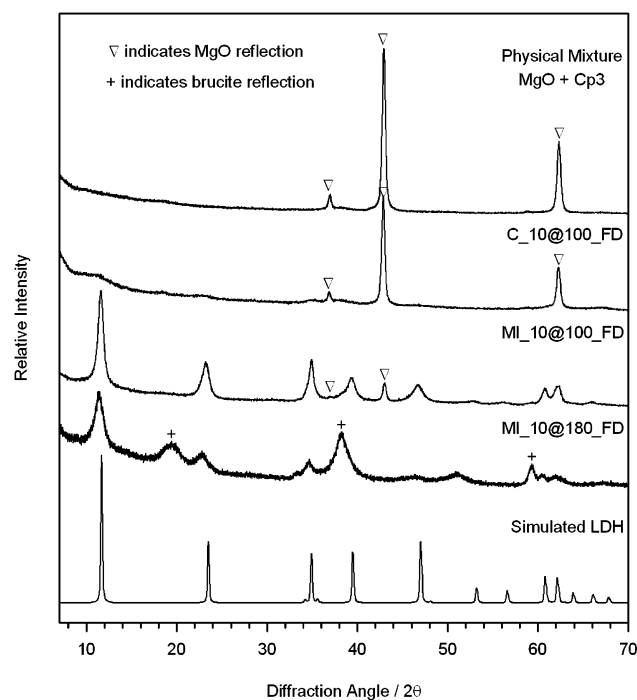


Fig. 1 PXRD patterns of the FD products obtained after 10 minutes of reaction compared with the PXRD pattern of the initial physical mixture and a simulated PXRD pattern of an Mg–Al LDH.

The use of MI during the reaction is seen to significantly increase the rate LDH formation. Strong reflections are visible corresponding well with those in the simulated LDH pattern (MI_{10@100_FD} and MI_{10@180_FD}). In contrast, the product resulting from the conventionally heated reaction (C_{10@100_FD}) exhibits little change from the initial physical mixture. Only a broad, weak reflection, assigned to the 003 basal reflection ($2\theta \approx 12^\circ$) indicates a small amount of conversion to LDH.

MgO reflections remain visible in the products reacted at 100 °C. These are not observed in the products from reaction at 180 °C, indicating that at this temperature the reaction kinetics are higher, in agreement with expected Arrhenius behaviour.

To study the influence of FD some slurries were dried in a Carbolite furnace at 70 °C for comparison. Fig. 2 shows the PXRD patterns of two furnace dried products collected after 10 minutes of reaction (conventionally, C_{10@100_CD} and using MI, MI_{10@100_CD}) at 100 °C. In contrast with the FD products, LDH reflections are clearly visible in the material obtained by conventional reaction. Additionally, no MgO reflections are observed in the product generated using

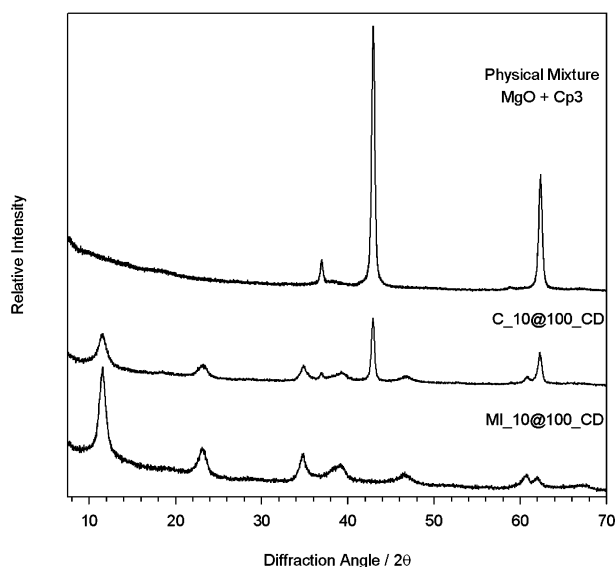


Fig. 2 PXRD patterns of products from slurries reacted for 10 minutes at 100 °C using (a) conventional and (b) MI heating, furnace dried at 70 °C. The PXRD pattern of the initial physical mixture is also shown.

MI. From these results it could be concluded that the reaction of MgO and Cp3 has reached completion after only 10 minutes of MI at 100 °C. This demonstrates the importance of accurately distinguishing the reaction time and avoiding the possibility of further chemical conversion when using *ex situ* analysis.

At 100 °C, only reflections corresponding to reactant MgO and an LDH phase are observed. This is in agreement with the findings of our *in situ* studies using energy dispersive X-ray diffraction.²¹ Any formation of brucite or boehmite, which would be the expected phases formed by the hydration of MgO or Cp3 respectively in this temperature range, are short lived, converting directly into LDH.

At 180 °C, however, formation of the impurity brucite is observed (Fig. 1, MI_10@180_FD). This indicates that at this temperature a change in the phase selectivity of the reaction occurs, with the hydration of MgO to Mg(OH)₂ now more favourable.

Characterisation of resultant LDH phases

For reaction times greater than 2 hours, little further change (shifts in reflection positions, identification of new phases *etc.*) in the products was observed by PXRD, independent of the heating method used. Fig. 3 shows the PXRD patterns and FTIR spectra of the FD products after reaction for 2 hours. Corresponding structural parameters are presented in Table 1. The Scherrer equation was used to estimate the average crystallite size, *t*, along the *c* axis by evaluating the full width at half maximum (FWHM) of the basal reflections of the resulting LDH phases. The FWHM were calculated using software installed in the instrument which uses a Gaussian fit. Table 2 compares the *t*, *c*₀ and *a*₀ parameters observed in the LDH products obtained after 10 and 120 minutes of reaction. The values should not be considered as the formal crystallite size as they do not account for line broadening due to stress-related or instrumental effects.²⁵ Furthermore, the shape of the LDH crystallites is neither spherical nor cubic. As the errors arising due to these assumptions are thought to be similar in all cases the values may be used as a reference to compare samples prepared by different synthetic routes.

The conventional and microwave products from reaction at 100 °C are single phase and appear to be isostructural. Observed LDH reflections agree well with the calculated structural parameters for the 3R₁ polytype (where the 012, 015 and 018 reflections are expected to be strong). The *a*₀ parameters (3.046 and 3.048 Å respectively) also correspond with the expected parameter for an LDH of composition *R* = 2.²⁶ Reflections in the LDH products prepared by MI are visibly narrower than

Table 2 Summary of estimated crystallite size (*t*) and structural parameters (*c*₀ and *a*₀) for LDH phases obtained

Preparation	time/min	<i>c</i> ₀ /Å	<i>a</i> ₀ /Å	<i>t</i> (003)/Å
Conventional, 100 °C	10	— ^a	— ^a	— ^a
Conventional, 100 °C	120	22.62	3.05	90
MI, 100 °C	10	23.05	3.05	70
MI, 100 °C	120	22.94	3.05	170
MI, 180 °C	10	23.27	3.06	80
MI, 180 °C	120	22.10	3.06	170

^a No observable LDH reflections in this product.

Table 1 Observed and calculated structural parameters for the LDH phases observed in Fig. 3

(a) C_120@100_FD				(b) MI_120@100_FD				(c) MI_120@180_FD			
<i>2θ</i> _{obs}	<i>d</i> _{obs}	<i>hkl</i>	<i>d</i> _{calc}	<i>2θ</i> _{obs}	<i>d</i> _{obs}	<i>hkl</i>	<i>d</i> _{calc}	<i>2θ</i> _{obs}	<i>d</i> _{obs}	<i>hkl</i>	<i>d</i> _{calc}
11.728	7.540	003	7.540	11.566	7.645	003	7.645	12.094	7.312	003	7.312
23.393	3.800	006	3.770	23.231	3.826	006	3.823	19.390	4.574	sl ^a /b ^b	4.573
34.964	2.564	012	2.569	34.820	2.574	012	2.578	24.222	3.671	006	3.656
39.441	2.283	015	2.279	39.320	2.290	015	2.288	34.228	2.618	101	2.621
46.801	1.939	018	1.929	46.821	1.939	018	1.942	34.764	2.574	012	2.567
52.972	1.727	1010	1.717	52.729	1.735	1010	1.731	37.898	2.372	104	2.379
60.789	1.523	110	1.523	60.727	1.524	110	1.524	44.967	2.014	107	2.019
62.109	1.493	113	1.493	62.016	1.495	113	1.493	54.295	1.688	1010	1.687
								59.317	1.557	b ^b	
								60.713	1.524	110	1.524
								62.159	1.492	113	1.492
<i>a</i> ₀	3.046	<i>c</i> ₀	22.620	<i>a</i> ₀	3.048	<i>c</i> ₀	22.935	<i>a</i> ₀	3.054	<i>c</i> ₀	22.098

^a sl indicates possible superlattice corresponding to the reflection most commonly expected given by $\sqrt{3}asin60$. ^b b indicates possible brucite reflection.

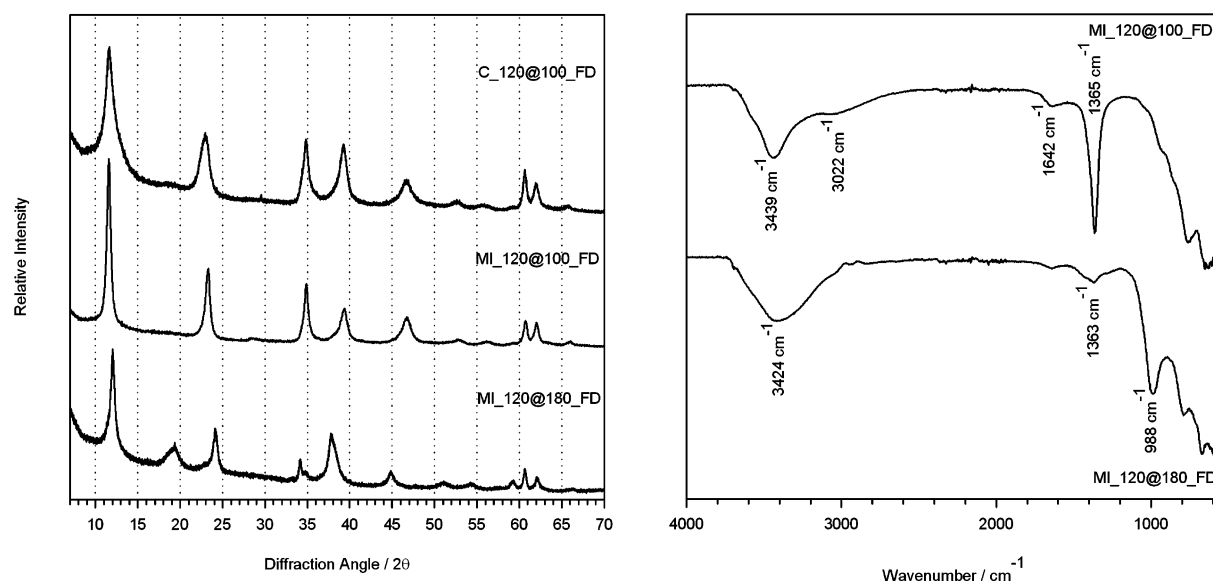


Fig. 3 PXRD patterns (left) and corresponding FTIR spectra (right) of products obtained after 2 hours of reaction at 100 °C (both conventionally and using MI) and at 180 °C using MI.

the reflections in the products from conventional synthesis. The estimated crystallite size of 176 Å for MI is almost double that of the conventional product at 91 Å, which is consistent with the observed increase in the kinetics using this heating method.

At 180 °C, although the PXRD pattern of the product obtained after 2 hours of reaction (Fig. 3, MI_120@180_FD) is similar to the pattern of the product collected after 10 minutes (Fig. 1, MI_10@180_FD), some evidence of further reaction is observed. The relative intensity of brucite compared to LDH reflections has decreased and the LDH reflections have narrowed. After 2 hours of reaction, the LDH reflections in the product correspond well to those previously reported for the 3R₂ polytype of LDH, with the expected shifts in the mid 2θ reflections (between 35–55°) clearly visible in the PXRD pattern.¹⁸ Observed values of d_{hkl} agree well with those calculated for the 101, 104 and 107 reflections (Table 1), which are expected to be strong in the 3R₂ polytype. The estimated crystallite size, 174 Å, is comparable with that of the LDH prepared by MI at 100 °C for the same reaction time (176 Å).

It is interesting to note (from the FTIR data) that the products from reaction at 100 °C contain a band at 1365 cm⁻¹, characteristic of the CO₃²⁻ anion. This absorption is not present in the FTIR spectra of the product prepared at 180 °C. It is known that complete elimination of carbonate from LDH is difficult due to the strong affinity of CO₃²⁻ within the interlayer.²⁴ The LDH product resulting from reaction at 180 °C, however, has a 3R₂ structure. No LDHs containing CO₃²⁻ are known to exist in this polytype which may be a factor prohibiting uptake of carbonate from atmospheric carbon dioxide.

SEM images of the reactant MgO and Cp3 compared with the materials obtained after 2 hours of reaction are shown in Fig. 4. Clear morphological differences are seen between reactants and products. Large agglomerated particles in which the familiar plate-like morphologies often associated with LDHs can be seen. These particles appear to be less densely agglomerated in the products of reaction at 180 °C (Fig. 4, h and i) compared with

those seen in the products from reaction at 100 °C, perhaps indicating less intergrowth of the primary crystallites. In all samples, a wide range of particle sizes are observed. For the product prepared using conventional heating, the plate-like features appear smaller than for the products prepared using MI. This difference in particle size supports the calculated difference estimated using the Scherrer equation.

Discussion and concluding remarks

MI has been shown to enhance the rate of LDH formation on reaction of the MgO–Al₂O₃–H₂O system, in agreement with the findings of Lim *et al.*²⁷ Several factors could contribute to the increased rate of reaction observed. Reaction temperatures can be achieved more rapidly using MI, since the MI penetrates the reacting mixture instantaneously providing efficient heat distribution. This reduces any lag time associated with heat conduction through the reaction vessel. Alternatively, increases in rate have also been attributed to the possibility of strong coupling between the MI and certain groups present, such as OH (known as strong absorbers) or have been ascribed to the occurrence of hot spots within the reacting mixture which lead to super heating.^{28,29}

Reaction at 180 °C successfully yielded a 3R₂ meixnerite-like LDH after just two hours, much faster than the previously reported conventional synthesis in which reaction times of 24 hours were reported. It was not possible to undertake a conventional synthesis at 180 °C for comparison with the microwave synthesis as the use of a different reaction vessel would have been necessary. Choice of reaction vessel has been observed to influence the reaction between MgO and Cp3 Al₂O₃, because different vessels have different heating profiles during reaction (depending on their size and thermal mass and the applied heating power).³⁰ The specific thermal conditions created during the reaction are critical in determining both the kinetics and phase selectivity of reaction. This is frequently

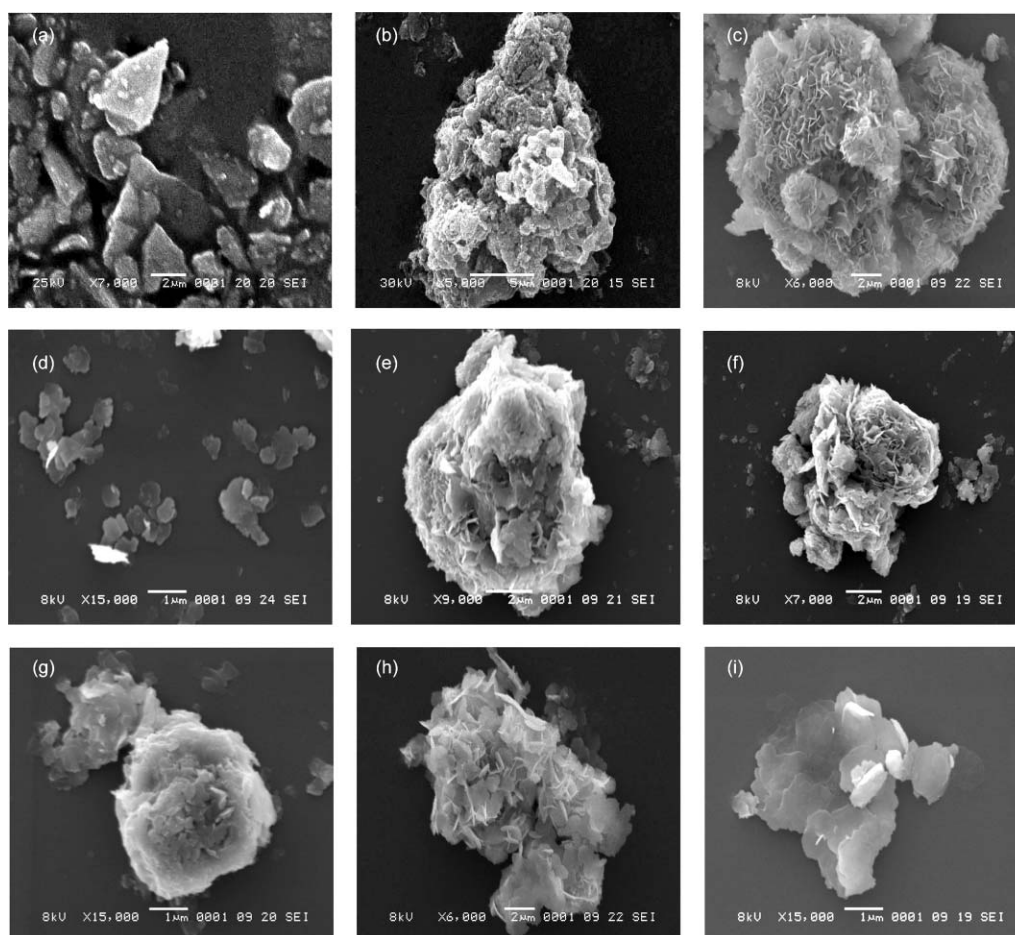


Fig. 4 SEM images of reactant (a) MgO and (b) Cp₃ Al₂O₃, compared with those of the products, (c and d) C₁₂₀@100_FD, (e, f and g) MI₁₂₀@100_FD and (h and i) MI₁₂₀@180_FD.

observed for systems where the products obtained are dependent on the reaction temperature.^{31,32}

The combination of microwave synthesis and freeze drying has been shown to be an effective approach for avoiding continued secondary reaction. Freeze drying effectively quenches the reaction enabling *ex situ* analysis at intermediate reaction stages. This allows increased sensitivity in phase detection compared to currently used *in situ* analytical techniques, where the presence of water reduces the achievable resolution.

These initial results indicate that increasing the reaction temperature from 100 to 180 °C changes the phase dynamics of the reaction, the hydration of MgO to Mg(OH)₂ becoming more significant at higher reaction temperatures. The morphological differences observed between the products may also have important implications in terms of their chemical reactivity. LDHs are widely used for intercalation chemistry and in the field of catalysis—applications where performance may be limited by the accessible surface area.³³ Dense aggregation of LDH crystallites by intergrowth may restrict accessibility to the gallery regions, thereby reducing reactivity of these compounds. The crystallite size of an LDH is also known to affect its physical properties, *e.g.* Albiston *et al.* reported that the rheology of Mg–Al LDH aqueous dispersions is critically affected by the primary LDH crystal size.³⁴

Acknowledgements

We would like to thank EPSRC for funding.

References

- 1 D. Tichit and B. Coq, *Catal. Technol.*, 2003, **7**, 206.
- 2 J.-H. Choy, S.-J. Choi, J.-M. Oh and T. Park, *Appl. Clay Sci.*, 2007, **36**, 122.
- 3 A. Roy, C. Forano, J. P. Besse, in *Layered Double Hydroxides: Present and Future*, ed. V. Rives, Nova Sci, Pub., 2001, ch.1, pp. 1.
- 4 D. G. Evans, R. C. T. Slade, in *Layered Double Hydroxides, Structure and Bonding*, ed. X. Duan and D. G. Evans, Springer-Verlag, Berlin, 2006, vol. 119, ch.1, pp. 1-87.
- 5 D. G. Evans and X. Duan, *Chem. Commun.*, 2006, **5**, 485.
- 6 J. W. Boclair and P. S. Braterman, *Chem. Mater.*, 1999, **11**, 298.
- 7 G. Mascolo, *Appl. Clay Sci.*, 1995, **10**, 21.
- 8 K. J. Rao, B. Vaidyanathan, M. Ganguli and P. A. Ramakrishnan, *Chem. Mater.*, 1999, **11**, 882.
- 9 S. Kannan and R. V. Jasra, *J. Mater. Chem.*, 2000, **10**, 2311.
- 10 D. Tichit, A. Rolland, F. Prinetto, G. Fetter, M. D. Martinez-Ortiz, M. A. Valenzuela and P. Bosch, *J. Mater. Chem.*, 2002, **12**, 3832.
- 11 M. Z. bin Hussein, Z. Zainal, A. H. Yahaya; and L. M. Ping, *Dyes Pigm.*, 2004, **63**, 135.
- 12 M. Z. bin Hussein, Z. Zainal, A. H. Yahaya and D. W. V. Foo, *J. Mater. Synth. Process.*, 2002, **10**, 89.
- 13 M. Z. bin Hussein, Z. Zainal, T. Y. Hin and O. W. Tat, *J. Microwave Power Electromagnetic Energy*, 2001, **36**, 113.
- 14 Z. J. Zhang, B. Lan, L. R. Feng, S. J. Lu and F. L. Qiu, *J. Inorg. Mater.*, 2004, **19**, 761.

- 15 Z. Xu, Y. Wu, H. He and D. Jiang, *Stud. Surf. Sci. Catal.*, 1994, **90**, 279.
- 16 E. S. Martin and A. Pearson, *US Pat.*, 5 514 361, 1996.
- 17 H. C. Greenwell, W. Jones, D. N. Stamires, P. O'Connor and M. F. Brady, *Green Chem.*, 2006, **8**, 1067.
- 18 S. P. Newman, W. Jones, P. O'Connor and D. N. Stamires, *J. Mater. Chem.*, 2002, **12**, 153.
- 19 A. S. Bookin and V. A. Drits, *Clays Clay Miner.*, 1993, **41**, 551.
- 20 V. Radha, P. Vishnu Kamath and C. Shivakumara, *J. Phys. Chem. B*, 2007, **111**, 3411.
- 21 S. Mitchell, T. Biswick, W. Jones, G. Williams and D. O'Hare, *Green Chem.*, 2007, **9**, 373.
- 22 D. M. Roy, R. Roy and E. F. Osborn, *Am. J. Sci.*, 1953, **251**, 337.
- 23 Standard 5 ml vials commercially available from Biotage AB, <http://www.biotage.com>.
- 24 M. Belloto, B. Rebours, O. Clause, J. Lynch, D. Bazin and E. Elkaim, *J. Phys. Chem.*, 1996, **100**, 8527.
- 25 P. Benito, F. M. Labajos, J. Rocha and V. Rives, *Microporous Mesoporous Mater.*, 2006, **94**, 148.
- 26 M. Kaneyoshi and W. Jones, *J. Mater. Chem.*, 1999, **9**, 805.
- 27 H. M. Lim, M. R. Kang, S. C. Lee, S-H Lee and K. J. Kim, *Mater. Sci. Forum*, 2005, **492–493**, 743.
- 28 F. J. Berry, L. E. Smart, P. S. Sai-Prasad, N. Lingaiah and P. Kanta-Rao, *Appl. Catal., A*, 2000, **204**, 191.
- 29 E. Reguera, C. Diaz-Aguila and H. Yee-Madeira, *J. Mater. Sci.*, 2005, **40**, 5331.
- 30 R. Hoogenboom, R. M. Paulus, A. Pilotti and U. S. Schubert, *Macromol. Rapid Commun.*, 2006, **27**, 1556.
- 31 W. Sun and J. Li, *Mater. Lett.*, 2006, **60**, 1599.
- 32 Y. C. Chua and X. Lu, *Langmuir*, 2007, **23**, 1701.
- 33 M. Adachi-Pagano, C. Forano and J. P. Besse, *J. Mater. Chem.*, 2003, **13**, 1988.
- 34 L. Albiston, K. R. Franklin, E. Lee and J. B. A. F. Smeulders, *J. Mater. Chem.*, 1996, **6**, 871.

Calix[*n*]arene sulfonic acids bearing pendant aliphatic chains as recyclable surfactant-type Brønsted acid catalysts for allylic alkylation with allyl alcohols in water†

Yu-Liang Liu, Li Liu,* Yi-Lin Wang, Yu-Chun Han, Dong Wang* and Yong-Jun Chen

Received 13th December 2007, Accepted 22nd February 2008

First published as an Advance Article on the web 20th March 2008

DOI: 10.1039/b719278a

Calix[*n*]arene sulfonic acids bearing pendant aliphatic chains were developed as surfactant-type Brønsted acid catalysts for allylic alkylation with allyl alcohols in water. The allylic alkylation products of aromatic compounds were obtained in 60–94% yields. The water-solution of the surfactant-type catalyst was recovered by means of simple extraction of water-insoluble products and centrifugation, which can be reused in the next cycle directly. After recycling seven times, the catalytic activity for the aqueous reaction still remained at a high level (92–96% yields).

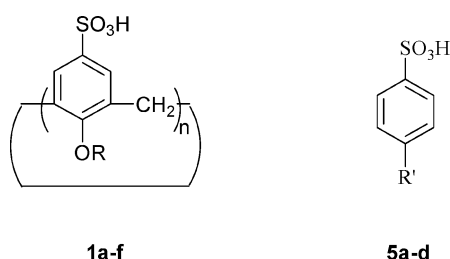
Introduction

Allylic alkylation is one of the most important carbon–carbon bond-forming reactions, which has been widely applied in the syntheses of many natural products and biologically active compounds.¹ Among them, allylic alkylation with allyl acetates or alcohols has attracted considerable attention. Although the hydroxyl group was considered an inefficient leaving group, the advantages of directly using allyl alcohol as an allylic reagent were noteworthy: no further functionalization was required for the activation of the hydroxyl group, and water was the sole byproduct of the reaction. Several catalysts suitable to the allylic alkylation reactions with allyl alcohols have been developed, including Brønsted acids,² Lewis acids,³ transition metal reagents⁴ and so on. On the other hand, there has been great progress in studying organic reactions in water, because of their synthetic efficiency and environmental friendliness.⁵ The development of the allylic alkylation with allyl alcohols in water for green chemistry should be very interesting to organic chemists. Oshima⁶ indicated that water enabled direct use of allyl alcohol for an allylic alkylation reaction in the presence of Pd(0) catalyst. In such a case, the reaction in water alone proceeded sluggishly and no reaction was observed in AcOEt, so that a water/AcOEt biphasic reaction system was employed. Kobayashi reported that the palladium-catalyzed substitutions of allyl alcohols could be carried out in water, but carboxylic acid was used as an activator.⁷ Most recently, it was reported that very similar reactions, the aqueous benzylation of aromatic and hetero-aromatic compounds with benzyl alcohols, could be catalyzed by a surfactant-type Brønsted acid (for example, dodecylbenzenesulfonic acid, DBSA).⁸ The use of a surfactant-type Brønsted acid as a catalyst played a crucial role for the catalytic

nucleophilic substitution in water. However, as indicated by Shimizu, the attempt to reuse the surfactant-type Brønsted acid (e.g. DBSA) in an aqueous reaction system failed.⁹ Considering the serious environmental problem caused by acid-pollution and the importance of recovering and reusing acid-catalysts in green synthesis,¹⁰ developing a recoverable and reusable surfactant-type Brønsted acid, which has efficient catalytic ability for the allylic alkylation in water, is still desirable. Herein, we would like to report the synthesis of calix[*n*]arene sulfonic acids bearing pendant aliphatic chains and their application as recoverable and reusable surfactant-type Brønsted acid catalysts to the allylation of aromatic and hetero-aromatic compounds with allyl alcohols in water.

Results and discussion

Previously, Shinkai and co-workers reported some water-soluble calixarene derivatives with surfactant activities.¹¹ The hexa-odum calix[6]arene sulfonates were found to be highly effective surfactants in aqueous Mukaiyama aldol reactions.¹² However, to our best knowledge, there have been few reports on the application of calixarene sulfonic acid as a Brønsted acid catalyst in aqueous organic reactions.⁹ Calix[*n*]arene sulfonic acid can be considered as a bunch of *p*-alkylbenzenesulfonic acids linked by methylene spacer, which provides a hydrophobic cavity. We envisioned that the use of these calixarene derivatives as surfactant-type acid catalysts should enhance the efficiency of catalytic allylic alkylation reaction in water and be helpful to overcome the difficulty in



Beijing National Laboratory for Molecular Science (BNLMS), Laboratory for Chemical Biology, Institute of Chemistry, Chinese Academy of Sciences, Beijing, 100080, China. E-mail: lliu@iccas.ac.cn; Fax: +8610-62554449; Tel: +8610-62554614

† Electronic supplementary information (ESI) available: Experimental procedure and characterization data. See DOI: 10.1039/b719278a

recycling surfactant-type Brønsted acid catalysts. Calix[*n*]arene derivatives (**1a–g**, *n* = 4, 6, 8) bearing a sulfonato group on the upper rim and the hydrophobic alkyl groups on the lower rim were synthesized based on the protocol by Shinkai.¹³ Initially, *para*-H-calix[6]arene-SO₃H (**1a**, *n* = 6, *R* = H) and *para*-Me-calix[6]arene-SO₃H (**1b**, *n* = 6, *R* = CH₃) as Brønsted acid catalysts (1 mol% H⁺) were employed in the reaction of indole **2a** with (*E*)-1,3-diphenylpropenol **3a** in water at room temperature for 18 h, respectively (Table 1, entries 1 and 2). The yields of the allylation product **4a** were low (23–26%). However, under the same reaction conditions, including the same catalyst loading (1 mol% H⁺), for the calix[6]arene-SO₃H bearing longer alkyl groups (**1c** and **1d**), the yields of **4a** increased noticeably to 74% and 83%, respectively (entries 3 and 4). The values of critical micelle concentration (cmc) of calix[*n*]arene-SO₃H (**1c–g**) were measured by means of microcalorimetry methods,¹⁴ which are listed in Table 1. Compared with **1a** and **1b**, the high catalytic abilities of **1c** and **1d** are attributed to the formation of micelles in the water in the course of the reaction. Meanwhile, the relatively small cmc values of **1c–g** indicated that the small amount of the catalyst was enough to form a micelle in water, *i.e.* surfactant catalyst loading could be reduced to a significant extent. However, when the alkyl group was dodecyl (**1e**), the yield of **4a** was decreased to 61% (entry 5). Based on Shinkai's suggestion,¹³ the reason was probably that **1e** behaved as a unimolecular micelle in water rather than forming a molecular aggregate. The size of the calix[*n*]arene cavity (*n* = 4 and 6) did not effect the yield of the reaction (entries 4 and 6), but in the case of **1g** (*n* = 8), the yield decreased slightly (entry 7), probably due to the formation of a bigger cavity, which had similar behavior to that of *p*-alkylbenzenesulfonic acid in water (entry 9).

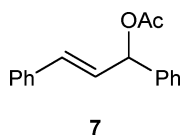
Under the condition of identical catalyst loading (1 mol% H⁺), the pH values of the aqueous solution of various catalysts

employed in the reaction are in the range of 2.7–3.4, except **1a** (Table 1). It was found that the yields of the reaction did not correlate with the acidity (pH) of the aqueous media containing sulfonic acid catalyst.

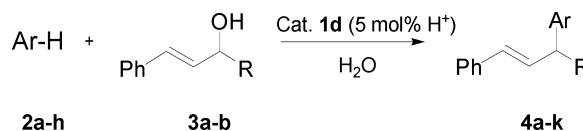
For comparison, *p*-toluenesulfonic acid (**5a**, TsOH) was used under the same reaction conditions. Although **5a** dissolves in water very well, the yield of **4a** is very poor, only 9.7% (entry 8). The use of polystyrene-supported sulfonic acid (**6**, PS-SO₃H) led the yield of **4a** to slightly increase to 49% (entry 12). The surfactant-type Brønsted acid (**5b**, DBSA) and **5d** could improve the yields of **4a** significantly (entries 9 and 11). In comparison of **5c** with **1c**, it can also be found that although they had the same pendant alkyl group (C₄H₉), calix[6]arene derivative **1c** exhibited higher catalytic ability, yields of **4a**: 74% vs. 45% (entry 3 and 10). In the absence of catalyst, no product was detected in the reaction system (entry 13).

In the summary of the above experimental results, it was suggested that the formation of micelles in water by using a surfactant-type catalyst played a crucial role in the catalytic allylic alkylation reactions with allyl alcohols in water. Surfactant-type calixarene sulfonic acid is favorable to form micelles in water even bearing shorter aliphatic chains. Moreover, the high catalytic efficiency could be reached by using a smaller amount of the catalyst.

On the other hand, allyl acetate (**7**) was used to react with **2a** in the presence of catalyst **1d** (1 mol% H⁺) in water, giving only 32% yield of alkylation product (**4a**). The use of water as a reaction media is of benefit to the sulfonic acid-catalyzed allylic alkylation with allyl alcohols.



Subsequently, various aromatic and hetero-aromatic compounds (**2a–h**) were employed to react with allylic substrate **3a** (*R* = Ph) in the presence of catalyst **1d** (5 mol% H⁺) at room temperature in water (Scheme 1), providing the alkylation products (**4a–h**) in good yields (70–94%) (Table 2). Furthermore, less activated allylic substrate **3b** (*R* = CH₃) was used in the surfactant-type sulfonic acid-catalyzed reaction with **2a–b** and **2h** in water. In order to obtain good yields, the reaction temperature should be increased to 40 °C for **3b**, however the poor regioselectivities were observed (*α*/*γ*: 0.83~1.3 : 1) (Table 2, entries 9–11).



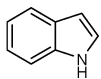
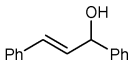
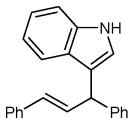
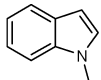
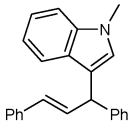
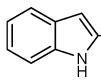
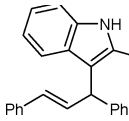
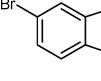
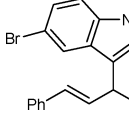
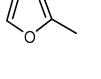
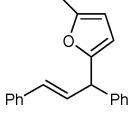
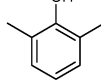
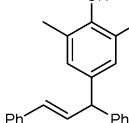
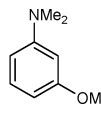
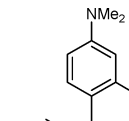
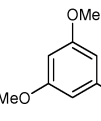
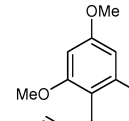
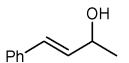
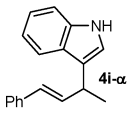
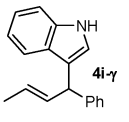
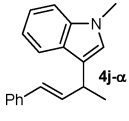
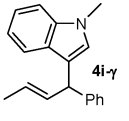
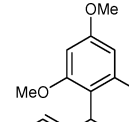
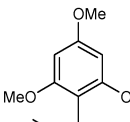
By selecting the reaction of **2b** with **3a** at room temperature in water as a model reaction, recycling experiments of the catalyst were performed. At first, **5b** (DBSA) was used in the reaction

Table 1 Screening of the catalysts based on the reaction of **2a** with **3a** in water^a

Entry	Catalyst	Yield ^b (%)	Cmc/nM	pK _a
1	1a , <i>n</i> = 6, <i>R</i> =H	23	—	5.80
2	1b , <i>n</i> = 6, <i>R</i> =CH ₃	26	—	2.78
3	1c , <i>n</i> = 6, <i>R</i> =C ₄ H ₉	74	0.014	2.96
4	1d , <i>n</i> = 6, <i>R</i> =C ₈ H ₁₇	83	0.069	3.11
5	1e , <i>n</i> = 6, <i>R</i> =C ₁₂ H ₂₅	61	0.027	3.40
6	1f , <i>n</i> = 4, <i>R</i> =C ₈ H ₁₇	82	0.012	3.18
7	1g , <i>n</i> = 8, <i>R</i> =C ₈ H ₁₇	74	0.021	3.10
8	5a , <i>R</i> '=H (TsOH)	10	—	2.90
9	5b , <i>R</i> '=C ₁₂ H ₂₅ (DBSA)	77	1.2	2.70
10	5c , <i>R</i> '=OC ₄ H ₉	45	36	2.92
11	5d , <i>R</i> '=OC ₈ H ₁₇	80	9.0	3.09
12	6 , PS-SO ₃ H (amberlyst-15)	49	—	3.10
13	None ^c	0 ^d	—	—

^a Catalyst loading: 1 mol% H⁺. ^b Isolated yield. ^c Without catalyst. ^d No product was detected.

Table 2 Calix[6]arene sulfonic acid-catalyzed allylic alkylation in water^a

Entry	Ar-H	Allylic alcohol	Temp/°C	Time/h	Product	Yield ^b (%)
1	2a 	3a 	r.t	6	 4a	83
2	2b 	3a	r.t	6	 4b	94
3	2c 	3a	r.t	2	 4c	70
4	2d 	3a	r.t	8	 4d	80
5	2e 	3a	r.t	3	 4e	81
6	2f 	3a	r.t	11	 4f	70
7	2g 	3a	r.t	12	 4g	71
8	2h 	3a	r.t	5	 4h	86
9	2a	3b 	40	6	 4i-α +  4i-γ (1.4 : 1)	60
10	2b	3b	40	24	 4j-α +  4j-γ (1.2 : 1)	86
11	2h	3b	40	24	 4k-α +  4k-γ (1.3 : 1)	94

^a Catalyst: **1d** (5 mol%). ^b Isolated yield.

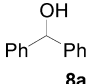
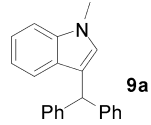
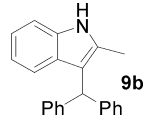
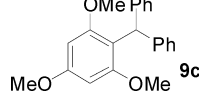
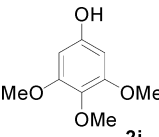
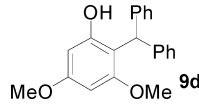
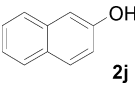
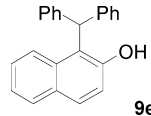
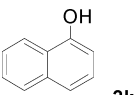
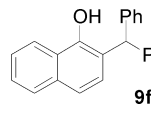
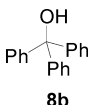
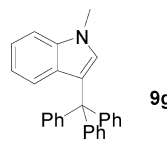
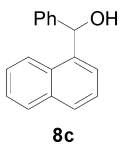
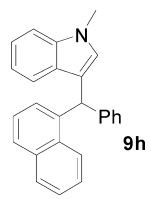
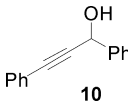
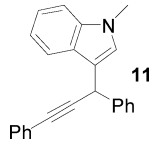
Table 3 Recycling of the calix[6]arene-SO₃H catalyst^a

Cycle	1	2	3	4	5	6	7
Time/h	6	6	6.5	6.5	6.5	7.5	7.5
Yield ^b (%)	94	96	95	93	92	94	93

^a The reaction of **2b** with **3a** in water at room temperature, catalyst **1d** (5 mol%). ^b Isolated yield.

to give the product **4b** at a yield of 80%.¹⁵ Unfortunately, after a second run, only trace of **4b** was detected on TLC. Similarly, the attempt to reuse the small molecule surfactant-type acid catalyst **5d** failed as well. To our delight, in the presence of catalyst **1d**, the reaction gave **4b** in 94% yield, even after seven cycles the yield of **4d** still remained at 93% (Table 3). The recycling procedure is very simple (Fig. 1). During the course of the reaction, an emulsion was formed (Fig. 1(a)). After

Table 4 Calix[6]arene-SO₃H catalyzed Friedel–Crafts alkylations in water^a

Entry	Ar-H	Alcohol	Time/h	Product	Yield ^b (%)
1	2b		48		95
2	2c	8a	24		77
3	2h	8a	38		82
4		8a	12		82
5		8a	24		75
6		8a	38		67
7	2b		18		94
8	2b		22		99
9	2b		48		69

^a catalyst:**1d** (5 mol% H⁺) reaction temperature: 80 °C. ^b isolated yield

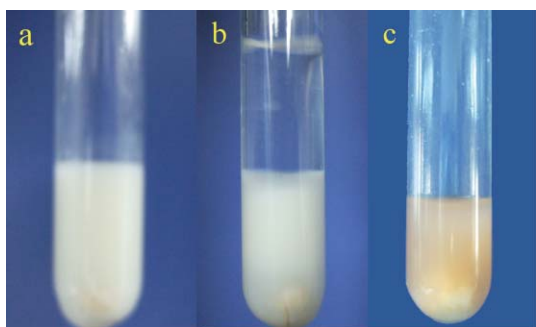
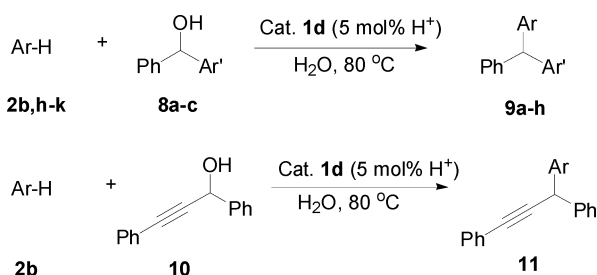


Fig. 1 The photos of recycling experiments (a) An emulsion system during the aqueous reaction. (b) A two-phase system after adding organic solvent, upper layer: a solution of the product in EtOAc, lower layer: an emulsion of the catalyst in water. (c) A water solution containing the catalyst for reuse.

the reaction completed, an organic solvent (ethyl acetate) was added to extract the water-insoluble product, and a two-phase system was generated, but the aqueous phase was found to still keep in emulative state (Fig. 1(b)). Through centrifugation, the two-phase system was separated more clearly. After the organic phase was removed, the obtained aqueous phase containing the catalyst (Fig. 1(c)) can be reused for the next run of the reaction directly. It was suggested that calixarene sulfonic acid would have poor solubility in aprotic organic solvent, such as ethyl acetate, ether and toluene. The phase separation, as well as recovery and reuse of the surfactant-type calix[*n*]arene sulfonic acid catalyst in water were performed. In contrast, the small molecule surfactant-type catalyst, such as DBSA, was able to dissolve in both water and organic solvent, leading to the strong loss of catalytic ability for the next aqueous reaction.

To examine the scope of the calixarene-SO₃H catalyst in aqueous reactions, the Friedel–Crafts alkylation with benzyl alcohols (**8a–c**) and propargyl alcohol (**10**) in the presence of catalyst **1d** (5 mol% H⁺) in water was carried out at 80 °C (Scheme 2). The aqueous reactions gave the corresponding products (**9a–h** and **11**) with good to excellent yields (Table 4). In comparison with allylic alcohols, the reactions with benzyl alcohols and propargyl alcohol need longer time and higher temperature.



Scheme 2

Conclusions

As a surfactant-type Brønsted acid catalyst, calix[*n*]arene sulfonic acid bearing aliphatic chains exhibited highly efficient catalytic ability for the allylic alkylation reactions with allyl

alcohols in water.‡ This kind of surfactant Brønsted acid catalyst can be recovered from an aqueous reaction system and reused many times without significant loss of catalytic ability. It provided an efficient and practical method to overcome the difficulties in recycling surfactant-type Brønsted acid catalysts from an aqueous reaction system.

Acknowledgements

We thank the National Natural Science Foundation of China and The Chinese Academy of Sciences for financial support.

References

- (a) For example, see: B. M. Trost and D. L. Van Vranken, *Chem. Rev.*, 1996, **96**, 395; (b) B. M. Trost and M. L. Crawley, *Chem. Rev.*, 2003, **103**, 2921; (c) M. Kimura, M. Futamata, R. Mukai and Y. Tamaru, *J. Am. Chem. Soc.*, 2005, **127**, 4592; (d) Y. Tamaru, *Eur. J. Org. Chem.*, 2005, 2647; (e) B. M. Trost and J. Quancard, *J. Am. Chem. Soc.*, 2006, **128**, 6314; (f) M. Bandini, A. Melloni, F. Piccinelli, R. Sinisi, S. Tommasi and A. Umami-Ronchi, *J. Am. Chem. Soc.*, 2006, **128**, 1424; (g) G. Helmchen, A. Dahnz, P. Dubon, M. Schelwies and R. Weihofen, *Chem. Commun.*, 2007, 675.
- (a) R. Sanz, A. Martinez, D. Miguel, J. M. Alvarez-Gutierrez and F. Rodriguez, *Adv. Synth. Catal.*, 2006, **348**, 1841; (b) R. Sanz, A. Martinez, J. M. Alvarez-Gutierrez and F. Rodriguez, *Eur. J. Org. Chem.*, 2006, 1383; (c) J. L. Bras and J. Muzart, *Tetrahedron*, 2007, **63**, 7942.
- (a) M. Yasuda, T. Somyo and A. Baba, *Angew. Chem., Int. Ed.*, 2006, **45**, 793; (b) M. Noji, Y. Konno and K. Ishii, *J. Org. Chem.*, 2007, **72**, 5151; (c) U. Jana, S. Biswas and S. Maiti, *Tetrahedron Lett.*, 2007, **48**, 4065; (d) J. S. Yadav, B. V. Subba Reddy, S. Aravind, G. G. K. S. Narayana Kumar and A. Srinivas Reddy, *Tetrahedron Lett.*, 2007, **48**, 6117; (e) U. Jana, S. Maiti and S. Biswas, *Tetrahedron Lett.*, 2007, **48**, 7160.
- (a) G. Onodera, H. Imajima, M. Yamanashi, Y. Nishibayashi, M. Hidai and S. Uemura, *Organometallics*, 2004, **23**, 5841; (b) B. M. Trost and J. Quancard, *J. Am. Chem. Soc.*, 2006, **128**, 6314; (c) J. Huang, L. Zhou and H. Jiang, *Angew. Chem., Int. Ed.*, 2006, **45**, 1945; (d) Y. Yokoyama, N. Takagi, H. Hikawa, S. Kaneko, N. Tsubaki and H. Okuno, *Adv. Synth. Catal.*, 2007, **349**, 662.
- (a) C.-J. Li, and T.-H. Chan, *Organic Reactions in Aqueous Media*, John Wiley, New York, USA, 1997; (b) P. A. Grieco, *Organic Synthesis in Water*, Blackie, Academic and Professional, London, UK, 1998; (c) A. Lubineau, and J. Auge, in *Modern Solvent in Organic Synthesis*, ed. P. Knochel, Springer-Verlag, Berlin, Heidelberg, 1999; (d) B. Cormils, and W. A. Hermann, *Aqueous-Phase Organometallic Catalysis*, Wiley-VCH, Weinheim, Germany, 2004; (e) C.-J. Li, and T.-H. Chan, *Comprehensive Organic Reactions in Aqueous Media*, Wiley-VCH, New York, USA, 2007.

‡ **Typical procedure for allylic alkylation** A mixture of indole **2a** (58.6 mg, 0.5 mmol), (*E*)-1,3-diphenylprop-2-en-1-ol **3a** (105.1 mg, 0.5 mmol) and **1d** (1.5 mg, 5 mol% H⁺) in water (2 mL) were stirred vigorously at room temperature for 18 h. The reaction mixture was extracted by ether (2 mL × 3), and the organic phase was collected, dried over anhydrous Na₂SO₄, and evaporated under reduced pressure to give the crude product, which was purified by flash chromatography on silica gel (eluent: petroleum ether : ethyl acetate = 12 : 1) to give a yellow solid **4a**¹⁶ (128.2 mg, 83% yield). **Typical procedure for recycling experiment** A mixture of *N*-methyl indole **2b** (63.9 μL, 0.5 mmol), **3a** (105 mg, 0.5 mmol) and **1d** (7.5 mg, 5 mol% H⁺) in water (2 mL) was stirred vigorously at room temperature for 6 h. When the reaction was finished by TLC detection, the reaction mixture was extracted by ethyl acetate (2 mL × 3), then two-phase was separated further by centrifugation. The organic phase was collected using a syringe, dried over anhydrous Na₂SO₄, and evaporated under reduced pressure to give a crude product, which was purified by flash chromatography on silica gel (eluent: petroleum ether : ethyl acetate = 12 : 1) to give a white solid **4b**¹⁷ (152 mg, 94% yield). The aqueous phase containing the catalyst was reused in the next cycle of aqueous reaction directly.

- 6 H. Kinoshita, H. Shinokubo and K. Oshima, *Org. Lett.*, 2004, **6**, 4085.
- 7 K. Manabe and S. Kobayashi, *Org. Lett.*, 2003, **5**, 3241.
- 8 S. Shirakawa and S. Kobayashi, *Org. Lett.*, 2007, **9**, 311.
- 9 For Shimizu's observation, see: S. Shimizu, N. Shimada and Y. Sasaki, *Green Chem.*, 2006, **8**, 608.
- 10 (a) P. T. Anastas and J. C. Wanner, *Green Chemistry: Theory and Practice*, Oxford University Press, New York, USA, 1998; (b) J. A. Gladysz, *Chem. Rev.*, 2002, **102**(10): special issue, *Recoverable catalysts and reagents*.
- 11 (a) S. Shinkai, H. Koreishi, S. Mori, T. Sone and O. Manabe, *Chem. Lett.*, 1985, 1033; (b) S. Shinkai, K. Araki and O. Manabe, *J. Chem. Soc., Chem. Commun.*, 1988, 187; (c) S. Shinkai, T. Arimura, K. Araki and H. Kawabata, *J. Chem. Soc., Perkin Trans. 1*, 1989, 2039.
- 12 (a) H.-T. Tian, Y.-J. Chen, D. Wang, C.-C. Zeng and C.-J. Li, *Tetrahedron Lett.*, 2000, **41**, 2529; (b) H.-T. Tian, Y.-J. Chen, D. Wang, Y.-P. Bu and C.-J. Li, *Tetrahedron Lett.*, 2000, **42**, 1803; (c) H.-T. Tian, H.-J. Li, Y.-J. Chen, D. Wang and C.-J. Li, *Ind. Eng. Chem. Res.*, 2002, **41**, 4523.
- 13 S. Shinkai, S. Mori, H. Koreishi, T. Takayuki and O. Manabe, *J. Am. Chem. Soc.*, 1986, **108**, 2409.
- 14 Y. Li, J. Reeve, Y. Wang, R. K. Thomas, J. Wang and H. Yan, *J. Phys. Chem. B*, 2005, **109**, 16070.
- 15 The same product 4b was obtained in 86% yield under the reaction conditions of 2b with 3a in water: 80 °C, 24 h, DBSA (10 mol%), see ref. 8.
- 16 T. Kajimoto, Y. Ishioka, T. Katoh and M. Node, *Bioorg. Med. Chem. Lett.*, 2006, **16**, 5736.
- 17 M. Westermaier and H. Mayr, *Org. Lett.*, 2006, **8**, 4791.

Commercially available molybdc compound-catalyzed ultra-deep desulfurization of fuels in ionic liquids

Wenshuai Zhu,^a Huaming Li,^{*a,b} Xue Jiang,^a Yongsheng Yan,^a Jidong Lu,^b Lining He^a and Jiexiang Xia^a

Received 28th January 2008, Accepted 6th March 2008

First published as an Advance Article on the web 25th March 2008

DOI: 10.1039/b801185k

A simple liquid–liquid extraction and catalytic oxidative desulfurization (ECODS) system composed of molybdc compound, 30% H₂O₂ and 1-butyl-3-methylimidazolium tetrafluoroborate ([bmim]BF₄) has been found suitable for the ultra-deep removal of dibenzothiophene (DBT) in model oil. The precatalyst of molybdc compound was oxidized with H₂O₂ to form peroxomolybdc compound, which was soluble in ionic liquid and dissolved in oil. The sulfur-containing compounds, such as benzothiophene (BT), DBT and 4,6-dimethyldibenzothiophene (4,6-DMDBT), in model oil were extracted into ionic liquid phase and oxidized to their corresponding sulfones by peroxomolybdc compound. In the case of the system containing model oil (DBT), H₂O₂, Na₂MoO₄·2H₂O and [bmim]BF₄, extraction and catalytic oxidation increased the sulfur removal to 99.0%, which was remarkably superior to mere solvent extraction with IL (13.6%) or catalytic oxidation without IL (4.1%). The desulfurization system could be recycled five times with very little decrease in activity.

Introduction

Ultra-deep desulfurization of transportation fuels is urgently needed as sulfur has brought forth great negative problems to engines and the environment. SO_x emission from automobile exhausts not only pollutes air greatly, but also irreversibly poisons the noble metal catalysts in automobiles. With more and more stringent regulatory constraints, it is a trend to achieve little-to-no sulfur fuels (S-content < 10 ppm).¹ In the conventional process, hydrodesulfurization (HDS) is used to remove thiols, sulfides and disulfides. However, owing to steric hindrance, it is difficult to remove some sulfur compounds such as dibenzothiophene (DBT) and its derivatives. In order to remove these compounds, severe operating conditions (*T* > 623 K, 30–100 bar) and large capital cost are needed.¹ Therefore, alternative desulfurization technologies have attracted wide attention.^{2–8}

Besides oxygen, hydrogen peroxide is the most economical and environmentally benign oxidant that might be used in desulfurization of fuels. More recently, oxidative desulfurization (ODS) with hydrogen peroxide combined with extraction is regarded as a promising strategy to achieve an ultra-low sulfur level.^{9–11} Organic sulfides can be oxidized selectively to sulfoxides and sulfones, which are then removed by polar extractants. The reported oxidative desulfurization systems include formic acid/H₂O₂,^{12,13} acetic acid/H₂O₂,¹⁴ polyoxometalate/H₂O₂,^{15–18} *etc.* Among these processes, polyoxometalate/H₂O₂ is considered as one of the most promising oxidative systems to deeply

remove organic sulfur. However, flammable and volatile organic compounds (VOCs) are usually employed as extractants, leading to further environmental and safety concerns.

Ionic liquids (ILs), as novel green solvents, have been extensively employed in green chemistry instead of organic solvents because of their low melting point, wide liquid range, negligible vapor pressure and good solubility characteristics, *etc.* The new approach for desulfurization of diesel fuels by extraction with ILs has been described.¹⁹ Many types of ILs have been attempted, such as [bmim]PF₆,^{19,20} [bmim]BF₄,^{19,20} [omim]BF₄,¹⁹ [bmim][CF₃SO₃],¹⁹ [omim][OCSO₄],¹⁹ [bmim]Cl/AlCl₃,¹⁹ [bmim]Cl/Cu₂Cl₂,²¹ [bmim]Cl/ZnCl₂,²² [bmim]Cl/SnCl₂,²² TMAC/AlCl₃,²³ [emim][EtSO₄],¹ [bmim][OCSO₄],¹ [hmim][Tf₂N],²⁴ [bmim][DBP],²⁵ [emim][DEP],²⁵ [BPy]BF₄.²⁶ However, the efficiency of sulfur removal has not been high, only in the range 10%–40%. Recently, it was shown that chemical oxidation in conjunction with IL extraction can increase the sulfur removal significantly. For instance, Wei²⁸ has reported that oxidation of DBT in water-immiscible [bmim]PF₆ resulted in a high oxidation rate and water-miscible [bmim]BF₄ led to a lower conversion. The oxidative desulfurization of fuels catalyzed by acidic ionic liquids [Hmin]BF₄²⁸ and [Hnmp]BF₄²⁹ in the presence of H₂O₂ has been investigated by the groups of Lu and Zhao, who found acidic ILs could decompose hydrogen peroxide to form hydroxyl radicals. The sulfur compounds are extracted into the IL phase and oxidized to their corresponding sulfones by the hydroxyl radicals. The results of these experiments indicated that the sulfur removal of DBT-containing model oil can reach more than 90%, which is superior to the simple extraction with IL. Based on the above summarizations, we conclude that polyoxometalate-catalyzed oxidation in conjunction with IL extraction can increase the sulfur removal significantly.

^aCollege of Chemistry and Chemical Engineering, Jiangsu University, 301 Xuefu Road, Zhenjiang, 212013, P. R. China

^bState Key Laboratory of Coal Combustion, Huazhong University of Science and Technology, Wuhan, 430074, P. R. China

Recently, we have successfully developed a system of [bmim]-BF₄ and [bmim]PF₆ doped with amphiphilic catalyst [WO(O₂)₂·Phen·H₂O] (Phen: 1, 10-phenanthroline monohydrate) for liquid–liquid extraction and catalytic oxidative desulfurization (ECODS).¹¹ Although the sulfur removal could reach 98.6%, too much H₂O₂ (O/S = 10/1) was consumed and the synthetic process of the catalyst was rather complicated. In addition, W-element was introduced into the oil phase owing to the use of amphiphilic catalyst. In this work, we employed commercially available molybdic compounds as catalysts and developed an ECODS system composed of 1-butyl-3-methylimidazolium tetrafluoroborate ([bmim]BF₄), H₂O₂ and catalysts such as Na₂MoO₄·2H₂O, H₂MoO₄, (NH₄)₆Mo₇O₂₄·4H₂O, H₃PMo₁₂O₄₀·13H₂O, (NH₄)₃PMo₁₂O₄₀·7H₂O and Na₃PMo₁₂O₄₀·7H₂O for deep removal of DBT in model oil. The ionic liquids [bmim]BF₄, 1-*n*-octyl-3-methylimidazolium tetrafluoroborate ([omim]BF₄), 1-butyl-3-methylimidazolium hexafluorophosphate ([bmim]PF₆), 1-*n*-octyl-3-methylimidazolium hexafluorophosphate ([omim]PF₆), 1-butyl-3-methylimidazolium trifluoroacetate ([bmim]TA) and 1-*n*-octyl-3-methylimidazolium trifluoroacetate ([omim]TA) doped with the catalyst were selected for the ECODS. Six ILs were immiscible with model oil, which not only served as extractants and reaction media but also stabilized hydrogen peroxide in the process of the reaction. DBT was extracted from the model oil and oxidized in the ionic liquid. These simple hydrophilic molybdic compounds not only possessed good catalytic activity but hardly contaminated the oil.

Results and discussion

Effect of different desulfurization systems on removal of DBT in *n*-octane

Three different desulfurization systems were conducted: extraction, extraction coupled with chemical oxidation and extraction coupled with catalytic oxidation. The results are listed in Table 1. Six ILs were immiscible with model oil, and the catalyst could dissolve in these ILs. However, aqueous hydrogen peroxide only dissolved in [bmim]BF₄, [bmim]TA and [omim]TA, and formed bi-phasic systems, in which the oil phase was the upper layer and IL phase, along with catalyst and oxidizing agent, was the lower layer. For [omim]BF₄, [bmim]PF₆ and [omim]PF₆, tri-

phasic systems were formed, in which the oil phase was the upper layer, aqueous hydrogen peroxide as oxidizing agent was in the middle and IL phase, along with catalyst, was the lowest layer.

When [bmim]BF₄ was used as extractant for DBT-containing model oil at 30 °C and 70 °C, the S-removal only reached 13.6% and 15.5% respectively. With addition of H₂O₂ in [bmim]BF₄, the S-removal of 31.5% was given after chemical oxidation. When Na₂MoO₄·2H₂O, H₂O₂ and IL were employed together, the removal of DBT increased sharply. This result indicated that IL played a significant role in the desulfurization system. In the case of the system comprising Na₂MoO₄·2H₂O, H₂O₂ and [bmim]BF₄, the sulfur content decreased from 1000 ppm to 10 ppm *via* extraction and catalytic oxidation, reaching 99.0% S-removal. However, the oxidative desulfurization system containing Na₂MoO₄·2H₂O and H₂O₂ only led to 4.1% S-removal in the absence of IL, which contributed to the decomposition of most hydrogen peroxide under 70 °C in the presence of Na₂MoO₄·2H₂O. Consequently, we concluded that IL not only served as an extractant and reaction media but also stabilized hydrogen peroxide at high temperature (70 °C), with Na₂MoO₄·2H₂O acting as catalyst. These experiments clearly demonstrated that a combination of catalytic oxidation and extraction in IL could deeply remove DBT from model oil, which was not only superior to the desulfurization system of H₂O₂/CH₃COOH/[bmim]BF₄,²⁷ but also comparable to our former work of H₂O₂/WO(O₂)₂·Phen·H₂O/[bmim]BF₄.¹¹ These results also indicated that the remarkable advantage of this process over the desulfurization of model oil by mere solvent extraction with IL or mere catalytic oxidation without IL. Similar trends were found in other ILs, which got the S-removal from 37.4% to 77.8% (Table 1, entry 2 to 6).

It may be pointed out that the nature of IL played an important role in S-removal. The desulfurization efficiency of [TA]⁻ anion-containing ILs was obviously inferior to [BF₄]⁻ and [PF₆]⁻ anion-containing ILs, which demonstrated [TA]⁻ may restrain the rate of oxidation of DBT. The efficiency of desulfurization was higher in water-miscible [bmim]BF₄ than that in water-immiscible [omim]BF₄, [bmim]PF₆ and [omim]PF₆ because of partitioning effects. Experimentally, a bi-phasic system (IL/oil) was formed in [bmim]BF₄, but a tri-phasic system (IL/H₂O₂/oil) was formed in [omim]BF₄, [bmim]PF₆ and [omim]PF₆.

Table 1 Comparison of different desulfurization systems of model diesel oil^a

Entry	Type of ILs	S-removal of different desulfurization system (%)				
		IL		IL + H ₂ O ₂	IL + Na ₂ MoO ₄ +H ₂ O ₂	Na ₂ MoO ₄ +H ₂ O ₂
		a	b			
1	[bmim]BF ₄	13.6	15.5	31.5	99.0	
2	[omim]BF ₄	18.0	21.2	35.0	67.6	
3	[bmim]PF ₆	11.1	14.6	39.2	69.8	
4	[omim]PF ₆	18.5	20.2	44.6	77.8	
5	[bmim]TA	12.9	15.0	30.5	49.0	
6	[omim]TA	17.0	20.5	32.1	37.4	
7	—					4.1

^a Model oil was prepared by dissolving DBT in *n*-octane to give solutions with an S-content of 1000 ppm. Reaction conditions: *T* = 70 °C, *t* = 3 h, model oil = 5 mL, IL = 1 mL, [*n*(DBT)/*n*(Catalyst)] = 20, [*n*(H₂O₂)/*n*(DBT)] = 4. a: The mixture was stirred at 30 °C for 15 min. b: The mixture was stirred at 70 °C for 3 h.

Effect of amount of catalyst on the removal of DBT

The desulfurization system containing $\text{Na}_2\text{MoO}_4 \cdot 2\text{H}_2\text{O}$, H_2O_2 and $[\text{bmim}]\text{BF}_4$ was used to investigate the effect of different amounts of catalyst. Fig. 1 displays the content of DBT remaining in *n*-octane vs. amount of catalyst. DBT/catalyst molar ratios of 100 : 1, 60 : 1, 40 : 1 and 20 : 1 were plotted. Increasing the amount of $\text{Na}_2\text{MoO}_4 \cdot 2\text{H}_2\text{O}$ in the IL resulted in an increase of S-removal. As can be seen, when the DBT and catalyst ratio was changed from 100 : 1 to 20 : 1, sulfur content decreased from 400 ppm to 50 ppm at 60 °C. These results indicated that the amount of catalyst in the reaction had a vital effect on DBT removal.

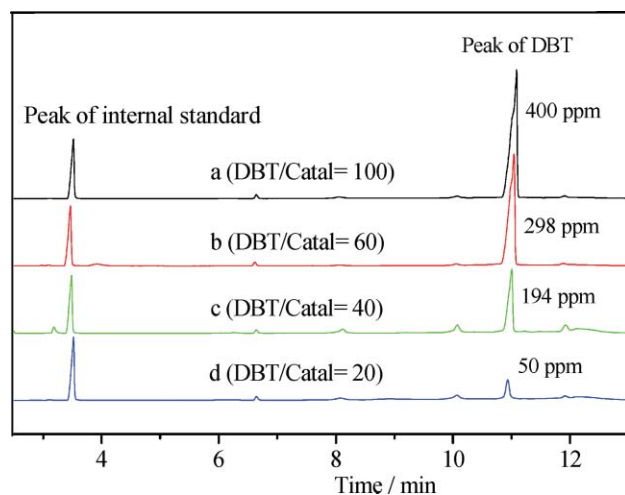


Fig. 1 Effect of amount of catalyst on the removal of DBT (GC-FID chromatograms). *Reaction conditions:* model oil = 5 mL, IL = 1 mL, $[\text{n}(\text{H}_2\text{O}_2)/\text{n}(\text{DBT}) = 4]$, $t = 3$ h, $T = 60$ °C.

Effect of the $\text{H}_2\text{O}_2/\text{DBT}$ molar ratios on the removal of DBT

To investigate the effect of the amount of oxidizing agent and reaction temperature on the oxidative properties, different $\text{H}_2\text{O}_2/\text{sulfur}$ (O/S) molar ratios on the removal of DBT at different temperatures are given in Fig. 2. O/S molar ratios of 2 : 1, 3 : 1, 4 : 1, 5 : 1 and 6 : 1 are plotted. As can be seen, when the O/S molar ratio was increased from 2 : 1 to 6 : 1, DBT removal increased at different temperatures. According to the stoichiometric reaction, 2 mol of hydrogen peroxide are consumed for oxidation of 1 mol of DBT to DBT sulfone (DBTO_2). It is noteworthy that there was a competition between the decomposition of hydrogen peroxide and DBT oxidation reaction. With stoichiometric amount of H_2O_2 , the S-removal at different temperatures followed the order 70 °C > 60 °C > 50 °C > 80 °C. When the O/S molar ratio was increased to 3, the S-removal followed a new order of 70 °C > 80 °C > 60 °C > 50 °C. These findings demonstrated the higher the reaction temperature was, the faster the oxidation rate of DBT and the decomposition rate of hydrogen peroxide were. With a ratio of O/S < 4, the sulfur removal was lower at 80 °C than at 70 °C because decomposition of hydrogen peroxide was prominent at higher temperature. When O/S ratio was above 4, the S-removal followed the order of 80 °C > 70 °C > 60 °C >

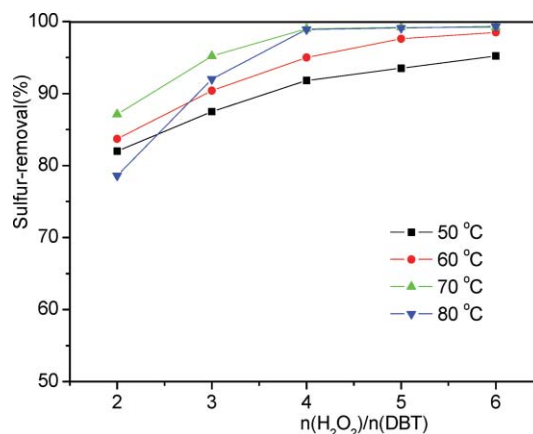


Fig. 2 Effect of the $\text{H}_2\text{O}_2/\text{DBT}$ molar ratios on the removal of DBT. *Reaction conditions:* model oil = 5 mL, IL = 1 mL, $[\text{n}(\text{DBT})/\text{n}(\text{Catalyst}) = 20]$, $t = 3$ h.

50 °C. These results also indicated the optimal O/S molar ratio was 4 at 70 °C.

Effect of time and temperature on the removal of DBT

The desulfurization system containing $\text{Na}_2\text{MoO}_4 \cdot 2\text{H}_2\text{O}$, H_2O_2 and $[\text{bmim}]\text{BF}_4$ was used to investigate the effect of various reaction time and temperatures. Fig. 3 displays S-removal of DBT in *n*-octane vs. reaction time at various temperatures. The data at time zero reflected the ability of $[\text{bmim}]\text{BF}_4$ to extract DBT from *n*-octane at room temperature. The sulfur content of the model oil decreased from its original value of 1000 ppm to 864 ppm. After a combination of extraction and catalytic oxidation, DBT was oxidized in the IL phase after it was extracted from *n*-octane. So a continuous decrease in the concentration of DBT in *n*-octane was observed at various temperatures. The higher the reaction temperature was, the faster the oxidation rate of DBT was. Sulfur removal reached 99.0% at 70 °C in 3 h, and 95.0%, 92.8% and 92.0% at 60, 50 and 40 °C, respectively.

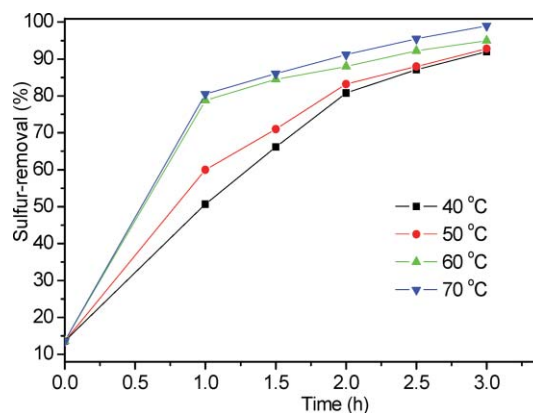


Fig. 3 Sulfur-removal after oxidation with $\text{Na}_2\text{MoO}_4 \cdot 2\text{H}_2\text{O}$ as catalyst in $[\text{bmim}]\text{BF}_4$ vs. reaction time at various temperatures. *Reaction conditions:* model oil = 5 mL, IL = 1 mL, $[\text{n}(\text{DBT})/\text{n}(\text{Catalyst}) = 20]$, $[\text{n}(\text{H}_2\text{O}_2)/\text{n}(\text{DBT}) = 4]$.

Table 2 The reactivity of different Mo-species catalysts for desulfurization^a

Entry	Catalyst	S-removal (%)	
		Without IL	Addition of IL
1	Na ₂ MoO ₄ ·2H ₂ O	4.1	99.0
2	H ₂ MoO ₄	18.6	94.2
3	(NH ₄) ₆ Mo ₇ O ₂₄ ·4H ₂ O	3.6	98.4
4	H ₃ PMo ₁₂ O ₄₀ ·13H ₂ O	49.7	92.6
5	(NH ₄) ₃ PMo ₁₂ O ₄₀ ·7H ₂ O	6.5	97.9
6	Na ₃ PMo ₁₂ O ₄₀ ·7H ₂ O	7.0	98.7

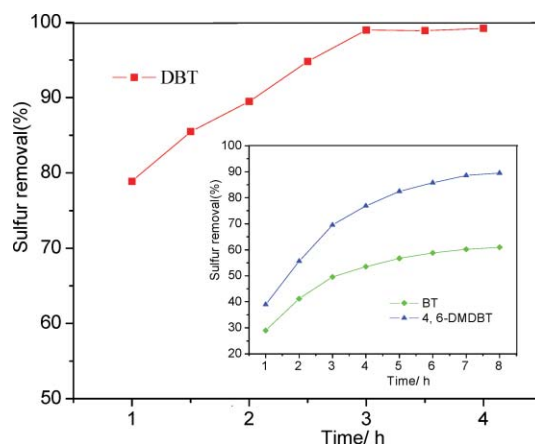
^a Reaction conditions: $T = 70\text{ }^{\circ}\text{C}$, $t = 3\text{ h}$, model oil = 5 mL, IL = 1 mL, $[n(\text{DBT})/n(\text{Catalyst}) = 20]$, $[n(\text{H}_2\text{O}_2)/n(\text{DBT}) = 4]$.

Influence of the different molybdc compounds

To compare the reactivity of the different Mo-species catalysts, the oxidation of DBT was carried out under the same reaction conditions. The results in Table 2 indicated the remarkable advantage of ECODS with IL process over the desulfurization by catalytic oxidation without IL. In the absence of IL, the S-removal was only 4.1% to 49.7%. With addition of IL, the S-removal increased sharply, reaching 92.6% to 99.0%. Comparing several molybdc compounds in oxidative system without IL, it was found that acids such as H₂MoO₄ and H₃PMo₁₂O₄₀·13H₂O reached a higher S-removal than salts. The cause of this phenomena lay in that acids (lower pH) could make better use of hydrogen peroxide among Mo-species catalysts. However, salts enabled quicker decomposition of hydrogen peroxide. With addition of IL, the oxidation efficiency was different. Salts such as Na₂MoO₄·2H₂O, (NH₄)₆Mo₇O₂₄·4H₂O, (NH₄)₃PMo₁₂O₄₀·7H₂O and Na₃PMo₁₂O₄₀·7H₂O yielded higher S-removal than acids. These results indicated that higher electrolyte strength of catalyst may contribute to better reactivity in IL.

Influence of the different substrates

To study the effect of the Na₂MoO₄·2H₂O in [bmim]BF₄ on the different sulfur compounds, the oxidation of three model sulfur compounds such as benzothiophene (BT), DBT and 4,6-dimethyldibenzothiophene (4,6-DMDBT) was carried out under the same conditions. As shown in Fig. 4, with the same reaction time, the S-removal through ECODS decreased in the order DBT > 4,6-DMDBT > BT. This order agreed well with the system of polyoxometalates/AcOH/H₂O₂.³⁰ The electron density on the sulfur atom on BT is significantly lower, leading to the lowest reactivity to BT. For DBT and 4,6-DMDBT, the electron density on the sulfur of the former is 5.756, as much as the latter (5.760).³⁰ Therefore, reactivity was mainly affected by the steric hindrance of the methyl groups, which became an obstacle for the approach of the sulfur atom to the catalytic active species in IL. The removal of BT, DBT and 4,6-DMDBT was 29.0%, 78.9% and 38.9% after 1 h, respectively. In the case of DBT, the sulfur removal could reach 99.0% in 3 h. However, the result hardly continued improving after 3 h. For BT and 4,6-DMDBT, 49.6% and 69.5% S-removal were achieved in 3 h and the results continue increasing after 3 h. In this experiment, the sulfur removal of BT and 4,6-DMDBT could reach 61.0% and 89.5% in 8 h, respectively.

**Fig. 4** Different substrates in the process of ECODS with Na₂MoO₄·2H₂O as catalyst. Reaction conditions: $T = 70\text{ }^{\circ}\text{C}$, model oil = 5 mL, [bmim]BF₄ = 1 mL, $[n(\text{S})/n(\text{Catalyst}) = 20]$, $[n(\text{H}_2\text{O}_2)/n(\text{S}) = 4]$.**Table 3** Recycle of [bmim]BF₄ containing Na₂MoO₄·2H₂O

Cycle	Sulfur removal (%)	
	IL (1 mL)	IL (3 mL)
1	99.0	97.4
2	98.2	98.2
3	97.5	98.0
4	93.8	97.6
5	90.0	97.3

$T = 70\text{ }^{\circ}\text{C}$, $t = 3\text{ h}$, model oil = 5 mL, $[n(\text{DBT})/n(\text{Catalyst}) = 20]$, $[n(\text{H}_2\text{O}_2)/n(\text{DBT}) = 4]$.

Effect of recycling of ionic liquid

The recycling of ECODS system for [bmim]BF₄ containing Na₂MoO₄·2H₂O and H₂O₂ was investigated in removal of DBT in model oil. The data in Table 3 indicated that catalytic systems could be recycled five times with an unnoticeable decrease in activity using 3 mL IL. However, the reactivity decreased from 99.0% to 90.0% after the recycling of the catalytic system for five times with 1 mL IL. According to our observation, more and more precipitation was produced after recycling for three times using 1 mL IL, which led to a decrease in activity in next run.

The determination of Mo-content in model oil

To investigate whether the metal catalyst was leached into the oil phase, the Mo-content determination in oil sample has been carried out by atomic emission spectrometry with inductively coupled plasma (ICP-OES). The results are listed in Table 4. For Na₂MoO₄·2H₂O, the Mo-content was 1.2 mg L⁻¹ in oil phase. The proportion of catalyst leached into the oil phase was 0.9% in the case of the [bmim]BF₄/catalyst/H₂O₂ system. However, this oil phase was washed by de-ionized water (10 mL × 2) and the Mo-content in oil decreased to zero. The Mo-content of other molybdc compounds in oil was very low as well. The results were different from those of the amphiphilic catalyst WO(O₂)₂·Phen·H₂O and MoO(O₂)₂·Phen, whose metal contents were 12.0 mg L⁻¹ and 12.5 mg L⁻¹ in oil. Moreover, after the oil phase was washed by de-ionized water (10 mL × 2), the metal-content in oil only decreased to a half.

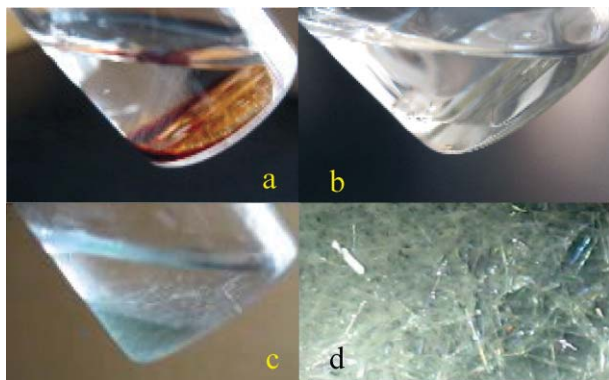
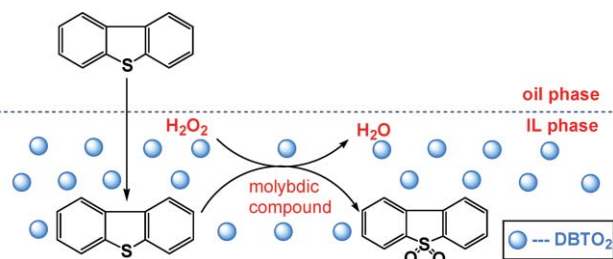
Table 4 Mo-content in model oil^a

Entry	Catalyst	Mo-content in oil/mg L ⁻¹
1	Na ₂ MoO ₄ ·2H ₂ O	1.2
2	H ₂ MoO ₄	0.5
3	(NH ₄) ₆ Mo ₇ O ₂₄ ·4H ₂ O	0.3
4	H ₃ PMo ₁₂ O ₄₀ ·24H ₂ O	0.9
5	(NH ₄) ₃ PMo ₁₂ O ₄₀ ·7H ₂ O	0.4
6	Na ₃ PMo ₁₂ O ₄₀ ·7H ₂ O	1.4
7	WO(O ₂) ₂ ·Phen·H ₂ O ¹¹	12.0
8	MoO(O ₂) ₂ ·Phen ¹¹	12.5

^a Model oil was prepared by dissolving DBT in *n*-octane to give solutions with S-content 1000 ppm. Reaction conditions: $T = 70\text{ }^{\circ}\text{C}$, $t = 3\text{ h}$, model oil = 5 mL, IL = 1 mL, $[n(\text{DBT})/n(\text{Catalyst}) = 20]$, $[n(\text{H}_2\text{O}_2)/n(\text{DBT}) = 4]$.

The process and mechanism of ECODS

DBT was chosen as a sulfur compound representative of those present in fuel. The extraction and catalytic oxidation desulfurization system for [bmim]BF₄ containing Na₂MoO₄·2H₂O and H₂O₂ was selected as a research model. Ionic liquid was immiscible with model oil, so formed a bi-phasic system. As for clarifying the process of oxidation, the photos of different desulfurization systems were taken (Fig. 5). The oxidative desulfurization system containing Na₂MoO₄·2H₂O and H₂O₂ (Fig. 5a) led to rather low sulfur removal in the absence of IL, which indicated that the oxidation hardly took place in oil phase. After addition of IL, the removal of sulfur increased sharply, which demonstrated that organic sulfur was oxidized in IL phase (Fig. 5b and c). The precatalyst of Na₂MoO₄·2H₂O was oxidized with H₂O₂ to form peroxomolybdic species Na₂[MoO(O₂)₂(OH)₂], which was soluble in ionic liquid. The sulfur-containing compounds in the model oil were extracted into IL phase and oxidized to their corresponding sulfones by the peroxomolybdic compound. A possible extraction and catalytic oxidation circle of ultra-deep desulfurization was given in Fig. 6. DBT first entered the IL phase and then was selectively oxidized to DBTO₂ (Fig. 5d). The sulfone accumulated in IL and could be easily separated from IL by centrifugation. Thereby, organic sulfur was removed from the model oil. In this way, ultra-deep desulfurization can be achieved.

**Fig. 5** Photos of different desulfurization systems.**Fig. 6** Suggested extraction and catalytic oxidation circle of ultra-deep desulfurization.

Conclusion

In this paper, commercially available molybdic compounds was dissolved in ILs ([bmim]BF₄, [omim]BF₄, [bmim]PF₆, [omim]PF₆, [bmim]TA and [omim]TA) to oxidize BT, DBT and 4,6-DMDBT with hydrogen peroxide for deep desulfurization under moderate conditions. The S-removal of DBT-containing model oil in [bmim]BF₄ could reach 99.0% at 70 °C for 3 h, which was the remarkable advantage of this process over the desulfurization by mere solvent extraction with IL or catalytic oxidation without IL. Moreover, the catalysts hardly dissolved in oil. The catalytic oxidation system containing Na₂MoO₄·2H₂O, H₂O₂ and [bmim]BF₄ could be recycled five times without a significant decrease in activity and oxidized sulfur could be reclaimed by centrifugation. The worldwide chemical industry is directing extensive efforts toward the efficient production of ILs, which will develop a simple, safe, reproducible and environmentally benign post-treatment to the traditional HDS for ultra-deep desulfurization.

Experimental

Preparation of ionic liquids and model oil

The ionic liquids [bmim]BF₄, [omim]BF₄, [bmim]PF₆, [omim]PF₆, [bmim]TA and [omim]TA were synthesized as mentioned in the literature procedure.^{31,32} Model oil was prepared by dissolving DBT, BT and 4, 6-DMDBT in *n*-octane to give a corresponding sulfur content of 1000, 1000 and 500 ppm.

Catalytic oxidative desulfurization of model oil

The oxidative desulfurization experiments were carried out in a home-made 40 mL two-necked flask. The mixture, containing 5 mL of model oil, 0.064 mL of 30 wt% H₂O₂ [$n(\text{H}_2\text{O}_2)/n(\text{DBT}) = 4$], 1 mL of IL and catalyst [$n(\text{S})/n(\text{Mo}) = 20$], was stirred vigorously at 70 °C for 3 h. After reaction was completed, the upper phase (model oil) was withdrawn and analyzed by gas chromatography, with nitrobenzene as internal standard, coupled with a flame ionization detector (GC-FID). A 15 m × 0.32 mm inner diameter × 1.0 μm film thickness SE-54 capillary column was used for separation.

Recycling of ionic liquid and reclamation of DBTO₂

At the end of each run, the IL phase (under-layer) was separated from the model oil phase and distilled in an oil-bath at 110 °C for 2 hours until H₂O₂ was removed entirely. The DBTO₂ and catalyst were not removed from the IL. The fresh H₂O₂ and

model oil were introduced for the next reaction under the same conditions as described above. By this procedure, the DBTO₂ accumulated in the IL phase in successive runs. After the last run, the IL phase was cooled at room temperature and the DBTO₂ precipitated from IL. The sulfone was reclaimed from IL by centrifugation.

Acknowledgements

This work was financially supported by the National Nature Science Foundation of China (No. 20676057, 20777029) and Jiangsu University Scientific Research Funding (No. 04JDG044).

References

- J. Esser, P. Wasserscheid and A. Jess, *Green Chem.*, 2004, **6**, 316.
- J. M. Campos-Martin, M. C. Capel-Sanchez and J. L. G. Fierro, *Green Chem.*, 2004, **6**, 557.
- C. Li, Z. X. Jiang, J. B. Gao, Y. X. Yang, S. J. Wang, F. P. Tian, F. X. Sun, X. P. Sun, P. L. Ying and C. R. Han, *Chem.–Eur. J.*, 2004, **10**, 2277.
- A. J. Hernandez-Maldonado and R. T. Yang, *Catal. Rev. Sci. Eng.*, 2004, **46**, 111.
- I. V. Babich and J. A. Moulijn, *Fuel*, 2003, **82**, 607.
- C. S. Song, *Catal. Today*, 2003, **86**, 211.
- E. Ito and J. A. R. Van Veen, *Catal. Today*, 2006, **116**, 446.
- H. Rang, J. Kann and V. Oja, *Oil Shale*, 2006, **23**, 164.
- L. F. Ramirez-Verduzco, E. Torres-Garcia, R. Gomez-Quintana, V. Gonzalez-Pena and F. Murrieta-Guevara, *Catal. Today*, 2004, **98**, 289.
- H. Y. Lü, J. B. Gao, Z. X. Jiang, F. Jing, Y. X. Yang, G. Wang and C. Li, *J. Catal.*, 2006, **239**, 369.
- W. S. Zhu, H. M. Li, X. Jiang, Y. S. Yan, J. D. Lu and J. X. Xia, *Energy Fuels*, 2007, **21**, 2514.
- S. Otsuki, T. Nonaka, N. Takashima, W. H. Qian, A. Ishihara, T. Imai and T. Kabe, *Energy Fuels*, 2000, **14**, 1232.
- G. X. Yu, S. X. Lu, H. Chen and Z. N. Zhu, *Energy Fuels*, 2005, **19**, 447.
- K. Yazu, M. Makino and K. Ukegawa, *Chem. Lett.*, 2004, **33**, 1306.
- D. Huang, Z. Zhai, Y. C. Lu, L. M. Yang and G. S. Luo, *Ind. Eng. Chem. Res.*, 2007, **46**, 1447.
- F. Al-Shahrani, T. Xiao, S. A. Llewellyn, S. Barri, Z. Jiang, H. Shi, G. Martinie and M. L. H. Green, *Appl. Catal., B*, 2007, **73**, 311.
- J. B. Gao, S. G. Wang, Z. X. Jiang, H. Y. Lu, Y. X. Yang, F. Jing and C. Li, *J. Mol. Catal. A: Chem.*, 2006, **258**, 261.
- M. Te, C. Fairbridge and Z. Ring, *Appl. Catal., A*, 2001, **219**, 267.
- A. Bosmann, L. Datsevich, A. Jess, A. Lauter, C. Schmitz, and P. Wasserscheid, *Chem. Commun.*, 2001, 2494.
- S. G. Zhang and Z. C. Zhang, *Green Chem.*, 2002, **4**, 376.
- C. P. Huang, B. H. Chen and J. Zhang, *Energy Fuels*, 2004, **18**, 1862.
- C. Z. Zhang, C. P. Huang, J. W. Li and C. Z. Qiao, *Chin. Chem. Res.*, 2005, **16**, 23.
- S. G. Zhang, Q. L. Zhang and Z. C. Zhang, *Ind. Eng. Chem. Res.*, 2004, **43**, 614.
- J. Planeta, P. Karasek and M. Roth, *Green Chem.*, 2006, **8**, 70.
- Y. Nie, C. X. Li, A. J. Sun, H. Meng and Z. H. Wang, *Energy Fuels*, 2006, **20**, 2083.
- J. L. Wang, D. S. Zhao, E. P. Zhou and Z. J. Dong, *Fuel Chem. Technol.*, 2007, **35**, 293.
- W. H. Lo, H. Y. Yang and G. T. Wei, *Green Chem.*, 2003, **5**, 639.
- L. Lu, S. F. Cheng, J. B. Gao, G. H. Gao and M. Y. He, *Energy Fuels*, 2007, **21**, 383.
- D. S. Zhao, J. L. Wang and E. P. Zhou, *Green Chem.*, 2007, **11**, 1219.
- C. Komintarachat and W. Trakarnpruk, *Ind. Eng. Chem. Res.*, 2006, **45**, 1853.
- J. G. Huddleston, A. E. Visser, W. M. Reichert, H. D. Willauer, G. A. Broker and R. D. Rogers, *Green Chem.*, 2001, **3**, 156.
- P. Bonhote, A. P. Dias, N. Papageorgiou, K. Kalyanasundaram and M. Gratzel, *Inorg. Chem.*, 1996, **35**, 1168.

Stereoselective oxidation of *R*-(+)-limonene by chloroperoxidase from *Caldariomyces fumago*

Sergio Águila,^a Rafael Vazquez-Duhalt,^{*b} Raunel Tinoco,^b Manuel Rivera,^b Gina Pecchi^a and Joel B. Alderete^a

Received 2nd January 2008, Accepted 2nd April 2008

First published as an Advance Article on the web 1st May 2008

DOI: 10.1039/b719992a

The oxidation of *R*-(+)-limonene by chloroperoxidase (CPO) from *Caldariomyces fumago* is reported. The reaction was performed in 60 mM phosphate buffer at pH 3.0 and 6.0, and in the absence and in the presence of chloride ions. In the absence of chloride ions, at both pH values, the reaction was regio and stereoselective with a diastomeric excess (*de*) >99% of (1*S*,2*S*)-4*R*-limonene-1,2-diol. On the other hand, when the reaction was carried out in the presence of chloride ions an enhancement in the reaction rate was observed, maintaining the regioselectivity, but not the stereoselectivity (*de* <5.4). The reaction products under these conditions were identified as (1*S*,2*S*)-4*R*-limonene-1,2-diol and (1*R*,2*R*)-4*R*-limonene-1,2-diol. It seems that in the absence of chloride ions the stereoselectivity is determined by stereospecific interaction of limonene with CPO active site, as supported by docking analysis, while in the presence of potassium chloride the limonene oxidation also occurs by the produced hypochlorite without stereoselectivity.

Introduction

Biocatalysis has been well recognized, for many years, as an excellent synthetic strategy for pharmacology,¹ food industry,² fine chemicals,³ and biofuels production,⁴ as well as for bioremediation.⁵ Doubtless, enzymatic transformations are an attractive alternative to the conventional homogeneous and heterogeneous catalytic processes, due to that their chemo-, regio- and stereospecificities, and they are a fundamental part of green chemistry.

Fragrances production is an interesting application field for biocatalysis. Fragrances, flavors and other organic products could be obtained by the enzymatic modification of natural compounds. The market recognizes when these products are produced by an environmentally friendly process, compared with those obtained by conventional chemical methods,⁶ having a higher market value. For fragrance or flavor production, several studies on terpene modifications have been performed, including biotechnological modifications of monoterpenoid compounds.⁷ Enzymatic processes are considered natural processes to obtain flavor products.⁸

The microbiological modification of the *R*-(+)-limonene has been widely studied. Bacteria, fungi and yeast have been used for the biotransformation, obtaining different products, such as carveol, carvone, epoxide derivatives and diol derivatives.⁹ In spite of the high regioselectivity of these biotransformations, the stereoselectivity is much lower. On the opposite,

enzymatic reactions are cleaner and show higher stereospecificity, when compared with whole cell transformations. Lipases have been used in the esterification and transesterification of monoterpenes,¹⁰ and hydroxylases in the hydroxylation of monoterpenes.⁸ Enzymatic oxidation of *R*-(+)-limonene by cytochrome P450 monooxygenases family has been studied,¹¹ in which only perillyl alcohol was obtained. Monoterpene transformation has been also performed by peroxidases.^{12,13}

Chloroperoxidase (CPO) from *Caldariomyces fumago* catalyzes different reactions such as hydroxylation and epoxidation of olefins with high yields and enantiomeric excess (*ee*).^{14–16} Oxygen transfer to carbon–carbon double bonds catalyzed by CPO has been investigated on a broad range of allylic cyclic mono-olefins.^{14,17} The effects of chain length, double bond position, substituted groups and *cis/trans*-stereochemistry on the enantioselectivity and reactivity of this enzyme have been discussed in mechanistic terms.¹⁴

In this work, the biocatalytic oxidation of *R*-(+)-limonene by CPO from *C. fumago* is studied. The effects of pH and the presence of chloride ions on the regio- and stereoselectivities of this reaction were determined.

Results and discussion

The oxidation of *R*-(+)-limonene by CPO in the presence of hydrogen peroxide and chloride ions was assayed and the reaction products were analyzed by GC-MS. Contrary to expected results, no epoxy derivatives could be found. The chromatogram showed the production of only two products, a mixture of diastomeric diols, **4** and **5** (Fig. 1). To corroborate the chemical nature of the products, 5 mL reactions were performed and the products were separated and collected by preparative

^aFacultad de Ciencias Químicas, Casilla 160-C, Universidad de Concepción, Concepción, Chile

^bInstituto de Biotecnología UNAM, Apartado Postal 510-3, Cuernavaca, Mor., 62210, México. E-mail: vazqduh@ibt.unam.mx; Fax: +(52) 777 317 2388

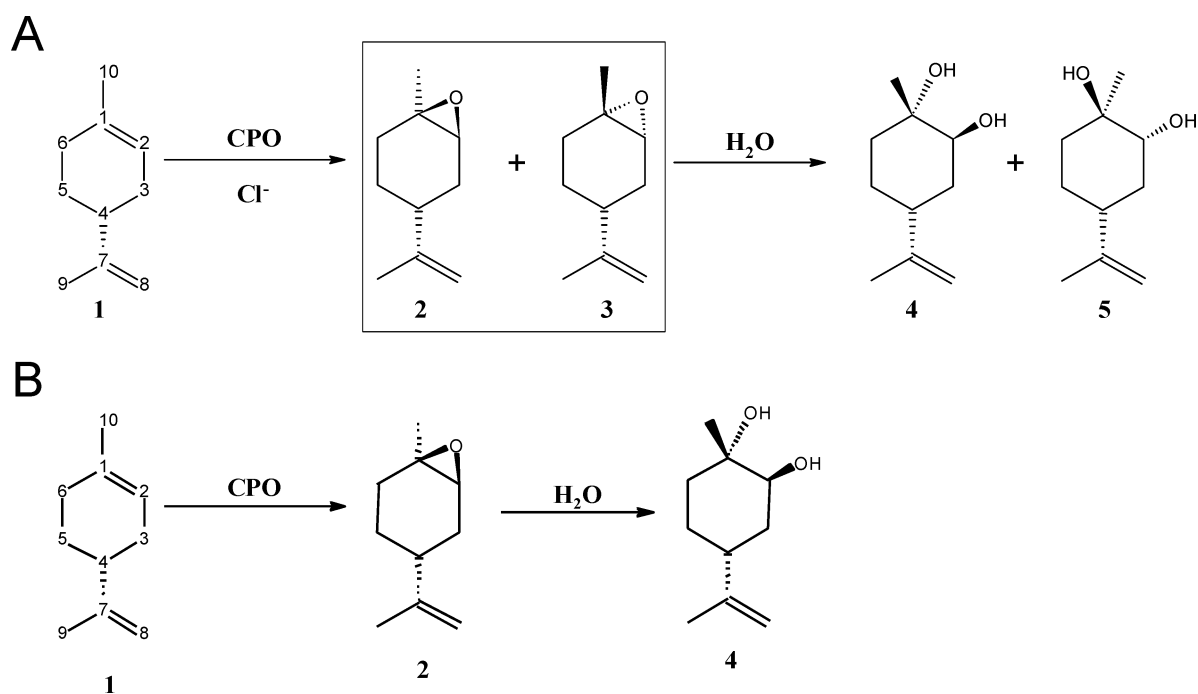


Fig. 1 Reaction products of oxidation of *R*-(+)-limonene. (A) In the presence of KCl and (B) in the absence of KCl.

HPLC. The products of the reaction 1*S*,2*S*,4*R*-limonene-1,2-diol **4** and 1*R*,2*R*,4*R*-limonene-1,2-diol **5** were characterized through the use of ^1H and ^{13}C NMR spectroscopies (see Experimental section). The oxidation occurred only in the ring double bond and no reaction occurred at the isopropenyl double bond, indicating a high regioselectivity of the reaction.

Chloroperoxidase from *C. fumago* is a versatile heme enzyme because of its catalytic diversity. CPO is a peroxide-dependent chlorinating enzyme and it also catalyzes peroxidase-, catalase- and cytochrome P450-type reactions of dehydrogenation, H_2O_2 decomposition and oxygen insertion, respectively.¹⁸ Each activity has different optimal conditions, for example, optimal halogenation activity is usually obtained in the presence of chloride ions and at pH 3, while peroxidase activity is preferentially performed at pH 6. In order to evaluate the effect of reaction conditions on the chemical nature of the products, the CPO transformation of limonene was carried out in the presence and in the absence of 30 mM KCl and at both pH 3 and pH 6. No chlorinated products were detected, even at pH 3 with KCl, and under all conditions only limonene-1,2-diols were found. In addition, no epoxidated intermediates **2** and **3** were detected in any of the reaction conditions tested. A spontaneous epoxide

hydrolysis during the reaction could be expected. In order to investigate the extent of hydrolysis of these epoxy intermediates, a mixture of **2** and **3** were incubated in aqueous medium in the absence of both CPO and H_2O_2 . The results showed that the derivative epoxides were spontaneously hydrolyzed, conducting to the formation of **4** and **5** diols, which were characterized by ^1H and ^{13}C NMR (see spectra in the Experimental section). It is well known that the epoxides in aqueous media have a natural tendency to be opened in either acid or alkaline media.^{12,19} In acidic medium the reaction occurs by a protonation of the epoxidic oxygen followed by the opening and the formation of an anti diol. In basic media, there is first an elimination of the geminal proton, then the epoxide is opened generating the corresponding diol.

Table 1 shows the CPO-mediated oxidation of *R*-(+)-limonene and the diastomeric excess, calculated according to eqn (1). Dramatic changes in the diastomeric excess were detected when potassium chloride was added to the reaction medium. In the reaction carried out in the absence of chloride only **4** was observed, with a diastomeric excess >99.0% at both pH 3 and 6. On the other hand, when the reaction was performed in the presence of chloride ions, the stereoselectivity disappears,

Table 1 Kinetic constants of CPO-mediated oxidation *R*-(+)-limonene and diastomeric excess (*de*)

pH	^a Chloride	k_{cat} (s^{-1})	K_{M} (μM)	$k_{\text{cat}}/K_{\text{M}}$ ($\text{s}^{-1} \mu\text{M}^{-1}$)	Product	<i>de</i> (%)
3	–	2.3	0.36	6.4	4	>99.0
6	–	11.8	0.34	34.7	4	>99.0
3	+	18.7	0.11	170.0	4 and 5	5.4
6	+	11.1	0.10	111.0	4 and 5	0.0

^a KCl 30 mM.

conducting to the formation of a diastomeric mixture of **4** and **5**. The induced loss of the reaction stereoselectivity in the presence of chloride ions occurs at both pH 3 and 6, with *de* values of 5.4% and 0%, respectively.

Fig. 1 shows a proposed reaction pathway of CPO-mediated oxidation of *R*-(+)-limonene. The transformation of *R*-(+)-limonene by CPO produced the epoxide intermediate **2** and **3**. The spontaneous hydrolysis of these epoxide derivatives produced the corresponding diastomeric mixture diols **4** and **5**. Similar results were reported for 1,3-cycloheptadiene and 1,3-cyclohexadiene,¹⁹ among others.¹²

Chirality is of vital importance in the manufacture of pharmaceuticals, pesticides, and other biochemicals. Indeed, with many compounds, one enantiomer may have a specific biological activity, while the other enantiomer has a completely different activity. Racemic mixtures of enantiomers, comprising half of each type, are relatively easy to prepare by existing methods, but are not a good choice for preparing pure enantiomeric intermediates and final products. Synthesis of pure enantiomer preparations requires use of chiral substrates, either as starting materials or as intermediates. The high stereoselectivity oxidation of diolefins by CPO has been previously pointed out by Hager¹⁶ and Colonna,²⁰ making CPO an interesting alternative for chiral synthesis.

Oxidation of alkenes to produce the corresponding epoxide is an industrially-relevant synthesis process. The search for methods of asymmetric synthesis of epoxides from olefins has been the subject of many chemical and biological studies. Olefins are abundantly available as natural products and as compounds produced by the chemical industry. Asymmetric epoxides have many advantages as electrophilic intermediates for stereochemical syntheses involving reactions with nucleophiles. After substantial research efforts worldwide, some enantioselective enzyme-catalyzed epoxidation processes have been scaled up.²¹ The production of enantiomerically pure epoxides is very desirable for many purposes, including chemical synthesis of chiral products.

Many different methods for the preparation of epoxides have been developed. On an industrial scale, the epoxidation of plant oils is currently carried out with the Prileschajew reaction, in which the unsaturated oil reacts with a perchloric acid. Soluble mineral acid, commonly sulfuric acid, is used as a catalyst for this reaction. Environmental concerns related to the disposal of salt formed during the final neutralization of the mineral acid and technical problems, such as corrosion and separation operations, are associated with this process.

Another method involves the use of certain titanium silicalite materials to catalyze olefin oxidation by hydrogen peroxide. The prior art related to titanium silicalite-catalyzed epoxidation teaches that it is beneficial to employ a hydrogen peroxide solution that does not contain large amounts of water and recommends the use of an organic solvent as a liquid medium for the epoxidation reaction. A complex solvent mixture containing aromatic hydrocarbons is preferred.

Finally, the Ishii–Venturello system (W^{VI}/P^V /phase transfer catalyst, PTC/ $H_2O/CHCl_3$) is able to catalyze the selective epoxidation of a variety of monoterpenes, including the limonene, to give the corresponding mono- and di-epoxides in good yields under mild conditions. However, the Ishii–Venturello system

has disadvantages since toxic and carcinogenic chlorocarbon solvents (CCl_4 , $CHCl_3$, CH_2Cl_2) are required for high epoxide yield. Besides, the catalyst is rapidly deactivated, likely due to catalyst decomposition by interaction with epoxides.

These industrial processes are far from being environmentally safe and this constitutes a strong driving force for modification of, or the search for, substitutes for these technologies. In addition of its reaction selectivity, enzymatic catalyzed processes could be an interesting green alternative for the epoxide production.

The origin of the CPO name is its ability to halogenate several substrates, such as 2-chlorodimedone, antipyrine, NADH, and barbituric acid.²² In addition, CPO is able to chlorinate polycyclic aromatic hydrocarbons,²³ fulvic acid,²⁴ and flavanones and flavones.²⁵ Under the assayed reaction conditions no halogenated product was detected, even at pH 3 and in the presence of chloride ions (Table 1). Nevertheless, CPO is also a potent epoxidation biocatalyst that displays moderate to high enantioselectivity on a wide variety of olefinic substrates. Many of the chiral synthons formed from the epoxidation of simple phenyl-derived olefins are very significant.²⁶ However, CPO-mediated halogenation of double bonds is well known. Unsaturated carboxylic acids, such as trans-cinnamic acid and its derivatives, were found to be halogenated by CPO.²⁷ The transformation of monoterpenes by CPO has been recently reported.²⁸ In the absence of halide ions, the terpenic alcohols were transformed to their respective aldehydes, while terpene hydrocarbons were not substrates for CPO under these conditions. In the presence of halide ions, all terpenes tested were transformed and the products of careen were analyzed and shown to be haloalcohols.

Kinetic constants of CPO in the *R*-(+)-limonene transformation at two different pHs and in the absence and in the presence of chloride ions were determined (Table 1). As reviewed before,¹⁵ CPO-mediated epoxidations are reactions orders of magnitude slower when compared with other CPO catalyzed reactions, such as chlorination, peroxidation and catalase. Nevertheless, the transformation rates obtained with *R*-(+)-limonene up to 18.7 s^{-1} are higher than those obtained in the epoxidation of styrene.²⁹ On the other hand, consistently with literature information for peroxidase reactions, the catalytic activity is higher at pH 6 than at pH 3 in the absence of chloride ions. Also it is known that independent to the halogenation reactions, the presence of chloride enhances the peroxidasic activity. On the other hand, the presence of chloride ions decrease three-times the affinity constant (K_M) for limonene at both pHs. Thus, at pH 3 the catalytic efficiency increases 25-fold in the presence of KCl when compared at the same pH but in the absence of KCl.

In order to explain the lack of stereospecificity when the reactions are carried out in the presence of halogen ions, we hypothesize that in the absence of chloride ions the stereoselectivity is determined by stereospecific interaction of limonene with CPO active sites, while in the presence of chloride, the limonene oxidation may also occur chemically, without selectivity, by reacting with hypochlorite molecules that could be produced by CPO.

It is proposed that CPO is able to produce free hypochlorite when it reacts with hydrogen peroxide in the presence of

chloride ions.³⁰ On the other hand, hypochlorite reacts with olefins to form epoxides.³¹ Ramakrishnan *et al.*³² showed nearly complete lack of stereoselectivity in the reaction of 2-methyl-4-propylcyclopentane-1,3-dione with CPO in the presence of KCl. In addition, when chloroperoxidase is supplied with chloride ions and hydrogen peroxide there is no stereoselective synthesis of halohydrins from *cis* or *trans* propenylphosphonic acid.³³ Likewise, chloroperoxidase produces racemic bromohydrins when propylene and styrene serve as halogen acceptors.³⁴

In terms of the enzyme structure and mechanism, the stereochemistry could be completely retained in the epoxidation reaction if the epoxide oxygen derives quantitatively from the peroxide. The concerted oxygen transfer should be carried out by the oxene mechanism, as occurred for cytochrome P450-catalyzed oxidations with molecular oxygen. Chloroperoxidase and cytochrome P450 thus catalyze comparable epoxidation reactions in which the ferryl oxygen is transferred to the olefin with retention of stereochemistry.³⁵ In addition, the persistence of stereospecificity at different pHs could be explained by the total lack of change in the position of Glu183 and surrounding residues when the pH is lowered from 6.0 to 3.0 or when ligands bind.³⁶

With the aim to investigate the high stereospecificity of the CPO activity on the *R*-(+)-limonene molecule in absence of chloride ions, docking calculations using *R*-(+)-limonene, *S*-(-)-limonene, and the epoxide intermediates **2** and **3** as ligands were evaluated. Using the ground state of CPO, *R*-(+)-limonene showed to be a better substrate, with an affinity constant of $188 \pm 4 \mu\text{M}$, than *S*-(-)-limonene, with an affinity constant one order of magnitude higher of 1.09 mM. The docking simulations give an estimated binding free energy (ΔG) for *S*-(-)-limonene and *R*-(+)-limonene of $-4.04 \text{ kcal mol}^{-1}$ and $-5.07 \text{ kcal mol}^{-1}$, respectively. The three-dimensional structures of reactive CPO intermediates, Compound I and Compound II, are not available yet, thus we have used for docking simulations the CPO ground state and the epoxide intermediates in order to estimate the interaction between iron–oxygen and the reactive limonene double bond (Fig. 2). Docking simulations with epoxide **2** showed interaction with several residues of the CPO active site (Table 2), while epoxide intermediate **3** was unable to interact in a favorable position, supporting the experimentally observed stereospecificity of the CPO reactions. Epoxide intermediate **2** showed a high affinity with a constant of $11.8 \pm 2.3 \mu\text{M}$, and a binding free energy of $-6.72 \text{ kcal mol}^{-1}$. The affinity increased one order of magnitude when compared to *R*-(+)-limonene. This difference could be explained by the packing interactions of the

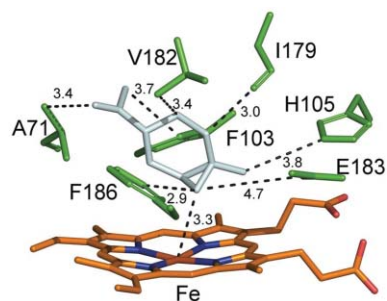


Fig. 2 Energy minimized model of limonene epoxide **2** docked in the catalytic site of ICPO represented in stick draw. The distances are represented in dark dash between different atoms of limonene intermediate and residues around the heme.

V182, I179, F103, F186, H105 and A71 residues around the active site of CPO (Fig. 2).

Recently, studies have shown in detail the interactions of the following residues: V67, N74, F103, H105, E183 and F186, around the catalytic site of CPO related with the binding of formate, acetate and nitrate.³⁷ The effect of these packing interactions probably drives the stereospecific complementarity with the limonene epoxide **2** and the Fe in the active site of CPO (see Fig. 2). This idea is in agreement with the kinetic data and the energetic and structural information found in the present study. The molecular modeling has been used to study the binding of 4,6-dimethyl dibenzothiophene with CPO in order to obtain information about the ligand recognition and interactions mechanism.³⁸ The molecular dynamic calculations showed the existence of two substrate binding sites in CPO with similar affinities for the substrate. The results were extended to carbazole as substrate. All this approximation was supported by experimental data reported previously. On the other hand, Sundaramoorthy *et al.*³⁶ have used *cis* β -methylstyrene and the corresponding epoxide product for a study providing a structural and energetic basis for the understanding of enantioselectivity in CPO-catalyzed epoxidation reactions.

The comparative analysis of distances between limonene epoxide **2** and both the heme and residues near the catalytic site of CPO are shown in Table 2. In our simulation, the van der Waals interaction between the epoxide oxygen of **2** and the heme Fe is around of 3.3 Å, and it is similar to the distance of 3.08 Å found between the oxygen and the iron of the peroxy radical of Compound 0, using the crystallographic model (PDB entry: 2j5m) recently reported.³⁹ However, the long Fe–O bond lengths reported in crystal structures of the ferryl forms of HRP, cytochrome c peroxidase, and myoglobin only varies from 1.84–1.92 Å.⁴⁰ The other five bond lengths of iron coordination bonds are an iron–histamine distance of $1.91 \pm 0.03 \text{ Å}$, and an iron–pyrrole nitrogen average distance of $2.02 \pm 0.02 \text{ Å}$. In the case of CPO, the Fe–O bond length is 1.63–1.65 Å for Compound I and 1.82 Å for Compound II, while the Fe–S distal coordination bond is 2.6–2.7 Å and 2–39 Å, respectively, both determined by X-ray absorption spectroscopy.⁴¹

It is important to point out that these results show that CPO is able to transform limonene with high regio- and stereoselectivity according to the reaction conditions, and that it is an interesting candidate for chiral enzymatic biosynthesis.

Table 2 Distances in Å between limonene epoxide **2** and residues around the catalytic site

Residues atom	Atom	Distance in Å	Atom of limonene
A71	CA	3.4	C8
F103	CE1	3.7	C9
H105	NE2	3.8	C10
I179	O	3.0	C6
V182	CG1	3.4	C5/C3
E183	OE2	4.7	Epoxide
F186	CE2	2.9	Epoxide
Heme	Fe	3.3	Epoxide

Experimental

Enzyme

Chloroperoxidase from *Caldariomyces fumago* 98362 was kindly donated by Dr Michael A. Pickard, University of Alberta, Canada. Purified enzyme preparation showed a Reinheitszahl coefficient (Rz) (A_{403}/A_{280}) of 1.41.

Chemicals

R-(+)-limonene **1**, mixture of (1*R*,2*S*,4*R*)-1,2-epoxy-*p*-menth-8-ene **2** and (1*S*,2*R*,4*R*)-1,2-epoxy-*p*-menth-8-ene **3** (epoxy-(+)-limonene mixture *cis/trans*), H₂O₂, were purchased from Sigma-Aldrich. Salt buffers were obtained from J. T. Baker (Phillipsburg, NJ, USA). Acetonitrile and other organic solvents (HPLC grade) were obtained from Fisher Scientific (Fairlawn, NJ, USA).

Enzymatic reaction conditions

The reaction mixture (1 ml) contained 22 pM CPO and from 0.15–0.80 μM *R*-(+)-limonene in 60 mM phosphate buffer pH 3.0 or 6.0 containing 15% acetonitrile. The reactions were performed at room temperature and started by adding 1 mM H₂O₂. The reaction progress was monitored by HPLC-UV (Perkin Elmer) equipped with a Series 200 quaternary pump, a diode array detector model 235C and a reverse-phase column (2.1 × 150 mm) Eclipse XDB-C₁₈ 5 μm (Agilent). The mobile phase was acetonitrile/water 65 : 35 at 0.5 ml min⁻¹. The decrease in the concentration of *R*-(+)-limonene was followed by measuring the decrease in their peak area at A₂₂₀ and correlated to a standard curve. The specific activity was estimated by measuring the mol oxidized substrate per mol CPO per unit of time. All reactions were done by triplicate, and the mean and standard deviations are reported.

Identification of the reaction products

To obtain enough amount of products for their identification, 5 ml reaction mixtures containing 0.8 μM *R*-(+)-limonene were treated with 22 pM CPO and 1 mM H₂O₂. The reaction was stopped after 10 min, extracted with CH₂Cl₂ and the organic fraction (1 μl) was injected in split mode (40 : 1) to GC-MS (Agilent GC: 6890 N, Mass selective detector: 5973 N). The products were identified with mass spectra. Identification of the different diastereomers was corroborated by comparison with known standards using GC-MS. The diastereomeric excess was calculated by using the following equation:

$$de = \left(\frac{A_4 - A_5}{A_4 + A_5} \right) 100 \quad (1)$$

A₄ and A₅ correspond to areas of compounds **4** and **5**, respectively. These areas were quantified by using an external standard (dodecane).

Preparation of standards

The preparation of dihydroxylated derivatives were made through the chemical hydrolysis in acid medium (pH = 3) of a mixture (1 : 3) (1*R*,2*S*,4*R*)-1,2-epoxy-*p*-menth-8-ene **2** and

(1*S*,2*R*,4*R*)-1,2-epoxy-*p*-menth-8-ene **3**. The products of the reaction 1*S*,2*S*,4*R*-limonene-1,2-diol **4** and 1*R*,2*R*,4*R*-limonene-1,2-diol **5** were characterized through ¹H and ¹³C NMR spectroscopy. The measurements were performed on a BRUKER AC 250 spectrometer, operating at 253.13 and 62.2 MHz for ¹H and ¹³C, respectively.

Spectral data

***R*-(+)-limonene 1.** $[\alpha]_D^{20} = +55.2^\circ$. MS (EI, 70 eV): *m/z* (relative intensity): 41 (24.2), 44 (31.9), 51 (10.6), 53 (28.5), 55 (14.0), 67 (87.1), 68 (100), 77 (24.7), 79 (28.4), 81 (9.5), 81 (10.9), 91 (26.9), 92 (29.2), 93 (45.3), 94 (11.9), 107 (9.3), 121 (25.9) and 136 (M⁺, 23.7). ¹H NMR (250 MHz, CDCl₃), δ : 4.65 (d, 2H, *J* = 10.2 Hz), 1.67 (s, 3H) and 1.19 (s, 3H). ¹³C NMR (62.4 MHz, CDCl₃), δ : 209.52, 149.92, 108.91, 75.38, 53.42, 39.72, 37.48, 34.65, 21.59 and 20.88.

(1*R*,2*S*,4*R*)-1,2-epoxy-*p*-menth-8-ene 2. *m/z*: 40 (29), 41 (65.9), 42 (13), 43 (82.7), 44 (23.6), 51 (19.8), 53 (37.4), 55 (44.1), 56 (10), 65 (16.6), 67 (100), 68 (66.7), 69 (31.8), 77 (27), 78 (11.4), 79 (49.5), 80 (13.7), 81 (43.9), 82 (19.2), 84 (10.1), 91 (54.1), 92 (29.1), 93 (54.3), 94 (33.5), 95 (35.7), 105 (23.2), 107 (22.4), 108 (26.9), 109 (18.3), 117 (12.4), 119 (28.9), 121 (13.8), 134 (13), 135 (4.2), 136 (4.7), 137 (9.1), 152 (M⁺, 2.9). ¹H NMR (250 MHz, CDCl₃), δ : 1.319 (s, H10), 1.35–2.18 (m, H3-H6), 1.690 (t, H9, *J*₈₋₉ = *J*_{8'-9} ≈ 1 Hz), 3.055 (br t, H2, *J*₂₋₃ = 2.9, *J*_{2-3'} ≈ 2.4 Hz), 4.660 (dq, H8, *J*_{8-8'} = 0.5 Hz), 4.722 (dq, H8'). ¹³C NMR (62.4 MHz, CDCl₃), δ : 20.82 (C9), 24.13 (C10), 25.69 (C5), 28.40 (C3) and 30.55 (C6), 35.99 (C4), 59.93 (C1), 60.17 (C2), 108.87 (C8), 148.79 (C7).

(1*S*,2*R*,4*R*)-1,2-epoxy-*p*-menth-8-ene 3. *m/z*: 41 (81.9), 43 (87.3), 44 (15.6), 45 (12.5), 51 (18.5), 53 (53.3), 55 (55.7), 56 (10.9), 63 (10.9), 65 (32.5), 67 (100), 68 (69.4), 70 (16.4), 71 (10.8), 77 (30.8), 79 (53.7), 80 (18), 81 (41.5), 82 (29.5), 91 (72.1), 92 (20.5), 93 (50.4), 94 (27.4), 95 (26), 105 (15.8), 107 (29.5), 108 (15.5), 109 (31), 117 (14.9), 119 (26), 123 (21.4), 137 (28.5) and 152 (M⁺, 0). ¹H NMR (250 MHz, CDCl₃), δ : 1.303 (s, H10), 1.35–2.18 (m, H3-H6), 1.667 (t, H9, *J*₈₋₉ = *J*_{8'-9} ≈ 1 Hz), 3.000 (br t, H2, *J*₂₋₃ = 2.9, *J*_{2-3'} ≈ 2.4 Hz), 4.660 (dq, H8, *J*_{8-8'} = 0.5 Hz), 4.722 (dq, H8'). ¹³C NMR (62.4 MHz, CDCl₃), δ : 19.97 (C9), 24.01 (C10), 25.69 (C5), 29.69 (C3) and 30.55 (C6), 40.52 (C4), 57.11 (C1), 58.92 (C2), 108.87 (C8) and 148.57 (C7).

1*S*,2*S*,4*R*-limonene-1,2-diol 4. MS (EI, 70 eV): *m/z* (relative intensity): 40 (12), 41 (62.3), 42 (10.4), 43 (100), 53 (29.2), 55 (49), 56 (14.1), 57 (25.6), 58 (32.3), 65 (11.9), 67 (74.5), 68 (43.2), 69 (48.1), 70 (14.5), 71 (95.3), 72 (11.5), 77 (12.6), 79 (23.7), 81 (45.9), 82 (39.8), 83 (16.5), 91 (15), 93 (27.3), 95 (23.6), 97 (13.7), 108 (40.2), 109 (32.1), 110 (12.3), 111 (14.3), 119 (14.5), 123 (10.1), 134 (10.2), 137 (15.9) and 152 (M⁺, 20.2). ¹H NMR (250.15 MHz, CDCl₃) δ : 4.71 (m, H8), 3.63 (t, H2, *J*_{H2eq-H3eq} = *J*_{H2eq-H3ax} = 2.8 Hz), 2.40–2.23 (m, H4), 1.95–1.50 (m, H3, H5 and H6), 1.73 (s, H8), 1.26 (3H, s, H10). ¹³C NMR (62.4 MHz, CDCl₃), δ : 71.3 (C1), 73.9 (C2), 33.9 (C3), 37.4 (C4), 26.6 (C5), 33.6 (C6), 149.3 (C7), 109.0 (C8), 21.0 (C9) and 26.1 (C10).

1*R*,2*R*,4*R*-limonene-1,2-diol 5. MS (EI, 70 eV): *m/z* (relative intensity): 40 (12), 41 (62.3), 42 (10.4), 43 (100), 53 (29.2), 55 (49), 56 (14.1), 57 (25.6), 58 (32.3), 65 (11.9), 67 (74.5), 68 (43.2),

69 (48.1), 70 (14.5), 71 (95.3), 72 (11.5), 77 (12.6), 79 (23.7), 81 (45.9), 82 (39.8), 83 (16.5), 91 (15), 93 (27.3), 95 (23.6), 97 (13.7), 108 (40.2), 109 (32.1), 110 (12.3), 111 (14.3), 119 (14.5), 123 (10.1), 134 (10.2), 137 (15.9) and 152 (M⁺, 20.2). ¹H NMR (250.15 MHz, CDCl₃) δ: 4.73 (m, H8), 3.57 (q, H2, $J_{\text{H2ax-H3eq}} = 4.5$, $J_{\text{H2ax-H3ax}} = 11.8$ Hz), 2.40–2.23 (m, H4), 1.95–1.50 (m, H3, H5 and H6), 1.56 (s, H8), 1.20 (3H, s, H10). ¹³C NMR (62.4 MHz, CDCl₃) δ: 73.9 (C1), 77.2 (C2), 36.1 (C3), 43.6 (C4), 28.6 (C5), 38.5 (C6), 148.5 (C7), 109.0 (C8), 18.9 (C9) and 20.9 (C10).

Docking simulations

The crystallographic model from *Caldariomyces fumago* chloroperoxidase (PDB entry: 1CPO) at 1.9 Å of resolution.⁴² was used as a flexible molecule receptor to automated docking simulations. The docking was performed using a Lamarckian genetic algorithm from AutoDock4 software package⁴³ with an initial population of 300 and 1×10^7 energy evaluations. The structure of limonene as a flexible ligand molecule was drawn using Chem3D Ultra molecular modeling software. The molecular dynamics was performed to optimize the geometry and the minimum energy structure with the next parameters step interval: 2.0 fs, frame intervals 10 fs: terminated after 1000 cycles with a heating/cooling rate of 1000 kcal atom⁻¹ ps⁻¹ at 300 K. The partial atomic charges (Gasteiger) and the rotatable bonds were added using AutoDock Tools 1.4.6⁴⁴ The Kollman and Gasteiger charges were added to 1CPO. The calculations of the van der Waals, H-bonds, electrostatics potential and desolvation free energies for grid map was done using AutoGrid4 program.⁴¹ The GRID procedures were used to define the binding site of the ligand. The grid spacing was established at 0.375 Å. The receptor fit within the following volume maximum and minimum coordinates (64.7, 26.07, 33.69) and (11.67, -22.99, -21.86) respectively. The grid map covered the maximum and minimum coordinates (42.9, 5.5, 9.65) and (30.159, -7.22, -2.341) respectively, fixing the residue E183. The lowest energy model was selected to further analysis. The models were evaluated using AutoDock Tools 1.4.6.⁴¹ and visualized using PyMol 0.99 computer program.⁴⁵

Conclusions

The oxidation of the *R*-(+)-limonene by CPO from *C. fumago* in absence of the chloride ions is regio- and highly diastereoselective. The catalytic efficiency was higher in the presence of chloride, maintaining the regioselectivity, but losing its diastereoselectivity. Halogenase activity of CPO was not observed at pH 3 under the experimental conditions. Substrate docking modeling showed that in the absence of chloride ions the stereospecificity is governed by the substrate-active site interaction, while in the presence of chlorine ions the CPO-mediated production of hypochlorite may produce a chemical oxidation to form a racemic mixture of epoxide intermediates. Thus, CPO-mediated reactions of terpenes is an interesting synthesis alternative to produce stereospecific epoxides.

Acknowledgements

This work has been funded by CONICYT and MECESUP UCH-408 (Chile) and by CONACYT (Mexico). All docking calculations were performed using the cluster Sputnik II computer technology donated by the Macroproyecto de Tecnologías de la Información y la Computación, UNAM under supervision and computational technical assistance of Ricardo Ciria, Roberto Bahena and Jérôme Verleyen.

References

- D. J. Pollard and J. M. Woodley, *Trends Biotechnol.*, 2007, **25**, 66–73.
- (a) J. Schrader, M. M. Etschmann, D. Sell, J. M. Hilmer and J. Rabenhorst, *Biotechnol. Lett.*, 2004, **26**, 463–472; (b) J. James and B. K. Simpson, *Crit. Rev. Food Sci. Nutr.*, 1996, **36**, 437–463.
- K. M. Koeller and C. H. Wong, *Nature*, 2001, **409**, 232–240.
- E. A. Bayer, R. Lamed and M. E. Himmel, *Curr. Opin. Biotechnol.*, 2007, **18**, 237–245.
- M. Alcalde, M. Ferrer, F. J. Plou and A. Ballesteros, *Trends Biotechnol.*, 2006, **24**, 281–287.
- P. S. J. Cheetham, *Adv. Biochem. Eng. Biotechnol.*, 1997, **55**, 1–49.
- (a) P. Gallezot, *Catal. Today*, 2007, **121**, 76–91; (b) H. Li, W. Lan, C. Cai, Y. Zhou and Y. Lin, *Chin. J. Anal. Chem.*, 2006, **34**, 946–950.
- J. Schrader, M. M. Etschmann, D. Sell, J. M. Hilmer and J. Rabenhorst, *Biotechnol. Lett.*, 2004, **26**, 463–472.
- (a) R. S. Dhavalikar and P. K. Bhattacharyya, *Indian J. Biochem.*, 1966, **3**, 144–517; (b) E. Bowen, *Potential by-products from microbial transformation of d-limonene*, Florida State Horticultural Society, Florida, 1975. p. 304; (c) Y. Noma, S. Yamasaki and Y. Asakawa, *Phytochemistry*, 1992, **31**, 2725–2727; (d) J. Onken and R. G. Berger, *J. Biotechnol.*, 1999, **69**, 163–168; (e) T. K. Cheong and P. J. Oriel, *Appl. Biochem. Biotechnol.*, 2000, **84–86**, 903–915; (f) W. A. Duetz, A. H. Fjällman, S. Ren, C. Jourdat and B. Witholt, *Appl. Environ. Microbiol.*, 2001, **67**, 2829–2832; (g) W. R. Abraham, H. M. Hoffmann, K. Kieslich, G. Reng and B. Stumpf, *Ciba Found. Symp.*, 1985, **111**, 146–160; (h) W-R. Abraham, B. Stumpf and K. Kieslich, *Appl. Microbiol. Biotechnol.*, 1986, **24**, 24–30; (i) B. B. Mukherjee, G. Kraidman and I. D. Hill, *Appl. Microbiol.*, 1973, **25**, 447–453; (j) L. Draczynska, *J. Basic Microbiol.*, 1987, **27**, 191–196.
- I. L. Gatfield, J-M. Hilmer and H. J. Bertram, *Chimia*, 2001, **55**, 397–401.
- E. G. Funhoff, U. Bauer, I. Garcia-Rubio, B. Witholt and J. B. van Beilen, *J. Bacteriol.*, 2006, **188**, 5220–5227.
- V. M. Dembitsky, *Tetrahedron*, 2003, **59**, 4701–4720.
- A. M. Azevedo, V. C. Martins, D. M. F. Prazeres, V. Vojinovic, J. M. S. Cabral, L. P. Fonseca and M. R. El-Gewely, *Biotechnol. Annu. Rev.*, 2003, **9**, 199–247.
- (a) M. P. J. Van Deurzen, F. Van Rantwijk and R. A. Sheldon, *Tetrahedron*, 1997, **53**, 13183–13220; (b) F. Van Rantwijk and R. A. Sheldon, *Curr. Opin. Biotechnol.*, 2000, **11**, 554–564.
- E. J. Allain, L. Deng and L. P. Hager, *J. Am. Chem. Soc.*, 1993, **115**, 4415–4416.
- (a) A. F. Dexter, F. J. Lakner, R. A. Campbell and L. P. Hager, *J. Am. Chem. Soc.*, 1995, **117**, 6412–6413; (b) F. J. Lakner and L. P. Hager, *J. Org. Chem.*, 1996, **61**, 3923–3925; (c) F. J. Lakner and L. P. Hager, *Tetrahedron: Asymmetry*, 1997, **8**, 3547–3550.
- (a) A. Zaks and D. R. Dodds, *J. Am. Chem. Soc.*, 1995, **117**, 10419–10424; (b) S. Hu and L. P. Hager, *Tetrahedron Lett.*, 1999, **40**, 1641–1644; (c) D. J. Bougioukou and I. Smonou, *Tetrahedron Lett.*, 2002, **43**, 339–342.
- (a) G. L. Kedderis, D. E. Rickert, R. N. Pandey and P. F. Hollenberg, *J. Biol. Chem.*, 1986, **261**, 15910–15914; (b) S. Kobayashi, M. Nakano, T. Kimura and A. P. Schaap, *Biochemistry*, 1987, **26**, 5019–5022; (c) M. B. McCarthy and R. E. White, *J. Biol. Chem.*, 1983, **258**, 9153–9158; (d) P. R. Ortiz de Montellano, Y. S. Choe, G. DePillis and C. E. Catalano, *J. Biol. Chem.*, 1987, **262**, 11641–11646.
- (a) C. Sanfilippo and G. Nicolosi, *Tetrahedron: Asymmetry*, 2002, **13**, 1889–1892; (b) C. Sanfilippo, A. Patti and G. Nicolosi, *Tetrahedron: Asymmetry*, 2000, **11**, 3269–3272.

- 20 S. Colonna, N. Gaggero, C. Richelmi and P. Pasta, *Trends Biotechnol.*, 1999, **17**, 163–168.
- 21 (a) S. Panke, M. Held, M. G. Wubbolts, B. Witholt and A. Schmid, *Biotechnol. Bioeng.*, 2002, **80**, 34–41; (b) A. Liese, K. Seelbach, and C. Wandrey, *Industrial Biotransformations: A Collection of Processes*, Wiley-VCH Verlag GmbH & Co. KGaA, Germany, 2000.
- 22 R. D. Libby, T. M. Beachy and A. K. Phipps, *J. Biol. Chem.*, 1996, **271**, 21820–21827.
- 23 R. Vazquez-Duhalt, M. Ayala and F. J. Marquez-Rocha, *Phytochemistry*, 2001, **58**, 929–933.
- 24 V. Niedan, I. Pavasars and G. Oberg, *Chemosphere*, 2000, **41**, 779–785.
- 25 P. Yaipakdee and L. W. Robertson, *Phytochemistry*, 2001, **57**, 341–347.
- 26 (a) K. M. Manoj, X. Yi, G. P. Rai and L. P. Hager, *Biochem. Biophys. Res. Commun.*, 1999, **266**, 301–303; (b) L. P. Hager, F. J. Lakner and A. Basavapathruni, *J. Mol. Catal. B: Enzym.*, 1998, **5**, 95–101.
- 27 H. Yamada, N. Itoh and Y. Izumi, *J. Biol. Chem.*, 1985, **260**, 11962–11969.
- 28 B. A. Kaup, U. Piantini, M. Wüst and J. Schrader, *Appl. Microbiol. Biotechnol.*, 2007, **73**, 1087–1096.
- 29 X. Yi, M. Mroczko Manoj K. M., X. Wang and L. P. Hager, *Proc. Natl. Acad. Sci. U. S. A.*, 1999, **96**, 12412–12417.
- 30 H. A. Wagenknecht and W. D. Woggon, *Chem. Biol.*, 1997, **4**, 367–372.
- 31 M. Klawonn, S. Bhor, G. Mehlretter, C. Döbler, C. Fischer and M. Beller, *Adv. Synth. Catal.*, 2003, **345**, 389–392.
- 32 K. Ramakrishnan, M. E. Oppenhuizen, S. Saunders and J. Fisher, *Biochemistry*, 1983, **22**, 3271–3277.
- 33 J. Kollonitsch, S. Marburg and L. M. Perkins, *J. Am. Chem. Soc.*, 1970, **92**, 4489–4490.
- 34 S. L. Neidleman and J. Geigert, *Biohalogenation: Principles, Basic Roles and Applications*, John Wiley and Sons, New York, 1986, p. 109.
- 35 P. R. Ortiz de Montellano, Y. S. Choe, G. D. DePillis and C. E. Catalano, *J. Biol. Chem.*, 1987, **262**, 11641–11646.
- 36 M. Sundaramoorthy, J. Terrier and T. L. Poulos, *Chem. Biol.*, 1998, **5**, 461–473.
- 37 K. Kuhnel, W. Blankenfeldt, J. Turner and I. Schlichting, *J. Biol. Chem.*, 2006, **281**, 23990–23998.
- 38 J. C. Basurto, J. Aburto, J. T. Ferrara and E. Torres, *Mol. Simul.*, 2007, **33**, 649–654.
- 39 K. Kuhnel, E. Derat, J. Turner, S. Shaik and I. Schlichting, *Proc. Natl. Acad. Sci. U. S. A.*, 2007, **104**, 99–104.
- 40 M. Chance, L. Powers, T. Poulos and B. Chance, *Biochemistry*, 1986, **25**, 1266–1270.
- 41 M. T. Green, J. H. Dawson and H. B. Gray, *Science*, 2004, **304**, 1653–1656.
- 42 M. Sundaramoorthy, J. M. Mauro, A. M. Sullivan, J. Turner and T. L. Poulos, *Acta Crystallogr., Sect. D: Biol. Crystallogr.*, 1995, **51**, 842–844.
- 43 G. M. Morris, D. S. Goodsell, R. S. Halliday, R. Huey, W. E. Hart, R. K. Belew and A. J. Olson, *J. Comput. Chem.*, 1998, **19**, 1639–1662.
- 44 F. Michel, R. H. Sanner, S. Dallakyan, S. Karnati, W. Lindstrom, G. M. Morris, B. Norledge, A. Omelchenko, D. Stoffler and G. Vareille, *AutoDock Tools*, 1999–2007.
- 45 W. L. DeLano, *The PyMOL Molecular Graphics System*, 2002, available from: <http://www.pymol.org>.

The application of calcined natural dolomitic rock as a solid base catalyst in triglyceride transesterification for biodiesel synthesis

Karen Wilson,^{*a} Chris Hardacre,^b Adam F. Lee,^{*a} Janine M. Montero^a and Lee Shellard^a

Received 10th January 2008, Accepted 11th March 2008

First published as an Advance Article on the web 3rd April 2008

DOI: 10.1039/b800455b

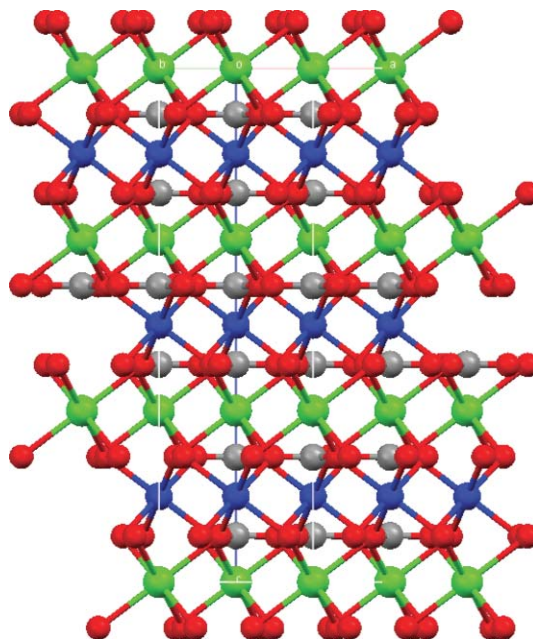
Natural dolomitic rock has been investigated in the transesterification of C₄ and C₈ triglycerides and olive oil with a view to determining its viability as a solid base catalyst for use in biodiesel synthesis. XRD reveals that the dolomitic rock comprised 77% dolomite and 23% magnesian calcite. The generation of basic sites requires calcination at 900 °C, which increases the surface area and transforms the mineral into MgO nanocrystallites dispersed over CaO particles. Calcined dolomitic rock exhibits high activity towards the liquid phase transesterification of glyceryl tributyrate and trioctanoate, and even olive oil, with methanol for biodiesel production.

Introduction

Biodiesel is a clean fuel source which is viewed as a viable alternative for dwindling petroleum-based diesel resources. It is synthesized *via* the transesterification of natural fats or oils (of vegetable or animal origin) with C₁–C₂ alcohols,^{1,2} using soluble acid or base catalysts.³ Commercial biodiesel production traditionally uses soluble bases such as Na or K alkoxides in this transesterification step, forming fatty acid methyl esters (FAME), which constitute biodiesel, together with glycerol by-product.⁴ Aqueous quenches subsequently required to remove the base and isolate biodiesel are problematic due to saponification and emulsification.² Complete removal of the base catalysts is essential as even trace residues in fuel corrode vehicle fuel tanks and injector systems. These quenching and processing steps also heavily contaminate the glycerol by-product with alkali salts and water, rendering it unusable directly as a commodity chemical.⁴ The use of a solid base catalyst offers several process advantages including the elimination of a quenching step (and associated contaminated water waste) to isolate the products, and the opportunity to operate in a continuous process.^{5,6}

A variety of solid bases are known including alkali or alkaline earth oxides, supported alkali metal ions, basic zeolites and clay minerals such as hydrotalcites.⁷ Alkaline earth oxides, in particular MgO^{8–10} and CaO,^{11,12} and hydrotalcites^{13,14,10} are potential solid bases for use in triacylglyceride (TAG) transesterification and have attracted attention in recent years. We recently reported that Li-doped CaO¹⁵ and Mg rich Mg–Al hydrotalcite materials¹³ are effective solid base catalysts for the transesterification of glyceryl tributyrate to methyl butanoate.

Building on our interest in the application of doped alkaline earth oxides we chose to investigate whether dolomitic rock could be employed as a solid base catalyst in biodiesel synthesis. The mineral dolomite (Scheme 1) is comprised of alternating layers of Mg(CO₃)–Ca(CO₃) and is structurally very similar to calcite (CaCO₃). Natural sources such as dolomitic rocks may also contain Ca-rich phases of magnesian calcite (Mg_xCa_{1–x}CO₃), which also adopt an alternating layered structure, in this instance of Ca(CO₃) and mixed Mg(CO₃)–Ca(CO₃).



Scheme 1 Structure of dolomite MgCa(CO₃)₂ (C–grey, Mg²⁺–blue, Ca²⁺–green, O^{2–}–red)

Dolomitic rocks have a high natural abundance and low toxicity, and in the UK are sourced mainly from quarries working Permian dolomites in Durham, South Yorkshire and Derbyshire.¹⁶ Recycling of powdered dolomitic rock generated at these quarries would add value to this readily available

^aDepartment of Chemistry, University of York, York, UK.
E-mail: kw13@york.ac.uk, afl2@york.ac.uk; Fax: +44 1904 432516;
Tel: +44 1904 432586

^bSchool of Chemistry & Chemical Engineering, Queen's University, Belfast, Northern Ireland. E-mail: c.hardacre@qub.ac.uk; Fax: +44 28 9097 4687; Tel: +44 28 9097 4592

source of waste mineral. In addition to uses in agriculture and construction, dolomite finds numerous industrial applications including iron and steel production, glass manufacturing and as fillers in plastics, paints, rubbers, adhesives and sealants.

The catalytic application of dolomite in biomass gasification¹⁷ has also attracted much attention as it is a cheap disposable naturally occurring material that can be used to significantly reduce the tar content of the product gas from a gasifier. Applications include steam-reforming of biomass-derived syngas¹⁸ and plastic waste elimination by co-gasification with coal and biomass.¹⁹ In addition, a nickel–dolomite catalyst has also been developed for use in steam reforming of naphthalene,²⁰ and gasification of tar with steam.^{21,22} The application of dolomite in other catalytic processes is less widely explored. Here, we report on the characterisation and application of dolomitic rock in the transesterification of triglycerides for biodiesel synthesis.

Experimental

Material preparation and characterisation

Natural dolomitic rock was mined from a deposit in Co. Fermanagh, Northern Ireland, and ground and sieved to particles of between 149–250 μm . Prior to use the material was calcined at 900 °C for 3 h in a static muffle furnace, then cooled in air to 100 °C prior to being transferred to a vacuum desiccator where they were stored prior to analysis and catalyst testing.

Thermogravimetric analysis (TGA) was performed using a Stanton Redcroft STA-780 between 20–1100 °C. Powder X-ray diffraction patterns were collected on a Bruker D8 diffractometer using Cu K α radiation and a Lynx Eye detector. The bulk Ca and Mg content of samples was determined by using a Hitachi atomic absorption spectrometer. DRIFTS spectra were obtained using a Thermo Avatar FTIR spectrometer. Samples were diluted with KBr powder (10 wt% in KBr), then loaded in an environmental cell and subjected to an additional drying under vacuum at 60 °C for 10 min prior to measurements to remove moisture physisorbed during air-exposure. Surface area measurements were performed by N₂ physisorption using a Quantachrom Nova instrument. To reduce errors with such a low surface area material, multipoint adsorption isotherms were measured on 0.5 g sample. Surface areas were calculated using the BET equation over the pressure range $P/P_0 = 0.02\text{--}0.2$, where a linear relationship was maintained. XPS measurements were performed using a Kratos AXIS HSi instrument equipped with a charge neutraliser and Mg K α X-ray source. Spectra were recorded at normal emission using an analyser pass energy of 20 eV, X-ray power of 159 W and were energy referenced to the valence band and adventitious carbon. Survey scans were recorded at 160 eV pass energy. SEM was undertaken on carbon supported samples imaged with a JEOL JSM-7000F field emission microscope.

Base strength was determined by Hammett indicators; ~25 mg of sample was shaken with 1 cm³ of a solution of Hammett indicator diluted in methanol and left to equilibrate for 2 h at which point no further colour change was observed. The colour on the catalyst was then noted. The following Hammett indicators were used: neutral red ($pK_{\text{BH}^+} = 6.8$), phenolphthalein ($pK_{\text{BH}^+} = 8.2$), Nile blue ($pK_{\text{BH}^+} = 10.1$), Tropaeolin-O ($pK_{\text{BH}^+} = 11$), 2,4-dinitroaniline ($pK_{\text{BH}^+} = 15$) and 4-chloro-2-nitroaniline

($pK_{\text{BH}^+} = 17.2$). Determination of basicity of porous solid base catalysts by such measurements remains controversial due to solvent-support interactions²³ and accessibility of the probe molecule within micropores.²⁴ Despite this, provided the polarity of the solvent used to suspend the solid and indicator is similar to that of the reaction media, semi-quantitative determination of the maximum solid base strength can be obtained. While Hammett indicator measurements are conventionally performed using non-polar solvents,²⁵ it was thus deemed appropriate to use methanol in this instance, as a measure of the base strength of the catalyst under reaction conditions would be determined. The base strength is quoted as being stronger than the weakest indicator which exhibits a colour change, but weaker than the strongest indicator that produces no change.

Transesterification reaction

Reactions were performed in a stirred batch reactor with samples withdrawn periodically for analysis using a Shimadzu GC17A gas chromatograph fitted with a DB1 capillary column (film thickness 0.25 μm , i.d. 0.32 mm, length 30 m), and AOC 20i autosampler. Transesterification reactions were performed at 333 K using 0.05 g of catalyst, 0.01 mol of glyceryl tributyrate or glyceryl trioctanoate (Aldrich 98%), 0.0025 mol hexyl ether (Aldrich 97%) as internal standard, and 0.3036 mol methanol (Fisher 98%). Olive oil transesterification was performed as above except that 0.16 g extra virgin olive oil (Sainsbury's own brand—UK supermarket chain) was used, equating to ~0.2 mmol triglyceride based on the majority glyceryltriolate component, and only 25 mg of calcined dolomite was added. Reactions were run for 3 h, with initial rates determined from the linear portion of the reaction profile at low conversion (<30%). Turn over frequencies are determined as initial rate conversion/mass of catalyst. Catalyst selectivity and overall mass balances (closure was >98%) were determined using reactant and product response factors derived from multipoint calibration curves. The errors in the conversions and selectivities are $\pm 2\%$ and $\pm 3\%$, respectively.

Results and discussion

Materials characterisation

The thermal stability of ground dolomitic rock (Fig. 1) was first examined by TGA which shows a small weight loss at

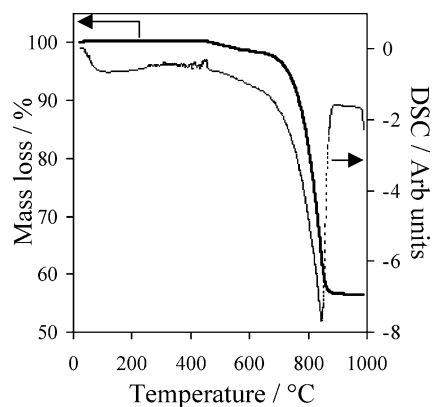


Fig. 1 TGA (bold line) and DSC (dotted line) analysis of dolomite.

Table 1 Textural properties and basicity of fresh and calcined dolomite

Sample	Surface area/m ² g ⁻¹	Mean Pore diameter/nm	Pore volume/cm ³ g ⁻¹	Hammett basicity
Fresh dolomite	3.2	3.5	5.6 × 10 ⁻³	pK _b < 6.8
900 °C calcined	8.0	11.9	4.8 × 10 ⁻²	11 < pK _b < 15

500 °C followed by a major exothermic weight loss at ~800 °C, which accounts for 43% of the material. Dolomite decomposes via $\text{MgCa}(\text{CO}_3)_2 \rightarrow \text{MgO} + \text{CaCO}_3 + \text{CO}_2$, with subsequent $\text{CaCO}_3 \rightarrow \text{CaO} + \text{CO}_2$,²⁶ which should give a total weight loss of ~47.7%. $\text{Mg}(\text{CO}_3)$ and $\text{Ca}(\text{CO}_3)$ are expected to give weight losses of 52 and 44%, respectively, the slight deviation suggests our natural dolomitic rock may be slightly calcite rich.

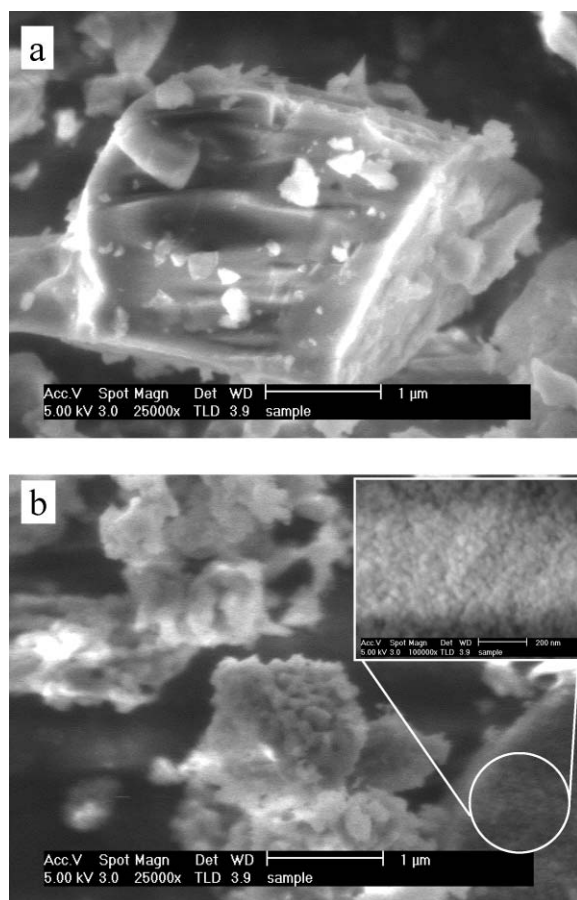
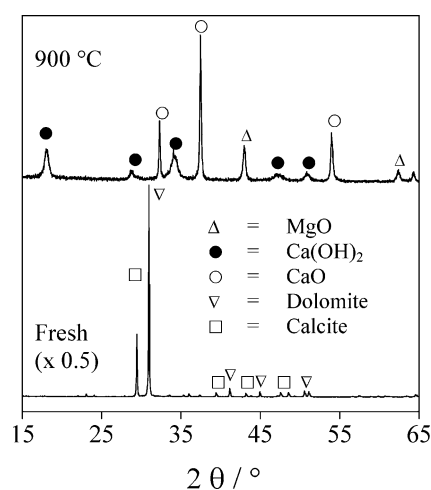
Fresh dolomite has a low surface area and negligible basicity (Table 1). Calcination at 900 °C changes both the structural and chemical properties of dolomite, as evidenced by an increased surface area and base strength. These are both likely associated with the evolution of CO₂, whose expulsion from the lattice is expected to fracture the crystallites, with the concomitant formation of extra base sites in the residual material.

The surface morphology of fresh and calcined dolomite was also examined by SEM (Fig. 2a–b). The parent material comprised large particles, exposing smooth planes or regularly faceted steps, with a high degree of crystallinity. Calcination fractures these particles, as expected from CO₂ expulsion from carbonate-rich areas, generating a high density of irregular,

pitted microcrystallites. Closer inspection of these highly textured surfaces reveals the presence of nanoparticles (~20 nm) explaining the rise in surface area (Fig. 2b inset).

Table 2 shows the corresponding elemental analysis, which reveals the atomic Ca : Mg ratio is ~2.5 times higher than that expected for $\text{CaMg}(\text{CO}_3)_2$. The simplest explanation is that our natural material is a calcium-rich dolomitic rock, probably containing additional calcite or magnesian calcite.²⁷ The bulk Ca and Mg contents both rise following calcination, reflecting CO₂ desorption. These changes are qualitatively mirrored by their analogous surface compositions, which also directly demonstrate the loss of surface carbon and oxygen. While the bulk ratio Ca : Mg ratio remains essentially constant during calcination, the surface becomes greatly Mg enriched, indicative of magnesium phase segregation during carbonate decomposition.

The crystallinity of fresh and calcined dolomite was further probed by powder XRD. The parent material exhibits major diffraction peaks at 29.4° and 30.9°, characteristic of the (104) reflections of calcite²⁸ and dolomite,²⁹ respectively (Fig. 3). Weaker reflections between 35–55° are also consistent with both these phases, confirming our natural dolomitic rock comprises a mixture of dolomite and calcite. Simulations of the (104) reflections suggests a composition of 77% dolomite : 23% calcite. Following calcination, reflections arising from dolomite and calcite are lost, coincident with the appearance of new crystalline phases that can be assigned to Ca(OH)₂ (18°, 29°, 34.3°, 47.2° and 50.9°), CaO (32.3°, 37.4° and 53.9°), and MgO (42.9° and 62.3°).³⁰

**Fig. 2** SEM of (a) fresh and (b) 900 °C calcined dolomite.**Fig. 3** XRD of fresh and 900 °C calcined dolomite.

Peakwidth analysis using the Scherrer equation reveals the nanocrystalline nature of these new phases, with volume averaged particle sizes ~30–65 nm for CaO, ~20–23 nm for MgO and ~7–13 nm for Ca(OH)₂. Note the discrepancy between bulk

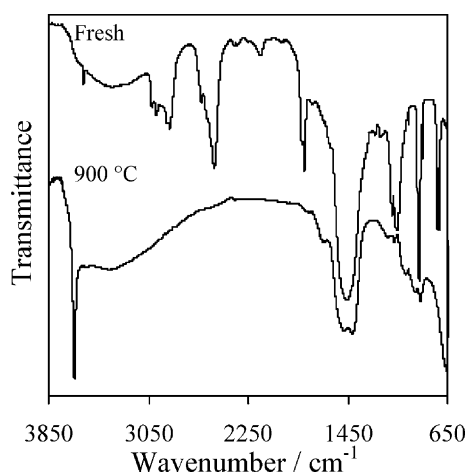
Table 2 Elemental and surface analysis of fresh and calcined dolomite

Sample	Bulk Mg ^a (wt%)	Bulk Ca ^a (wt%)	Bulk atomic Ca : Mg	Surface Mg ^b (wt%) ^b	Surface Ca (wt%)	Surface O (wt%)	Surface C (wt%)	Surface atomic Ca : Mg
Fresh dolomite	1.9	18.0	2.3	4.6	24.8	55.2	15.4	3.3
900 °C calcined	4.6	39.9	2.2	14.8	24.9	50.4	9.9	1.0

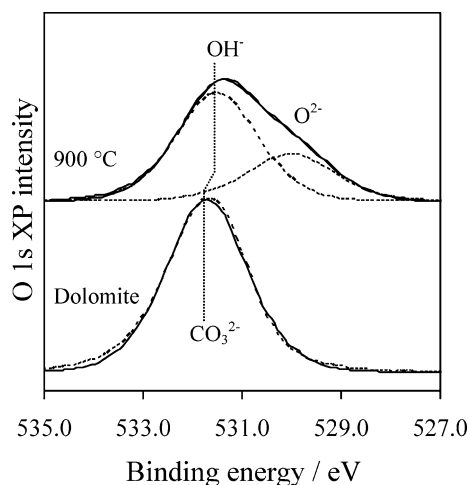
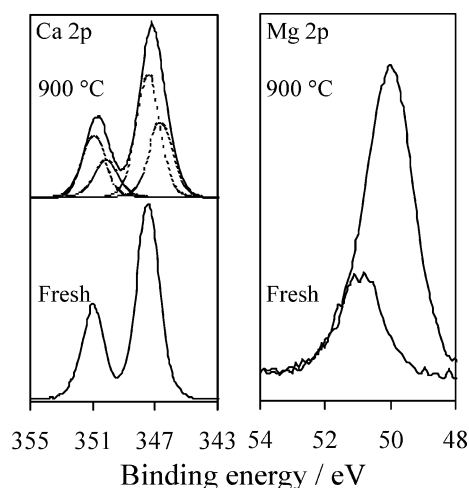
^a From atomic absorption (batch-batch variability in bulk composition of ground dolomite samples ~0.25 wt%). ^b From XPS quantification based upon above elements. Survey scans also revealed Al (1.8 and 6.5 wt%) and Si (3.5 and 1.2 wt%) in fresh and calcined materials, respectively.

and surface Ca : Mg ratios rules out the possibility of complete dolomite phase separation into discrete CaO (or hydroxide) and MgO particles.

DRIFT spectra of the fresh material (Fig. 4) show bands at 730, 883 and 1468 cm⁻¹, characteristic of dolomite,³¹ with the 1468 cm⁻¹ peak associated with lattice CO₃²⁻. Closer inspection reveals a small peak at 714 cm⁻¹, attributable to magnesian calcite or calcite. The 1800 and 2535 cm⁻¹ peaks are combination bands, while the cluster around 3000 cm⁻¹ reflect organic residues. Calcination eliminates all peaks bar the feature associated with CO₃²⁻, which splits into two new components at 1427 and 1496 cm⁻¹. These modes most likely arise from the ν_s and ν_{as} O–C–O stretches of unidentate bound carbonate adsorbed at the surface of oxide/hydroxide nanocrystals. Such a capping carbonate adlayer is consistent with previous observations that calcined CaO readsorbs atmospheric CO₂ to form amorphous CaCO₃.³² A sharp band at 3646 cm⁻¹ also develops in the O–H stretching region after heating, attributable to surface Ca(OH)₂.³¹ The observation of Ca(OH)₂ in both DRIFT and XRD is consistent with measurements on calcined limestone which show hydration of CaO occurs more rapidly than for MgO.³³

**Fig. 4** DRIFT spectra of fresh and 900 °C calcined dolomite samples.

High resolution O 1s XP spectra in Fig. 5 show only a single oxygen environment at 531.7 eV within the parent dolomite, consistent with the binding energy for CO₃²⁻. Thermal processing produces new states at 530.0 and 531.5 eV, characteristic of surface O²⁻ and hydroxyl groups, respectively. Fig. 6 shows the corresponding Ca and Mg 2p spectra. The Ca and Mg 2p_{3/2} components of fresh dolomite lie at 347.4 and 50.9 eV, representative of CaCO₃¹² and MgCO₃.³⁴ Calcination broadens

**Fig. 5** O 1s XP spectra of fresh and 900 °C calcined dolomite.**Fig. 6** Ca 2p and Mg 2p regions for fresh and 900 °C calcined dolomite.

the Ca peaks, and peak fitting reveals the presence of two distinct chemical states at 346.6 and 347.4 eV. We respectively assign these to surface Ca(OH)₂ and CaCO₃ (presumably formed by adventitious adsorption of CO₂ in accordance with the DRIFTS measurements).³⁵ A concomitant downshift in the Mg 2p_{3/2} peak to 50 eV is attributed to the formation of MgO nanoparticles.³⁴

Transesterification reaction

Dolomite samples were subsequently examined for their activity in the transesterification of triglycerides with methanol. Fig. 7 and 8 show the reaction profiles for the transesterification of C₄ and C₈ triglycerides using 900 °C calcined dolomitic rock.

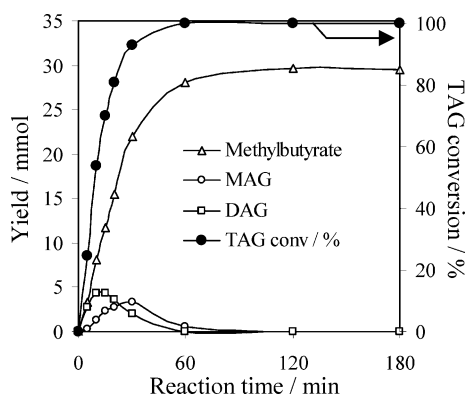


Fig. 7 Reaction profile for 900 °C calcined dolomite catalysed transesterification of tributylglyceride with methanol at 60 °C.

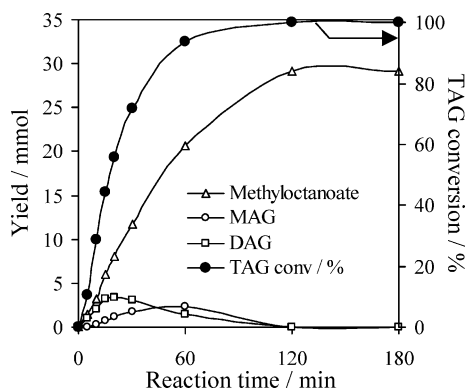


Fig. 8 Reaction profile for 900 °C calcined dolomite catalysed transesterification of trioctylglyceride with methanol at 60 °C.

Material which was uncalcined, or only heated to 600 °C (just above the first decomposition in TGA), was inactive for transesterification, as expected from its lack of base sites. Complete conversion of both TAGs, and their respective mono- and diacyl glyceride (MAG/DAG) intermediates, to the corresponding methyl esters was observed in less than 3 h irrespective of substrate chain length.

Table 3 shows the calculated turnover frequency (TOF) for dolomite catalysed transesterification. For the C₄ TAG a TOF of 587 mmol h⁻¹ g⁻¹ cat is observed, which greatly exceeds that reported for other solid base catalysts in this model reaction.^{13,15} To our knowledge the results in Fig. 8 represent the first report of C₈ TAG transesterification, which proceeds with a lower TOF of 347 mmol h⁻¹ g⁻¹ cat. This reduced TOF compared with the C₄ TAG is possibly indicative of slower diffusion of the bulkier triglyceride into the catalyst microstructure. Catalyst reuse was evaluated in transesterification of the C₄ TAG, with

95% conversion and >98% selectivity to FAME observed after 3 h reaction.

In order to test the applicability of our dolomitic solid base catalysts to commercial plant feedstocks, we also screened them against commercially available olive oil. Olive oil comprises mainly glyceryl trioleate, a C₁₈ unsaturated triglyceride, along with a few percent of triglycerides wherein the oleate chains are substituted for linoleic (C₁₈ doubly unsaturated) or palmitate (C₁₆ saturated). Dolomite calcined at 900 °C again proved effective for the production under mild conditions (Fig. 9), with the final biodiesel composition preserving the initial 90 : 10 : 1 (oleate : linoleate : palmitate) TAG ratios. This new dolomite-derived solid base again achieved excellent conversions of tripalmitate and trilinoleate of >90% within 3 h reaction, with a good performance of ~88% trioleate conversion.

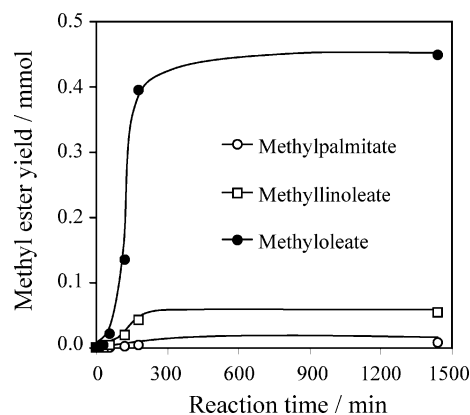


Fig. 9 Reaction profile for 900 °C calcined dolomite catalysed transesterification of olive oil with methanol at 60 °C.

To make a comparison of these values with those from the literature under similar conditions, we have determined TOFs based on the mass of oil and catalyst used in our reaction. For our reaction at 60 °C, we calculate a TOF of 2.9 g_(oil)h⁻¹g_(cat)⁻¹ which compares favourably with values reported for rapeseed oil transesterification at 65 °C where TOF of 1.66 g_(oil)h⁻¹g_(cat)⁻¹ and 0.14 g_(oil)h⁻¹g_(cat)⁻¹ are observed for bulk CaO and MgO, respectively.³⁶ Activities reported for bulk CaO are however very variable and can depend on surface sample pretreatment and microcrystallinity with values ranging between 2.5 to 45 g_(oil)h⁻¹g_(cat)⁻¹ reported in sunflower oil transesterification.¹² Indeed it has recently been reported that the MgO catalysed transesterification of sunflower oil is significantly enhanced through the use of nanocrystalline MgO.⁹

Overall, these results demonstrate the versatility of calcined dolomite as a solid base for transesterification of oils and finds

Table 3 TOF and conversions of solid bases in transesterification of TAGs after 3 h at 60 °C

Catalyst	TAG	Conversion ^b (%)	Selectivity (%)	TOF/mmole h ⁻¹ g ⁻¹ cat
900 °C dolomite	C ₄	100	>98	587
900 °C dolomite	C ₈	100	>98	347
1.2 wt% Li/CaO ¹⁵	C ₄	100	>98	160
Mg _{2.9} Al hydrotalcite ¹³	C ₄	74.3	75 ^a	162

^a Other residual products were mono- and diglycerides intermediates as determined by GC-MS. ^b In all cases blank reactions show <10% TAG conversion after 24 h.

a valuable application for an waste material currently generated at stone quarries.

Conclusions

The application of calcined dolomitic rock has been investigated in the transesterification of triglycerides for biodiesel synthesis. Fresh dolomitic rock comprised approximately 77% dolomite and 23% magnesian calcite. High temperature calcination reveals Mg surface segregation as MgO nanocrystals dispersed over CaO/(OH)₂ particles. CO₂ evolved during calcination increases both the surface area and basicity of natural dolomite. Calcined dolomite is an effective catalyst for the transesterification of C₄, C₈ and even long-chain C₁₆₋₁₈ triglyceride mixtures with methanol. The TOF for tributyrat conversion to methyl butanoate are the highest reported for any solid base to date. Catalytic transesterification rates are slower for more bulky TAGs, and may reflect mass transport limitations in accessing base sites.

Notes and references

- H. Fukuda, A. Kondo and H. Noda, *J. Biosci. Bioeng.*, 2001, **92**, 405.
- F. Ma and M. A. Hanna, *Bioresour. Technol.*, 1999, **70**, 1.
- B. Freedman, R. O. Butterfield and E. H. Pryde, *J. Am. Oil Chem. Soc.*, 1986, **63**, 1375.
- S. Gryglewicz, *Bioresour. Technol.*, 1999, **70**, 249.
- Y. Ono and T. Baba, *Catal. Today*, 1997, **38**, 321.
- K. Narasimharao, A. F. Lee and K. Wilson, *J. Biobased Mater. Bioenerg.*, 2007, **1**, 1.
- K. Tanabe, M. Misono, Y. Ono and H. Hattori, *Stud. Surf. Sci. Catal.*, 1989, **51**.
- E. Li and V. Rudolph, *Energy Fuels*, 2008, **22**, 145.
- M. Verziu, B. Cojocara, J. Hu, R. Richards, C. Ciuculescu, P. Filip and V. I. Parvulescu, *Green Chem.*, 2008, **10**, 373.
- M. Di Serio, M. Ledda, M. Cozzolino, G. Minitillo, R. Tesser and E. Santacesaria, *Ind. Eng. Chem. Res.*, 2006, **45**, 3009.
- X. J. Liu, H. Y. He, Y. J. Wang, S. L. Zhu and X. L. Piao, *Fuel*, 2008, **87**, 216.
- M. Lopez Granados, M. D. Zafra Poves, D. Martin Alonso, R. Mariscal, F. Cabello Galisteo, R. Moreno-Tost, J. Santamarı and J. L. G. Fierro, *Appl. Catal., B*, 2007, **73**, 317.
- D. G. Cantrell, L. J. Gillie, A. F. Lee and K. Wilson, *Appl. Catal., A*, 2005, **287**, 183.
- J. L. Shumaker, C. Crofcheck, S. A. Tackett, E. Santillan-Jimenez and M. Crocker, *Catal. Lett.*, 2007, **115**, 56.
- R. S. Watkins, A. F. Lee and K. Wilson, *Green Chem.*, 2004, **6**, 335.
- D. Highley, A. Bloodworth, and R. Bate, *Dolomite-Mineral planning factsheet*, British Geological Survey, 2006.
- D. Sutton, B. Kelleher and J. R. H. Ross, *Fuel Process. Technol.*, 2001, **73**, 155.
- R. L. Bain, *Ind. Eng. Chem. Res.*, 2005, **44**, 7945.
- M. P. Aznar, M. A. Caballero, J. A. Sancho and E. Frances, *Fuel Process. Technol.*, 2006, **87**, 409.
- T. J. Wang, J. Chang, C. Z. Wu, Y. Fu and Y. Chen, *Biomass Bioenerg.*, 2005, **28**, 508.
- J. Srinakruang, K. Sato, T. Vitidsant and K. Fujimoto, *Catal. Commun.*, 2005, **6**, 437.
- T. J. Wang, J. Chang, P. Lv and J. X. Zhu, *Energy Fuels*, 2005, **19**, 22.
- D. Farcasiu, A. Ghenciu, G. Marino and K. D. Rose, *J. Am. Chem. Soc.*, 1997, **119**, 11826.
- B. C. Gates and T. K. Cheung, *Top. Catal.*, 1998, **6**, 41.
- H. A. Benesi, *J. Am. Chem. Soc.*, 1956, **78**, 4590; T. Yamanka and K. Tanabe, *J. Phys. Chem.*, 1975, **79**, 2409.
- H. Galai, M. Pijolat, K. Nahdi and M. Trabelsi-Ayadi, *Solid State Ionics*, 2007, **178**, 1039.
- K. Wright, R. T. Cygan and B. Slater, *Geochim. Cosmochim. Acta*, 2002, **66**, 2541.
- E. N. Maslen, V. A. Strel'tsov, N. R. Strel'tsova and N. Ishizawa, *Acta Crystallogr., Sect. B: Struct. Sci.*, 1995, **51**, 929.
- V. A. Drits, D. K. McCarty, B. Sakharov and K. L. Milliken, *Can. Mineral.*, 2005, **43**, 1255.
- Powder Diffraction Database, PDF MainEx Lib, Version 9.0.133, Bruker Analytical X-ray Systems GmbH, 1997.
- S. Gunasekaran and G. Anbalagan, *J. Raman Spectrosc.*, 2007, **38**, 846.
- H.-J. Freund and M. W. Roberts, *Surf. Sci. Rep.*, 1996, **25**, 225.
- J. Lanas and J. I. Alvarez, *Thermochim. Acta*, 2004, **423**, 1.
- D. K. Aswala, K. P. Muthea, S. Tawdeb, S. Chodhuryb, N. Bagkarb, A. Singha, S. K. Guptaa and J. V. Yakhmia, *J. Cryst. Growth*, 2002, **236**, 661.
- P. Liu, T. Kendelewicz, G. E. Brown Jr., G. A. Parks and P. Pianetta, *Surf. Sci.*, 1998, **416**, 326.
- S. Yan, H. Lu and B. Liang, *Energy Fuels*, 2008, **22**, 646.

Solvent-modulated reactivity of PCl_3 with amines†

Eric Jean Amigues, Christopher Hardacre,* Gillian Keane and Marie Eugenie Migaud*

Received 6th December 2007, Accepted 12th February 2008

First published as an Advance Article on the web 20th March 2008

DOI: 10.1039/b718849h

The reactivity of phosphorus trichloride towards amines in ionic liquids has been investigated and compared with that in conventional organic solvents. In addition to easing the synthetic procedures thus far required for the preparation of aminochlorophosphines in molecular solvents, for example the ability to operate at 20 °C, under non-anhydrous and high concentration conditions with short reaction times and rapid addition of reagents, bis{(trifluoromethyl)sulfonyl}imide-based ionic liquids offer a tight control over the selectivity during the reaction and offer access to monoamination and bisamination products in high yields and chemoselectivity. Furthermore, these ionic liquids offer a unique storage medium for these highly moisture sensitive aminochlorophosphines.

Introduction

The past decade has seen a revolution in the field of biomedicine through high-density DNA microarrays and biochips.¹ Improvements in DNA microarray technology can be readily associated with improved oligodeoxynucleotide synthesis based on efficient phosphoramidite coupling chemistry.² The increased availability of the phosphoramidite reagents and improved coupling methods has facilitated these exciting developments. However, phosphoramidite reagents still remain expensive to make, difficult to store and, most importantly, lack the chemical variation in order to improve on the overall yields of oligonucleotide polymerisation reactions. Moreover, phosphoramidites containing amino groups other than diisopropylamino have been shown to increase both the reaction rates and isolated yields,³ but due to their greater moisture sensitivity coupled with the fact that the synthesis is more difficult than the analogous diisopropylamine derivatives, these molecules are currently under-used.

The current standard procedures to access the synthetic precursor, alkoxydiisopropylaminochlorophosphine, to the nucleoside phosphoramidite derivatives used as reagents in oligonucleotide syntheses,⁴ require the preliminary treatment of excess PCl_3 with a highly purified alcohol, often cyanoethanol, to yield the alkoxydichlorophosphine. This alkoxydichlorophosphine is then purified *via* distillation and reacted with an excess of diisopropylamine. While this route has been highly optimised in organic solvents, in particular diethyl ether and hexane, there remains significant room for improvement.⁵ Alternatively, attempts to synthesise alkylaminodichlorophosphines

((RNH) PCl_2 and (R_2N) PCl_2) as starting materials to access alkoxyalkylaminochlorophosphines (RNH) $\text{PCl}(\text{OR}')$ and alkoxydialkylaminochlorophosphines (R_2N) $\text{PCl}(\text{OR}')$ in molecular solvents are often plagued by difficulties in achieving specific substitution resulting in low chemoselectivities and the need to use an excess of one of the reagents.⁶

Additionally, the difficulties encountered to favour the production of (RNH) PCl_2 over that of (RNH) $_2\text{PCl}$ is plagued by the high instability towards hydrolysis of the reaction products in solvents such as diethyl ether and hexane, thus resulting in decreased crude yields and need of purification. In a few instances, chemoselective control over the substitution pattern is achieved by increasing the steric hindrance around the phosphorus centre by use of bulky amine reactants and by using excess PCl_3 .⁷ Yet, this approach produces alkylaminodichlorophosphines of little use in oligonucleotides synthesis. High chemoselectivity has been reached in the formation of monoalkylaminodichlorophosphines ((RNH) PCl_2) in organic solvents by using silylated amine^{8,9} or lithiated amine precursors^{10–12} in order to minimise the proportion of bis- and tri-substituted aminophosphine products. Although successful, these conditions to prepare monoalkylaminodichlorophosphines ((RNH) PCl_2) are only suitable for small scale production. In other words, there is currently no scalable method that offers access to a broad range of monoalkylaminodichlorophosphines.

Consequently, while unhindered alkoxymonoalkylaminochlorophosphines have great potential in their application in oligodeoxynucleotide synthesis, the current limitations associated with the synthesis of their synthetic precursors have had a major impact on their lack of application. Therefore, facile synthesis of these aminodichlorophosphines could offer not only opportunities in accessing a broader range of phosphoramidites on large scale but also new opportunities to further improve upon solid phase synthesis of therapeutic agents such as antisense oligonucleotides.¹³

Herein, we report the easily scalable chemoselective synthesis of a range of aminochlorophosphines achieved using ionic liquids. Recently, the chemistry of PCl_3 in ionic liquids has

QUILL/School of Chemistry and Chemical Engineering, Queen's University Belfast, Stranmillis Road, Belfast, Northern Ireland, UK BT9 5AG. E-mail: c.hardacre@qub.ac.uk, m.migaud@qub.ac.uk; Fax: +44 28 9097 4687

† Electronic supplementary information (ESI) available: ¹H NMR, ¹³C NMR and ³¹P NMR spectra following large scale synthesis in [C_4mim][NTf_2] and isolation of dichlorodiisopropylaminophosphine (**7f**). See DOI: 10.1039/b718849h

been reported.¹⁴ Therein, the hydrolytic stability of PCl_3 was found to be enhanced in the ionic liquid media. In addition, its reactivity towards various charged nucleophiles, including sulfates and fluoride ions, was examined with the formation of mixed anhydride-P(III) species as well as PF_3 being observed. In this paper, enhanced chemoselectivity of PCl_3 in a range of non-dried bis((trifluoromethyl)sulfonyl)imide ($[\text{NTf}_2]^-$)-based ionic liquids (Fig. 1) towards a range of primary (Scheme 1) and secondary amines is shown over molecular solvents.

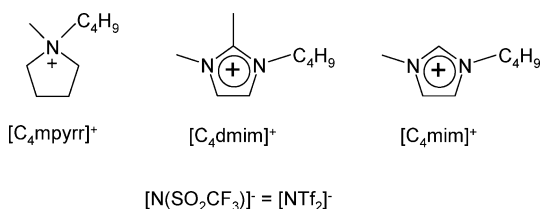


Fig. 1 Ionic liquids employed in this study.

Results and discussion

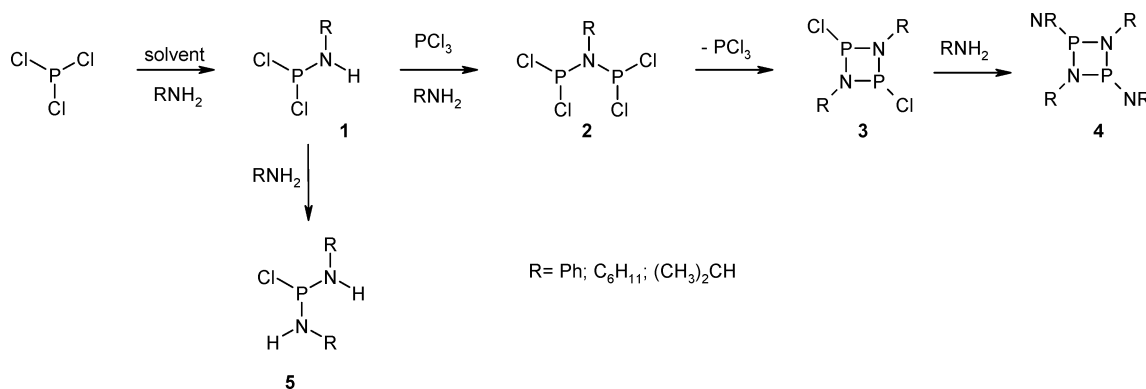
Methodology employed

Stoichiometric ratios between reagents were maintained throughout the experiments in order to maximise atom efficiency with respect to conversion, yields and chemoselectivity for both PCl_3 and the amines investigated. The results in the ionic liquids were compared with those found in hexane as the latter is commonly used in PCl_3 and aminodichlorophosphine

chemistry¹⁵ and provides a better hydrophobic environment than diethyl ether in order to monitor the reactions over extended time periods. The $[\text{NTf}_2]^-$ -based ionic liquids were used in the study as these provided the best balance between solubility of PCl_3 and non-reactivity of the anion whilst providing an environment whereby the presence of water did not lead to hydrolysis. This environment may be contrasted with that found in ionic liquids containing basic anions such as acetate and hydrogensulfate, for example. These ionic liquids have two effects. They increase the K_w of water in the ionic liquid and thus increasing the concentration of OH^- ¹⁶ which acts as a nucleophile and reacts with PCl_3 leading to hydrolysis products. Secondly, these basic anions can act as nucleophiles which directly react with PCl_3 leading to mixed anhydrides, as found previously for mesylate and ethylsulfate based ionic liquids.¹⁴

In the present work, each permutation of ionic liquid ($[\text{C}_4\text{pyrr}][\text{NTf}_2]$, $[\text{C}_4\text{mim}][\text{NTf}_2]$ and $[\text{C}_4\text{dmim}][\text{NTf}_2]$) and stoichiometric ratios of PCl_3 , amine and Hünig's base was examined and the product distribution over time determined and compared with reactions in hexane. As an exemplar, results as a function of solvent selection obtained for isopropyl amine (Table 1) and diisopropyl amine (Table 2) are presented. The results presented in Tables 3 and 4 are the optimal results obtained after evaluation of a full set of experiments for each stoichiometric ratio and for all amines/ionic liquids investigated.

The yields used for the preparation of such tables were determined as a function of ^{31}P NMR peak integration ratio, where the percentage yield corresponds to the ratio of the peak area of a given compound to the total of peak areas of



Scheme 1 Reaction scheme showing the progressive amination of PCl_3 with primary amines.

Table 1 Summary of product distribution of reactions of PCl_3 with isopropyl amine in the absence of Hünig's base in a series of ionic liquids and in hexane; data obtained after 150 min at 20°C

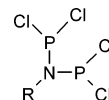
Amine	Solvent	PCl_3 : NHR_2	Percentage distribution				Hydrolysis or adduct product
			PCl_3	Cl_2PNHR (1)	(2)	$\text{ClP}(\text{NHR})_2$ (5)	
Isopropyl amine	$[\text{C}_4\text{mim}][\text{NTf}_2]$	1 : 2	6	59	35	—	—
	$[\text{C}_4\text{dmim}][\text{NTf}_2]$	1 : 2	48	33	19	—	—
	$[\text{C}_4\text{mpyrr}][\text{NTf}_2]$	1 : 2	21	55	24	—	—
	Hexane	1 : 2	62	6	6	—	26

Table 2 Summary of product distribution of reactions of PCl_3 with diisopropyl amine in the presence of Hünig's base in a series of ionic liquids and in hexane; data obtained after 150 min at 20 °C

Amine	Solvent	PCl_3 : NHR_2 : Hünig's Base	Percentage distribution			
			PCl_3	Cl_2PNR_2 (7)	$\text{CIP}(\text{NR}_2)_2$ (8)	Hydrolysis
Diisopropyl amine	$[\text{C}_4\text{mim}][\text{NTf}_2]$	1 : 1 : 1	—	100	—	—
	$[\text{C}_4\text{dmim}][\text{NTf}_2]$	1 : 1 : 1	16	84	—	—
	$[\text{C}_4\text{mpyrr}][\text{NTf}_2]$	1 : 1 : 1	—	100	—	—
	Hexane	1 : 1 : 1	25	75	—	—

Table 3 Summary of product distribution of reactions of PCl_3 with primary amines in the presence and absence of Hünig's base in ionic liquids and in hexane; data obtained after 150 min at 20 °C

Amine	Solvent	PCl_3 : NHR_2 : Hünig's Base	Percentage distribution				Hydrolysis or adduct product
			PCl_3	Cl_2PNHR (1)	(2)	$\text{CIP}(\text{NHR})_2$ (5)	
Aniline (a)	$[\text{C}_4\text{mpyrr}][\text{NTf}_2]$	1 : 2 : 0	9	80	11	—	—
	Hexane	—	58	—	29	—	13 ^a
	$[\text{C}_4\text{dmim}][\text{NTf}_2]$	1 : 1 : 1	13	84	3	—	—
	Hexane	—	74	—	26	—	—
	$[\text{C}_4\text{mpyrr}][\text{NTf}_2]$	1 : 2 : 2	—	9	—	91	—
Cyclohexyl amine (b)	$[\text{C}_4\text{mpyrr}][\text{NTf}_2]$	1 : 2 : 0	17	83	—	—	—
	Hexane	—	47	47	6	—	—
	$[\text{C}_4\text{mim}][\text{NTf}_2]$	1 : 1 : 1	—	—	97	—	10 ^b
	Hexane	—	20	—	80	—	3 ^b
	$[\text{C}_4\text{dmim}][\text{NTf}_2]$	1 : 2 : 2	21	—	79	—	—
Isopropyl amine (c)	$[\text{C}_4\text{mim}][\text{NTf}_2]$	1 : 2 : 0	71	—	29	—	—
	Hexane	—	6	59	35	—	—
	$[\text{C}_4\text{mim}][\text{NTf}_2]$	1 : 1 : 1	62	6	6	—	26 ^b
	Hexane	—	28	—	72	—	—
	$[\text{C}_4\text{dmim}][\text{NTf}_2]$	1 : 2 : 2	50	—	50	—	—
Hexane	—	23	—	77	—	—	
Hexane	—	19	—	81	—	—	



^a Adduct product. ^b Hydrolysis product.

all phosphorus-containing species, and hence corresponds to a mole ratio of phosphorus containing compounds. Typical sets of ^{31}P NMR spectra were taken after 30, 90 and 150 min at 20 °C to present product distribution as a function of time. Fig. 2 illustrates examples of such data sets. In all three cases, the progression of product distribution is clearly identified. It must be noted that at this reagent ratio (PCl_3 : amine : base; 1 : 2 : 2 ratio), there is rapid disappearance of PCl_3 and formation of the monoaminated product. Furthermore, the second amine substitution occurs only once all PCl_3 has been converted. Similarly, the reaction rates of the second amination appear to be slower than that of the first amination. NMR tube experiments were initially conducted in order to obtain “*in situ*” data. While the product distributions under such conditions were consistent with those obtained in reaction vessels where magnetic stirring was applied, lack of stirring resulted in slow reagent mass transfer and much increased reaction time (min vs. days).

Primary amine reactions

Table 3 summarises the results from a ^{31}P NMR study of the sequential dehydrochloride coupling of trichlorophosphine with

aniline, cyclohexylamine and isopropylamine in ionic liquids and hexane. In each reaction, a number of products were identified (Scheme 1) whose distribution, although relatively simple within a given set of conditions used, was strongly dependant on the ratio of reactants/base employed. In general, enhanced chemoselectivity is observed in the ionic liquids compared with in hexane and it is proposed that this occurs *via* a modulation of the amines' reactivity. Under each set of reaction conditions, the amine reacts with PCl_3 to form a mole of HCl. In order to increase the conversion, the HCl must be removed to shift the equilibrium towards the products. This is achieved by the use of Hünig's base or a second mole equivalent of the reactant amine. There are differences in the selectivity and extent of reaction where the reactant amine is used as the base compared with Hünig's base, as well as differences depending on the solvent used. The $\text{p}K_a$ of the base in each solvent in each case determines the extent of reaction and the change in selectivity.

In hexane, in the presence of two equivalents of primary amine, PCl_3 reacted slowly to form *N,N*-bis(dichlorophosphino)-alkyl- and aryl-amine (2), in addition to a transient species, likely to be an amine-adduct of PCl_3 , such as $[(\text{PhNH}_2)\text{PCl}_3]$. It should be noted that the latter was only

Table 4 Summary of product distribution of reactions of PCl_3 with secondary amines in the presence and absence of Hünig's base in ionic liquids and in hexane; data obtained after 150 min at 20 °C

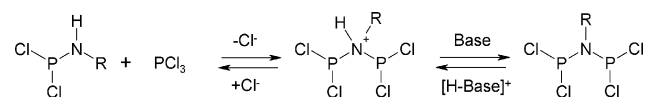
Amine	Solvent	PCl_3 : NHR_2 : Hünig's Base	Percentage distribution				
			PCl_3	Cl_2PNR_2 (7)	$\text{ClP}(\text{NR}_2)_2$ (8)	$\text{P}(\text{NR}_2)_3$ (9)	Hydrolysis (6)
Morpholine (d)	$[\text{C}_4\text{mpyrr}][\text{NTf}_2]$	1 : 2 : 0	23	77	—	—	—
	Hexane	—	8	77	—	—	15
	$[\text{C}_4\text{dmim}][\text{NTf}_2]$ or $[\text{C}_4\text{mpyrr}][\text{NTf}_2]$	1 : 1 : 1	—	100	—	—	—
	Hexane	—	45	50	5	—	—
Piperidine (e)	$[\text{C}_4\text{mpyrr}][\text{NTf}_2]$	1 : 2 : 0	—	—	—	—	100
	Hexane	—	13	67	20	—	—
	$[\text{C}_4\text{mim}][\text{NTf}_2]$ or $[\text{C}_4\text{mpyrr}][\text{NTf}_2]$	1 : 1 : 1	—	—	—	—	—
	Hexane	—	67	33	—	—	—
Diisopropyl amine (f)	$[\text{C}_4\text{mpyrr}][\text{NTf}_2]$	1 : 2 : 0	—	—	—	—	—
	Hexane	—	48	48	4	—	—
	$[\text{C}_4\text{mim}][\text{NTf}_2]$ or $[\text{C}_4\text{mpyrr}][\text{NTf}_2]$	1 : 2 : 2	—	—	—	—	—
	Hexane	—	—	21	67	12	—
Diethyl amine (g)	$[\text{C}_4\text{dmim}][\text{NTf}_2]$	1 : 2 : 0	—	100	—	—	—
	Hexane	—	25	75	—	—	—
	$[\text{C}_4\text{mim}][\text{NTf}_2]$ or $[\text{C}_4\text{mpyrr}][\text{NTf}_2]$	1 : 1 : 1	—	100	—	—	—
	Hexane	—	—	26	44	—	30
Diethyl amine (g)	$[\text{C}_4\text{mim}][\text{NTf}_2]$	1 : 2 : 0	—	100	—	—	—
	Hexane	—	10	75	15	—	—
	$[\text{C}_4\text{mim}][\text{NTf}_2]$	1 : 1 : 1	—	100	—	—	—
	Hexane	—	8	77	15	—	—

formed as minor component, and then only in the absence of Hünig's base. Despite the fact that PCl_3 was not used in excess, a significant amount remained unreacted. In the presence of Hünig's base, no diazadichlorodiphosphetidine (3) or diaminodiazadiphosphetidine (4) were detected nor was the proposed adduct material, even when two equivalents of Hünig's base and two equivalents of the primary amine were used. In hexane, with the exception that no diazadiphosphetidine derivative was formed, similar product distributions to those found for aniline were also observed for cyclohexylamine and isopropylamine, with no monoamination product (1) detectable.

In comparison with hexane, a significant difference increase in the activity and selectivity of the reactions was observed using $[\text{NTf}_2]^-$ -based ionic liquids as the solvent. In the case of aniline, when a two fold excess of aniline and Hünig's base was used, bis(phenylamino)chlorophosphine (5a) was the major product, with the reaction in $[\text{C}_4\text{mpyrr}][\text{NTf}_2]$ forming over 90% bis-substituted material in addition to a small amount of the mono-substituted product. In the presence of two equivalents of amine or one equivalent of amine and one equivalent of Hünig's base, the principal component of the reaction of aniline and PCl_3 was the monoaminodichlorophosphine (1a), with, in the case of $[\text{C}_4\text{mpyrr}][\text{NTf}_2]$, complete conversion of PCl_3 into (1a) and phosphetidine (2a) after 150 min. Although similar product distributions were observed for a 1 : 2 ratio of PCl_3 :primary amine in the case of aniline, cyclohexylamine and isopropylamine, significant changes in the product distribution was found in the case of cyclohexylamine and isopropylamine compared with aniline in the presence of Hünig's base. In the

case of the alkylamines, phosphetidine (2b) and (2c) are formed, exclusively.

This switch in behavior of aniline compared with cyclohexylamine and isopropylamine in the absence and presence of Hünig's base may be explained by a combination of their relative basicity and nucleophilicity and the formation of the charged intermediate from the aminodichlorophosphine ($(\text{RNH})\text{PCl}_2$). Scheme 2 shows the proposed reaction mechanism for the formation of the amine bridged species from the monoaminated dichlorophosphine. In the case of aniline, irrespective of whether a strong base is present in the form of Hünig's base, only monoamination of the PCl_3 is observed. Although aniline is nucleophilic enough to displace the Cl^- in PCl_3 and is a strong enough base to deprotonate the cation intermediate, the nucleophilicity of the monoaminated dichlorophosphine, *i.e.* $\text{PCl}_2(\text{NHR})$, is reduced in comparison with that of the free amine due to the presence of the electron withdrawing effect of the PCl_2 group. This decrease in reactivity of the nitrogen centre in $\text{PCl}_2(\text{NHPh})$, reduces the formation of the cationic intermediate for the bridged species and the equilibrium lies towards the reactants favoring the monoaminated product. In the case of cyclohexylamine and isopropylamine, in the absence of Hünig's base the monoaminated product is also favored but

**Scheme 2** Reaction scheme showing the reaction intermediate during the transformation of monoaminated dichlorophosphine to *N,N*-bis(dichlorophosphino)alkylamine.

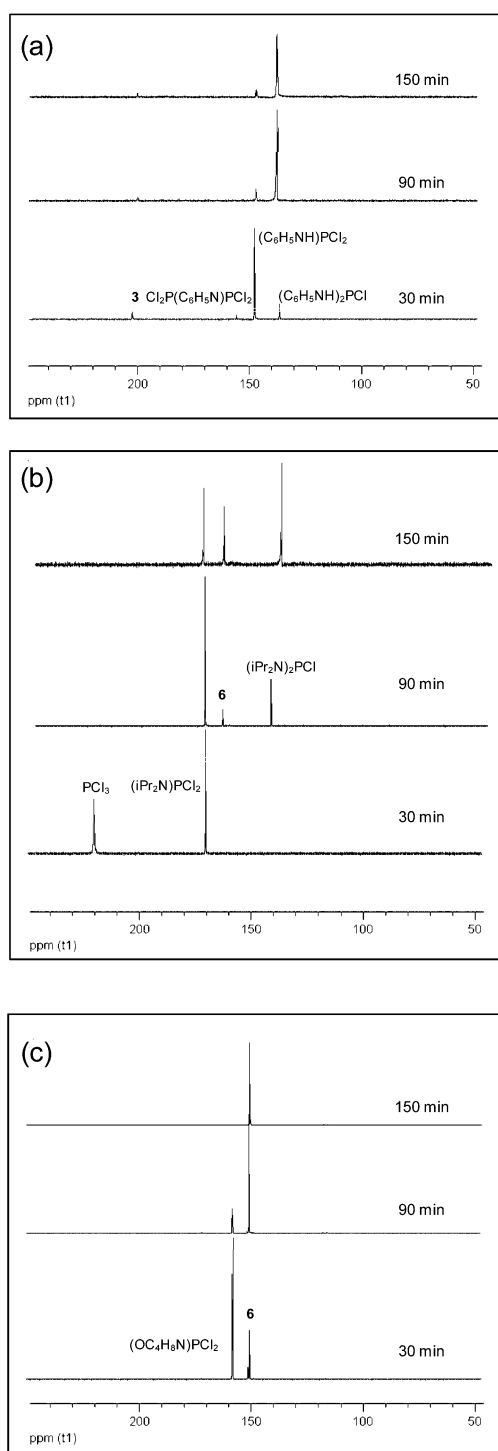


Fig. 2 ^{31}P NMR spectra taken after 30, 90 and 150 min of the reaction between one equivalent of PCl_3 and two molar equivalents of (a) aniline, (b) diisopropyl amine and (c) morpholine in the presence of two molar equivalents of Hünig's base in $[\text{C}_4\text{mpyr}][\text{NTf}_2]$ at 20°C .

in the presence of the strong base the bridged species is formed predominantly. For these amines, the fact that the bridging species does form under some reaction conditions, indicates that, although the nucleophilicity will again reduce going from the free amine to the $\text{PCl}_2(\text{NHR})$ species, the nitrogen centre is still sufficiently reactive to form the cationic intermediate

for the bridged species due to the inductive electron donating effect of the alkyl substituents. This may be compared with the case for the equivalent aniline based species where the nucleophilicity of nitrogen lone pair of electrons is reduced by the presence of the aromatic ring. Unlike the free cyclohexylamine or isopropylamine, which are much weaker bases than Hünig's base (ethyl-diisopropylamine (Hünig's base): $\text{p}K_{\text{a}}$ 11.4 vs. cyclohexylamine $\text{p}K_{\text{a}}$ 10.7), in the presence of the tertiary amine, the cationic intermediate is deprotonated in the ionic liquid and the equilibrium is shifted to the bridged species. Interestingly, a comparison of the results found in hexane and the ionic liquid shows that the $\text{p}K_{\text{a}}$ must be very different in each solvent. In the case of hexane, both the alkyl primary and tertiary amines are sufficiently basic to deprotonate the cationic intermediate, whereas in the ionic liquid only Hünig's base has a high enough $\text{p}K_{\text{a}}$.

It has been shown recently that aromatics and ionic liquids form ordered structures through, for example π - π or methyl- π interactions.¹⁷ Therefore, to confirm that the selectivity differences observed are due to the nucleophilicity/basicity of the amine used and not due to a specific ordering within the solvent, the reactivity of benzylamine was examined. Irrespective of the conditions used, in both hexane and ionic liquids, similar product distributions and rates of reactions were found to those observed with cyclohexylamine under equivalent conditions.

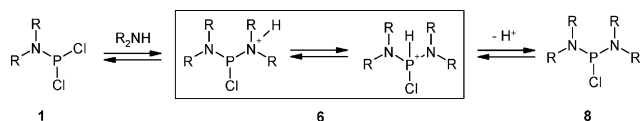
These observations greatly differ from the results reported by Burford *et al.*, as well as those indicating the exclusive formation of dimeric phosphetidine species **3** and **4**.^{18,19} Burford *et al.* reported the sequential dehydrochloride coupling of trichlorophosphine with sub-equivalent amounts of aniline and 2,6-diisopropyl-aniline in both toluene and hexane.¹⁹ Unlike with aniline, with 2,6-diisopropyl-aniline phosphetidines were minor products, indicating that steric interactions were controlling the outcomes of the reactions. It can therefore be concluded that the ionic liquids modulate the basicity of the amine used as well as the nucleophilic reactivity of each amines and the corresponding aminodichlorophosphine towards PCl_3 , thus providing genuine chemoselectivity towards monoaminated product formation.

Secondary amine reactions

Table 4 summarises the results of reacting a range of secondary amines with PCl_3 in ionic liquids and hexane. As expected, compared with the primary amines (Table 3), higher reactivity was observed for the secondary amines due to their increased nucleophilicity. In addition, as found for primary amines, the reactions of secondary amines with PCl_3 showed higher conversions in the ionic liquids than in hexane (Table 4). For example, in the absence of Hünig's base, quantitative conversion was not observed when hexane was used as the solvent, except in the case of diisopropylamine. In contrast, quantitative conversion was found in the ionic liquids for all the secondary amines reacted under similar conditions, even in the absence of the Hünig's base. Moreover, higher selectivity was achievable, in general, in the ionic liquids compared with hexane. For example, complete mono-amination of PCl_3 was achieved very easily in ionic liquids with all the secondary amines studied, whereas a mixture of unreacted PCl_3 , monoaminated, bisaminated and, in some cases,

tris-aminated phosphines were observed in hexane in addition to hydrolysis. With diisopropylamine it was also possible to obtain, in $[C_4mpyrr][NTf_2]$, > 95% yield of bisaminated product after 360 min, where a ratio of 1 : 2 : 2 (PCl_3 : amine : Hünig's base) was used.

Some differences in the product distributions were observed as a function of the amine employed. All secondary amines showed rapid quantitative formation of the monoaminated dichlorophosphine using either a ratio of PCl_3 : amine : Hünig's base of 1 : 2 : 0 and 1 : 1 : 1 in the ionic liquids. In the case of piperidine, no further amination is observed even in the presence of two-equivalent excess of piperidine and Hünig's base (1 : 2 : 2); however, an intermediate at 150.2 ppm which was not the bisaminated phosphine and which did not further react even with extended reaction time was formed. In contrast, under these conditions, the dichlorodiisopropylaminophosphine reacted further to form a stable intermediate with a ^{31}P NMR chemical shift of 163.0 ppm which gradually reacted to form the bisaminated product at 143.0 ppm. Fig. 3 shows the ^{31}P NMR spectra corresponding to the formation of the bisaminated phosphine as a function of time in ionic liquids in the presence of a two-equivalent excess of secondary amine and Hünig's base. These spectra may be compared with equivalent ^{31}P NMR spectra obtained in the presence of one-equivalent of secondary amine and Hünig's base showing the formation of the monoaminated product only (Fig. 3). The intermediate (**6**) formed is thought to be the species formed during nucleophilic attack of the amine on the monoaminated product prior to deprotonation, as shown in Scheme 3. Diethylamine exhibited a similar reactivity at high amine : Hünig's base ratios with the formation of the equivalent bisaminated cationic intermediate which slowly converted to the bisdialkylaminochlorophosphine.



Scheme 3 Reaction scheme showing the formation of the cationic intermediate following nucleophilic attack of a secondary amine on the monoaminated dichlorophosphine.

Interestingly, the intermediates observed in the ionic liquids were not observed under any conditions in hexane supporting the proposal that this is a charged species which is stabilized by the ionic environment. Although some selectivity to the monoaminated product can be obtained in hexane, this is strongly dependent on the ratios of amine, base and PCl_3 . For example, using a 1 : 2 : 2 ratio (PCl_3 : amine : Hünig's base) rapid formation of a mixture of mono-, bis- and trisdialkylaminophosphines was observed for piperidine.

In general, no hydrolysis products were detected by ^{31}P NMR in the ionic liquids compared with up to 26% observed in the dry hexane experiments. This hydrolysis is thought to have occurred during transfer of the sample for NMR characterisation, observations indicative of the hydrolytic instability of these aminodichlorophosphines in organic solvents. During the reaction of 2 equivalents of diethylamine and Hünig's base with PCl_3 , hydrolysis was observed in the ionic liquids in contrast with the high hydrolytic stability of many of the reactions

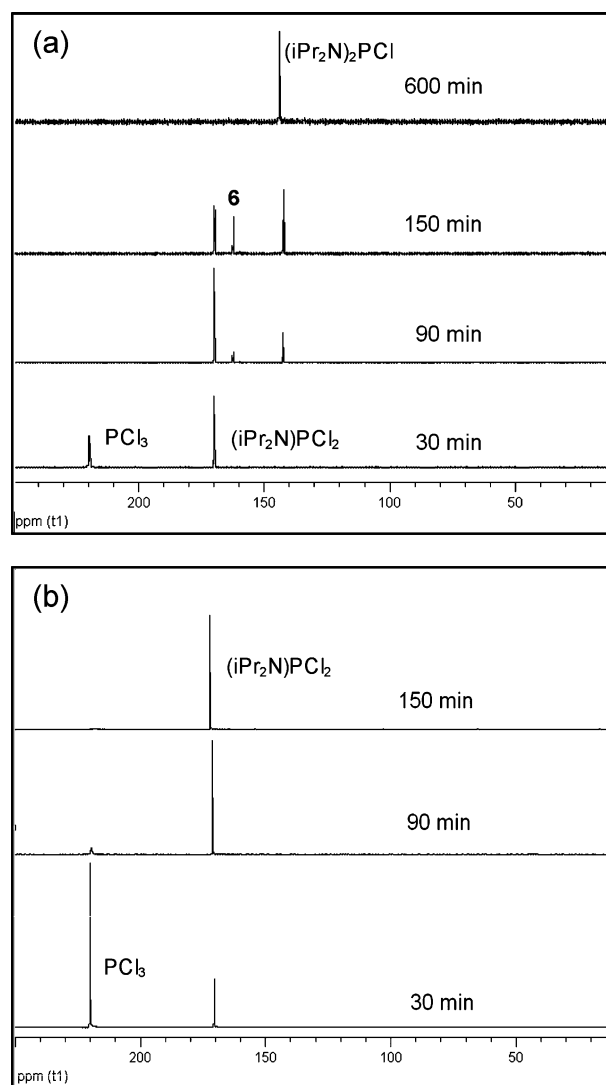


Fig. 3 ^{31}P NMR spectra as a function of reaction time during the reaction of PCl_3 with (a) two equivalents of $HNiPr_2$ and Hünig's base and (b) one equivalent of $HNiPr_2$ and Hünig's base in $[C_4mpyrr][NTf_2]$ at 20 °C.

performed. On further examination, it was shown that hydrolysis was strongly influenced by the concentration/mole ratio of amine/base in the ionic liquid. The increased hydrolytic stability in ionic liquids has been attributed to the fact that the water is strongly bound to the ionic liquid and is well dispersed throughout the solvent resulting in "deactivation of the water".¹⁴ However, in the presence of competing molecules which may hydrogen bond to the solvent, some of the water is displaced thus promoting hydrolysis. This effect is highly concentration dependent, for example, hydrolysis was only observed in the case of diisopropylamine when used in a ratio of 1 : 3 : 3 (PCl_3 : diisopropylamine : Hünig's base) and when PCl_3 was present in the ionic liquid at 0.13 mole fraction, with respect to the ionic liquid. At lower mole fraction concentration (e.g. 0.1 mole fraction) or at a ratio of 1 : 2 : 2 (PCl_3 : diisopropylamine : Hünig's base) such hydrolysis is not observed, hence the versatility of the synthetic procedures.

Interestingly, the chemoselectivity enhancement of the ionic liquid over hexane for the reactions of secondary amines occurs even if the ionic liquid is used in small concentrations, as an additive. For example, a large-scale reaction was performed to form dichlorodiisopropylaminophosphine from reaction of PCl_3 (0.40 moles) with diisopropylamine (0.40 moles) in the presence of Hünig's base (0.40 moles) and $[\text{C}_4\text{mim}][\text{NTf}_2]$ (0.075 moles) at 20 °C. At the higher concentration the reaction proceeded more slowly than observed under dilute conditions but still did not require practical precautions such as cooling down of the system to control the expected exothermic reaction between PCl_3 and diisopropylamine, as required in organic solvents. Similar chemoselectivity was obtained as observed at more dilute concentrations with quantitative conversion observed by ^{31}P NMR. Fig. 4 shows the evolution of the product distribution followed by ^{31}P NMR over the first 74 h of the reaction. After five days, quantitative conversion to the monoaminated dichlorophosphine product had occurred. Once the reaction was complete, the product was distilled from the reaction mixture at 84 °C under 0.1 mmHg and yielded 60% of pure isolated product.

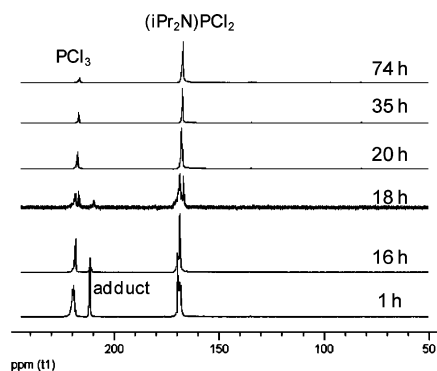


Fig. 4 Evolution of the product distribution followed by ^{31}P NMR over 74 h of the reaction between PCl_3 , diisopropylamine and Hünig's base at a molar ratio of 1 : 2 : 2 and an initial PCl_3 mole ratio of 85% in $[\text{C}_4\text{mim}][\text{NTf}_2]$ at 20 °C.

Two work-up procedures were investigated, namely distillation and solvent extraction. Using distillation, some decomposition of the ionic liquid was found and this limited the recyclability of the ionic liquid but allowed separation of the desired and side products. However, solvent extraction did lead to efficient recycling of the ionic liquid. The side products were also extracted and required distillation to separate the products subsequently. The ammonium salts still present in the ionic liquids after extraction of the phosphorus containing compounds with an appropriate organic solvent (hexane, diethyl ether) were removed by a simple aqueous wash. The ionic liquids were then dried under vacuum and left open to the air to equilibrate with respect to their water content and could be recycled over four times. However, some optimisation with respect to identifying the best extracting solvent for a given aminochlorophosphine thus synthesized was needed. For example, diisopropylaminodichlorophosphine was extracted from $[\text{C}_4\text{mim}][\text{NTf}_2]$ using hexane producing isolated yields similar to those obtained by distillation.

The high concentrations used in the reaction performed in the ionic liquid cannot be undertaken in organic solvents such

as hexane due to the increased viscosity of the reaction mixture as the reaction proceeds. In the presence of the ionic liquids, the trialkylammonium chloride salt, formed by the neutralization of the HCl during the amination, dissolved allowing for the reaction mixture to remain fluid. In contrast, the salt precipitated from hexane resulted in thick slurry which was difficult to stir. This slurry resulted in poor mass transfer, reducing the overall yield of the reaction and required filtration under inert atmosphere before workup to isolate the monoaminated chlorophosphine formed. Even at low concentration, this ammonium salt precipitated in hexane while the $[\text{C}_4\text{mim}][\text{NTf}_2]$ remained solid-free, see ESI.† Additionally, the reaction was carried out at 20 °C with no need for control of the reagents' addition rates, unlike reactions carried out in hexane. The fact that, for a given solvent, the chemoselectivity was similar under high and low concentration conditions indicates that the enhanced chemoselectivity found in the ionic liquids compared with hexane is unlikely to be associated with mass transfer effects due to the precipitation of the salt from the hexane.

As found previously with PCl_3 , although highly air and hydrolytically unstable, once formed, alkylaminodichlorophosphines and dialkylaminodichlorophosphines were found to be stabilized with respect to hydrolysis in the "wet" ionic liquid. For example, dichlorodiisopropylaminophosphine was stored in air with 0.06 mole ratio with respect to $[\text{C}_4\text{dmim}][\text{NTf}_2]$ with <5% hydrolysis over a period of 8 months.

Conclusions

In conclusion, $[\text{NTf}_2]^-$ -based ionic liquids provide a unique environment for the highly chemoselective production and storage of mono, bis and triaminated phosphines at 20 °C. High yielding monoamination of PCl_3 can be achieved with primary amines in the absence of strong base under scalable reaction conditions. Furthermore, $[\text{C}_4\text{mim}][\text{NTf}_2]$ provides an excellent environment for finely controlled reaction conditions to prepare the monoalkylaminophosphetidines also in high yields. Chemoselectivity with respect to the formation of monoaminated and bisaminated chlorophosphines on reaction of PCl_3 with aromatic amines can be achieved under controlled conditions using $[\text{C}_4\text{mpyr}][\text{NTf}_2]$ as solvent and one or two equivalents of amine and Hünig's base, respectively. Similar high selectivity and faster reaction times can be achieved for secondary amines in the ionic liquids. These high selectivities are difficult to achieve using molecular solvents and require the use of excess reagents, derivatised starting materials and careful control of the reaction conditions, for example concentration, temperature and water content. Very importantly, secondary amines were found to react with the same efficacy under the same temperature and rate of reagent addition conditions in highly concentrated solutions (*i.e.* additive amounts of ionic liquids) as in diluted ionic liquid-solutions. This allows for the possibility of using small quantities of the expensive $[\text{NTf}_2]^-$ -based ionic liquids rather than in solvent volumes for the large scale production of dichlorodialkylaminophosphines.

Overall, ionic liquids provide an opportunity to use of stoichiometric ratios of PCl_3 and amine to obtain high selectivity of the desired product without the additional waste of PCl_3 which must be removed when used in large excess or the need to make

a specific amine nucleophile, *e.g.* the anion. These reactions may be carried out at high concentration thus limiting the amount of solvent used without pretreatment of the ionic liquid which may be used wet. The ionic liquid media significantly reduces the waste compared with reactions performed in conventional organic solvents.

Experimental

General procedures

The product distribution of the reaction of PCl_3 with amines was examined *in situ* by ^{31}P NMR, ^1H - ^{31}P coupled NMR. Large scale reactions were carried out in order to establish a protocol for product isolation and to examine the product stability in ionic liquids. Three sets of parallel experiments using 1-butyl-3-methylimidazolium bis{(trifluoromethyl)sulfonyl}imide ($[\text{C}_4\text{mim}][\text{NTf}_2]$), 1-butyl-2,3-dimethylimidazolium bis{(trifluoromethyl)sulfonyl}imide ($[\text{C}_4\text{dmim}][\text{NTf}_2]$), and 1-butyl-1-methyl-pyrrolidinium bis{(trifluoromethyl)sulfonyl}imide ($[\text{C}_4\text{mpyr}][\text{NTf}_2]$) were carried out. These ionic liquids were prepared in house using standard literature methods²⁰ from the appropriate halide salt. Water content and bromide content were measured for each ionic liquid using Karl Fischer titration and ion chromatography, respectively. In each case, the bromide levels were below 5 ppm and the water content was between 0.09 and 0.21 wt%. The ionic liquids were used without drying.

For each set of experiments, the molar ratio between PCl_3 (Aldrich, 98%), the nucleophilic amine and the base, ethyldiisopropylamine (Sigma Aldrich, redistilled, 99.5%) were varied. The amines investigated were aniline, cyclohexylamine, isopropylamine, piperidine, morpholine, diethylamine and diisopropylamine which were obtained from Aldrich and distilled over calcium hydride prior to use.

In general, in order to benchmark the results in the ionic liquids, the experiments were performed in *n*-hexane (Aldrich) which was distilled over calcium hydride and stored with molecular sieves (4 Å). The reactions were monitored over time for up to 150 min and were carried out at 20 °C under an argon atmosphere whilst stirring using a magnetic follower.

Spectroscopic details

All the ^{31}P , ^{31}P - ^1H nuclear magnetic resonance spectra were recorded on a Bruker AC 300 (Avance) at 25 °C by directly transferring samples into the NMR tube with no addition of deuterated solvents. The ^{31}P NMR chemical shifts were recorded in parts per million (ppm) relative to an external probe (sealed capillary tube inside the NMR tube sample) of triethylphosphate ($\text{PO}(\text{OEt})_3$) in CDCl_3 (solvent used for locking/shimming optimisation). The $\text{PO}(\text{OEt})_3$ probe was referenced at 0.2 ppm.

General experimental for each reaction condition studied

Reaction conditions where a ratio of 1 : 2, PCl_3 : amine was used.

In 1.5 cm³ of solvent, 0.8 mmol of PCl_3 (66 μl) and 1.6 mmol of a given amine were combined and stirred under argon at *ca.* 20 °C. After 30 min, a 0.5 cm³ aliquot was removed for analysis

by ^{31}P and ^{31}P - ^1H NMR spectroscopy, and then hourly, up to 150 min.

Reaction conditions where a ratio of 1 : 1 : 1, PCl_3 : amine : Hünig's base was used. In 1.5 cm³ of solvent, 0.8 mmol of PCl_3 (66 μl), 0.8 mmol of distilled amine and 0.8 mmol of ethyldiisopropylamine (Hünig's base, 130 μl) were combined and stirred under argon at *ca.* 20 °C. A 0.5 cm³ aliquot was removed for analysis by ^{31}P and ^{31}P - ^1H NMR spectroscopy after 30 min and then hourly, for up to 150 min.

Reaction conditions where a ratio of 1 : 2 : 2, PCl_3 : amine : Hünig's base was used. In 1.5 cm³ of solvent 0.8 mmol of PCl_3 (66 μl), 1.6 mmol of distilled amine and 1.6 mmol of ethyldiisopropylamine (Hünig's base, 260 μl) were combined and stirred under argon at *ca.* 20 °C. A 0.5 cm³ aliquot was removed for analysis by ^{31}P and ^{31}P - ^1H NMR spectroscopy after 30 min and then hourly, for up to 150 min.

Product identification under optimized conditions

Dichlorophenylaminophosphine (1a). The aliquot contained 84% of the named compound (^{31}P , δ , 148.5 ppm, ^{31}P - ^1H coupled, d, $J_{\text{P-NH}} = 36.8$ Hz; ^{15}N , δ , 57.3 ppm, ^{31}P - ^{15}N coupled $J_{\text{P-N}} = 89$ Hz) after 150 min using a 1 : 1 : 1, PCl_3 : amine : Hünig's base ratio in $[\text{C}_4\text{dmim}][\text{NTf}_2]$. EI-MS; *m/z* ($\text{M}-\text{H}^+$) 193.1. This compound was also formed in 80% yield when two equivalents of amine and no Hünig's base were used in $[\text{C}_4\text{mpyr}][\text{NTf}_2]$.

***N,N*-bis-(Dichlorophosphino)phenylamine (2a).** The aliquot contained 83% of the named compound (^{31}P , δ , 155.5 ppm; ^{31}P - ^{15}N coupled $J_{\text{P-N}} = 93$ Hz) after 90 min using a 1 : 2 : 2, PCl_3 : amine : Hünig's base ratio in hexane.²¹

Aniline-phosphorus trichloride adduct

The aliquot contained 13% of the proposed adduct compound (^{31}P , δ , 201.1 ppm, ^{31}P - ^1H coupled, t, $J_{\text{P-NH}} = 29.9$ Hz) after 150 min in hexane using a 1 : 2, PCl_3 : amine : Hünig's base ratio.

Chlorobisphenylaminophosphine (5a). The aliquot contained 91% of the named compound (^{31}P , δ , 138.7 ppm) after only 90 min using 1 : 2 : 2, PCl_3 : amine : Hünig's base ratio in $[\text{C}_4\text{mpyr}][\text{NTf}_2]$.

Dichlorocyclohexylaminophosphine (1b). The aliquot contained 47% of the named compound (^{31}P , δ , 157.2 ppm, ^{31}P - ^1H coupled, d, $J_{\text{P-NH}} = 36.8$ Hz; ^1H , δ , 8.3 (br, NH), 3.52 (m, *CHNP*); ^{13}C 50.6 ppm (CNP)) after 150 min using a 1 : 2, PCl_3 : amine ratio in $[\text{C}_4\text{mpyr}][\text{NTf}_2]$.

***N,N*-bis(Dichlorophosphino)cyclohexylamine (2b).** The aliquot contained 97% of the named compound (^{31}P , δ , 170.3 ppm; ^1H , δ , 4.08 (m, *CHNP*); ^{13}C δ , 52.8 ppm (CNP)) after 150 min using a 1 : 1 : 1, PCl_3 : amine : Hünig's base ratio in $[\text{C}_4\text{mim}][\text{NTf}_2]$.²²

Dichloroisopropylaminophosphine (1c). The aliquot contained 71% of this compound in $[\text{C}_4\text{mim}][\text{NTf}_2]$ after 150 min (^{31}P , δ , 157.3 ppm, ^{31}P - ^1H coupled, d, $J_{\text{P-NH}} = 48.6$ Hz; ^{13}C , δ , 44.6, 23.3 ppm) after 150 min, using a 1 : 2, PCl_3 : amine ratio.

***N,N*-bis-(Dichlorophosphino)isopropylamine (2c).** The aliquot contained 72% of *N,N*-bis(dichlorophosphino)isopropylamine in [C₄mim][NTf₂] (³¹P, δ , 170.4 ppm; ¹³C, δ , 45.8, 24.0 ppm) after 150 min using a 1 : 1 : 1, PCl₃ : amine : Hünig's base ratio.²³

Morpholine intermediate (6). The aliquot contained 100% of the named compound (³¹P, δ , 150.2 ppm) after 150 min in [C₄mpyrr][NTf₂] using a reaction condition of 1 : 2 : 2, PCl₃ : amine : Hünig's base reaction conditions.

Dichloromorpholinophosphine (7d). The aliquot contained 100% of the named compound (³¹P, δ , 157.7 ppm, ³¹P–¹H coupled, *d*, $J_{\text{P-NH}} = 7.4$ Hz) after 90 min in [C₄mpyrr][NTf₂] using a ratio of 1 : 1 : 1, PCl₃ : amine : Hünig's base.²⁴

Dichloropiperidinophosphine (7e). The aliquot contained 100% of the named compound (³¹P, δ , 157.8 ppm, ³¹P–¹H coupled, *t*, $J_{\text{P-NH}} = 8.3$ Hz) after only 90 min using a 1 : 1 : 1, PCl₃ : amine : Hünig's base ratio in [C₄mpyrr][NTf₂]. This result was also observed in the [C₄mim][NTf₂].²⁵

Dichlorodiisopropylaminophosphine (7f). The aliquot contained 100% of the named compound (³¹P, δ , 169.4 ppm, ³¹P–¹H coupled, *t*, $J_{\text{P-NH}} = 12.8$ Hz) after 150 min using a 1 : 1 : 1, PCl₃ : amine : Hünig's base ratio in [C₄mpyrr][NTf₂].²⁶

Chlorobisdiisopropylaminophosphine (8f). The aliquot contained 44% of the named compound (³¹P, δ , 143.0 ppm, ³¹P–¹H coupled, *t*, $J_{\text{P-NH}} = 11.4$ Hz) after 150 min using a 1 : 2 : 2, PCl₃ : amine : Hünig's base ratio in [C₄mpyrr][NTf₂]. After 180 min 85% of this compound was observed.²⁷

Dichlorodiethylaminophosphine (7g). The aliquot contained 100% of compound **11** (³¹P, δ , 162.6 ppm) after 150 min using a 1 : 1 : 1, PCl₃ : amine : Hünig's base ratio in [C₄mim][NTf₂].²⁸

Chlorobisdiethylaminophosphine (8g). The aliquot contained 67% of the named compound (³¹P, δ , 156.0 ppm) after 150 min, along with mono- (³¹P, δ , 162.0 ppm) and tris- (³¹P, δ , 119.0 ppm) substituted products in hexane using a 1 : 2 : 2, PCl₃ : amine : Hünig's base ratio.²⁹

Dichlorobenzylaminophosphine

The aliquot contained 77% of the named compound (³¹P, δ , 162.0 ppm, *d*, $J_{\text{P-NH}} = 51.3$ Hz) after only 90 min in [C₄mpyrr][NTf₂] using a 1 : 2 : 0, PCl₃ : amine : Hünig's base ratio.

N,N-bis(Dichlorophosphino)benzylamine

The aliquot contained 56% of *N,N*-bis(dichlorophosphino)benzylamine (³¹P, δ , 168.0 ppm) after 150 min in [C₄mpyrr][NTf₂] using a 1 : 1 : 1, PCl₃ : amine : Hünig's base ratio.

Large scale synthesis of dichlorodiisopropylaminophosphine (7f). To 0.075 mol of the ionic liquid [C₄mim][NTf₂] was added 0.40 mol of PCl₃ (34.90 cm³) under argon. A mixture of 0.40 mol of distilled diisopropylamine (56.10 cm³) and 0.40 mol of distilled ethyldiisopropylamine (Hünig's base, 69.68 cm³) was then added slowly *via* an addition funnel over 15 min. Aliquots were removed for analysis by ³¹P and ³¹P–¹H NMR. After

three days, the named compound was distilled from the ionic liquid under vacuum (0.1 mmHg) at 84 °C into a flask containing a small amount of stabilizing ionic liquid, [C₄dmm][NTf₂] (7.00 g). The clear liquid was obtained in 60% isolated yield. The remainder was left un-distilled. ¹H NMR (300 MHz, CDCl₃, δ ppm relative to TMS) 3.9 (hept, 2H, $J = 4.1$ Hz, 2 \times CH), 1.3 (d, 12 H, $J = 8.3$ Hz, 4 \times CH₃). ¹³C NMR (75 MHz, CDCl₃, δ ppm relative to CDCl₃) $\delta = 48.2$ (d, $J = 7.5$ Hz), 23.6 (d, $J = 7.5$ Hz). ³¹P, δ , 169.4 ppm, ³¹P–¹H coupled, *t*, $J_{\text{P-NH}} = 12.8$ Hz.

Acknowledgements

We acknowledge QUILL and DEL for funding (GK), Merck KGaA for financial support (EA) and the donation of ionic liquids and EPSRC for funding under a Portfolio Partnership. Maeve O'Neill is acknowledged for providing initial results.

References

- 1 I. Wick and G. Hardiman, *Curr. Opin. Drug Discovery Dev.*, 2005, **8**, 347–354.
- 2 K. Dill and A. McShea A., *Drug Discovery Today: Technol.*, 2005, **2**, 261–266.
- 3 K. L. Fearon, B. L. Hirschbein, M. F. Foy, M. Q. Nguyen, A. Okruszek, S. N. McCurdy, J. E. Frediani, L. A. Dedionisio, A. M. Raible, E. N. Cagle and V. Boyd, *Nucleic Acids Res.*, 1998, **26**, 3813–3824.
- 4 K. Akaji, *Reagents for glycoside, nucleotide and peptide synthesis*, ed. D. Crich, John Wiley & Sons, Chichester, 2005.
- 5 R. Gukathasan, M. Massoudipour, I. Gupta, A. Chowdhury, S. Pulst, S. Ratnam, Y. S. Sanghvi and S. A. Laneman, *J. Organomet. Chem.*, 2005, **690**, 2603–2607.
- 6 A. B. Burg and P. J. Slota, *J. Am. Chem. Soc.*, 1958, **80**, 1107–1109; P. Marchand, A. Meffre, B. Donnadiou, D. Taton, Y. Gnanou, M. Destarac, F. Leising, A.-M. Caminade and J.-P. Majoral, *Phosphorus, Sulfur Silicon Relat. Elem.*, 2007, **182**, 1233–1244; K. Gholivand, Z. Shariatnia, Z. A. Tabasi and A. Tadjarodi, *Heteroat. Chem.*, 2006, **17**, 337–343.
- 7 F. Riviere, S. Ito and M. Yoshifuji, *Tetrahedron Lett.*, 2002, **43**, 119–122; N. Burford, T. S. Cameron, K. D. Conroy, B. Ellis, C. L. B. Macdonald, R. Ovans, A. D. Phillips, P. J. Ragogna and D. Walsh, *Can. J. Chem.*, 2002, **80**, 1404–1409; D. Polet, A. Alexakis, K. Tissot-Croset, C. Corminboeuf and K. Ditrich, *Chem.–Eur. J.*, 2006, **12**, 3596–3609.
- 8 E. W. Abel, *J. Chem. Soc.*, 1965, 57–61.
- 9 G. Bettermann, D. Schomburg and R. Schmutzler, *Phosphorus Sulfur Relat. Elem.*, 1986, **28**, 327–336.
- 10 A. L. Spek, F. J. J. de Kanter, A. W. Ehlers, A. M. Mills, M. Lutz, M. Schakel, K. Lammertsma, R. H. Lemmens, N. van der Riet and M. L. G. Borst, *Chem.–Eur. J.*, 2005, **11**, 3631–3642.
- 11 W. C. Zhang and X. M. Zhang, *Angew. Chem., Int. Ed.*, 2006, **45**, 5515–5518.
- 12 W. Zhang, C.-J. Wang, W. Gao and X. Zhang, *Tetrahedron Lett.*, 2005, **46**, 6087–6090.
- 13 M. H. Caruthers, A. D. Barone, S. L. Beaucage, D. R. Dodds, E. F. Fisher, L. J. McBride, M. Matteucci, Z. Stabinsky and J. Y. Tang, *Methods Enzymol.*, 1987, **154**, 287–313.
- 14 E. Amigues, C. Hardacre, G. Keane, M. Migaud and M. O'Neill, *Chem. Commun.*, 2006, 72–74.
- 15 e.g. E. Drent, R. van Dijk, R. van Ginkel, B. van Oort and R. I. Pugh, *Chem. Commun.*, 2002, 964–965; E. J. Nurminen, J. K. Mattinen and H. Loennberg, *J. Chem. Soc., Perkin Trans. 2*, 1998, **7**, 1621–1628.
- 16 D. R. MacFarlane, J. M. Pringle, K. M. Johansson, S. A. Forsyth and M. Forsyth, *Chem. Commun.*, 2006, 1905–1917.
- 17 J. D. Holbrey, W. M. Reichert, M. Nieuwenhuyzen, O. Sheppard, C. Hardacre and R. D. Rogers, *Chem. Commun.*, 2003, 476–477; C. G. Hanke, A. Johansson, J. B. Harper and R. M. Lynden-Bell, *Chem. Phys. Lett.*, 2003, **374**, 85–90; J. B. Harper and R. M. Lynden-Bell, *Mol. Phys.*, 2004, **102**, 85–94; M. Deetlefs, C. Hardacre,

- M. Nieuwenhuyzen, O. Sheppard and A. K. Soper, *J. Phys. Chem. B*, 2005, **109**, 1593–1598.
- 18 A. R. Davies, A. T. Dronsfield, R. N. Haszeldine and D. R. Taylor, *J. Chem. Soc., Perkin Trans. 1*, 1973, 379–385.
- 19 N. Burford, T. S. Cameron, K. D. Conroy, B. Ellis, C. L. B. Macdonald, R. Ovans, A. D. Philips, P. J. Ragona and D. Walsh, *Can. J. Chem.*, 2002, **80**, 1404–1409.
- 20 P. Bonhôte, A. Dias, N. Papageorgiou, K. Kalyanasundaram and M. Grätzel, *Inorg. Chem.*, 1996, **35**, 1168–1178.
- 21 H.-J. Chen, J. M. Barendt, R. C. Haltiwanger, T. G. Hill and A. D. Norman, *Phosphorus Sulfur Relat. Elem.*, 1986, **26**, 155–162.
- 22 F. Dodds, F. Garcia, R. A. Kowenicki, S. P. Parsons, M. McPartlin and D. S. Wright, *Dalton Trans.*, 2006, **35**, 4235–4243.
- 23 R. Jefferson, J. F. Nixon, T. M. Painter, T. R. Keat and L. Stobbs, *J. Chem. Soc., Dalton Trans.*, 1973, 1414–1419.
- 24 J. Cornforth, R. H. Cornforth and R. T. Gray, *J. Chem. Soc., Perkin Trans. 1*, 1982, **10**, 2289–2298.
- 25 S. E. Denmark, X. Su, Y. Nishigaichi, D. M. Coe, K.-T. Wong, S. B. D. Winter and J. Y. Choi, *J. Org. Chem.*, 1999, **64**, 1958–1967.
- 26 M. J. Overett, K. Blann, A. Bollmann, J. T. Dixon, F. Hess, E. Killian, H. Maumela, D. H. Morgan, A. Neveling and S. Otto, *Chem. Commun.*, 2005, 622–624.
- 27 A. Wilk, M. K. Chmielewski, A. Grajkowski, L. R. Phillips and S. L. Beaucage, *J. Org. Chem.*, 2002, **67**, 6430–6438.
- 28 J. P. Linthoudt, E. V. Berghe and G. P. Kelen G. P., *Spectrochim. Acta, Part A*, 1980, **36**, 315–320.
- 29 D. J. Dellinger, D. M. Sheehan, N. K. Christensen, J. G. Lindberg and M. H. Caruthers, *J. Am. Chem. Soc.*, 2003, **125**, 940–950.

Potential of 'nanofluids' to further intensify microreactors

Xiaolei Fan,^a Haisheng Chen,^b Yulong Ding,^b Pawel K. Plucinski^a and Alexei A. Lapkin^{*a}

Received 20th November 2007, Accepted 11th March 2008

First published as an Advance Article on the web 1st April 2008

DOI: 10.1039/b717943j

Recent discovery of high enhancement of heat transfer in nanofluids may be applicable to the area of process intensification of chemical reactors through integration of the functionalities of reaction and heat transfer in compact multifunctional reactors. This may lead to the reduction in the processes footprint and energy intensity over the process life cycle, allow easier implementation of highly exothermic and endothermic reactions, and enable rapid quenching of reactions. A nanofluid based on benign TiO₂ material dispersed in ethylene glycol has been studied in an integrated reactor–heat exchanger. An up to 35% increase in the overall heat transfer coefficient was measured in the steady state continuous experiments. This resulted in a closer temperature control in the reaction of selective reduction of an aromatic aldehyde by molecular hydrogen and very rapid change in the temperature of reaction under dynamic reaction control.

Introduction

Process intensification (PI), a term coined in the 1980s,^{1–3} encompasses the many different approaches leading ultimately to chemical processes that are: inherently safe, reduce or eliminate the need for on-site inventory of toxic/hazardous compounds, energy efficient and are characterised by a small footprint.^{4,5} Some examples of PI approaches include intensification of mass and heat transfer in microreactors^{6–8} and high shear reactors, *e.g.*, spinning disk⁹ and impinging jets, the use of neoteric solvents, *e.g.*, sc-CO₂,¹⁰ and ionic liquids.¹¹ Amongst many PI approaches, ionic liquids and compact reactors–heat exchangers are being commercialised at a very rapid pace.¹²

The principle of intensification in micro- and compact reactors is in the reduction of the length scales across which mass and heat transfer should occur, which allows the performing of highly exothermic and endothermic reactions safely, and to couple reactions with different heat effects. For example, selective oxidation of aromatic alcohols by molecular oxygen has been demonstrated at up to 24 atm undiluted oxygen pressure, which was enabled by (i) highly efficient heat removal in an integral micro-heat exchanger and (ii) the absence of gas-phase volume in which an explosive mixture of hydrocarbon vapour and oxygen may be produced.⁷

The main mechanisms by which an enhancement of heat transfer is achieved in microstructured heat exchangers, compared with conventional heat exchangers, are (i) the reduction of the material of construction conduction resistance (very thin barrier between the process fluid and the heat transfer medium), and (ii) by enhancing the convective heat transfer coefficient, the latter being achieved through design of the geometry of

the 100s of microns width scale heat transfer fluid channels.¹³ Taking this concept to the extreme will give a design with very thin walls and very narrow channels. The resulting heat transfer fluid pressure drop and, consequently, high pumping power, will negate the increase in the effectiveness of heat transfer, by increasing the overall process energy requirement. Thus, there exists an upper bound in efficiency of microreactors, given by the overall process energy optimisation. The remaining possibilities in further increasing the efficiency of micro-heat exchangers are the modification of the surface¹⁴ or an enhancement in the thermal properties and behaviour of the heat transfer fluid itself.

The latter approach has recently attracted a significant interest through the emergence of a new field of 'nanofluids', the term coined at Argonne National Labs.¹⁵ A nanofluid is a stable dilute suspension of nanoparticles in a heat transfer fluid, which alters the heat transfer characteristics of the base fluid. According to the classic effective medium (mean field or Maxwell) theory of heat transfer, an increase in the volume fraction of nanoparticles with a higher thermal conductivity than that of the base fluid, results in an increase in the effective thermal conductivity, as given by Hamilton and Crosser:¹⁶

$$\frac{k_{\text{nf}}}{k_{\text{f}}} = \frac{k_{\text{p}} + 2k_{\text{f}} - 2\phi(k_{\text{f}} - k_{\text{p}})}{k_{\text{p}} + 2k_{\text{f}} + \phi(k_{\text{f}} - k_{\text{p}})} \quad (1)$$

where k_{nf} , k_{f} and k_{p} are thermal conductivities of the nanofluid, base fluid and suspended particle, respectively, and ϕ is the particle volume fraction.

According to eqn (1) only a marginal increase in the thermal conductivity of a nanofluid could be expected. For example, a typical volume fraction of nanoparticles of 1 vol% gives an enhancement in thermal conductivity of *ca.* 3%. However, experimental results can be found in the literature with significantly better^{15,17,18} and significantly worse¹⁹ $k_{\text{nf}}/k_{\text{f}}$ ratios, as well as those supporting the basic Maxwell theory.²⁰ The exciting unexpectedly high increase in the thermal conductivity above the prediction of the classic theory resulted in a sharp increase in the interest in nanofluids. Fig. 1 summarises some recent

^aCatalysis and Reaction Engineering Group, Department of Chemical Engineering, University of Bath, Bath, BA2 7AY, UK.
E-mail: a.lapkin@bath.ac.uk; Fax: +44 1225 385713; Tel: +44 1225 383369

^bInstitute of Particle Science and Engineering, University of Leeds, Leeds, LS2 9JT, UK

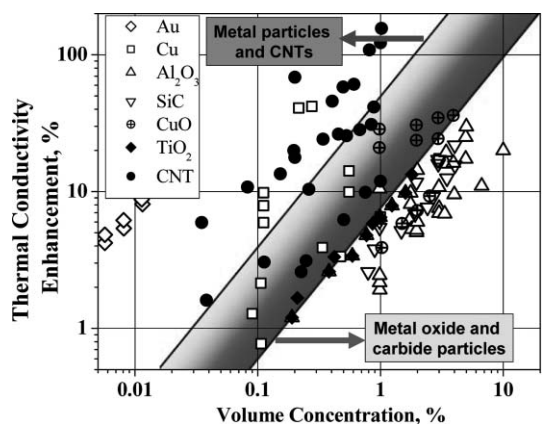


Fig. 1 Recent research data on the thermal conductivity of nanofluids. Adapted from ref. 21.

literature data of thermal conductivity of nanofluids (the shaded area shows the overlap in experimental data between nanofluids based on nanoparticles with high effective thermal conduction, such as metals, and low thermal conduction, such as oxides).²¹

A number of theories were proposed to explain this phenomenon.^{22,23} The emerging consensus among the nanofluids community, however, is that if clustering of nanoparticles is taken into account and the volume fraction is adjusted for the effective density/volume of the cluster, the heat conduction enhancement fits well to that predicted by eqn (1).^{24,25} The deterioration of heat conduction below the mean field theory has been shown to result from a significant interfacial heat transfer resistance in the case of poor wetting of nanoparticles by the base fluid.²⁶ Therefore, the chemistry of nanoparticles and fundamental knowledge of nanoparticle aggregation behaviour are the key to designing new and effective nanofluids for heat transfer applications. There remains a possibility of higher enhancement of conductive heat transfer, if particle-to-particle conduction pathways are generated above the percolation threshold in the case of the high aspect ratio nanoparticles, such as carbon nanotubes.^{27–29}

In most practical applications, the heat transfer fluid is not stationary, as in the case of heat conduction measurements described above. The convective heat transfer coefficient becomes more important and, according to the fundamental theory, heat transfer may be enhanced, remain unchanged or even be worse in the presence of nanoparticles, depending on how affected are the three parameters: heat conductivity of nanofluids (k_{nf}), thermal boundary layer thickness (δ_t) and properties of the heat transfer surface, where the effects of the former two parameters are shown, for the case of turbulent flow, by eqn (2):

$$h = k_{nf}/\delta_t \quad (2)$$

where h is the convective heat transfer coefficient. The effect of the heat transfer surface properties is reflected in the total heat flux.

There is very little experimental or theoretical data on the convective heat transfer in micro heat exchangers. It was shown experimentally, that an enhancement in heat transfer efficiency, expressed as thermal resistance ($K W^{-1}$), of ca. 13% can be achieved only at low heat transfer fluid flowrate.³⁰ Pronounced fouling of micro heat exchanger by nanoparticles at higher

flowrates was shown to be responsible for poor performance of nanofluids. In another study, a more pronounced enhancement of the heat transfer coefficient was found in the entrance region of a laminar flow in a microchannel.³¹ Theoretical calculations not based on convective heat transfer theory are underestimating the enhancement in the flow regime, even if high conductive heat transfer enhancement is assumed.³²

To the best knowledge of the authors, there have been no studies concerning application of nanofluids in chemical microreactors until now. The aim of this study is to evaluate performance of nanofluids in a structured compact reactor–heat exchanger. Enhancement of the overall heat transfer coefficient, stability of nanofluids and feasibility of rapid reaction quenching were studied in detail and comparison of the increased efficiency vs. the penalty of higher pumping power was made.

Experimental

Nanofluids

Dry TiO_2 nanoparticles and pure ethylene glycol (EG) were used to make nanofluids. The nanoparticles (P25 TiO_2 , purity better than 99.5%) were purchased from Degussa and ethylene glycol (>99.0%) was from Alfa Aesar. Both were used as received. The primary nanoparticles are spherical with approximately 25 nm diameter (by SEM and HRTEM). However, they are in the form of large agglomerates. The method of preparation of nanofluids employed in this work is described in detail elsewhere.¹⁸ TiO_2 -EG nanofluids with concentrations of 0.5, 2.0 and 4.0% by weight, corresponding respectively to 0.10, 0.43 and 0.86% by volume, were produced. As the dry TiO_2 nanoparticles were in the form of agglomerates, an ultrasonic bath (Nickel Electro Ltd, UK) was used to break the agglomerates. The average particle size of the resulting nanofluids was measured to be 50–150 nm by using dynamic light scattering (Malvern Nanosizer, Malvern Instruments), suggesting the presence of agglomerates in the colloid, rather than well separated seed particles. The TiO_2 -EG nanofluids were found to be stable for over two months at ambient temperature.

Compact structured reactor

Details of the reactor were disclosed elsewhere.^{7,33} In this study a square reaction channel with side of 3 mm and length of 100 mm was packed with 0.2 g of 1%wt Pt/C catalysts produced by Engelhard, using microspherical (particle diameter about 130 μm) mesoporous carbon support developed by MAST Carbons Ltd (UK). The catalyst was diluted with glass spheres (ca. 160 μm diameter) to fill the reaction channel completely.

The experimental system for performing convective heat transfer experiments and hydrogenation reaction is shown schematically in Fig. 2. Heat transfer fluid was heated and pumped into the compact heat exchange module by a recirculating bath (RCB, Haake DC30, DC10). A needle valve was used to control the flow rate of heat transfer fluid. Four K-type thermocouples (WATLOW) were used to measure temperature of heat transfer fluid inlet (T_1), outlet (T_2), process liquid inlet (T_3) and outlet (T_4). Three thermo-wells were placed along the length of each reaction channel at 13, 48 and 80% (T_5-T_7) from the inlet respectively. The thickness of the metal plate between

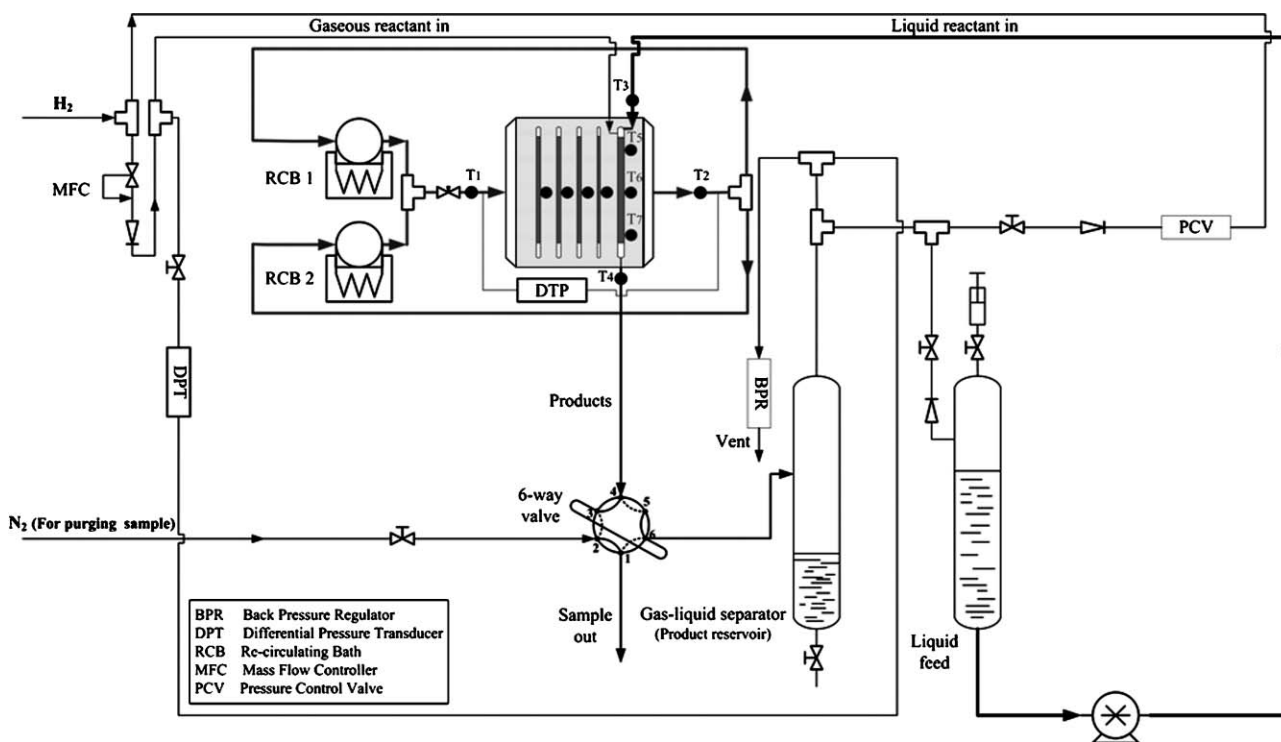


Fig. 2 Experimental rig for heat transfer and hydrogenation of benzaldehyde experiments.

thermocouples and the reaction channel was 100 μm , ensuring a reasonably quick response. Micro-thermocouples (Tempcon Instrumentation, UK) were used to measure temperature of the reaction channel wall.

In hydrogenation experiments, a 0.2 M benzaldehyde solution in 2-propanol was placed in the stainless steel feed vessel connected to a pump (Kontron Instruments, HPLC pump 422). Hydrogen flow rate was controlled by mass flow controllers (MFC, Brooks 5850 s). The outlet from the micro-reactor was connected *via* a low dead-volume six-way valve to a receiving vessel, which also served as a gas-liquid separator. The feed and receiving vessels were connected in order to equalise the pressure. The operating pressure was set by a back pressure regulator (BPR, Brooks 5866) and the pressure drop across the reactor was measured using a Bronkhorst differential pressure transducer (DPT).

Physical properties of nanofluids

The thermal conductivity was measured by using a KD2 thermal property meter (Labcell Ltd., UK), which is based on the transient hot wire method. The KD2 meter has a probe with 60 mm length and 0.9 mm diameter, which integrates in its interior a heating element and a thermo-resistor, and is connected to a microprocessor for controlling and conducting the measurements. The KD2 meter was calibrated by using distilled water and pure EG before any set of measurements. A thermostat bath (GD 120-S12, Grant, UK) was used to maintain the temperature uniformity within 0.02 K. At least five measurements were taken for each concentration of the nanofluids at a given temperature to ensure the uncertainty of measurements within 3%. Fig. 3 shows the relative thermal conductivity of

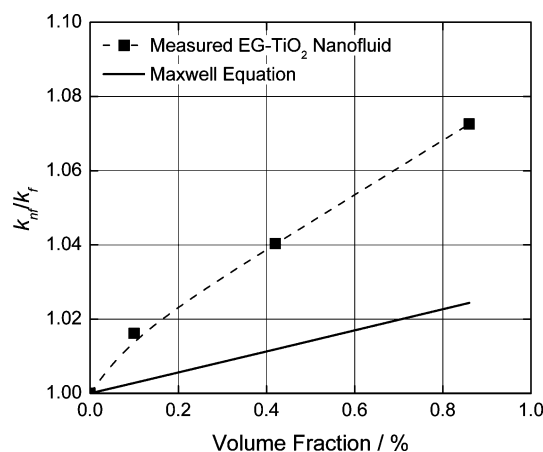


Fig. 3 Relative thermal conductivity of nanofluids (k_m/k_f) as a function of nanoparticle volume fraction.

nanofluids against the pure EG as a function of nanoparticle concentration together with the prediction of the conventional Maxwell equation at ambient temperature. It can be seen that the thermal conductivity of nanofluids increases with increasing nanoparticle concentration. The measured thermal conductivity of the nanofluids is higher than the predictions of the Maxwell equation even with the experimental error taken into account.

A Bohlin CVO rheometer (Malvern Instruments, UK) was used to measure nanofluids viscosity. Over the shear rate range (1–3000 s^{-1}) used in the measurements, TiO₂-EG nanofluids were confirmed as Newtonian fluids. Calibrations were conducted against standard solutions on weekly basis over the duration of this work to ensure accurate measurements of nanofluid viscosity. Three measurements were taken for each test and

the maximum uncertainty of viscosity was found to be $\sim 2.0\%$. The measured relative viscosity of nanofluids is plotted against nanoparticle volume fraction in Fig. 4. It can be seen that the viscosity of nanofluids increases with the increase of nanoparticle volume fraction. Also included in Fig. 4 is the prediction of the Einstein equation for dilute non-interacting suspensions of spherical particles ($\mu_{nf}/\mu_f = 1 + 2.5\phi$), showing that the Einstein equation under-predicts the experimental data.

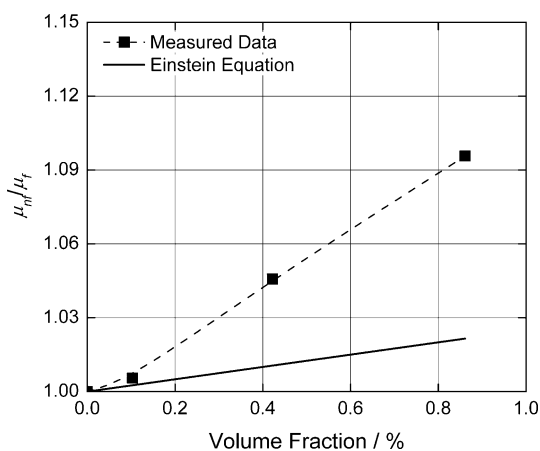


Fig. 4 Relative viscosity of nanofluids (μ_{nf}/μ_f) as a function of nanoparticle volume fraction.

Based on the nanoparticle and base fluid densities, the nanofluid density is calculated as eqn (3).³⁴

$$\rho_{nf} = \phi \rho_p + (1 - \phi) \rho_f \quad (3)$$

where ϕ is the volumetric fraction of nanoparticles and the subscripts p , f and nf refer to the nanoparticles, base liquid and nanofluids, respectively.

Assuming that the nanoparticles and the base liquid fluid are in thermal equilibrium, the specific heat capacity of the nanofluid can be estimated by:

$$c_{p,nf} = \phi \frac{\rho_p}{\rho_{nf}} c_{p,particle} + (1 - \phi) \frac{\rho_f}{\rho_{nf}} c_{p,f} \quad (4)$$

Table 1 shows the properties of the base liquid as well as for different concentrations of TiO_2 . It can be seen that the density and the heat capacity of nanofluids are very close to those of the base liquid.

Evaluation of the heat transfer performance of nanofluids

The overall experimental heat transfer coefficient, $h_{(exp)}$, was used to evaluate the heat transfer performance of different heat

transfer fluids. Based on the energy conservation equation:

$$\begin{aligned} \dot{q} [Js^{-1}] &= C_{p,HTF} \dot{m}_{HTF} (T_2 - T_1) = C_{p,P} \dot{m}_p (T_4 - T_3) \\ &= h_{(exp)} A f_t \Delta \vartheta_m \end{aligned} \quad (5)$$

And then $h_{(exp)}$ can be calculated as eqn (6):

$$h_{(exp)} [Js^{-1}m^{-2}K^{-1}] = \frac{C_{p,P} \dot{m}_p (T_4 - T_3)}{A f_t \Delta \vartheta_m} \quad (6)$$

In eqn (5) and (6), subscripts HTF and P refer to heat transfer fluid and process liquid, \dot{m} is the mass flow rate, A is the effective heat transfer area, and $\Delta \vartheta_m$ is the log-mean temperature difference, defined as:

$$\Delta \vartheta_m = \frac{(T_1 - T_4) - (T_2 - T_3)}{\ln[(T_1 - T_4)/(T_2 - T_3)]} \quad (7)$$

Log mean temperature is usually defined for counter flow heat exchangers. Therefore, a correction factor f_t was introduced in eqn (6) to account for the cross flow heat exchange process used in this study. Derivation of f_t can be found in the literature.³⁵

Results and discussion

Enhancement of heat transfer in micro heat exchanger

The potential enhancement of the overall heat transfer coefficient was studied in the steady state experiments in the absence of reaction with only water as a process fluid. Fig. 5 shows the recorded process fluid temperature at outlet (measured by T_4 , see Fig. 2) as a function of overall mass flowrate of heat

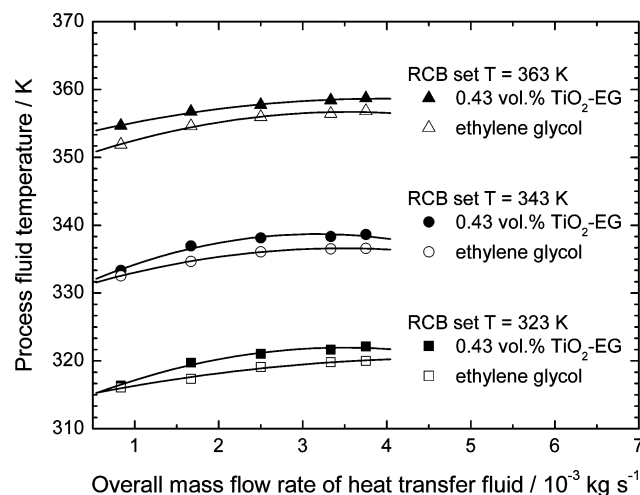


Fig. 5 Process fluid (water) temperature at reactor outlet as a function of overall mass flow rate of the heat transfer fluid.

Table 1 Thermal properties of TiO_2 -EG nanofluids at 303 K and 100 kPa

Thermal properties	Nanoparticle volume fraction in base liquid			
	$\phi = 0\%$	$\phi = 0.10\%$	$\phi = 0.43\%$	$\phi = 0.86\%$
ρ (kg m^{-3})	1110	1113	1123	1137
c_p ($\text{kJ kg}^{-1} \text{K}^{-1}$)	2.430	2.423	2.391	2.370
μ ($\text{kg m}^{-1} \text{s}^{-1}$)	1.410×10^{-2}	1.418×10^{-2}	1.474×10^{-2}	1.545×10^{-2}
k ($\text{W m}^{-1} \text{K}^{-1}$)	0.2530	0.2571	0.2632	0.2714

TiO_2 properties: $\rho_{\text{TiO}_2} = 4200 \text{ kg m}^{-3}$, $C_{p,\text{TiO}_2} = 0.54 \text{ kJ kg}^{-1} \text{K}^{-1}$, $k_{\text{TiO}_2} = 11.70 \text{ W m}^{-1} \text{K}^{-1}$.

transfer fluid (HTF) for both the base liquid and the TiO₂-EG nanofluids.

As it can be seen, the increase in T_4 with increasing of the overall HTF mass flow rate follows a similar pattern for both pure EG and TiO₂-EG nanofluids. Higher temperatures (T_4) were achieved using nanofluids as HTF compared with those using pure EG at the same flow rates. This indicates that more heat was transferred to the process fluid, according to eqn (5), by introducing nanoparticles into the base liquid. Therefore, convective heat transfer was improved by using nanofluids (note that the heat capacity and density of nanofluids are approximately the same as those of the base liquid due to low particle concentrations, see Table 1).

Fig. 6 shows the measured relative heat transfer coefficient of nanofluids (calculated by eqn (6)) as a function of TiO₂ nanoparticle volume fraction. The heat transfer coefficient of nanofluids increased rapidly with increasing nanoparticle concentration under the conditions used in this work.

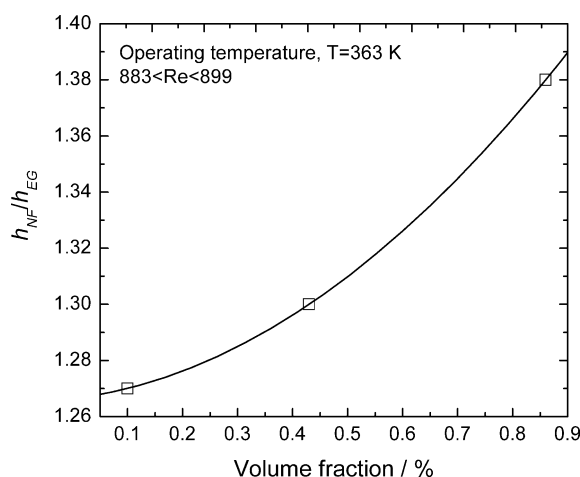


Fig. 6 Increment of overall relative heat transfer coefficient as a function of TiO₂ nanoparticle volume fraction.

Fig. 7 shows the temperature dependence of the measured overall heat transfer coefficient of nanofluids. The higher the temperature, the higher is the relative enhancement over pure EG. This is likely to be associated with an increase in convective

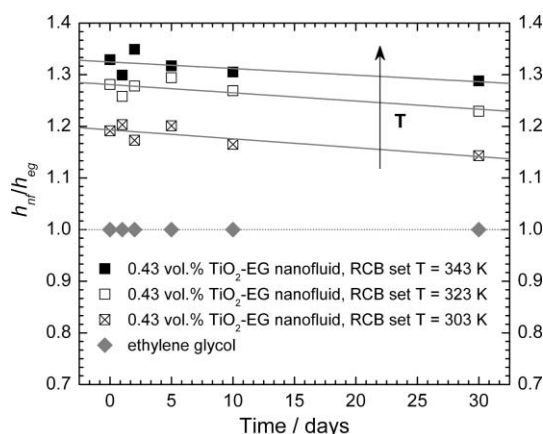


Fig. 7 Overall relative heat transfer coefficient of 0.43%vol TiO₂-EG nanofluid as a function of time, overall mass flow rate = 5×10^{-3} kg s⁻¹.

heat transfer due to a decrease in viscosity of the base liquid with increasing temperature. A recent study³⁶ showed that TiO₂ (P25)-EG nanofluid behaves as a Newtonian fluid over 0–8%wt concentration of nanoparticles, and the presence of nanoparticles does not affect the temperature dependence of the shear viscosity of the base EG fluid. The temperature dependent enhancement can be explained, at least qualitatively, by eqn (2). An increase in temperature leads to a decrease in viscosity, and hence a decrease in the thermal boundary layer. An increase in temperature also increases thermal conductivity.^{29,36} These factors, according to eqn (2), result in an increase in heat transfer, which corresponds to our observations.

The enhancement in the heat transfer coefficient slowly degraded over time. Fig. 7 shows the results over a period of 30 days, which give *ca.* 0.15% day⁻¹ loss in the enhancement effect for the 0.43%vol nanofluid. The exact reasons for this requires further investigation but it is believed to be associated with the gradual clustering of nanoparticles and sedimentation of the larger clusters in the low shear areas of the heat transfer system, most likely in the recirculating bath. This is supported by the dynamic light scattering measurements of the nanofluids, which showed an increased average particle size after 30 days.

There was no noticeable deposition of nanoparticles on the micro heat exchanger surfaces as evidenced by the retention of the enhancement upon change from the older nanofluid samples to a fresh sample. However, it was also noticed that elevated temperatures significantly accelerated aggregation and if strongly aggregated suspension of nanoparticles was circulated through the micro heat exchanger structure, serious fouling of surfaces occurs, requiring long sonication to remove the deposits.

Pressure drop and pumping power

As shown above, heat transfer process in the micro channel heat exchanger was intensified considerably using nanofluids. However, the enhanced heat transfer coefficient came with a small penalty of pressure increase, arising from a few percent increase of viscosity (Fig. 4). With conventional heat transfer fluids, an increase of heat transfer coefficient by a factor of 100% typically incurs a pressure drop penalty of ~1000%.³⁷ By using nanofluids, the penalty could be greatly reduced.

In comparison with pure base heat transfer liquid, introduction of nanoparticles leads to the increase in pressure drop and hence pumping power (see Fig. 8). Therefore, the overall system energy efficiency must be considered, since the enhancement in the heat transfer may be negated by the increase in the required pumping power. Given that replacement of heat transfer fluid leaves the rest of the system unchanged, we can compare the ratio of the heat transfer enhancement to the pumping power penalty, expressed as performance factor ζ_{PF} , see eqn (8). Thus, if the performance factor is equal to or above unity, the introduction of nanofluids will have a positive effect on the overall energy balance of the system. Performance factors of nanofluids with different TiO₂ concentrations are plotted against overall mass flow rate in Fig. 9.

$$\zeta_{PF} = \frac{\Delta \dot{q}}{\Delta P_{\text{pumping}}} = \frac{(\dot{q}_{nf} - \dot{q}_f)}{(P_{\text{pumping},nf} - P_{\text{pumping},f})} \quad (8)$$

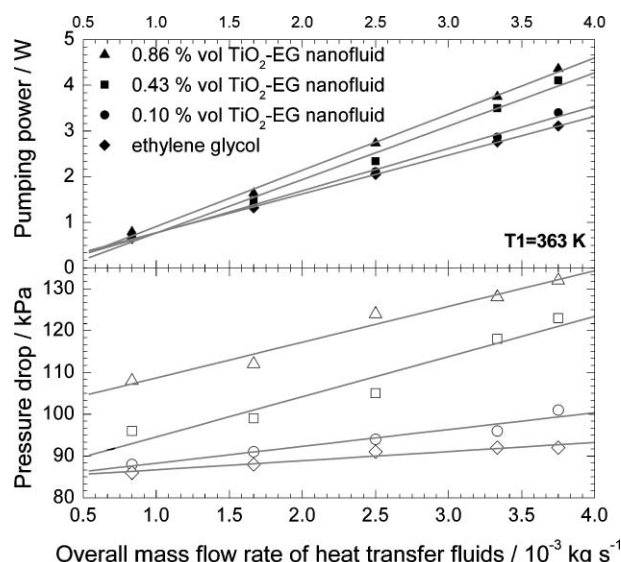


Fig. 8 Dependence of pressure drop across micro-heat exchange module and of pumping power on the overall mass flow rate and nanoparticle concentration of the heat transfer fluids. The pressure drop was measured across the whole device and includes the effects of inlet and outlet headers.

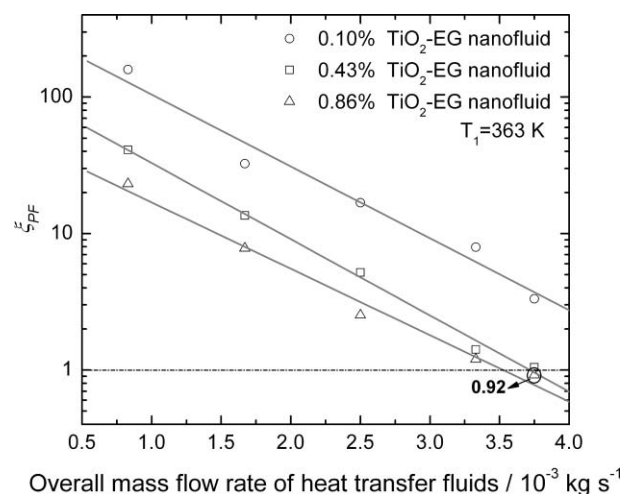


Fig. 9 Performance factor (ζ_{PF}) of TiO_2 -EG nanofluids as a function of overall mass flow rate of HTF.

where \dot{q} is the heat transferred to the process liquid, calculated by eqn (5) and P_{pumping} is pumping power, calculated by:

$$P_{\text{pumping}} = \Delta p \dot{v} \quad (9)$$

where \dot{v} is the average volumetric flow rate of the HTF.

As shown in Fig. 9, ζ_{PF} decreases with the increase in TiO_2 nanoparticle concentration for a given flow rate, as well as with increasing of the overall flow rate for a given concentration of nanoparticles. Performance factors remain above unity for most of the flow rates and nanofluids concentrations, which means the whole system is more energy efficient with the nanofluids as compared with a pure base liquid. The results show that the heat transfer increase in the compact reactor–heat exchanger due to nanofluids can be obtained with a moderate increase in the pumping power within a certain range of mass flow rates. However, it should be understood, that the energy demand for

the manufacture of nanoparticles should also be included in the overall energy assessment, considering the process within the wider life cycle system boundary. A lower than unity value of the performance parameter, obtained at high nanofluid flowrate and with high concentration of nanoparticles shows the regime under which the use of nanofluids is less economical.

Dynamic experiments

In the dynamic experiments, the two re-circulating baths, containing either EG or TiO_2 -EG nanofluids and set at two different temperatures, were used and the flow rapidly switched between them to direct a heat transfer fluid with a different temperature into the reactor system, as shown in Fig. 2. The dynamics of quenching of the process fluid, water, is shown in Fig. 10. In dynamic experiments, the lower temperature set by RCB2 for different HTFs was always 303 K. The off-set from the lower set temperature is due to the thermal mass of the reactor. Cooling of the reactor itself is under a different and much slower dynamics, which does not affect the dynamics of the process fluid quenching.

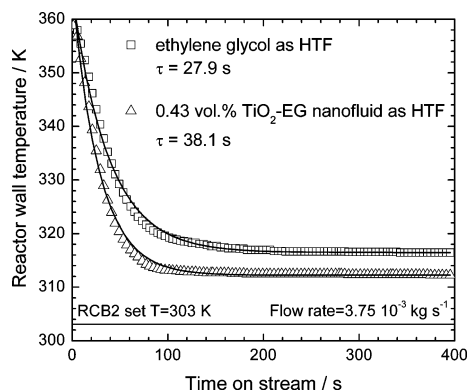


Fig. 10 Comparison of the temperature profiles of the quenching experiment based on EG and 0.43%vol TiO_2 -EG nanofluid. Symbols: experimental data points, solid lines: model fit.

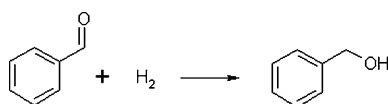
Eq. (10) describes the reactor wall temperature change over time in the dynamic quenching experiments:

$$T_w = T_\infty + (T_0 - T_\infty)e^{-t/\tau} \quad (10)$$

where T_w , T_0 and T_∞ are instantaneous reactor wall temperature, initial reactor wall temperature and reactor wall temperature at the final steady state; τ is the process time constant. The fit of eqn (10) for pure EG and the 0.43%vol TiO_2 -EG nanofluid to the experimental data and the calculated time constants are shown in Fig. 10.

Time constants calculated from this model are 27.9 s for the TiO_2 -EG nanofluid and 38.1 s for pure EG. Smaller τ of the system with nanofluid compared with pure EG means the reactor responds quicker to the temperature change. The apparent rate of cooling of the working fluid with EG only is 0.7 K s^{-1} , whereas with the nanofluid it is increased to 1.1 K s^{-1} , which is a 57% increase. Such an increase in the rate of temperature change should also have a pronounced effect on the rate of quenching of chemical reactions, since the temperature effect is enhanced by the exponential dependence of reaction rate on temperature.

To investigate the potential dynamic quenching of a chemical reaction in the compact reactor, the reaction of selective reduction of an aromatic aldehyde to an alcohol was studied. Reaction of reduction of benzaldehyde, shown in Scheme 1 is mildly exothermic, with a standard reaction enthalpy of -67 kJ mol^{-1} . The reaction was performed under continuous flow conditions in the compact reactor–heat exchanger developed earlier.⁷ Under isothermal conditions reaction reached steady state within 10 minutes, after which conversion and selectivity data were recorded.



Scheme 1 Reduction of benzaldehyde.

Fig. 11 shows the temperature dependence of conversion of benzaldehyde and yield of benzyl alcohol, using 1%wt Pt/C catalyst. Isothermal conditions were kept at all conversion levels. The decrease in the yield at temperatures above 330 K is due to two factors: (i) formation of higher molecular weight products, as proven by mass spectroscopy and the regeneration of the catalysts by washing with non-polar solvents, and (ii) the temperature dependence of adsorption of reactants and products on the catalyst. The former factor, the formation of the higher molecular weight by-products, does slowly deactivate the catalysts. However, this rate is insignificant within the timescale of the dynamic quenching experiment. The temperature dependence of adsorption of reactants and products results in the reversible temperature dependence of the overall conversion. This effect is being exploited to demonstrate the dynamic switch between reaction regimes.

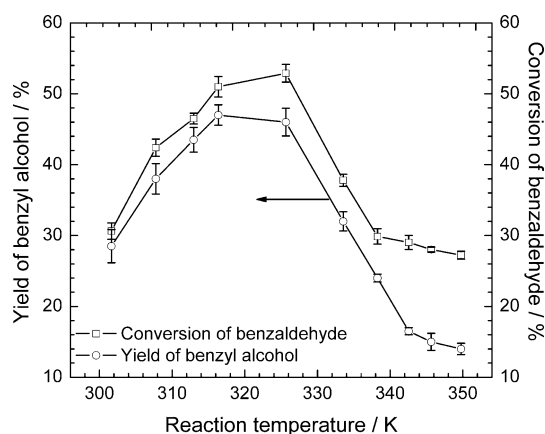


Fig. 11 Yield of benzyl alcohol and benzaldehyde conversion in the compact reactor–heat exchanger as a function of the reaction temperature. $P = 8 \text{ bar}$, $F_{\text{Liquid}} = 1 \text{ mL min}^{-1}$, $F_{\text{Gas}} = 16 \text{ mL(STP) min}^{-1}$.

Fig. 12 shows results of the experiment, in which the temperature of the heat transfer fluid was changed step-wise from 353 to 303 K and the response of the reaction was followed by taking samples at intervals of 120 s. Based on the data we can estimate the rate of transition from one steady state to the second, assuming the rate processes to be first order. Thus, in the case of ethylene glycol only the rate is $ca. 1.1 \times 10^{-4} \text{ mol L}^{-1} \text{ s}^{-1}$, whereas in the case of the nanofluid this rate increased to $ca.$

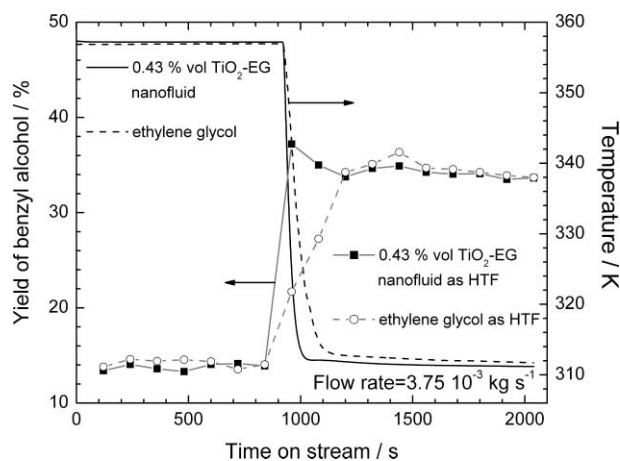


Fig. 12 Benzyl alcohol concentration in the outlet of the reactor as a function of the reaction temperature. $P = 8 \text{ bar}$, $F_{\text{Gas}} = 16 \text{ mL(STP) min}^{-1}$.

$3.9 \times 10^{-4} \text{ mol L}^{-1} \text{ s}^{-1}$. It is worth emphasizing that the rate of change between the two steady states is significantly underestimated, since due to the slow sampling technique we were unable to collect the concentration data sufficiently fast to obtain the data-points in the transient regime. The likely actual rate of this transition is expected to be even higher.

The significant increase in the rate of response of chemical reaction to the change in temperature of the working fluid may open interesting new opportunities for rapid quenching of chemical reactions in compact multifunctional systems. This should be especially important for the development of sequential transformations in a single unit operation, or for inducing rapid phase changes in the process stream.

Conclusions

Further intensification of heat transfer in a compact reactor–heat exchanger with nanofluids was confirmed and enhancement in the overall heat transfer coefficient of up to $ca. 35\%$, compared with the corresponding base fluid, was observed studying the specific case of TiO_2 nanoparticles in ethylene glycol. Nanoparticle agglomeration was believed to be responsible for the slow decrease in performance of TiO_2 -EG nanofluids.

We have shown that the penalty for introduction of nanoparticles due to the increased pressure drop is small, and a considerable increase in the overall energy efficiency can be attained. This is in strong contrast with conventional heat exchangers. Results showed that the compact reactor–heat exchanger system became more efficient with nanofluids for most of the conditions used in present study.

The results of dynamic experiments demonstrated that the compact reactor–heat exchanger has a significantly faster dynamic response when nanofluids are used. The quick dynamic response of the reactor can be employed for rapid switching of reaction conditions, *e.g.*, rapid quenching of reactions, which was shown in the example of temperature dependent reaction selectivity.

There is a significant potential of nanofluids for novel applications in flow chemistry and catalytic reaction engineering, and

the minimum feasible outcome is the significant reduction in the overall process energy requirement.

Acknowledgements

Part of this work was funded *via* the Engineering and Physical Sciences Research Council Discipline Hopping grants to AL (EP/D000564/1) and YD (EP/D000645/1). XF is grateful to ORS award and University of Bath Research Studentship.

References

- 1 A. I. Stankiewicz and J. A. Moulijn, *Chem. Eng. Prog.*, 2000, **96**, 22–34.
- 2 W. T. Cross and C. Ramshaw, *Chem. Eng. Res. Des.*, 1986, **64**, 293–301.
- 3 J. F. Jenck, F. Agterberg and M. J. Droscher, *Green Chem.*, 2004, **6**, 544–556.
- 4 S. Becht, R. Franke, A. Geißelmann and H. Hahn, *Chem. Eng. Technol.*, 2007, **30**, 295–299.
- 5 A. Tonkovich, D. Kuhlmann, A. Gogers, M. J. S. Fitzgerald, R. Arora and T. Yuschak, *Chem. Eng. Res. Des.*, 2005, **83**, 634–639.
- 6 C. H. Phillips, G. Lauschke and H. Peerhossaini, *Appl. Thermal Eng.*, 1997, **17**, 809–824.
- 7 D. V. Bavykin, A. A. Lapkin, S. T. Kolaczowski and P. K. Plucinski, *Appl. Catal., A*, 2005, **288**, 165–174.
- 8 W. Ehrfeld, V. Hessel and H. Löwe, *Microreactors*, Wiley-VCH, Weinheim, 2000.
- 9 A. Aoune and C. Ramshaw, *Int. J. Heat Mass Transfer*, 1999, **42**, 1432–1445.
- 10 P. G. Jessop, *J. Supercrit. Fluids*, 2006, **38**, 211–231.
- 11 *Ionic liquids in synthesis*, ed. P. Wasserscheid and T. Welton, Wiley-VCH, Weinheim, Germany, 2007.
- 12 M. Freemantle, in *Chem. Eng. News*, 2003, p. 9.
- 13 D. B. Tuckerman and R. F. W. Pease, *IEEE Electron. Device Lett.*, 1981, **EDL-2**, 126–129.
- 14 W. M. Kays and A. L. London, *Compact heat exchangers*, McGraw Hill Higher Education, 1984.
- 15 J. A. Eastman, S. U. S. Choi, S. Li, W. Yu and L. J. Thompson, *Appl. Phys. Lett.*, 2001, **78**, 718–720.
- 16 R. L. Hamilton and O. K. Crosser, *Ind. Eng. Chem. Fundam.*, 1962, **1**, 187–191.
- 17 S. Lee, S. U. S. Choi, S. Li and J. A. Eastman, *Trans. ASME, J. Heat Transfer*, 1999, **121**, 280–289.
- 18 D. Wen and Y. Ding, *Int. J. Heat Mass Transfer*, 2004, **47**, 5181–5188.
- 19 S. K. Das, N. Putra and W. Roetzel, *Int. J. Heat Mass Transfer*, 2003, **46**, 851–862.
- 20 S. K. Das, S. U. S. Choi and H. E. Patel, *Heat Transfer Eng.*, 2006, **27**, 3–19.
- 21 Y. Ding, H. Chen, L. Wang, C. Yang, Y. He, W. Yang, W. Lee, L. Zhang and R. Huo, *KONA*, 2007, **25**, 23–38.
- 22 P. Keblinski, S. R. Phillpot, S. U. S. Choi and J. A. Eastman, *Int. J. Heat Mass Transfer*, 2002, **45**, 855–863.
- 23 R. Prasher, W. Evans, P. Meakin, J. Fish, P. Phelan and P. Keblinski, *Appl. Phys. Lett.*, 2006, **89**, 143119.
- 24 J. Eapen, W. C. Williams, J. Buongiorno, L.-W. Hu, S. Yip, R. Rusconi and R. Piazza, *Phys. Rev. Lett.*, 2007, **99**, article number: 095901.
- 25 *Nanofluids: Fundamentals and Applications*, Copper Mountain, Colorado, USA, 2007.
- 26 S. Shenogin, L. Xue, R. Ozisik, P. Keblinski and D. G. Cahill, *J. Appl. Phys.*, 2004, **95**, 8136–8144.
- 27 D. Wen and Y. Ding, *J. Thermophys. Heat Transfer*, 2004, **18**, 481–485.
- 28 H. Hong, J. Wensel, F. Liang, W. E. Billups and W. Roy, *J. Thermophys. Heat Transfer*, 2007, **21**, 234–236.
- 29 Y. Ding, H. Alias, D. Wen and R. A. Williams, *Int. J. Heat Fluid Flow*, 2006, **49**, 240–250.
- 30 R. Chein and J. Chuang, *Int. J. Thermal Sci.*, 2007, **46**, 57–66.
- 31 J. Lee and I. Mudawar, *Int. J. Heat Mass Transfer*, 2007, **50**, 452–463.
- 32 S. P. Jang and S. U. S. Choi, *Appl. Thermal Eng.*, 2006, **26**, 2457–2463.
- 33 P. K. Plucinski, D. V. Bavykin, S. T. Kolaczowski and A. A. Lapkin, *Ind. Eng. Chem. Res.*, 2005, **44**, 9683–9690.
- 34 B. C. Pak and Y. I. Cho, *Exp. Heat Transfer*, 1998, **11**, 151–170.
- 35 W. S. Janna, *Engineering Heat Transfer*, PWS Publishers, Boston, USA, 1986.
- 36 H. Chen, Y. Ding, Y. He and C. Tan, *Chem. Phys. Lett.*, 2007, **444**, 333–337.
- 37 S. U. S. Choi, in *2nd Korean-American Scientists and Engineers Association Research Trend Study Project Review and the Korea-U.S. Technical Conference on Strategic Technologies*, Vienna, VA, USA, 1998.

Moderate route for the utilization of CO₂-microwave induced copolymerization with cyclohexene oxide using highly efficient double metal cyanide complex catalysts based on Zn₃[Co(CN)₆][†]

Manju Mampambath Dharman, Ji-Yeon Ahn, Mi-Kyung Lee, Hye-Lim Shim, Kyung-Hoon Kim, Il Kim and Dae-Won Park*

Received 21st January 2008, Accepted 28th February 2008

First published as an Advance Article on the web 20th March 2008

DOI: 10.1039/b801132j

Zn₃[Co(CN)₆] based double metal cyanide complexes are currently used as catalysts for both the ring-opening polymerization of epoxides and the copolymerization of epoxides and CO₂. This paper reports an environmentally friendly route for the copolymerization of cyclohexene oxide (CHO) with CO₂ using microwave irradiation. The reaction occurred over a faster reaction time (2–30 min) and a much lower pressure (9.7 bar) than conventional methodologies giving a high molecular weight (19.3 kg mol⁻¹) polycarbonate with a higher level of CO₂ incorporation ($f_{\text{CO}_2} = 75\%$). The catalysts were prepared from an aqueous solution of ZnX₂ and K₃[Co(CN)₆] using *tert*-butanol and polyethers as complexing agents. All the catalysts were characterized by elemental analysis, ICP-OES, XRD, XPS and IR spectroscopy. The catalysts were found to be highly selective for the copolymer with a high TOF (TOF = 25 177 h⁻¹) values. Unlike conventional synthesis, there was no induction period noticed for the catalyst to initiate copolymerization. The high reactivity and excellent properties of the copolymer might be due to the higher activation of CHO by microwaves due to its high polarizability and higher dielectric constant.

Introduction

Microwaves, which reside in an area of the electromagnetic spectrum between infrared radiation and radio waves, have shown considerable potential in improving chemical reactions over the past few years. The rapid increase in the number of publications and the availability of reliable microwave instrumentation has increased the level of interest in this non-conventional energy. A better performance in terms of conversion, selectivity and reaction time has been established using this technique in an environmentally friendly way. After the first publication, several studies and reviews have reported the utilization of microwaves in organic synthesis.^{1–13} The main attributes of microwave assisted organic synthesis is the dramatic acceleration of chemical reactions as a consequence of the high heating rate (5–1000 fold) than conventional heating methods. It was demonstrated that microwaves can induce some transformations that are practically impossible using conventional heating methods. In addition, the shorter reaction time unlocks the conceptualization for new ideas and allows repetition to produce modified protocols for various synthetic reactions.

The world is confronted with a major crisis of climate change due to the increased evolution of greenhouse gases, with CO₂ being the main culprit. Therefore, its effective utilization has

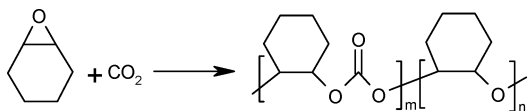
become an interesting area of research among scientists. This can be achieved by exploiting CO₂ as a feedstock through chemical reactions to generate valuable products. Being a promising step towards the sequestration of CO₂, the cycloaddition or copolymerization of CO₂ with epoxides to cyclic carbonates or polycarbonates has attracted considerable attention. Polycarbonates are categorized as specialty polymers with the characteristics of engineering thermoplastics.¹⁴ Industrially, polycarbonates are synthesized from alcohols and phosgene, a highly toxic carbonyl source. In a search for an environmentally benign counterpart of phosgene, the coupling of CO₂ with epoxides catalyzed by Et₂Zn/H₂O was first discovered by Inoue *et al.* in 1969.¹⁵ The aliphatic polycarbonates obtained from CO₂ and epoxides have properties, such as low toxicity and biodegradability. Although CO₂ has promising feedstock properties, such as being inexpensive, abundant, non-flammable and non-toxic, its high thermodynamic stability has rendered it inert to chemical reactions. Therefore, the exploration of efficient catalysts for CO₂ utilization is still an ongoing process. To date, several catalysts have been reported and reviewed for the effective utilization of CO₂ including double metal cyanide complexes (DMC).^{16,17} DMC complexes are considered to be good catalysts for the ring opening polymerization of epoxides. In our previous work, copolymers of various epoxides with CO₂ were synthesized successfully employing various DMC catalysts through conventional methods.^{17b,c}

The pressurized reaction in microwaves was a technological challenge until the first report on the cycloaddition reaction of CO₂ with epoxides.¹⁸ In this study, a series of Zn^X-Co based DMC catalysts were synthesized by varying the complexing

Division of Chemical Engineering, Pusan National University, Gungjung-gu, Busan, 609-735, Korea. E-mail: dwpark@pusan.ac.kr; Fax: +82 51-512-8563; Tel: 82 51-510-2399

[†] Electronic supplementary information (ESI) available: Detailed characterization of catalysts and polymers. See DOI: 10.1039/b801132j

agents and zinc halides. Their effect on the copolymerization of cyclohexene oxide with CO₂ (Scheme 1) under microwave irradiation was examined by varying the amount of catalyst, CO₂ pressure, microwave power and irradiation time. In addition, the effects of various DMC catalysts were investigated.



Scheme 1 Copolymerization of cyclohexene oxide with CO₂.

Results and discussion

The DMC complexes consisting of zinc hexacyanometalate were characterized by their unique prussian blue structure (Fig. 1). These complexes are generally prepared by a precipitation reaction between K₃[M(CN)₆] (where M can be Cr, Co, Fe *etc.*) and metal salts (*e.g.* ZnCl₂, ZnSO₄, CoCl₂ *etc.*) with the complexing agents. The role of the complexing agents in the synthesis of the DMC complexes was confirmed by their enhanced catalytic activity towards the ring opening polymerization of propylene oxide as well as the copolymerization of epoxides with CO₂.²⁰ This increase in catalytic activity is affected by the crystallinity of the catalyst. The DMC complexes prepared in the absence of any complexing agents were highly crystalline and had lower catalytic activity. This deformation of the crystal structure is essential for its catalytic activity, which can be modified not only by adding complexing agents but also through various preparation conditions such as the presence of an excess of metal salts, temperature and washing and drying conditions. ZnCl₂ was found to be an effective precursor for preparing the catalysts. Recent studies reported the improvement in catalytic activity by the presence of excess ZnCl₂ for both the ring opening polymerization of epoxides and its copolymerization with

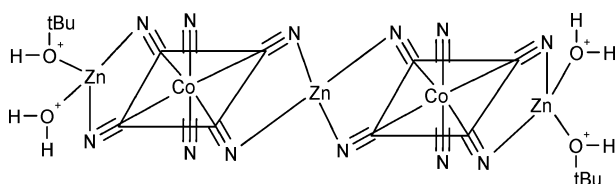


Fig. 1 Tentative structure of Zn^x-Co based DMC complex catalyst.

Table 1 XPS results of Zn^x-Co based DMC complexes

Element ^a	Zn(2p)	Co(2p)	C(1 s)	N(1 s)	O(1 s)	X
DMC-1	B.E./eV At. (%)	780.3 1.1	285.8 23.7	398.5 7.7	531.6 4.4	198.0 1.2
DMC-2	B.E./eV At. (%)	780.8 3.7	284.6 51.2	399.1 21.6	531.3 8.7	198.8 3.9
DMC-3	B.E./eV At. (%)	779.4 1.5	284.6 63.1	398.1 10.7	531.2 16.5	197.7 3.4
DMC-4	B.E./eV At. (%)	779.3 3.5	285.9 59.2	398.9 18.2	531.7 11.4	68.4 1.3
DMC-5	B.E./eV At. (%)	780.0 3.4	286.3 55.2	399.5 23.8	532.5 8.2	618.1 0.1

^a B.E.: Binding energy; At.: Atomic ratio.

CO₂.^{20a} Starting from K₃[Co(CN)₆], various DMC complexes were synthesized as catalysts by varying ZnX₂ and complexing agents.

Characterization of DMC catalysts

The surface formulation of the catalysts was examined by XPS and XRD, and the electronic properties were determined by FTIR. Table 1 summarizes the XPS results. The binding energy of the zinc atom of ZnCl₂ (1023.7eV) was higher than all the DMC catalysts formed after complexation. This shift might be due to the fact that the introduction of complexing agents into the DMC complexes makes the zinc atom of Zn₃[Co(CN)₆] coordinate with the oxygen atom of the complexing agent.

It is believed that incorporation of complexing agents during the synthesis of DMC complexes enhances their catalytic activity due to a change in crystallinity.^{20b} Further improvements were accomplished by low molecular weight functional polymers and organic compounds as complexing agents, which substantially reduced the crystallinity of the complex.^{17b,c} Three types of polyethers were used as complexing agents in addition to *tert*-butanol, PEG-PPG-PEG, PTMEG and PPG. The surface properties and crystal structure of the catalysts synthesized were examined by XRD (Fig. 2). XRD pattern showed that

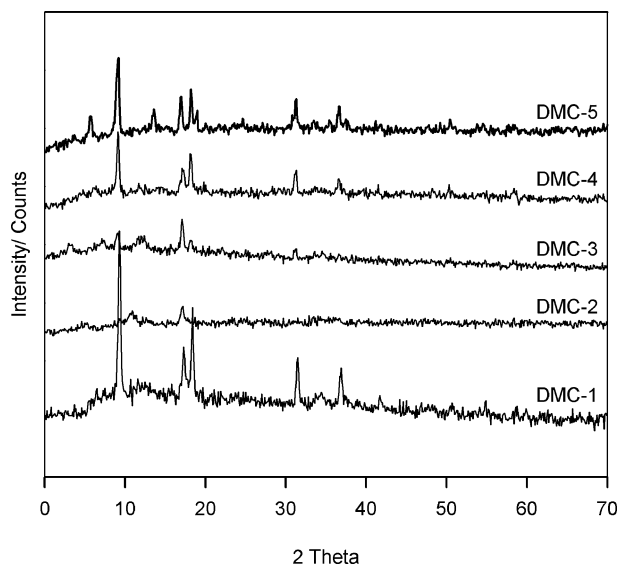


Fig. 2 XRD patterns of various Zn^x-Co DMC complexes.

all the catalysts were amorphous with no peaks corresponding to ZnCl_2 . The DMC-2 catalyst prepared using $t\text{-BuOH}$ and PTMEG as complexing agents showed the lowest crystallinity. On the other hand, the DMC-1, DMC-3, DMC-4 and DMC-5 catalysts showed a cubic lattice (d values: 5.13, 3.63 and 2.56 Å). The catalysts were further characterized by FTIR spectroscopy (Fig. 3). All the DMC complexes showed a shift of the $\nu(\text{CN})$ band from 2127 cm^{-1} in $\text{K}_3\text{Co}(\text{CN})_6$ to 2192 cm^{-1} in DMC-1, DMC-2 and DMC-4, and 2196 cm^{-1} in DMC-3 and DMC-5. The $\nu(\text{CN})$ of free CN^- is 2080 cm^{-1} .²¹ The $\nu(\text{CN})$ shift to higher frequencies suggests that CN^- acts as a σ -donor by donating electrons to Co^{3+} at the same time as the π -electron donor by chelating to Zn^{2+} .

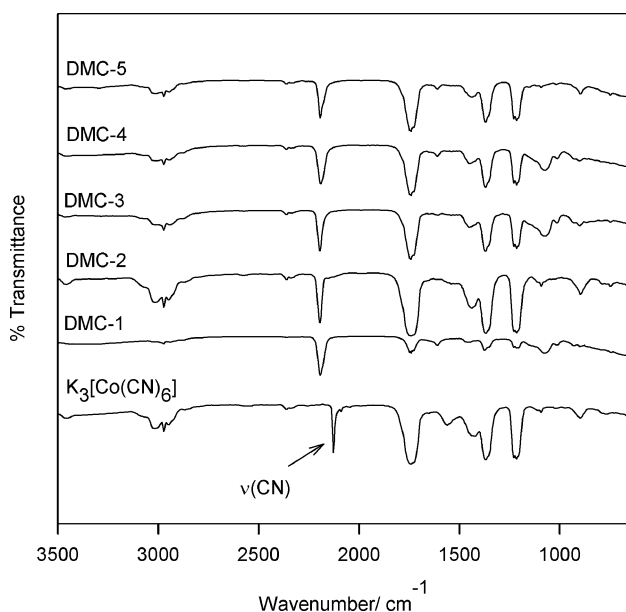


Fig. 3 FT-IR spectra of various $\text{Zn}^x\text{-Co}$ DMC complexes.

Heating characteristics of $\text{CHO}/\text{CO}_2/\text{catalyst}$ mixtures under microwave irradiation

The temperature profiles for reaction mixtures at various reaction conditions were measured since the heat effect of microwave energy had significant influence on the copolymerization of CHO and CO_2 . Fig. 4 shows the effect of microwave power and catalyst amount on the temperature of the reaction mixture using DMC-1 as catalyst ($P_{\text{CO}_2} = 9.7\text{ bar}$). The temperature increased rapidly to the high value within 15 min and then it increased slowly until a constant value was reached. The higher the microwave power and catalyst amount, the higher the equilibrium temperature.

The heating behavior of reaction mixtures with different monomer concentration (DMC-1 = 0.005 g, 100 W, $P_{\text{CO}_2} = 9.7\text{ bar}$) and various DMC catalysts (0.005 g, 100 W, $P_{\text{CO}_2} = 9.7\text{ bar}$) was also investigated and the results are shown in Fig. 5. On increasing the monomer concentration the equilibrium temperature increases steadily. On the other hand, in the case of DMC-2 and DMC-3 the thermal equilibrium at 100 W showed an abrupt variation in temperature whereas DMC-4 and DMC-5 followed the same behavior as DMC-1.

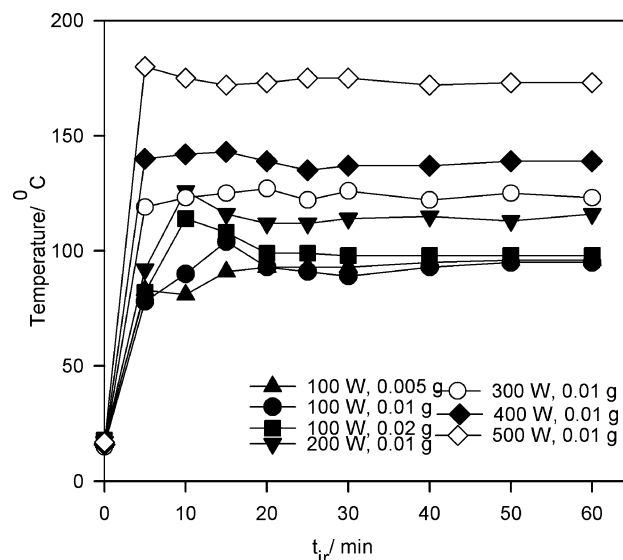


Fig. 4 Heat effect of microwave energy at different microwave power and catalyst amount.

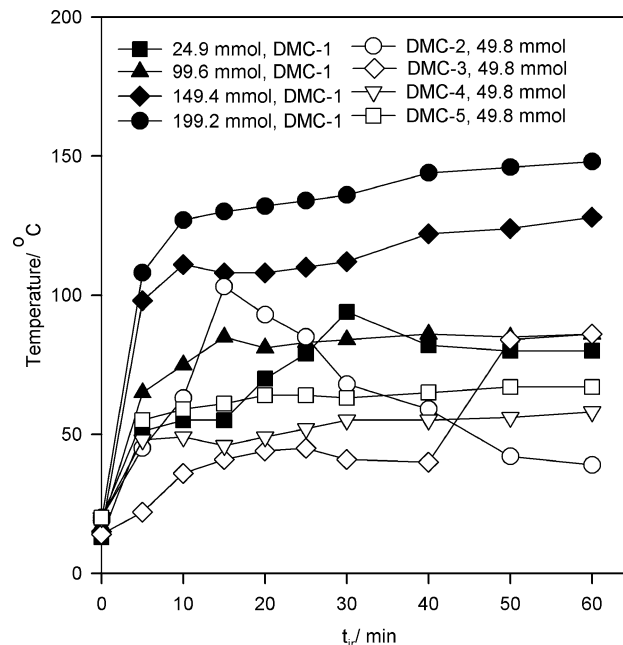


Fig. 5 Heat effect of microwave energy at different monomer concentration and DMC catalysts.

Influence of crystallinity and non-stoichiometry of catalysts

The copolymerization of CHO and CO_2 was carried out under microwave irradiation under various reaction conditions. The isolated polymer was identified by FT-IR (Fig. 6), $^1\text{H-NMR}$ (Fig. 7) and $^{13}\text{C-NMR}$ (δ 153.8, 153.0 ($-\text{C}(\text{O})$), 79.6, 76.3 ($-\text{O}-\text{C}(\text{H})-$), 29.2, 28.5 ($-\text{CH}_2$), 22.8, 22.0 ($-\text{CH}_2$)) spectroscopy. The strong absorption at 1749 cm^{-1} shown in the IR spectra corresponds to the stretching vibration of the carbonyl group. The absence of a peak at 1800 cm^{-1} in the FT-IR spectra of the reaction mixture ruled out cyclohexene carbonate formation during copolymerization. The amount of carbonate linkage was determined by integrating the $^1\text{H-NMR}$ peaks corresponding to the methine protons of polycarbonate and polyether at

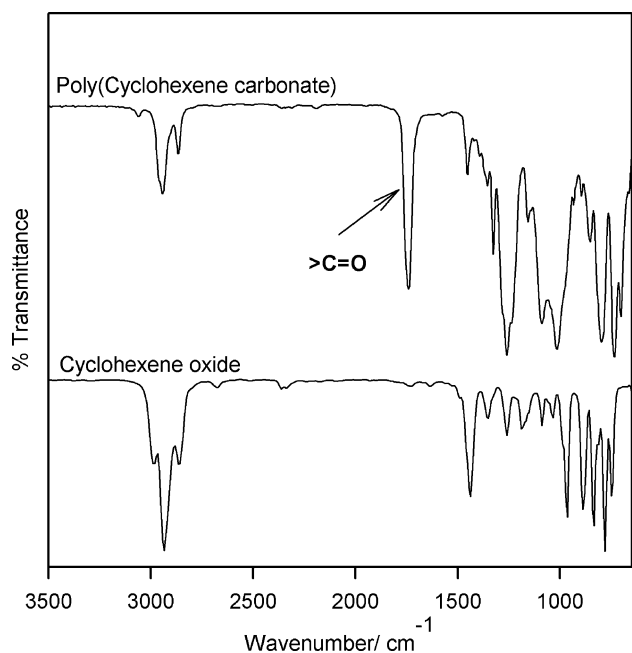


Fig. 6 FT-IR spectra of cyclohexene oxide and poly (cyclohexene carbonate).

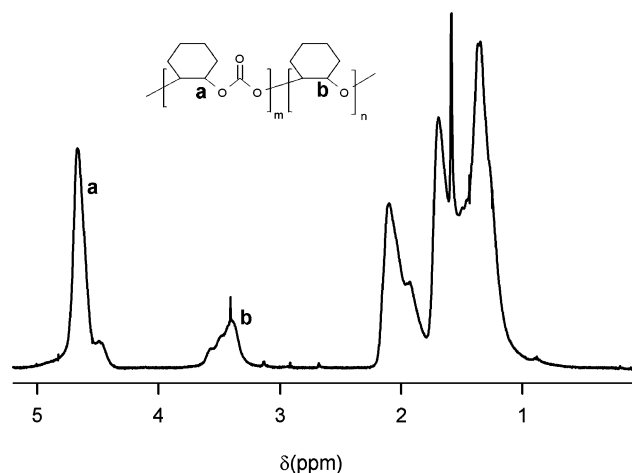


Fig. 7 ¹H-NMR spectra of poly(cyclohexene carbonate) containing ether linkage.

4.6 and 3.45 ppm, respectively. Table 2 shows the overall compositions of the DMC catalysts based on the EA and ICP-OES results. The corresponding activity was measured in terms of the turn over frequency (TOF). From these results,

the catalysts exhibited a non-stoichiometric nature regardless of the same preparation conditions. The activity of the catalyst varied according to the crystallinity and non-stoichiometric nature of the catalysts. Overall, the crystallinity of the DMC complexes increased in the order DMC-2 < DMC-3 < DMC-4 ≤ DMC-1 < DMC-5, whereas the activity of DMC catalysts showed a reverse order. The DMC-2 catalyst with the lowest crystallinity showed the highest TOF value whereas DMC-5 with the highest crystallinity showed the lowest activity. The low activity of DMC-5 catalyst might also be due to the absence of excess ZnI₂ in the catalyst composition (Table 2), which is an activator for the polymerization reactions.^{20a} The molecular weight and total yield of the product formed from DMC-5 (109 g g⁻¹ Zn) was much lower than that produced using the other DMC catalysts; DMC-1 (1409 g g⁻¹ Zn), DMC-2 (1967 g g⁻¹ Zn), DMC-3 (513 g g⁻¹ Zn), DMC-4 (493 g g⁻¹ Zn). Considering the polymer properties, DMC-1 showed excellent activity with a high molecular weight and higher level of CO₂ incorporation and this catalyst was used in further polymerization studies.

Effect of microwave irradiation parameters

In order to optimize the polymerization reactions under microwave irradiation, the polymerizations were performed using DMC-1 as the catalyst at different reaction conditions. Table 3 shows the effect of various reaction parameters on the copolymerization of CHO with CO₂. The influence of the CO₂ pressure and catalyst loading on the copolymerization of CO₂ with CHO are summarized as entries 1–6. In a multiphase system, the dissolution and mass transfer of CO₂ in CHO are two important reaction parameters that affect the product properties. CO₂ being an inert monomer requires effective activation for excellent polymer properties otherwise the copolymerization of CHO with CO₂ can be suppressed by the competitive homopolymerization of CHO. Considering entries 1, 2 and 6, a steady increase in molecular weight and CO₂ incorporation were observed with increasing pressure from 3.4 to 9.7 bar. 35% CO₂ incorporation was observed at a very short time of 4.5 min (entry 6), at which time the reaction mixture becomes too viscous resulting in significant impediment to the diffusion of CO₂. At lower pressure, a shorter reaction time and the viscosity of the reaction mixture might lead to a lower CO₂ concentration in the bulk due to a delay in mass transfer. The entries 5–9 lists the effect of microwave power on the polymerization time (*t_p*) at which the reaction mixture becomes too viscous for the efficient diffusion of the gaseous monomer. These results showed that a lower power is suitable for the copolymerization reaction. However, at

Table 2 Non-stoichiometric molecular formula of DMC complexes^a

Catalyst	Possible molecular formula ^b	<i>M_n</i> ^c	PDI ^c	<i>f</i> _{CO₂} (%) ^d	TOF ^e
DMC-1	Zn ₃ [Co(CN) ₆] ₂ ·0.27ZnCl ₂ ·0.31 ^t BuOH·0.42H ₂ O	14500	1.5	74.0	3910
DMC-2	Zn ₃ [Co(CN) ₆] ₂ ·0.25ZnCl ₂ ·0.45 ^t BuOH	11171	1.4	63.7	6594
DMC-3	Zn ₃ [Co(CN) ₆] ₂ ·0.20ZnCl ₂ ·0.61 ^t BuOH	8355	1.5	55.9	6167
DMC-4	Zn ₃ [Co(CN) ₆] ₂ ·0.15ZnBr ₂ ·0.44 ^t BuOH	13471	1.4	39.6	3671
DMC-5	Zn ₃ [Co(CN) ₆] ₂ ·0.062 ^t BuOH·1.8H ₂ O	745	1.0	63.3	2120

^a Polymerization condition: CHO = 49.8 mmol, catalyst = 0.005 g, *P*_{CO₂} = 9.7 bar, MW power = 100 W, *t_r* = 30 min. ^b Based on ICP-OES and elemental analyses. ^c Obtained from GPC analysis. ^d Estimated by ¹H-NMR (*f*_{CO₂}(%) = {carbonate linkage/[carbonate linkage + ether linkage]} × 100). ^e Turn over frequency (moles of CHO consumed/moles of Zn-hour).

Table 3 Effect of reaction parameters on copolymerization of CHO and CO₂^a

Entry	[CHO]/mmol	Catalyst amount/g	MW power/W	P _{CO₂} /bar	t _p ^b ;t _{ir} ^c /min	M _n ^d	PDI ^d	f _{CO₂} (%) ^e	TOF ^f
1	49.8	0.01	200	3.4	5.0	2673	2.1	17.0	12681
2	49.8	0.01	200	6.9	4.5	3557	2.0	29.0	14146
3	49.8	0.005	100	9.7	30.0	14500	1.5	74.0	3910
4	49.8	0.02	100	9.7	6.0	7487	1.5	20.0	5429
5	49.8	0.01	100	9.7	13.0	7640	1.7	56.3	4882
6	49.8	0.01	200	9.7	4.5	7573	1.5	35.5	14117
7	49.8	0.01	300	9.7	4.0	6982	1.4	32.5	15914
8	49.8	0.01	400	9.7	3.5	6058	1.6	19.2	18336
9	49.8	0.01	500	9.7	2.5	4856	1.6	9.7	25177
10	24.9	0.005	100	9.7	30.0	19312	1.6	75.0	1970
11	99.6	0.005	100	9.7	30.0	14976	1.2	71.0	7033
12	149.4	0.005	100	9.7	30.0	11429	1.2	57.0	10848
13	199.2	0.005	100	9.7	30.0	10850	1.2	51.0	14516
14	49.8	0.01	100	9.7	13.0;23.0	13238	1.4	62.5	2793
15	49.8	0.01	100	9.7	13.0;33.0	16875	1.4	53.6	1953
16	49.8	0.01	100	9.7	13.0;43.0	10974	1.4	56.5	1500

^a Polymerization condition: Catalyst = DMC-1. ^b Time of polymerization. ^c Time of microwave irradiation. ^d Obtained from GPC analysis. ^e Estimated by ¹H-NMR (f_{CO₂} (%) = {carbonate linkage/[carbonate linkage + ether linkage]} × 100). ^f Turn over frequency (moles of CHO consumed/moles of Zn-h).

higher microwave power, the polymerization time was reduced to 2.5 min with the highest CHO conversion (TOF = 25 177 at 500 W). On the other hand, the molecular weight and f_{CO₂} showed a steady decrease with increased power. This is because at higher microwave power, homopolymerization might dominate the copolymerization and the less reactive CO₂ co-monomer would not be activated.

As evidenced from entries 3–5 in Table 3, both the molecular weight and f_{CO₂} were influenced by the catalyst concentration. A higher amount of catalyst leads to a significant decrease in carbonate content. At higher catalyst concentration, the [CHO]/[Zn] ratio becomes lower, which results in the activation of CHO rather than CO₂ giving a lower f_{CO₂} with a lower molecular weight and carbonate content.²² Entries 4 and 5 shows with increasing catalyst amount from 0.01 g to 0.02 g, the molecular weight exhibited narrow fluctuations whereas the f_{CO₂} value decreased to 20 with decreasing polymerization time (t_p = 6 min). However, the TOF increased at higher catalyst loading. The same effect was observed by changing the monomer concentration instead of the amount of catalyst, as shown as entries 10–13 in Table 3. With increasing monomer concentration, the viscosity of the reaction mixture was not significantly affected under microwave irradiation. After 30 min irradiation at 100 W, a lower [CHO]/[Zn] ratio gave a polycarbonate of M_n = 19.3 (kg mol⁻¹) and f_{CO₂} = 75. This was the highest molecular weight and highest level of CO₂ incorporation of the copolymer in a shorter reaction time and lower pressure using the same type of Zn–Co based DMC catalyst through conventional means. In addition to classical heating methods, it was reported that the catalyst requires pre-activation to initiate the polymerization reaction.^{23a} Compared with the reported conventional copolymerization, there was a significant increase in the activity of the catalyst under microwave irradiation with no remarkable induction period for catalyst initiation. The probable reason may be the rapid polarization of CHO under microwave irradiation. This explains the reduction in t_p with increase in microwave power 100–500 W (entries 5–9). This fact is further supported by Lee *et al.* in which the addition of quaternary

ammonium salt with DMC complex reduced the induction time considerably by rapid polarization of epoxide, which in turn lowered the energy of activation.^{23b} Moreover the catalyst was capable of producing high molecular weight polycarbonate from the monomer, which is 4000 times higher than the weight of the catalyst. However, both M_n and f_{CO₂} were lower at this ratio (entries 12, 13).

After 13 min irradiation at 100 W, the reaction mixture became highly viscous and could not be stirred. The viscous reaction mixture was irradiated for a prolonged time to determine the influence of microwave irradiation, even after t_p. After 33 min irradiation (entry 15), the polymer molecular weight increased but the f_{CO₂} decreased than that of 23 min irradiation (entry 14). This can be explained by the fact that the diffusion of CO₂ became difficult due to the highly viscous nature of the reaction mixture but the microwaves were successful in activating the remaining unreacted CHO, as shown by the significant increase in molecular weight. Further irradiation (43 min, entry 16) with microwaves has a detrimental effect on the polymeric properties. Prolonged irradiation can cause the depolymerization of the polycarbonate produced, substantially reducing the molecular weight. Fig. 8 shows the proposed reaction mechanism for the DMC catalyzed copolymerization of CHO and CO₂. In this case, ring opening of CHO was expected to be the initiation reaction for polymerization followed by the addition of CO₂.

The effectiveness of microwave irradiation depends both on the polarizability and dielectric constant.²⁴ The ability to polarize under the influence of microwaves is expected to be higher for CHO on account of its high polarizability (α) and dielectric constant (ε_r) [α = 10.83 × 10⁻²⁴ cm³; ε_r = 9.1 (20 °C)] than CO₂ [α = 2.76 × 10⁻²⁴ cm³; ε_r = 1.6 (20 °C)]. To the best of our knowledge, the molecular weight of the polycarbonate formed from CHO and CO₂ using the DMC catalyst under microwave irradiation was the highest reported thus far in a shorter reaction time and lower pressure. A higher TOF was observed in all cases compared with DMC catalyzed conventional methods. According to the literature, the low molecular weight polycarbonate was attributed to the insertion of CHO requiring

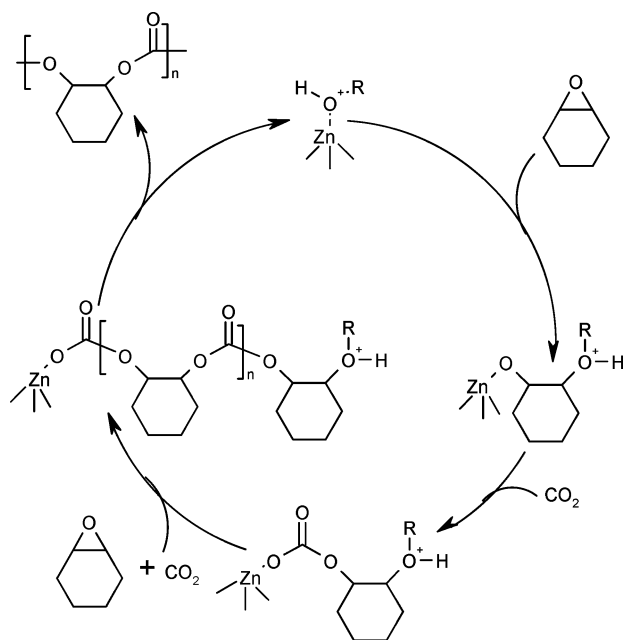


Fig. 8 Plausible reaction mechanism for the copolymerization of CHO and CO₂.

higher activation energy than for the insertion of CO₂ into the CHO terminal due to the steric hindrance of CHO.^{17d} Therefore, classical heating methods require a high temperature to obtain high molecular weight polycarbonate in a shorter reaction time. On the other hand, a lower temperature is favorable for the incorporation of CO₂. However, the reaction time necessary for achieving considerable conversion is quite high. Nevertheless, a high CO₂ pressure is needed in both cases. Under the influence of microwaves, CHO molecules become activated easily in a shorter reaction time, resulting in a high molecular weight polymer. A lower f_{CO_2} might be justified by the delay in the mass transfer of CO₂ into the bulk of the CHO due to the high viscosity of the reaction mixture and/or the lack of sufficient pressure for CO₂ to become activated by microwaves. Overall, microwave induced copolymerization produced good results within a shorter reaction time. In addition, a lower pressure was needed to obtain a high molecular weight polycarbonate containing considerable levels of CO₂ incorporation compared with conventional methodologies.

Experimental

Materials

Zinc chloride ($\geq 98\%$), zinc bromide ($\geq 98\%$), zinc iodide ($\geq 98\%$), potassium hexacyanocobaltate(III) (K₃Co(CN)₆), tertiary butyl alcohol (99+%) were purchased from Aldrich and used without further purification. Poly(ethylene glycol)-block-poly(propylene glycol)-block-poly(ethylene glycol) (PEG-PPG-PEG; $M_n = 1,100$), poly(propylene glycol) (PPG; $M_n = 725$) were purchased from Aldrich whereas poly(tetramethylene ether glycol) (PTMEG; $M_n = 1800$) was received from BASF Korea. Cyclohexene oxide (CHO, 98%) was purchased from Aldrich, refluxed over calcium hydride and distilled before use. Carbon dioxide of 99.999% purity was used without further purification.

CH₂Cl₂ and CH₃OH were obtained from SK Chemicals, Korea and used as such.

Catalyst synthesis

All DMC catalysts based on Zn^x-Co were synthesized according to the reported procedure elsewhere.¹⁹ The following methodology was used to prepare DMC-1. Solution 1 was prepared by dissolving 0.01 M of potassium hexacyanocobaltate(III) in 40 mL of distilled water. Solution 2 was prepared by dissolving 0.1 mol of ZnCl₂ in 100 mL of distilled water and 20 mL of *tert*-butanol. Solution 3 was prepared by dissolving 15 mL of tri-block copolymer, PEG-PPG-PEG, in 2 mL of distilled water and 40 mL of *tert*-butanol. Solution 2 was added slowly to solution 1 over a 1 h period at 50 °C with vigorous stirring, which resulted in the precipitation of a white solid. Solution 3 was then added to the above reaction mixture over a 10 min period with constant stirring for a further 1 h. The resulting solid was filtered, washed thoroughly with distilled water and dried at 60 °C for several hours under vacuum. DMC-2 and DMC-3 were synthesized using PTMEG and PPG as the complexing agent, respectively, and DMC-4 and DMC-5 were prepared using ZnBr₂ and ZnI₂ as the zinc salt, respectively. The catalysts were characterized by X-ray diffraction (XRD), X-ray photoelectron spectroscopy (XPS), Fourier transform infra-red spectroscopy (FT-IR), elemental analysis (EA) and inductively coupled plasma optical emission spectroscopy (ICP-OES).

Analyses

The wide-angle X-ray diffraction (WAXD) patterns of the DMC catalyst were obtained using a Rigaku with a RINT2000 wide angle goniometer 185 using Cu K α at 40 kV and 30 mA at a rate of 4° min⁻¹ ranging from 5–80°. XPS analysis was carried out using an ESCALAB 250 induced electron emission spectrometer with Al K α (1486.6 eV, 12 mA, 20 kV), carbon as the reference. The FT-IR spectra of the catalysts were obtained in transmission mode using React IR. Elemental analysis of the catalysts was carried out using a Vario EL III analyzer. The metal content of the catalysts was obtained from ICP-OES analysis using ULTIMA2 CHR (1.5 kW, 40.68 MHz, 130–800 mm) with mono chromat HDD and a poly chromat PMT detector. ¹H-nuclear magnetic resonance (NMR, 300 MHz) and ¹³C-NMR (75 MHz) spectra of the polymers were obtained on a Varian Gemini 2000 using CDCl₃ as solvent. The molecular weights and polydispersity index (PDI) of the polymers were measured by gel permeation chromatography (GPC) using a Waters 515 HPLC pump and Waters 2410 refractive index detector, operated at 25 °C. THF was used as the eluent and the calibration was performed using polystyrene standards. A multimode microwave reactor (KMIC 2KW) containing the source with a continuously adjustable power from 0 to 2 kW using a 3-stub tuner operating at a frequency of 2.450 GHz was utilized for the reactions. The surface temperature of the reactor was measured by an IR temperature detector.

Microwave assisted copolymerization of CHO with CO₂

The copolymerization of CHO with CO₂ was carried out in a 100 mL Pyrex glass reactor equipped with a magnetic stirrer.

In a typical copolymerization reaction, the required amount of catalyst was placed in the reactor and the desired amount of CHO was then added. The reactor was then capped with the reactor head inside the microwave cavity, purged several times with CO₂ and then pressurized to the desired value. The reaction was started by microwave irradiation at a particular microwave power for a set time with constant stirring. Two reaction times were used in this process; (1) t_p , which is the time for polymerization at which the reaction mixture becomes highly viscous and stops stirring, (2) t_{ir} , which is the total time for microwave irradiation. During copolymerization, the pressure inside the reactor was maintained using a cracking pressure valve set to 21 bar. After the stipulated time, polymerization was stopped by cooling the reaction mixture to room temperature and the CO₂ remaining inside the reactor was vented off. The product was dissolved in dichloromethane and filtered to remove the catalyst. The polymer formed was precipitated by adding excess methanol, filtered and dried under vacuum at 60 °C. The conversion of CHO was obtained from GC analysis and the polymer yield was calculated gravimetrically.

Conclusion

DMC catalysts based on Zn₃[Co(CN)₆]₂ were used for the microwave induced copolymerization of CHO with CO₂. The route was found to be successful for the synthesis of polycarbonate containing a considerable level of CO₂ incorporation at a lower pressure and shorter reaction time. In addition, the use of microwaves for the activation of CHO in copolymerization is a green technique that does not require solvents and is capable of furnishing high molecular weight copolymer. Complexing agents and zinc halides used for the synthesis of DMC catalysts had a significant effect on the catalytic activity for the copolymerization reaction. Microwave induced solventless copolymerization including gaseous monomers is expected to provide a new paradigm for the development of green technology.

Acknowledgements

The authors are grateful to Korea Science and Engineering Foundation (R01-2007-000-10183-0) and Brain Korea 21 project for the financial support for this work and to Korea Basic Science Institute (Busan) for catalyst characterizations.

References

- 1 R. Gedye, F. Smith, K. Westaway, H. Ali, L. Baldisera, L. Laberge and J. Rousell, *Tetrahedron Lett.*, 1986, **27**, 279.
- 2 (a) M. Neüchter, B. Ondruschka, W. Bonrath and A. Gum, *Green Chem.*, 2004, **6**, 128; (b) S. A. Galema, *Chem. Soc. Rev.*, 1997, **26**, 233; (c) N. E. Leadbeater, H. M. Torenus and H. Tye, *Comb. Chem. High Throughput Screen.*, 2004, **7**, 511; (d) M. Kidwai, *Pure Appl. Chem.*,

- 2001, **73**, 147; (e) L. Perreux and A. Loupy, *Tetrahedron*, 2001, **57**, 9199.
- 3 (a) C. O. Kappe, *Angew. Chem., Int. Ed.*, 2004, **43**, 6250; (b) A. K. Bose, M. J. Manhas, B. K. Banik and E. W. Robb, *Res. Chem. Intermed.*, 1994, **20**, 1; (c) C. R. Strauss and R. W. Trainor, *Aust. J. Chem.*, 1995, **48**, 1665; (d) S. Caddick, *Tetrahedron*, 1995, **51**, 10403.
- 4 (a) A. Loupy, G. Bram and J. Sansoulet, *New J. Chem.*, 1992, **16**, 233; (b) R. S. Varma, *Tetrahedron*, 2002, **58**, 1235.
- 5 A. de la Hoz, A. Díaz-Ortiz, A. Moreno and F. Langa, *Eur. J. Org. Chem.*, 2000, **4**, 3659.
- 6 N. Elander, J. R. Jones, S. Y. Lu and S. Stone-Elander, *Chem. Soc. Rev.*, 2000, **29**, 239.
- 7 F. Langa, P. de la Cruz, E. Espiñadora, J. J. García, M. C. Pérez and A. de la Hoz, *Carbon*, 2000, **38**, 1641.
- 8 (a) L. Zong, S. Zhou, N. Sgriccia, M. C. Hawley and L. C. Kempel, *J. Microwave Power Electromagn. Energ.*, 2003, **38**, 49; (b) F. Wiesbrock, R. Hoogenboom, M. A. M. Leenen, M. A. R. Meier and U. S. Schubert, *Macromolecules*, 2005, **38**, 5025; (c) H. Stange and A. Greiner, *Macromol. Rapid Commun.*, 2007, **28**, 504.
- 9 Y. Xu and Q.-X. Guo, *Heterocycles*, 2004, **63**, 903.
- 10 S. K. Das, *Synlett*, 2004, 915.
- 11 M. Larhed, C. Moberg and A. Hallberg, *Acc. Chem. Res.*, 2002, **35**, 717.
- 12 C. O. Kappe, *Curr. Opin. Chem. Biol.*, 2002, **6**, 314.
- 13 (a) R. S. Varma, *Green Chem.*, 1999, **1**, 43; (b) A. K. Bose, M. S. Manhas, S. N. Ganguly, A. H. Sharma and B. K. Banik, *Synthesis*, 2002, **11**, 1578.
- 14 W. Kuran, in *Polymeric Material Encyclopedia*, CRC Press, 1996, vol. 9.
- 15 S. Inoue, H. Koinuma and T. Tsuruta, *J. Polym. Sci., Polym. Lett. Ed.*, 1969, **7**, 287.
- 16 (a) M. Yoshida and M. Ihara, *Chem.–Eur. J.*, 2004, **10**, 2886; (b) G. W. Coates and D. R. Moore, *Angew. Chem., Int. Ed.*, 2004, **43**, 6618; (c) D. J. Darensbourg and M. W. Holtcamp, *Coord. Chem. Rev.*, 1996, **153**, 155; (d) T. A. Zevaco, A. Janssen, J. Sypien and E. Dinjus, *Green Chem.*, 2005, **7**, 659; (e) X. B. Lu, L. Shi, Y. M. Wang, R. Zhang, Y. J. Zhang, X. J. Peng, Z. C. Zhang and B. Li, *J. Am. Chem. Soc.*, 2006, **128**, 1664.
- 17 (a) D. J. Darensbourg, M. J. Adams and J. C. Yarbrough, *Inorg. Chem.*, 2001, **40**, 6543; (b) I. Kim, M. J. Yi, S. H. Byun, D. W. Park, B. U. Kim and C. S. Ha, *Macromol. Symp.*, 2005, **224**, 181; (c) I. Kim, M. J. Yi, K. J. Lee, D. W. Park, B. U. Kim and C. S. Ha, *Catal. Today*, 2006, **111**, 292; (d) S. Chen, G.-R. Qi, Z.-J. Hua and H.-Q. Yan, *J. Polym. Sci., Part A: Polym. Chem.*, 2004, **42**, 5284.
- 18 (a) U. Kreher, C. R. Strauss and D. Walter, Proceedings of ECSOC-5, The Fifth International Conference on Synthetic Organic Chemistry, Basel, Switzerland, 2001; (b) F. Ono, K. Qiao, D. Tomida and C. Yokoyama, *J. Mol. Catal. A: Chem.*, 2007, **263**, 223.
- 19 R. Srivastava, D. Srinivas and P. Ratnasamy, *J. Catal.*, 2006, **241**, 34.
- 20 (a) X.-H. Zhang, Z.-J. Hua, S. Chen, F. Liu, X.-Ke. Sun and G.-R. Qi, *Appl. Catal., A: Gen.*, 2007, **325**, 91; (b) S. Chen, Z. Hua, Z. Fang and G. Qi, *Polymer*, 2004, **45**, 6519; (c) Y. J. Huang, G. R. Qi and L. S. Chen, *Appl. Catal., A: Gen.*, 2003, **240**, 263; (d) S. Chen and L. Chen, *Colloid Polym. Sci.*, 2004, **282**, 1033.
- 21 K. Nakamoto, *Infrared and Raman spectra of inorganic and coordination compounds*, Wiley, 3rd edn, 1978, p. 266.
- 22 (a) Y. Xiao, Z. Wang and K. Ding, *Chem.–Eur. J.*, 2005, **11**, 3668; (b) B. Y. Lee, H. Y. Kwon, S. Y. Lee, S. J. Na, S.-I. Han, H. Yun, H. Lee and Y.-W. Park, *J. Am. Chem. Soc.*, 2005, **127**, 3031.
- 23 (a) W. J. Kruper, (Jr.) and D. J. Swart, *US Pat.*, 4 500 704, 1985; (b) S. Lee, S. T. Baek, K. Anas, C. S. Ha, D. W. Park, J. W. Lee and I. Kim, *Polymer*, 2007, **48**, 4361.
- 24 A. Loupy, *Microwaves in Organic Synthesis*, Wiley, p. 4.

Using a biphasic ionic liquid/water reaction system to improve oxygenase-catalysed biotransformation with whole cells

Robert J. Cornmell,^a Catherine L. Winder,^b Stephanie Schuler,^a Royston Goodacre^b and Gill Stephens^{*a}

Received 29th October 2007, Accepted 17th March 2008

First published as an Advance Article on the web 11th April 2008

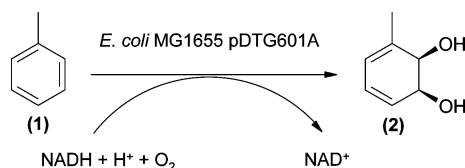
DOI: 10.1039/b716602h

Whole cells are usually used for oxygenase-catalysed biotransformations to ensure efficient cofactor recycling and to avoid problems with purification and stability of these complex, multi-subunit enzymes. Productivity in oxygenase-catalysed biotransformations is frequently restricted by toxicity of the substrates to the cells, but attempting to solve this problem using two-liquid phase reaction systems with conventional solvents provides only modest improvements in productivity. Therefore, we developed new, two phase systems using water-immiscible ionic liquids. Even though [NMeOct₃][NTf₂] and [P_{6,6,6,14}][NTf₂], inhibited growth of *Escherichia coli* by 39% and 23% respectively, both ionic liquids could be used to improve toluene dioxygenase-catalysed conversion of toluene to toluene *cis*-glycol using recombinant *E. coli* cells. The two-liquid phase reaction system improved resistance to toluene toxicity by 8-fold, and product concentrations increased by 2.5-fold in shake flask cultures. Product concentrations and specific product yields were improved by 200% and 238% respectively in bioreactors with an unrestricted oxygen supply.

Introduction

We wish to report the first oxygenase-catalysed biotransformation using whole cells in a biphasic ionic liquid/water reaction system. The use of ionic liquids for biotransformations with isolated enzymes is becoming well established because of their versatility and their improved safety and environmental credentials compared with conventional molecular solvents.^{1,2} By contrast, the use of whole cell biocatalysts in ionic liquids is much less well developed, and has been restricted so far to hydrolyses and a range of reductions.^{3–8} Herein we report the application of ionic liquids to obtain increased product concentrations using toluene dioxygenase expressed in a recombinant *Escherichia coli* strain.

Like many other oxygenase-catalysed biotransformations, the use of toluene dioxygenase to produce synthetically important *cis* diols^{9–12} (Scheme 1) is hindered by low productivities due to inhibition of the whole cell biocatalyst by substrate toxicity.^{13–15}



Scheme 1 Toluene dioxygenase-catalysed dihydroxylation of toluene to toluene *cis*-glycol.

^aSchool of Chemical Engineering and Analytical Science, Manchester Interdisciplinary Biocentre, University of Manchester, 131 Princess Street, M1 7DN, Manchester, UK.

E-mail: gill.stephens@manchester.ac.uk; Fax: +44 161 3068918; Tel: +44 161 3064377

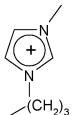
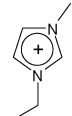
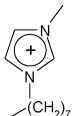
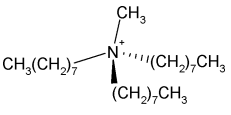
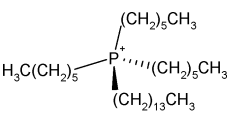
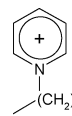
^bSchool of Chemistry, Manchester Interdisciplinary Biocentre, University of Manchester, 131 Princess Street, M1 7DN, Manchester, UK

Two-liquid phase reaction systems should provide a simple method to overcome the inhibition.^{16–21} These systems involve the use of a nontoxic, water-immiscible organic solvent as a second liquid phase in the reaction mixture. The solvent dissolves the substrate preferentially, and thus maintains a sub-inhibitory concentration of the substrate in the aqueous phase. The solvent phase also acts as a reservoir for the substrate, because the substrate equilibrates between the two phases as the cells convert it to product in the aqueous phase. Unfortunately, wide application of this technology has been hindered by the extremely restricted range of biocompatible molecular solvents.^{17,20,22} Thus, optimum biocatalyst performance is only obtained when there is a serendipitous match between the physical properties of the substrate and one of the biocompatible organic solvents.^{17,22} No such match is available for the toluene dioxygenase reaction; for example, using tetradecane as the water-immiscible phase provides only modest increases in product concentration using recombinant *E. coli* strains as the biocatalyst (1.2–1.4-fold).^{23,24} Therefore, it is clear that a wider range of biocompatible, water-immiscible solvents is needed, and hydrophobic ionic liquids were obvious candidates for testing.

Results and discussion

The first step was to identify biocompatible ionic liquids to test in the biotransformation. For redox biotransformations using whole cell biocatalysts, the required level of biocompatibility is to maintain cell viability and metabolic activity in the presence of the solvent, so that the cells can recycle the cofactor. Conventional growth rate and viable count measurements provide a reliable and comprehensive measure of cellular integrity and metabolic potential, whereas ionic liquid-induced changes in cell

Table 1 Effect of ionic liquids on growth of *E. coli*

Cation	Anion	
	[Cl] ⁻	[NTf ₂] ⁻
 [BMim]⁺	Water miscible (nd)	Toxic ($\mu = 0 \text{ h}^{-1}$)
 [EMim]⁺	Water miscible (nd)	Toxic ($\mu = 0 \text{ h}^{-1}$)
 [OMim]⁺	Toxic ($\mu = 0 \text{ h}^{-1}$)	na
 [NMeOct₃]⁺	Toxic ($\mu = 0 \text{ h}^{-1}$)	Biocompatible ($\mu = 0.219 \pm 0.01 \text{ h}^{-1}$)
 [P_{6,6,6,14}]⁺	Toxic ($\mu = 0 \text{ h}^{-1}$)	Biocompatible ($\mu = 0.276 \pm 0.006 \text{ h}^{-1}$)
 [NDecPy]⁺	na	Toxic ($\mu = 0 \text{ h}^{-1}$)
Tetradecane (phase ratio 0.23) No solvent (control)	$\mu = 0.336 \text{ h}^{-1} (\pm 0.006)$ $\mu = 0.357 \text{ h}^{-1}$	

E. coli MG1655 was grown in the presence of ionic liquids with the cations and anions shown at phase ratios from 0.0025 to 0.4 (solvent volume/total volume). "Biocompatible, $\mu = x \text{ h}^{-1}$ " gives the growth rate (μ) at a phase ratio of 0.23; "Toxic, $\mu = 0 \text{ h}^{-1}$ " indicates that there was no growth at any concentration tested; nd, not determined for the reason stated; na, not available. The growth rates (μ) without solvent and with tetradecane were also measured as controls. Data are the average for 5 replicates. The percentage inhibition was calculated from eqn (1).

$$\% \text{ inhibition} = \frac{[\mu_{\text{control}} - \mu_{\text{solvent}}]100}{\mu_{\text{control}}} \quad (1)$$

morphology complicate quantitative measurements of viability using vital stains. Therefore, we measured growth rates for *E. coli* MG1655 using high-throughput nephelometry in the presence of various water-immiscible ionic liquids (Table 1). Control cultures were grown in the absence of solvent, and with tetradecane. We used the host strain without the recombinant plasmid to examine the effect of the ionic liquids alone, since this would avoid physiological complications caused by maintenance

of the high copy number plasmid, over expression of the biocatalyst genes and the biotransformation.

In the absence of biotransformation, tetradecane inhibited growth by only 5.9% compared with growth in the absence of solvent (Table 1) when added to a phase ratio of 0.23 (solvent volume/total volume). [P_{6,6,6,14}][NTf₂] was more inhibitory than tetradecane but was, nevertheless, the least inhibitory of the ionic liquids tested, with 23% inhibition at a phase ratio of

0.23. [NMeOct₃][NTf₂] inhibited growth by 39% at a phase ratio of 0.23. Thus, both of these ionic liquids were sufficiently biocompatible to allow growth at reasonable rates. By contrast, none of the other water-immiscible ionic liquids tested allowed growth. Thus, changing the anion to chloride resulted in complete growth inhibition even when the phase ratio of [P_{6,6,6,14}][Cl] and [NMeOct₃][Cl] was decreased to 0.0025. [OMim][Cl] was also inhibitory. The homologues with shorter side chains are water miscible, and, therefore, were not tested. We did not test the [PF₆] anion, since it hydrolyses in water to form HF.^{25,26}

Since [NMeOct₃][NTf₂] and [P_{6,6,6,14}][NTf₂] were found to be biocompatible, we tested a wider range of [NTf₂] salts for biocompatibility, but [BMim][NTf₂], [EMim][NTf₂] and [NDecPy][NTf₂] inhibited growth completely at phase ratios between 0.0025 and 0.4. This demonstrates that both the cation and anion determine toxicity in a rather unpredictable manner. Furthermore, the sensitivity to ionic liquids varies between different species, since [BMim][NTf₂] is suitable for use with *Lactobacillus kefir*,³ but not *E. coli*.

Since [NMeOct₃][NTf₂] and [P_{6,6,6,14}][NTf₂] were sufficiently biocompatible to allow growth of *E. coli* MG1655, we tested their effect on the toluene dioxygenase-catalysed biotransformation of toluene **1** to toluene *cis*-glycol **2** (Scheme 1) using growing cultures of the recombinant *E. coli* strain, MG1655 pDTG601A. The substrate **1** dissolved preferentially in the ionic liquids, and we found that the *K_D* values were 0.68 and 0.60 in the [NMeOct₃][NTf₂]/media and [P_{6,6,6,14}][NTf₂]/media systems, respectively. In contrast, **2** partitioned completely into the aqueous phase when solutions of **2** (5 mM and 10 mM) were equilibrated with [NMeOct₃][NTf₂] and [P_{6,6,6,14}][NTf₂] (phase ratio 0.23).

We determined that the optimum initial toluene concentration for the biotransformation in single phase aqueous cultures was 3.76 mmol l⁻¹ at 50 ml scale. When the biotransformation was tested using [NMeOct₃][NTf₂] and [P_{6,6,6,14}][NTf₂] under the same conditions as a benchmark, the reaction rate and final product concentrations were unaffected by the presence of either ionic liquid (Fig. 1). The overall chemical yield of product in each reaction system remained unchanged at 87–90% (± 4%) after 20 h. As reported previously,²³ a small quantity of 3-methylcatechol (0.5–0.62 mM) was also formed.

Although product formation was unaffected by the ionic liquids, viable counts were slightly lower (Fig. 1). Furthermore, the growth rate of the cells during the biotransformation was 0.25 h⁻¹ and 0.21 h⁻¹ in the presence of [P_{6,6,6,14}][NTf₂] and [NMeOct₃][NTf₂] respectively, compared to 0.37 h⁻¹ for control biotransformations without solvent. Therefore, cell growth was more sensitive to inhibition by the ionic liquids than the biotransformation. This is unsurprising because growth depends on a great many cellular reactions that are potentially prone to inhibition, whereas the biotransformation presents far fewer targets for inhibition, since it depends only on the dioxygenase and a few supporting reactions.

The toxicity of the ionic liquids was intensified during the biotransformation. Thus, [P_{6,6,6,14}][NTf₂] inhibited growth by 32% during the biotransformation, compared with 23% in the absence of toluene and the recombinant plasmid (Table 1). Similarly, [NMeOct₃][NTf₂] inhibited growth by 43% during the biotransformation, compared with 39% in the absence of

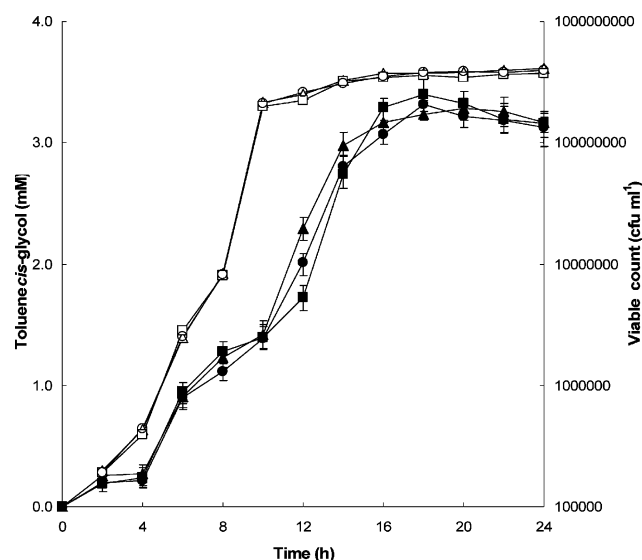


Fig. 1 Effect of ionic liquids on biotransformation of toluene at the optimum concentration (3.76 mmol l⁻¹) by *E. coli* MG1655(pDTG601A). Concentrations of toluene *cis*-glycol (closed symbols) and viable counts (open symbols) were measured for cultures grown without additions (▲, △) or in the presence of [P_{6,6,6,14}][NTf₂] (●, ○) or [NMeOct₃][NTf₂] (■, □). Data points are the average of 3 replicates and error bars show the maximum variance from the mean.

toluene. On the other hand, the growth rate under biotransformation conditions in the absence of solvent was 3.6% higher than in control cultures without biotransformation. Therefore, the presence of substrate, product, recombinant plasmid and inducer intensify the growth inhibition by the ionic liquids but do not affect the biotransformation.

Since [NMeOct₃][NTf₂] and [P_{6,6,6,14}][NTf₂] did not have any adverse effects on the biotransformation, they were good candidates for further development of the two-liquid phase reaction system with ionic liquids. Therefore, we tested the ability of the ionic liquids to protect the cells from toluene toxicity, by checking for growth over a range of toluene concentrations. In cultures grown without solvent, the maximum toluene concentration tolerated by the biocatalyst was 9.4 mmol l⁻¹, since growth was inhibited completely at higher concentrations. There was still significant inhibition with 9.4 mmol l⁻¹ toluene, since the final biomass concentration was only 59% of the concentration in the cultures grown with the optimum toluene concentration (3.76 mmol l⁻¹).

In the two-liquid phase system with either [NMeOct₃][NTf₂] or [P_{6,6,6,14}][NTf₂] (phase ratio 0.23), the maximum toluene concentration tolerated was 75.2 mmol l⁻¹. This was an 8-fold increase compared with the control cultures without ionic liquid. Therefore, the ionic liquids were extremely effective in protecting the cells from toluene toxicity.

The protection against toluene toxicity made it possible to run the biotransformation with a greatly increased toluene concentration. This was extremely beneficial, since it resulted in a 2.5-fold increase in toluene *cis*-glycol concentration (to *ca.* 20 mM) in the presence of the ionic liquids compared with the single phase system (Table 2). This is much better than the improvement available using recombinant *E. coli* with tetradecane as the solvent, which only gives a maximum of

Table 2 Effect of ionic liquids on biotransformation of toluene and on the maximum toluene concentration tolerated by the cells

Reaction system	Substrate 1 concentration/mmol l ⁻¹	Product 2 concentration/mM	Product yield 2 (%)	Specific yield of 2/mmol g ⁻¹ dry weight
Aqueous	9.4	8.31 (± 0.36)	88.4 (± 3.8)	0.83 (± 0.04)
[P _{6,6,6,14}][NTf ₂]	75.2	20.7 (± 0.13)	27.5 (± 0.17)	2.68 (± 0.02)
[NMeOct ₃][NTf ₂]	75.2	20.3 (± 0.46)	27.0 (± 0.6)	2.89 (± 0.07)

E. coli MG1655 pDTG601A was grown in the presence and absence of ionic liquids (3 replicates), with the maximum concentration of toluene tolerated in the reaction system under test conditions. Product concentration, chemical yield and specific yield were measured after 24 h.

1.2- to 1.4-fold increase depending on the culture system.^{23,24} Most importantly, the product concentration with the ionic liquids was 10.5-fold higher than in the two phase system with tetradecane.²⁴

There was no evident difference between the performance of the two ionic liquids in the 50 ml scale biotransformations, even though [NMeOct₃][NTf₂] inhibited growth more than [P_{6,6,6,14}][NTf₂]. This further emphasises that the biotransformation is not affected by the growth inhibition caused by the ionic liquid. It is also important to note that there was no emulsion formation in any of the cultures grown with the ionic liquids, whereas there are serious problems with emulsification when tetradecane is used, due to release of surface active materials by the cells.^{27–30}

The only problem was that the conversion of toluene to toluene *cis*-glycol was incomplete (27% yield). However, the oxygen supply was restricted to the air available in the culture headspace because the culture vessels had to be sealed to prevent loss of substrate. This suggested that the incomplete conversion could be due to oxygen limitation (it should be noted that this is unrelated to the low solubility of oxygen in ionic liquids,³¹ since the cells were in the aqueous phase and oxygen is reasonably soluble in water). This hypothesis was tested by using a bioreactor for the biotransformation (at 1.25 L scale) so that an unrestricted oxygen supply could be provided. Thus, the dissolved oxygen concentration was maintained above 5% by automatic control of the stirrer speed.

Initially, we grew triplicate control cultures in the bioreactor in the absence of the ionic liquids, using a feed of liquid toluene. *E. coli* is extremely sensitive to liquid toluene, and this meant that growth and product formation varied significantly between the replicate control cultures (Fig. 2). Thus, the final toluene *cis*-glycol concentration was 26 mM, 19 mM and 9.6 mM in the three replicate biotransformations, and the specific product yields were 5.5, 3.2 and 1.69 mmol g⁻¹ dry weight cells respectively. In each case, product formation stopped when the cells had stopped growing and had begun to lyse. We suggest that the variability was due to exposure of the cells to droplets of liquid toluene, which is known to be extremely growth inhibitory compared with dissolved toluene.³²

The next step was to repeat the biotransformations with ionic liquid. [P_{6,6,6,14}][NTf₂] (phase ratio 0.23) was chosen as the water-immiscible phase because it was less inhibitory than [NMeOct₃][NTf₂], and because it is cheaper and more readily

available in bulk. Nevertheless, the number of replicate cultures had to be limited to two due to the cost of these experiments (£1500 for the ionic liquid alone) It should be noted that industrial implementation would increase demand and drive down the cost, whilst further cost reductions can be achieved by recycling the solvent, as for any other solvent in an industrial process.

Using the ionic liquid allowed the use of significantly higher feed rates of liquid toluene (Fig. 2). In theory, the maximum feed rate should be 8 times higher than the cells would tolerate in the absence of the ionic liquid, since the toluene concentration tolerated in flask cultures increased 8-fold in the presence of ionic liquid. However, we started the toluene feed more cautiously than this, at the same rate as the control, and then increased the feed rate as quickly as possible thereafter, by checking that there was no growth inhibition, cell lysis or inhibition of product formation after each increase in rate. Therefore, it was possible to adjust the toluene feed rate by trial and error to give a substantial increase over the rate tolerated by control cultures. This resulted in a significant increase in mean product concentration (55.5 ± 22.5 mM) compared with the flask cultures (20.7 ± 0.13 mM), indicating that productivity was indeed limited by the oxygen supply in the flasks. Like the cultures without ionic liquids, the biotransformations stopped when the cells stopped growing and the viable count had begun to fall. We assumed that the death of the cells had caused irreversible loss of activity.

The final product yields per unit biomass were very similar in the replicate cultures, at 12.5 mmol g⁻¹ dry weight cells and 10.9 mmol g⁻¹ dry weight cells for replicate 1 and 2, respectively. However, the final toluene *cis*-glycol concentration in replicate 1 was 2.3-times higher (78 mM) than in replicate 2 (33 mM). By contrast, product formation was very reproducible in the flask cultures. In the flasks, the toluene was dissolved directly in the ionic liquid at the start of the experiment, whereas liquid toluene was fed continuously to the two-phase medium in the bioreactor. This meant that each droplet of liquid toluene would have to equilibrate between the two liquid phases, and the cells would be exposed periodically to high levels of liquid toluene in the aqueous phase on a random basis. We suggest that this would be sufficient to cause the observed variations in cell growth and product formation in the bioreactor.

Despite the variations in product concentration, it was evident that the average specific product yield in the presence of [P_{6,6,6,14}][NTf₂] in the bioreactor was significantly

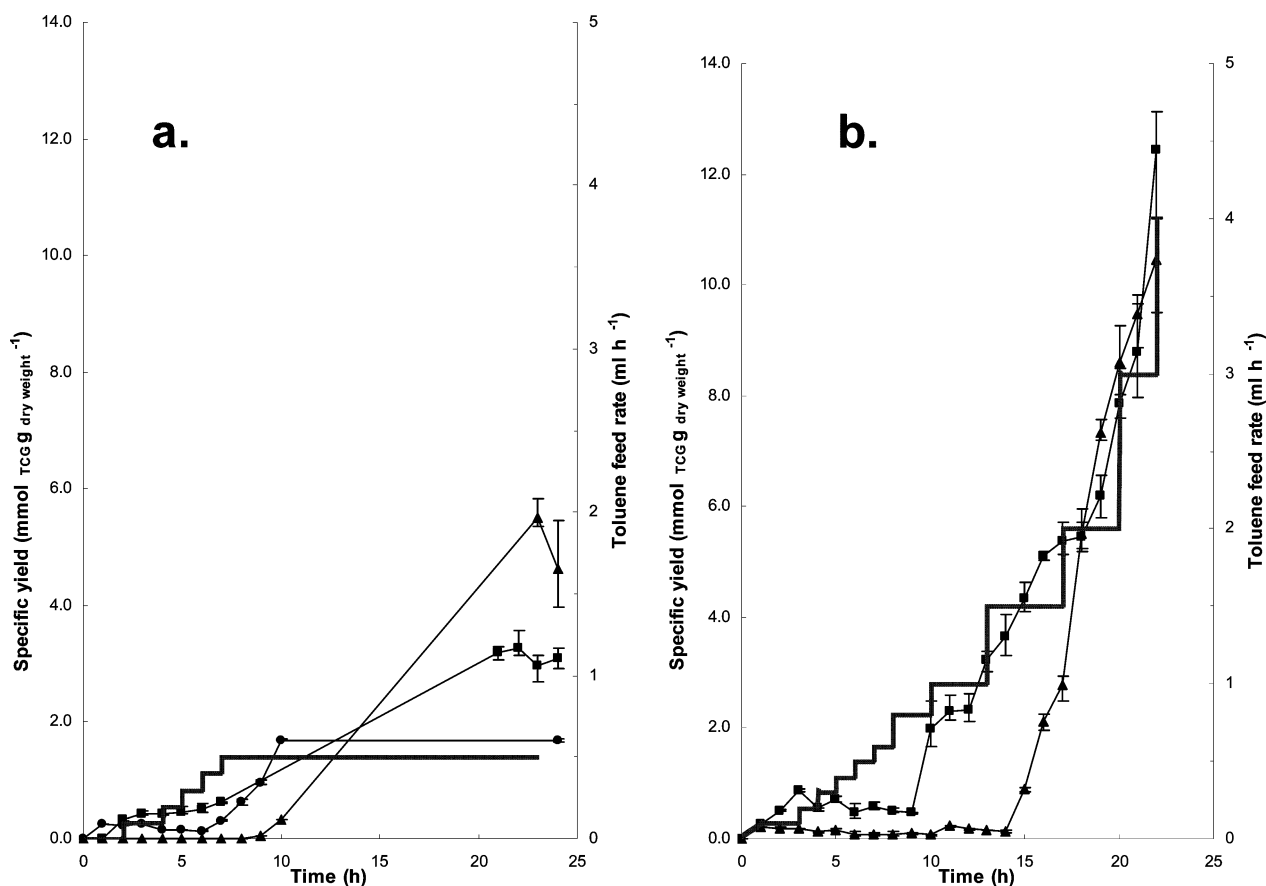


Fig. 2 Effect of $[P_{6,6,6,14}][NTf_2]$ on toluene *cis*-glycol production in bioreactors using *E. coli* MG1655(pDTG601A). *E. coli* MG1655 pDTG601A was grown at 1.25 L scale in bioreactor cultures with a feed of liquid toluene in the absence (a; 3 replicate cultures, ●, ▲, ■) and presence of $[P_{6,6,6,14}][NTf_2]$ at a phase ratio of 0.23 (b; 2 replicate cultures, ●, ▲). Specific yields of toluene *cis*-glycol are expressed as $mmol_{TCG} g^{-1} dry weight$, and are the average of 3 replicate analyses. Error bars show the maximum variance from the mean. Toluene feed rates (thick continuous line) are provided in the right hand axis.

better ($11.7 mmol g^{-1} dry weight$) than in the flask cultures ($2.68 mmol g^{-1} dry weight$) and in the monophasic biotransformations in the bioreactor ($3.46 mmol g^{-1} dry weight$). It should be noted that the chemical yields cannot be calculated accurately, because the reactor was sparged with air and this would strip the volatile substrate, toluene, out of the reactor at a significant rate. However, an approximate calculation of the *minimum* yield can be based on the total volume of toluene added during the fermentation (270 mmol). Thus, the apparent minimum product yields were 36% and 15%, calculated as $mmol_{TCG}/mmol_{toluene\ added} \times 100$. The stripping of toluene by the air flow would mean that the *actual* yields should be significantly higher than this.

Further work is now needed to optimise the regimes for growth and toluene feeding to obtain reproducible biotransformation in the presence of ionic liquids in bioreactors, although the current cost of the ionic liquid takes this beyond the scope of academic research.

Experimental

Chemicals: Authentic toluene *cis*-glycol samples were kindly provided by Chris Allen (Queen's University, Belfast). Ionic liquids were obtained as follows: [OMim][Cl] and [NDecPy][Cl]

from Ken Seddon (QUILL, Queen's University, Belfast); [NMeOct₃][NTf₂], from Solvent Innovation; [BMim][NTf₂], [EMim][PF₆], [EMim][NTf₂], [NMeOct₃][Cl], $[P_{6,6,6,14}][Cl]$ and $[P_{6,6,6,14}][NTf_2]$ from Sigma-Aldrich. Other chemicals were from Sigma-Aldrich unless stated otherwise.

Measurement of growth rates: Growth rates of *E. coli* K12 strain MG1655³³ were measured in MSX medium²⁷ in microcultures (200 μ l including solvent) using a Bioscreen C incubator/plate reader (Thermo Labsystems, Franklin, MA). Biotransformation of toluene was tested using *E. coli* MG1655 transformed³⁴ with pDTG601A³⁵ (provided by Rebecca Parales, University of California, Davis).

Biotransformations: Cultures for small scale biotransformations (50 ml)²⁷ were grown at 37 °C and 200 rpm with toluene in the presence or absence of solvents at a phase ratio of 0.23. Isopropyl- β -D-thiogalactoside (IPTG; 1 mM) was added after 5 h. All solvents were self sterile, since there was no microbial growth when 1 ml solvent was incubated in sterile medium for 30 h at 37 °C. The phase ratio was kept constant by taking samples from both the aqueous and solvent phases in the required volume ratio.

Larger scale biotransformations were performed in a Pierre Guerin bioreactor (Mauze, France) fitted with a 2 L vessel and operated at a working volume of 1.25L. Double strength

MS medium with ampicillin (100 $\mu\text{g ml}^{-1}$) was inoculated with 750 μl of a culture which had been grown in MSX medium²⁷ with 100 $\mu\text{g ml}^{-1}$ ampicillin for 18 h at 37 °C. The culture was grown for approximately 15 h at 37 °C, pH 6.8 ± 0.1 (controlled by automatic addition of 1 M HCl or 1 M NaOH), and a dissolved oxygen concentration above 5%, maintained by automatic control of stirrer speed (minimum 200 rpm) with an air flow of 25 l h⁻¹. Foaming was controlled by manual addition of the minimum volume of polypropylene glycol (P2000, 3% v/v) needed to break any foam, as soon as it began to form. When the OD_{680nm} reached 2.0, the pH was increased to 7.2 to prevent decomposition of toluene *cis*-glycol, and IPTG (1 mM) was added 30 min later, together with a feed of liquid toluene, added using a syringe pump (model 100 series, KD Scientific, USA). For cultures grown without ionic liquid, the toluene feed rate was maintained at 0.1 ml h⁻¹ for 2 h, and then increased every hour at a rate of 0.1 ml h⁻¹ to 0.5 ml h⁻¹, and then maintained at this rate for a further 17 h. Overall, this meant that 90 mmol toluene were fed to the cultures. A feed of glucose salts solution^{15,27} was started after 2 h, when the glucose in the culture medium had been depleted, and was fed at a rate sufficient to continue exponential growth of the bacteria, whilst also providing an electron donor for the biotransformation. The final culture volume was 1.25 L, after addition of the feeds and removal of samples. For the two phase reactions, the initial culture volume was 963 mL. [P_{6,6,6,14}][NTf₂] (287 mL) was pumped into the bioreactor when the OD was 2, so that the total culture volume was 1.25 L. The cells were allowed to adapt for 2 h before beginning the biotransformation as described above. The toluene feed was begun at 0.1 ml h⁻¹ for 2 h, and was increased hourly by 0.1 ml h⁻¹ until a rate of 0.8 ml h⁻¹ was established. After 10 h, the feed rate was increased to 1 ml h⁻¹, then further increased to 1.5 ml h⁻¹ at 13 h; at 17 h, the feed was increased to 2 ml h⁻¹ and then to 3 ml h⁻¹ at 20 h. A final toluene feed rate of 4 ml h⁻¹ was established at 22 h and held for 2 h. Overall, 270 mmol toluene were fed to the cultures. As before, the glucose feed was started after 2 h, but further aliquots of ionic liquid were added to compensate for increased culture volume due to glucose feeding, and thus keep the phase ratio as constant as possible. It was unnecessary to remove ionic liquid from the cultures to compensate for sampling, because the cultures were completely mixed, and all samples contained both the ionic liquid and aqueous phases in the correct phase ratio. The phases were allowed to separate before chemical analysis of the aqueous phase. The volume of the culture was 1.25 L at the end of the fermentation, including the ionic liquid.

Analytical methods: Product concentrations were determined by HPLC as described previously²⁷ except that a Spherisorb ODS (2) stainless steel analytical column (25 cm \times 4.6 mm, 5 μm particle size) was used. Viable counts were measured by plating serial dilutions of cultures in physiological saline (0.9% NaCl) on LB agar containing ampicillin (100 $\mu\text{g ml}^{-1}$).

Conclusion

The water-immiscible ionic liquids, [NMeOct₃][NTf₂] and [P_{6,6,6,14}][NTf₂], are biocompatible for *E. coli*, and have been used successfully to improve productivity and yield in the toluene dioxygenase-catalysed conversion of toluene to toluene

cis-glycol using a recombinant *E. coli* strain. To our knowledge, this is the first demonstration that ionic liquids can be used to improve an oxygenase-catalysed biotransformation using whole cells. The ionic liquids protect the biocatalyst from substrate toxicity by altering the availability of toluene in the aqueous phase. Therefore, using ionic liquids allows the formation of significantly higher product concentrations than in aqueous reaction systems or the conventional two-liquid phase system containing tetradecane. This alone is sufficient motive for further development of ionic liquid based reaction systems for redox biotransformations. The additional benefits accruing from lack of solvent emulsification, improved safety and lower environmental impact will push whole cell biocatalysis in ionic liquids to a much higher position on the research agenda.

Acknowledgements

This work was supported by the Engineering and Biological Systems committee of the UK Biotechnology and Biological Sciences Research Council. We thank Ken Seddon (QUILL, Queen's University, Belfast) for providing ionic liquids and for numerous helpful discussions. We are also grateful to Chris Allen (Queen's University, Belfast) for providing analytical standards and Rebecca Parales (University of California, Davis) for providing the plasmid, pDTG601A.

Notes and references

- 1 S. Park and R. J. Kazlauskas, *Curr. Opin. Biotechnol.*, 2003, **14**, 432–437.
- 2 F. van Rantwijk, R. M. Lau and R. A. Sheldon, *Trends Biotechnol.*, 2003, **21**, 131–138.
- 3 H. Pfruender, M. Amidjojo, U. Kragl and D. Weuster-Botz, *Angew. Chem., Int. Ed.*, 2004, **43**, 4529–4531.
- 4 S. G. Cull, J. D. Holbrey, V. Vargas-Mora, K. R. Seddon and G. J. Lye, *Biotechnol. Bioeng.*, 2000, **69**, 227–233.
- 5 M. D. Baumann, A. J. Daugulis and P. G. Jessop, *Appl. Microbiol. Biotechnol.*, 2005, **67**, 131–137.
- 6 M. Okochi, I. Nakagawa, T. Kobayashi, S. Hayashi, S. Furusaki and H. Honda, *J. Biotechnol.*, 2007, **128**, 376–382.
- 7 Y. Fatima, H. Kansal, P. Soni and U. C. Banerjee, *Process Biochem.*, 2007, **42**, 1412–1418.
- 8 S. Brautigam, S. Bringer-Meyer and D. Weuster-Botz, *Tetrahedron: Asym.*, 2007, **18**, 1883–1887.
- 9 T. Hudlicky, H. Luna, J. D. Price and F. Rulin, *J. Org. Chem.*, 1990, **55**, 4683–4687.
- 10 T. Hudlicky, D. Gonzalez and D. T. Gibson, *Aldrichim. Acta*, 1999, **32**, 35–62.
- 11 D. R. Boyd, N. D. Sharma and C. C. R. Allen, *Curr. Opin. Biotechnol.*, 2001, **12**, 564–573.
- 12 D. R. Boyd and G. N. Sheldrake, *Nat. Prod. Rep.*, 1998, **15**, 309–324.
- 13 D. R. Boyd, N. D. Sharma, B. Byrne, M. V. Hand, J. F. Malone, G. N. Sheldrake, J. Blacker and H. Dalton, *J. Chem. Soc., Perkin Trans. 1*, 1998, 1935–1943.
- 14 D. R. Boyd, N. D. Sharma, N. I. Bowers, J. Duffy, J. S. Harrison and H. Dalton, *J. Chem. Soc., Perkin Trans. 1*, 2000, **9**, 1345–1350.
- 15 R. O. Jenkins, G. M. Stephens and H. Dalton, *Biotechnol. Bioeng.*, 1987, **29**, 873–883.
- 16 K. Jablczynski, W. Wieckowski and A. Klein, *Z. Anorg. Allg. Chem.*, 1925, **143**, 343.
- 17 C. Laane, S. Boeren, K. Vos and C. Veeger, *Biotechnol. Bioeng.*, 1987, **30**, 81–87.
- 18 M. D. Lilly, *Philos. Trans. R. Soc. London, Ser. B*, 1983, **300**, 391–398.
- 19 G. J. Lye and J. M. Woodley, in *Multiphase Bioreactor Design*, ed. J. M. S. Cabral, M. Mota and J. Tramper, Taylor and Francis, London, Editon edn, 2001, p. 115.
- 20 G. J. Salter and D. B. Kell, *Crit. Rev. Biotechnol.*, 1995, **15**, 139–177.

- 21 M. Vermue, J. Sikkema, A. Verheul, R. Bakker and J. Tramper, *Biotechnol. Bioeng.*, 1993, **42**, 747–758.
- 22 A. J. J. Straathof, *Biotechnol. Prog.*, 2003, **19**, 755–762.
- 23 P. Phumathon and G. M. Stephens, *Enzyme Microb. Technol.*, 1999, **25**, 810–819.
- 24 J. T. Tsai, L. P. Wahbi, G. A. Dervakos and G. M. Stephens, *Biotechnol. Lett.*, 1996, **18**, 241–244.
- 25 K. R. Seddon, A. Stark and M. J. Torres, *Pure Appl. Chem.*, 2000, **72**, 2275–2287.
- 26 A. E. Visser, R. P. Swatloski, W. M. Reichert, S. T. Griffin and R. D. Rogers, *Ind. Eng. Chem. Res.*, 2000, **39**, 3596–3604.
- 27 L. P. Wahbi, D. Gokhale, S. Minter and G. M. Stephens, *Enzyme Microb. Technol.*, 1996, **19**, 297–306.
- 28 H. Baldascini and D. B. Janssen, *Enzyme Microb. Technol.*, 2005, **36**, 285–293.
- 29 A. Schmid, A. Kollmer and B. Witholt, *Enzyme Microb. Technol.*, 1998, **22**, 487–493.
- 30 J. Kieboom, J. J. Dennis, J. A. M. de Bont and G. J. Zylstra, *J. Biol. Chem.*, 1998, **273**, 85–91.
- 31 J. L. Anthony, E. J. Maginn and J. F. Brennecke, *J. Phys. Chem. B*, 2002, **106**, 7315–7320.
- 32 C. J. Hack, J. M. Woodley, M. D. Lilly and J. M. Liddell, *Enzyme Microb. Technol.*, 2000, **26**, 530–536.
- 33 F. R. Blattner, G. Plunkett, C. A. Bloch, N. T. Perna, V. Burland, M. Riley, J. ColladoVides, J. D. Glasner, C. K. Rode, G. F. Mayhew, J. Gregor, N. W. Davis, H. A. Kirkpatrick, M. A. Goeden, D. J. Rose, B. Mau and Y. Shao, *Science*, 1997, **277**, 1453–1462.
- 34 D. Hanahan, *J. Mol. Biol.*, 1983, **166**, 557–580.
- 35 G. J. Zylstra and D. T. Gibson, *J. Biol. Chem.*, 1989, **264**, 14940–14946.

Efficient subtilisin immobilization in chitosan, and peptide synthesis using chitosan–subtilisin biocatalytic films

Duncan J. Macquarrie*^a and Anna Bacheva*^b

Received 14th January 2008, Accepted 25th March 2008

First published as an Advance Article on the web 18th April 2008

DOI: 10.1039/b800584b

The immobilization of serine protease subtilisin Carlsberg on/in chitosan, a hydrophilic biopolymer was investigated in this study. Using different techniques, biocatalysts in the form of gels, fibers and films were prepared. Subtilisin loading and biocatalytic properties of obtained samples were studied. The optimal method of enzyme incorporation was pre-mixing of chitosan acetate and enzyme solutions, then air-drying and treatment with glutaraldehyde. It was found that this form of biocomposite has the highest loading capacity (up to 20 mg protein g⁻¹ support) and good mechanical properties. The dependence of subtilisin loading on the starting concentration of the enzyme during immobilization shows the maximum loading at [E] = 15 mg mL⁻¹. The dependence of subtilisin loading and activity on the concentration of the glutaraldehyde was explored. The biocatalytic films were active catalysts for peptide bond formation (with 25–92% product yield) in nonaqueous media, demonstrating high activity and stability under these conditions. They are also active in aqueous media, bringing about the reverse reaction, and can therefore be used for either peptide bond formation or cleavage.

Introduction

The natural role of chitin is to serve as the basis of an insects exoskeleton or shell of crustaceans, krill, shrimp and squid pen, defending the organism from the aggressive environment. Large volumes of chitin are available as they form a waste stream from the fishing industry. Adding value to chitosan is thus an important goal. Chitosan, a partially deacetylated chitin derivative, has been used as a protective shell for enzymes, protecting them from various inactivation factors which can arise during biotechnological processes.¹ One of the biggest advantages of chitosan over chitin and other potential support/protective materials (e.g. silica) is that slightly acidic solutions of chitosan can be readily cast into beads, films, fibres or gels, allowing for a great flexibility in the physical manipulation of chitosan thus lending to it unique potential as a catalyst support with potential for fixation in reactors and for continuous processing. Chitosan is a hydrophilic polymer that mimics the natural hydrophilic microenvironment of globular proteins, which work in aqueous solutions. Chitosan could thus function as a protective shell and/or a carrier depending on the immobilization method.¹ Physical adsorption, introduction into polymer network (entrapment) or covalent fixation of enzyme—all these diverse techniques could be used for enzyme immobilization on chitosan films. More broadly, chitosan is becoming increasingly important as a support for a wide range of catalytic systems.^{2,3}

Based on this idea we have prepared biocatalysts from subtilisin, immobilized on/in chitosan and studied their properties. To the best of our knowledge, subtilisin has not before been supported in/on chitosan. Subtilisin has been immobilized on different supports, including silica, organically modified silica and polymeric gels.^{4–9} While activity was clearly demonstrated in these systems, it is difficult to compare results directly, as different systems under different conditions were investigated. Despite this, we believe that chitosan has distinct advantages over the other supports due to (a) its renewable nature—it is currently available in large quantities as a waste product from the fishing industry and (b) its excellent film-forming ability, allowing attachment to reactor walls for advanced processing.

Due to the pH-sensitivity of the enzyme, we have modified the process for the preparation of the chitosan–enzyme system, so as to minimise the acidity of the dissolution step and the requirement for strongly basic conditions in the precipitation stage.

Results and discussion

Biocatalysts used in biotransformations should meet several criteria, for example: (i) they should be rigid enough not to be destroyed during reaction, (ii) they should be easily removed from the reaction mixture after the end of the reaction, (iii) the preparation process should proceed under mild conditions to protect enzymatic activity, and (iv) reuse should be straightforward. In our previous works^{6–9} it was shown that subtilisin immobilized on PVA cryogel, a hydrophilic polymer support, was active and stable in aqueous and organic media.

We decided to obtain biocomposites from chitosan, natural hydrophilic polymer, and serine protease subtilisin, one of the most prospective biocatalysts in enzymatic peptide synthesis.

^aCentre of Excellence in Green Chemistry, Department of Chemistry, University of York, Heslington, York, UK YO10 5DD. E-mail: djm13@york.ac.uk; Fax: +44 (0)1904 432705; Tel: +44 (0)1904 424533

^bChemistry Department, M V Lomonosov Moscow State University, 119991, Moscow, Russia. E-mail: anbach@genebee.msu.ru; Fax: +7 (495) 9328846; Tel: +7 (495) 9395529

In this biocomposite, enzyme should be entrapped into a polysaccharide network maintained by H-bonds. To make more robust biocomposites, samples should be precipitated and in some cases crosslinked.

Three types of the composite materials (film, fibres and gel) were prepared by dissolution of chitosan in dilute acid and addition of enzyme solution. We found that this process could also be carried out at a pH closer to neutral by preparing chitosan acetate first of all from dilute acetic acid solutions of chitosan, and then re-dissolving the salt in water. Resulting mixture was placed into a 10 mL glass vial, and re-precipitation of chitosan was then effected by one of following means: (1) air-drying (film (1)); (2) addition of 4M NaOH (gel (2)); (3) addition of 30% tripolyphosphate crosslinker solution (soft gel (3)); (4) addition of glutaraldehyde (GA) crosslinker (Fig. 1) solution of concentration 2% (gel (4)); (5) addition of GA solution of concentration 1% and 4 M NaOH (gel (5)); (6) addition of 3 M Na₂SO₄ crosslinker (fibres (6)). (The 4 M NaOH can be replaced by 4 M NaCl, which contains 0.1 M NaOH, with very similar results.)

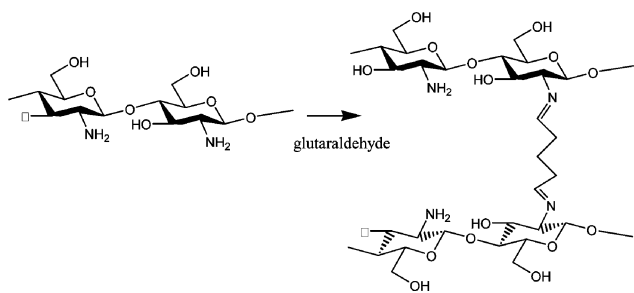


Fig. 1 Crosslinking of chitosan using glutaraldehyde.

Then the obtained preparations (except (6)) were washed with Tris-HCl buffer until no protein could be detected in the washings using optical absorbance at 280 nm. The amount of enzyme adsorbed was determined by measuring the residual enzyme after adsorption and comparing this to the original quantity.

It was found that all of these techniques gave composites containing enzyme, although the levels of protein incorporation differed drastically, as did specific activity, measured by hydrolysis of the chromogenic substrate Z-Ala-Ala-Leu↓pNA **12**, where Z = carbobenzyloxy, pNA = p-nitroanilide, and ↓ = the bond cleaved by the enzyme. The results of the experiments are summarized in Table 1 and Fig. 2.

The highest loading was observed in the crosslinked gels, but most active were fibres formed by Na₂SO₄ addition; however, subtilisin leached off this biocatalyst very easily as it was not well fixed on the support; moreover, the fibres were very soft

Table 1 Properties of subtilisin–chitosan biocomposites

Sample number	Sample preparation, additive	Loading/mg protein g ⁻¹ biocatalyst	Specific activity/g ⁻¹ biocatalyst
1	Film	0.81	0.0389
2	Gel (NaOH)	0.61	0.0474
3	Gel (TPP)	8.1	0.06
4	Gel (2%GA)	35.8	1.1
5	Gel (1%GA + NaOH)	22.3	0.42
6	Fibres (Na ₂ SO ₄), unwashed	20	8.7

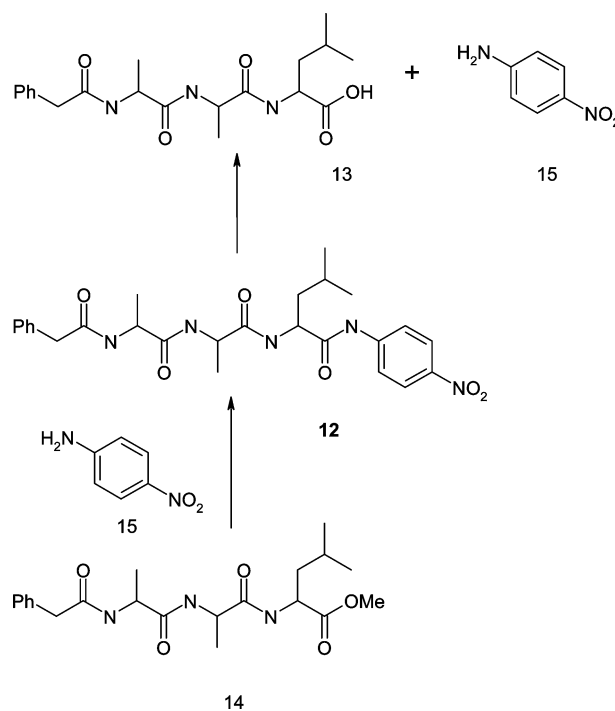


Fig. 2 Peptide synthesis and hydrolysis.

and inconvenient in use. Leaching was not observed for the other immobilization techniques.

Treatment by GA gave a material with better mechanical properties and higher activity than the other crosslinkers. GA has two aldehyde functionalities and is able to form covalent bonds both between NH₂ groups of enzyme and chitosan and between NH₂ groups from different chitosan chains. For these samples the dependence of loading on starting enzyme concentration was studied (Fig. 3). The degree of loading increased with increasing enzyme concentration, qualitatively following a typical Langmuir adsorption model, but after 15 mg mL⁻¹ the curve reached a plateau and further increase in concentration had no effect on loading, revealing a limit of subtilisin incorporation into the chitosan gel.

Loading and enzymatic activity of subtilisin–chitosan gels were studied depending on glutaraldehyde concentration (Table 2).

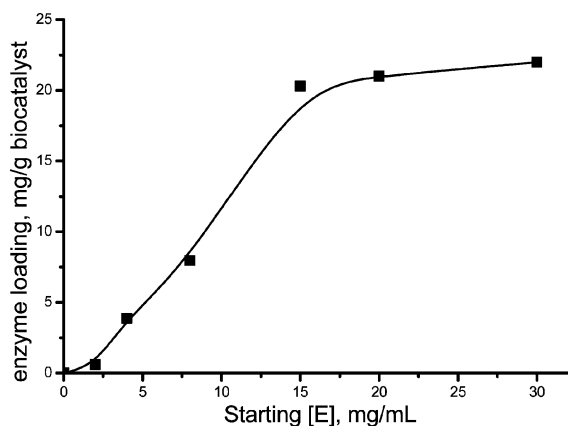


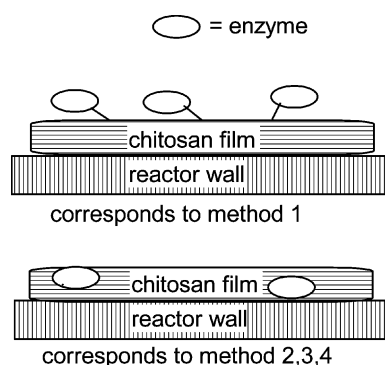
Fig. 3 Dependence of loading on starting enzyme concentration.

Table 2 Hydrolytic properties of subtilisin–chitosan gels depending on GA concentration

Sample number	[GA] (%)	Loading/mg protein g ⁻¹ biocatalyst	Specific activity/g ⁻¹ biocatalyst	Specific activity/mg ⁻¹ enzyme for hydrolysis
5	1	22.3	0.42	0.02
4	2	35	1.1	0.03
7	2.5	20.2	0.7	0.06

It was shown that optimal GA concentration for chitosan–subtilisin gels was in the range 1–2%, as gels obtained in these conditions possess maximum activity. Probably higher GA concentration leads to high crosslinking degree of chitosan, thus limiting substrate diffusion to the enzyme active centre.

Having demonstrated the basic activity of chitosan–subtilisin composites, we moved on to preparing composites immobilized in a reactor. Simple drying of chitosan solution leads to film formation. The film obtained adheres to the surface of reaction vessel (standard round bottom flask), meaning that we can readily make biocatalytic coatings using this technique. Films from chitosan–subtilisin biocomposite, crosslinked with GA, were obtained by 4 methods: (1) obtaining chitosan film, treatment by GA and then by subtilisin solution (sandwich), (2) mixing subtilisin and chitosan solutions and then addition of GA before drying, (3) as (2) but addition of GA after drying and (4) as (3) but the film was lyophilised (Fig. 4). Protein loading for biocomposite films appeared to be comparable to, and in some cases even higher than gels. All samples were active in hydrolysis, especially “sandwich”. However, in low water media, where the enzyme catalyses peptide bond formation, this biocatalyst was inactive probably due to full exposure of enzyme into denaturing organic solvent. The other biocatalytic films were active catalysts

**Fig. 4** Representation of film formation strategies.

for peptide bond formation in nonaqueous media in reaction (1) thus possessing high activity and stability under these conditions (Table 3).

The best biocatalytic properties were shown by the film obtained from chitosan–subtilisin mixture with addition of 0.5% GA before drying. After optimization of the preparation technique we chose several samples with high activity, which were capable of 25–92% yields in the formation of the tetrapeptide Z-Ala-Ala-Leu-Phe-pNA in dimethylformamide–acetonitrile (6/4) solution.

The films were mechanically stable after several uses and prolonged storage (several weeks). Activity was essentially unchanged on reuse over a period of 3–4 days (99–100% of original), but after 3 weeks storage in dry conditions had dropped to 82% of the original value.

Experimental

Subtilisin Carlsberg and chitosan (85% deacetylated, from crab shells) were obtained from Sigma. All other chemicals (crosslinkers, *etc.*) were obtained from Aldrich. All solvents and salts were of analytical grade or additionally purified. Peptides and peptide derivatives Glp-Ala-Ala-Leu-pNA (where Glp- is pyroglutamyl residue), Z-Ala-Ala-Leu-OCH₃ and Phe-pNA were obtained according to the procedures described by Getun *et al.*¹⁰ Reverse-phase HPLC analyses were performed on liquid chromatograph Altex Model 110A (United States) with column Microsorb-MV C8 (4.6 × 250 mm, Rainin Instrument Company, Inc., United States) with elution by linear gradients of acetonitrile 10–70% for 26.2 min in 0.1% TFA at the rate of 1 mL min⁻¹ with detection at 220 and 280 nm.

Amino acid analyses were performed on a Hitachi-835 amino acid analyzer (Japan) after sample hydrolysis in 5.7 M HCl at 105°C in evacuated ampoules for 48 h.

Preparation of subtilisin–chitosan biocomposites

To chitosan solution (1 mL, 1 wt% chitosan) in 2% acetic acid, the subtilisin solution (250 μL, 40 mg mL⁻¹ in phosphate buffer pH 8.0) was added, and mixture was agitated for 1 h. The solution was then placed into 10 mL glass (or round bottom flask) and air-dried to obtain film (1); alternatively, gels were obtained by treatment of the mixture by

- (1) addition of 0.1 mL 4 M NaOH solution (2);
- (2) addition of 30% tripolyphosphate solution at a level of 0.5% concentration in the mixture (gel (3));
- (3) addition of 50% glutaraldehyde solution to 2% (gel (4)) or 2.5% (gel (7)) concentration in the mixture;

Table 3 Properties of subtilisin–chitosan films, obtained using GA addition in peptide formation according to Fig. 2

Sample number	Sample preparation	[GA] (%)	Loading/mg protein g ⁻¹ biocatalyst	Specific activity/g biocatalyst	Yield of 12 (%)
8	Sandwich	0.5	44.34	0.64	0
9	GA addition	0.25	0.343	3.1	25
	Before drying	0.5	65	0.84	92
10	GA addition	0.25	0.42	3.5	80
	After drying	0.5	27	0.5	85
11	Lyophilization	0.25	8	8	62
		0.5	50	12.7	60

(4) addition of 0.1 mL 4 M NaOH solution and 50% glutaraldehyde solution to 1% concentration in the mixture (gel (5));

(5) addition of 3 M Na₂SO₄ solution (0.2 mL) (fibres (6)).

Different subtilisin concentrations in the subtilisin–chitosan mixture were obtained using consequent dilution of 150 mg mL⁻¹ subtilisin solution which were then added to the initial chitosan solution. The biocatalyst obtained was washed 3 times with 0.05 M Tris-HCl buffer pH 8.2 to block all remaining –CHO groups. The amount of immobilized protein was calculated from the data of amino acid analysis (for samples prepared with different subtilisin concentrations) or from UV absorbance at 280 nm of starting subtilisin solution subtracting absorbance of washings at 280 nm.

Different films were formed from chitosan acetate (2% chitosan solution in 2% acetic acid was precipitated by 10-fold volume of acetone, filtered, dried and ground). This was then re-dissolved in acetate buffer pH 5.0 (1 mL, 1 wt%) and mixed with subtilisin solutions in the same buffer (250 μL, 75 mg mL⁻¹). Then glutaraldehyde was added either before drying (5% solution, to obtain 0.5 and 1% concentration in the mixture, (9)) or after drying (0.25 or 0.5% solution, 2 mL (10)). Samples (11) were prepared by same way as (10) the only difference was that film was lyophilized instead of drying. The obtained samples were washed 3 times with 0.05 M Tris-HCl buffer pH 8.2. In the case of sample (8) solution of acetate chitosan in acetate buffer pH 5.0 (1 mL, 1 wt%) was dried to obtain film, then treated with 2 mL of 0.5% glutaraldehyde solution during 2 h, and subtilisin solution ((250 μL, 40 mg mL⁻¹) was added. After incubation during 24 h at +4 °C the sample was washed 3 times with 0.05 M Tris-HCl buffer pH 8.2.

Determination of immobilized subtilisin hydrolytic activity against Glp-Ala-Ala-Leu-pNA

Glp-Ala-Ala-Leu-pNA solution in DMF (50 μL, 5 mg mL⁻¹) was added to 2 mL of 0.05 M Tris/HCl buffer (pH 8.3) containing 1.5 mM CaCl₂, and the mixture was incubated at 20 °C for 10 min. Then a weighed sample of chitosan–subtilisin was added, and the mixture was incubated at 20 °C, absorbance was measured every minute with periodical shaking until its absorbance at 410 nm reached 0.1–0.4. The reaction was stopped with 1 mL of 50% acetic acid. In control samples there was reverse order of addition of the biocatalyst and acetic acid.

The specific activity was calculated according to the formula:

$$(A_{410} - A_{c410}) \times V_0 t \times m_{\text{biocat}} \times 8.9$$

where A_{410} is the absorption of the mixture at 410 nm, A_{c410} is the

absorption of the control sample, V_0 is the total volume of the sample (mL), t is the time of reaction (min), m_{biocat} is the weight of the biocatalyst (g), and 8.9 is the molar extinction coefficient of *p*-nitroaniline (mM⁻¹ cm⁻¹).

An activity unit is defined as the amount of enzyme that liberates 1 μmol of *p*-nitroaniline per 1 min under the condition described above.

Synthesis of Z-Ala-Ala-Leu-Phe-pNA by immobilized subtilisin

A portion of immobilized subtilisin (3–7 mg) was added to the solution of Z-Ala-Ala-Leu-OMe (5.1 mg, 12 μmol) and Phe-pNA (3.4 mg, 12 μmol) in 380 μL of the mixture of dimethylformamide–acetonitrile 6/4. The reaction suspension was shaken at 20 °C, with 5 μL samples being periodically taken for HPLC-analysis.

Conclusions

We have demonstrated that chitosan-immobilized subtilisin possesses both hydrolytic (in aqueous media) and synthetic (in low water media) activities. In general hydrolytic activity of biocomposite films containing GA was higher than for biocatalysts prepared without crosslinker. These films can be attached to the walls of a reaction vessel and used in both media. We have shown that biocatalytic films prepared in this work are characterized by preparative simplicity, high activity and stability in different media under very mild conditions.

Notes and references

- 1 B. Krajewska, *Enzyme Microb. Technol.*, 2004, **35**, 126.
- 2 E. Guibal, *Prog. Polym. Sci.*, 2005, **30**, 71.
- 3 D. J. Macquarrie and J. J. E. Hardy, *Ind. Eng. Chem. Res.*, 2005, **44**, 8499.
- 4 P. H. Fromm, M. E. Rezac, K. Würges and P. Czermak, *AIChE J.*, 2007, **53**, 237.
- 5 L. Ferreira, M. A. Ramos, J. S. Dordick and M. H. Gil, *J. Mol. Catal. B: Enzym.*, 2003, **21**, 189.
- 6 A. V. Bacheva, F. M. Plieva, E. N. Lysogorskaya, I. Yu Filippova and V. I. Lozinsky, *Bioorg. Med. Chem. Lett.*, 2001, **11**, 1005.
- 7 I. Yu Filippova, A. V. Bacheva, O. V. Baibak, F. M. Plieva, E. N. Lysogorskaya, E. S. Oksenoit and V. I. Lozinsky, *RAS Bull.*, 2001, **50**, 1896.
- 8 A. V. Bacheva, O. V. Baibak, A. V. Belyaeva, E. N. Lysogorskaya, E. S. Oksenoit, V. I. Lozinsky and I. Yu Filippova, *Russ. J. Bioorg. Chem.*, 2003, **29**, 502.
- 9 A. V. Bacheva, O. V. Baibak, A. V. Belyaeva, E. S. Oksenoit, T. I. Velichko, E. N. Lysogorskaya, A. K. Gladilin, V. I. Lozinsky and I. Yu Filippova, *Biochemistry (Moscow)*, 2003, **68**, 1896.
- 10 I. V. Getun, I. Y. Fillipova, E. N. Lysorgskaya, E. S. Oksenoit, V. V. Anisimova, S. V. Kolobanova, A. V. Bacheva and V. M. Stepanov, *Bioorg. Med. Chem. Lett.*, 1997, **20**, 2692.

Designing enzyme-compatible ionic liquids that can dissolve carbohydrates†

Hua Zhao,^{*a} Gary A. Baker,^b Zhiyan Song,^a Olarongbe Olubajo,^a Tanisha Crittle^a and Darkeysha Peters^a

Received 8th February 2008, Accepted 25th March 2008

First published as an Advance Article on the web 25th April 2008

DOI: 10.1039/b801489b

Recently, there is a rising interest in dissolving a variety of carbohydrates (such as sugars, starch and cellulose) in ionic liquids (ILs). The solutions of carbohydrates are then conveniently subject to chemical or physical modifications. However, one serious disadvantage of these ILs is their strong tendency in denaturing enzymes. This drawback prohibits the dissolved carbohydrates from being transformed by enzymatic reactions. In the present study, we designed a series of ILs that are able to dissolve carbohydrates but do not considerably inactivate the immobilized lipase B from *Candida antarctica*. These ILs consist of glycol-substituted cations and acetate anions. They could dissolve more than 10% (wt) cellulose and up to 80% (wt) D-glucose. The transesterification activities of the lipase in these ILs are very comparable with those in hydrophobic ILs. The hydrogen-bond forming anions, oxygen-containing cations, and low cation bulkiness promote the carbohydrate dissolution, while the low anion concentration appears essential for the enzyme stabilization. Therefore, an optimization could be achieved through a fine design of IL structures. To demonstrate the potential applications of these ILs, we performed the enzymatic transesterifications of methyl methacrylate with D-glucose and cellulose, respectively, both fully dissolved in ionic media. In the case of D-glucose, conversions up to 80% were obtained; and in the case of cellulose, conversions up to 89% and isolated yields up to 66% were achieved.

Introduction

It has been very challenging to catalyze the reactions on carbohydrates using insoluble enzymes in organic solvents because carbohydrates are not readily soluble in most organic solvents.¹ Unprotected sugars are only soluble in a few solvents such as pyridine and dimethylformamide (DMF). But these solvents induce low enzyme activities although a number of lipases and proteases retained some catalytic properties in them.² Alternatively, Cao *et al.*³ demonstrated the solid-phase esterification of D-glucose with fatty acids in organic solvents (such as *t*-butanol) catalyzed by immobilized lipases. However, these methods are not practical for starch and cellulose as they are not soluble in these solvents and less reactive than simple sugars. A detouring method is to prepare the derivatives of polysaccharides, and then dissolve them in organic solvents for biocatalytic processing (for example, using cellulose acetate as the substrate⁴).

Instead of making carbohydrates soluble, other attempts were made to solubilize the enzymes in organic solvents by either chemical modification or formation of reversed micelles of enzymes, but both methods have serious drawbacks.⁵ The Dordick group^{6,7} developed a simple technique in dissolving enzymes in organic solvents with low concentrations of

surfactants. Relying on this methodology, the transesterifications of solid β -cyclodextrin, amylose, hydroxy ethyl cellulose, and cellulose were carried out in isooctane or pyridine using soluble subtilisin Calsberg.^{5,8,9} Although enzymes were made soluble in organic solvents, carbohydrates were still suspended in solutions as heterogeneous systems, resulting in slow reaction rates and incomplete reactions.

Recently, ionic liquids (ILs), as non-volatile organic solvents, have been found capable of dissolving cellulose and other carbohydrates to a great extent. As summarized in Table 1, ILs based on chloride (Cl^-), dicyanamide (dca^-), formate (HCOO^-) and acetate (OAc^-) could dissolve up to 10–20% (wt) cellulose, and $>100 \text{ g L}^{-1}$ other carbohydrates such as β -D-glucose, sucrose, lactose, and β -cyclodextrin. More recently, ILs were used in dissolving portions of woods. For example, [BMIM]Cl could dissolve considerable amounts of cellulosic materials and lignin from different wood samples over 24 h at 100 °C.¹⁰ Another study¹¹ reported the dissolution of up to 8% (wt) wood in chloride-based ILs. The solubilization of carbohydrates in ILs has enabled a number of chemical derivatizations of these natural products in homogeneous systems,^{11–18} as well as the cellulose regeneration for a variety of applications (such as enzymatic hydrolysis,^{11,19} blending with wool keratin,²⁰ and producing enzyme-encapsulated films²¹).

Unfortunately, since carbohydrate-dissolving ILs are typically composed of anions of Cl^- , dca^- , HCOO^- and OAc^- , these anions form strong hydrogen-bonds with carbohydrates for dissolving them.²² For this reason, these ILs are more likely to denature enzymes,^{23–25} preventing a further enzymatic modification of dissolved carbohydrates in ILs. To overcome this obstacle, we aim to design new ILs that are able to dissolve

^aChemistry Program, Savannah State University, Savannah, GA, 31404, USA. E-mail: zhaoh@savstate.edu, huazhao98@gmail.com

^bChemical Sciences Division, Oak Ridge National Laboratory, Oak Ridge, TN, 37831, USA

† Electronic supplementary information (ESI) available: Preparation of ILs and synthesis of glycol-substituted ILs. See DOI: 10.1039/b801489b

Table 1 Solubility of carbohydrates in some ILs^a

IL	Carbohydrate	Solubility
[BMIM]Cl	Cellulose	10 wt% (100 °C), ⁴³ 25 wt% (microwave, 3–5 s pulses), ⁴³ 10–18% (83 °C) ^{15,17}
	Wool keratin fibers	11 wt% (130 °C) ²⁰
	Eucalyptus pulp	≥13.6% (85 °C) ⁴⁴
[EMIM]Cl	Solucell 1175 cellulose	16 wt% (100 °C) ³⁸
	Eucalyptus pulp	≥15.8% (85 °C) ⁴⁴
[AMIM]Cl	Cellulose	8–14.5 wt% (80 °C) ^{45,46}
	Solucell 1175 cellulose	10 wt% (100 °C) ³⁸
	KZO3 (1085) cellulose	12.5 wt% (100 °C) ³⁸
[BDMIM]Cl	Eucalyptus pulp	≥12.8% (85 °C) ⁴⁴
[BMPy]Cl	Cellulose	12–39% (105 °C) ¹⁵
[AdMIM]Br	Cellulose	4–12% (80 °C) ¹⁷
[BMIM][dca]	β-D-Glucose	145 g L ⁻¹ (25 °C) ¹³
	Sucrose	195 g L ⁻¹ (25 °C), ¹³ 282 g L ⁻¹ (60 °C) ¹³
	Lactose	225 g L ⁻¹ (75 °C) ¹³
	β-Cyclodextrin	750 g L ⁻¹ (75 °C) ¹³
	Amylose	4 g L ⁻¹ (25 °C) ¹³
	β-D-Glucose	91 g L ⁻¹ (25 °C) ¹³
[MoeMIM][dca]	Sucrose	220 g L ⁻¹ (25 °C) ¹³
[MomMIM][dca]	Sucrose	249 g L ⁻¹ (25 °C), ¹³ 352 g L ⁻¹ (60 °C) ¹³
[AMIM][HCOO]	Cellulose	10–20 wt% (60–85 °C) ⁴⁷
[EMIM][OAc]	Eucalyptus pulp	≥13.5% (85 °C) ⁴⁴
[BMIM][OAc]	Eucalyptus pulp	≥13.2% (85 °C) ⁴⁴
[EMIM][(MeO)(R)PO ₂]	Microcrystalline cellulose (DP 250)	10 wt% (45–65 °C) ⁴⁸
[MoeMIM][BF ₄]	β-D-Glucose	5 mg mL ⁻¹ (55 °C) ⁴⁹

^a BMIM = 1-Butyl-3-methylimidazolium, EMIM = 1-ethyl-3-methylimidazolium, AMIM = 1-allyl-3-methylimidazolium, BDMIM = 1-butyl-2,3-dimethylimidazolium, BMPy = 3-methyl-*N*-butylpyridinium, AdMIM = 1-allyl-2,3-dimethylimidazolium, dca = dicyanamide, MoeMIM = 1-methoxyethyl-3-methylimidazolium, MomMIM = 1-methoxymethyl-3-methylimidazolium, [(MeO)(R)PO₂]⁻ where R = H, Me or MeO.

carbohydrates but do not considerably inactivate enzymes. Since the high molar concentration of anions in ILs is responsible for the enzyme denaturation, we hypothesized that a lower anion concentration could reduce the enzyme-inactivating nature of ILs. Therefore, a longer substituent on the cation would increase the molecular weight and thus decrease the anion concentration of an IL. However, a longer alkyl chain on the cation would dramatically increase the melting-point and viscosity of the resulting IL. On the other hand, glycols and their derivatives are known having low melting-points and low viscosities. Therefore, poly(ethylene oxide)s (PEOs) were incorporated into cationic or anionic units to produce the liquid state of ion conductive polymers.^{26,27} In particular, various ILs have been synthesized by grafting alkyloxy substituents (ether or alcohol groups) onto the imidazolium ring^{13,28–38} or pyridinium ring.^{39,40} The inclusion of alkyloxy or alkyloxyalkyl groups could lower the melting-points of the resulting organic salts, yielding room-temperature ILs in most cases. In addition, the oxygen atoms embedded in the glycol chain may act as hydrogen-bond acceptors, interacting with carbohydrates to dissolve them. Following this rationale, we synthesized a series of imidazolium and tetraalkylammonium ILs carrying glycol-substituents in the side chain, and then determined the solubilities of sugars and cellulose in these new solvents. To examine their enzyme compatibility, we conducted the transesterification of *N*-acetyl-L-phenylalanine ethyl ester with 1-propanol in these ILs catalyzed by Novozyme 435 (immobilized lipase B from *Candida antarctica*). Although this reaction is commonly used as the activity assay of α -chymotrypsin,^{41,42} due to the non-volatility of the substrate and its moderate reaction rate, we found this reaction is also suitable for probing the lipase activity.

Furthermore, we demonstrated the enzymatic transformations of D-glucose and cellulose respectively, both dissolved in ILs.

Experimental

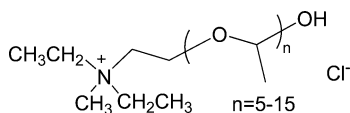
General

The following chemicals were purchased from Sigma-Aldrich (St. Louis, MO, USA): *N*-acetyl-L-phenylalanine ethyl ester (Ac-L-Phe-OEt), 1-ethyl-3-methylimidazolium bromide ([EMIM]Br), 1-ethyl-3-methylimidazolium chloride ([EMIM]Cl), 1-ethyl-3-methylimidazolium acetate ([EMIM][OAc]), 1-butyl-3-methylimidazolium bromide ([BMIM]Br), 1-butyl-3-methylimidazolium chloride ([BMIM]Cl), 1-hexyl-3-methylimidazolium chloride ([HMIM]Cl), bis(trifluoromethane)sulfonimide lithium salt (Li[Tf₂N]), sodium dicyanamide (Na[dca]), sodium acetate, phosphorus pentoxide (P₂O₅), D-glucose, sucrose, imidazole, *N*-methylimidazole, diethylene glycol monomethyl ether (≥99.6%), triethylene glycol monomethyl ether (≥97.0% GC), methoxypolyethylene glycol 350 {average mol. wt 350, empirical formula as CH₃(OEt)₇OH}, bromoethane, diethylamine, Amberlite® IRA-400 Cl resin, Avicel® PH-101 [microcrystalline cellulose (MCC), particle size 50 μm, DP 225, produced by FMC Corp.], triphenylmethyl chloride (known as trityl chloride), and methyl methacrylate.

Tetraethylene glycol monomethyl ether (98%) was obtained from the Alfa Aesar Company (Ward Hill, MA, USA). Ethylene glycol mono-2-chloroethyl ether (>98.0% GC), 2-[2-(2-chloroethoxy)ethoxy]ethanol (>96.0% GC), dipropylene glycol monomethyl ether (mixture of isomers)

(> 98.0% GC), tripropylene glycol monomethyl ether (mixture of isomers) (> 93.0% GC) were purchased from TCI America.

Benzenesulfonyl chloride (99%) and hexadecyltrimethylammonium hydroxide (25% in methanol) were acquired from Acros Organics. AMMOENG™ 110 (short as [Amm110]Cl, Scheme 1) was obtained from Solvent Innovation GmbH (Nattermannallee, Germany) as a colorless liquid (mp < -65 °C, density = 1.03 g cm⁻³ at 20 °C, viscosity = 495 mPa s at 20 °C, pH = 3.83 and conductivity = 0.090 mS cm⁻¹). *N,N*-Dimethylethanolammonium acetate, ([MM(EtOH)NH][OAc], purity 99%, water content 0.29%, colorless), bis(2-methoxyethyl)ammonium acetate ([[(MeOEt)₂NH₂][OAc], purity 99%, water content 0.13%, yellow), *N,N*-dimethyl-2-methoxyethylammonium acetate ([MM(MeOEt)NH][OAc], purity 99%, water content 1.0%, colorless), *N*-methyl-bis(2-methoxyethyl)ammonium acetate ([M(MeOEt)₂NH][OAc], purity 99%, water content 0.22%, yellow) were purchased from Bioniqs Ltd (York, UK). Novozyme 435[®] obtained from Sigma-Aldrich is a thermally stable lipase B from *Candida antarctica* (CaLB) immobilized on acrylic resin (0.3–0.9 mm in diameter and 0.430 g cm⁻³ in bulk density).



Scheme 1 Structure of AMMOENG™ 110 ([Amm110]Cl).

Preparation of ILs

All Tf₂N⁻ based ILs ([Choline][Tf₂N] (9), [Amm110][Tf₂N] (16), [EMIM][Tf₂N] (2), [BMIM][Tf₂N] (3), and [HMIM][Tf₂N] (4)) were synthesized through a precipitation reaction (for procedures see ESI†).⁵⁰

All dca⁻ or HCOO⁻ based ILs ([Choline][dca] (10), [Amm110][dca] (17), [Amm110][HCOO] (18), [BMIM][dca] (12), and [BMIM][HCOO] (6)) were prepared through an anion-exchange method (for procedures see ESI†). Dried Acros[®] 3A molecular sieves were added into ILs during storage.

A common method^{28,29,37} of grafting a glycol chain onto the imidazole ring is to firstly prepare the brominated or chlorinated glycol through reacting glycol (or its derivatives) with thionyl chloride in the presence of pyridine; the halogenated glycol and *N*-alkylimidazole are then refluxed in acetonitrile (or DMF) for 2–3 days to produce the desired ILs. Although this approach is effective, it involves the use of thionyl chloride, and the first

step of reactions requires an absolutely anhydrous environment. Another approach described by the Wasserscheid's group³⁶ utilized less toxic substances and was conducted under milder conditions. As illustrated in Scheme 2, current study adopted this method with a slight modification (for procedures and characterizations see ESI†).

Dissolution of sugars and cellulose

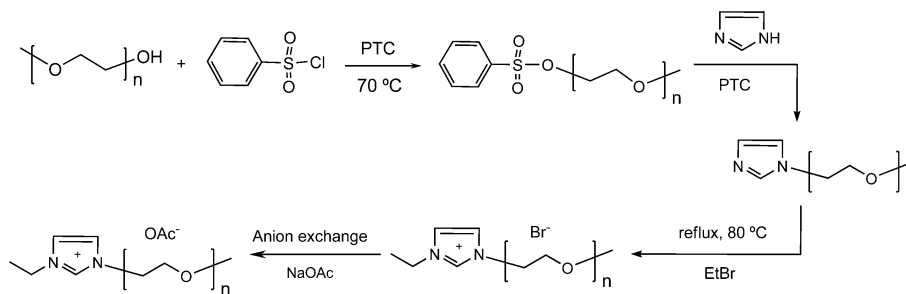
An IL (1.0 g) in a glass tube was immersed in an oil bath at a certain temperature. Samples of sugar or cellulose were added into the IL carefully at an increment of 5 mg. After a vigorous agitation, the IL solution should turn clear before the next increment was added. When the IL solution did not become clear after 1 h of sample addition, the saturation limit was reached.

Enzymatic transesterification of Ac-L-Phe-OEt with 1-PrOH

The enzyme was dried over P₂O₅ for at least 24 h. 1-Propanol (1-PrOH) was dried by anhydrous MgSO₄, and ILs were dried by Acros[®] 3A molecular sieves before use. Eighty microliters of Ac-L-Phe-OEt solution in 1-propanol was added into a volumetric vial, followed by the addition of solvent (IL or organic solvent) to make a 1.0 mL solution. The final concentrations of Ac-L-Phe-OEt and 1-propanol were 32 mM and 1.07 M respectively. The reaction vial was sealed and incubated in a water bath at 60 °C with a constant stirring. At time zero, the reaction was initiated by adding 20 mg Novozyme 435 into the mixture. Samples (50 µL each) were taken at intervals and each sample was diluted with 100 µL HPLC eluent. The eluent consisted of 65% (v/v) acetonitrile and 35% (v/v) aqueous acetate buffer (0.05 M, pH 4.5). The flow rate was 1.0 mL min⁻¹. The LC-10AT Shimadzu HPLC is equipped with a SPD-10A UV-visible dual wavelength detector, and a Shimadzu Premier C18 column (150 mm × 4.6 mm, particle size 5 µm). The detection wavelength was 258 nm. The injection volume was 20 µL. All experiments were run in duplicate. The peak areas of Ac-L-Phe-OPr were recorded and converted into concentrations. Since the standard curves (HPLC peak area vs. concentration) of Ac-L-Phe and Ac-L-Phe-OEt at 258 nm were very close, their averaged values were used as the standard curve of Ac-L-Phe-OPr. Laszlo and Compton⁴¹ also did not distinguish the difference between UV-responses of these compounds at 258 nm.

Enzyme stability in IL

A stock solution of 25 mM 4-nitrophenyl acetate was prepared in methanol. A dilute solution of 4-nitrophenyl acetate (1.0 mM)



Scheme 2 Synthesis of imidazolium ILs containing alkyloxyalkyl-chain ([Me(OEt)_n-Et-Im][OAc]).

was prepared by adding 1.0 mL of the stock solution slowly into 0.1 M phosphate buffer (pH 7.4) to make 25.0 mL solution. This aqueous solution was always prepared freshly before use.

10 mg Novozyme 435 (dried over P₂O₅) was incubated in 0.5 mL IL in the presence of substrates (32 mM Ac-L-Phe-OEt and 1.07 M 1-propanol) at 60 °C under agitation. After a certain incubation time, 10.0 mL distilled water was added into the reaction mixture, followed by filtration. The enzyme particles were washed with distilled water several times to remove residual IL. This incubated enzyme was then added into 2.0 mL 1.0 mM 4-nitrophenyl acetate solution at 20 °C under vigorous stirring. At 2 min of reaction time, the enzyme particles were removed by a filtration. The absorbance of filtrate was quickly determined at 405 nm by a Shimadzu UV-Mini-1240 spectrophotometer. The blank was the 1.0 mM 4-nitrophenyl acetate solution right before the reaction. The residual activity was calculated from the ratio of product absorbance.

The protein content in IL after the enzyme incubation was determined by the Bradford reagent: 50 µL IL (after the enzyme incubation) was diluted by 200 µL distilled water; 50 µL of the diluted solution was mixed with 1.5 mL Bradford reagent for 5 min at room temperature; the protein concentration was determined by the absorbance at 595 nm (blank was 50 µL of 20% (v/v) IL solution and 1.5 mL Bradford reagent). The protein standard curve was generated from standard solutions of bovine serum albumin (BSA).

Enzymatic transesterification of methyl methacrylate with D-glucose

D-Glucose (100 mM) and methyl methacrylate (100 mM) were completely dissolved in 2.0 mL IL at 60 °C. At time zero, the reaction was initiated by adding 40 mg Novozyme 435. At intervals, samples (50 µL each) were taken from the reaction mixture and diluted by the HPLC eluent (100 µL). The eluent consisted of 40% (v/v) acetonitrile and 60% (v/v) aqueous acetate buffer (0.05 M, pH 4.5). The HPLC column was Phenomenex® sphereclone C18 column (250 mm × 4.60 mm, particle size 5 µm). The detection wavelength was 258 nm. The injection volume was 20 µL. The conversion of methyl methacrylate was calculated from integration of the corresponding HPLC peak. All experiments were run in duplicate. To determine the acylation position, D-glucose-¹³C₆ was used as the reactant to repeat the above reaction. After 24 h, the reaction mixture was dissolved in D₂O/DMSO-d₆ (50/50, v/v) for analysis of ¹³C spectrum. The peak positions were compared with the spectrum of pure D-glucose-¹³C₆ in D₂O/DMSO-d₆ (50/50, v/v).

6-O-Tritylation of cellulose in [BMIM]Cl

The 6-O-tritylation of cellulose in an IL was based on a literature method.⁵¹ 0.2 g (anhydroglucose unit AGU = 1.23 mmol, 1 equiv.) cellulose was dissolved in 1.8 g [BMIM]Cl at 100 °C, followed by the addition of trityl chloride (2.06 g, 7.38 mmol, 6 equiv.) and pyridine (1.0 mL, 12.3 mmol, 10 equiv.). The reaction mixture was stirred at 100 °C in an oil bath for 3 h, and then precipitated in 40 mL methanol. The product was filtered and washed with methanol several times, and then dried at 40 °C in an oven for 24 h. Following the literature method,⁵¹

the final product was confirmed to be 6-O-trityl cellulose with a degree of substitution about 1.

Enzymatic transesterification of methyl methacrylate with cellulose

0.04 g Avivel PH-101 (anhydroglucose unit AGU = 0.25 mmol) or 6-O-trityl cellulose was completely dissolved in 2.0 g IL at 110 °C. After cooling to room temperature, 40 µL methyl methacrylate (150 mM) was added into the cellulose solution. The reaction mixture was sealed and vigorously stirred at 60 °C. At time zero, the reaction was initiated by adding 30 mg Novozyme 435. To determine the conversion of methyl methacrylate, at intervals, samples (50 µL each) were taken from the reaction mixture and each sample was diluted by the HPLC eluent (100 µL). The eluent consisted of 40% (v/v) acetonitrile and 60% (v/v) aqueous acetate buffer (0.05 M, pH 4.5). The cellulose and its ester precipitated from the eluent. After stirring and then centrifugation, the clear supernatant was injected into the HPLC. The injection volume was 20 µL. The HPLC column was Phenomenex® sphereclone C18 column (250 mm × 4.60 mm, particle size 5 µm). The detection wavelength was 258 nm. The conversion of methyl methacrylate was calculated from the integration of the corresponding HPLC peak. At the end of the reaction (72 h), the enzyme particles were removed from the solution either by decantation (if particles settled) or through filtration (may lose some product on the filter paper). Distilled water was added into the clear solution to precipitate out the cellulose ester. The cellulose ester was washed six times with water, and three times with acetone during a vacuum filtration (in the case of 6-O-trityl cellulose, centrifugation was used to precipitate the ester from the solution because the product particles were too small for regular filtration). The product was dried in an oven at 40 °C for 24 h. Granular samples of cellulose or cellulose ester were pressed into clear KBr pellets. The FT-IR spectra were measured using a Shimadzu IRPrestige-21 spectrometer through averaging 32 scans at 2 cm⁻¹ resolution (Happ-Genzel apodization). All experiments were run in duplicate.

Results and discussion

Effect of anions on cellulose dissolution

To dissolve carbohydrates, ILs usually carry anions of Cl⁻, dca⁻, HCOO⁻, or OAc⁻ as suggested by Table 1. Their capability in forming hydrogen bonds is considered the main mechanism of carbohydrate dissolution in ILs. For example, ¹³C and ^{35/37}Cl NMR relaxation measurements on [BMIM]Cl confirmed that chloride ions interact with the cellulose -OH groups in a 1 : 1 stoichiometry.²² Molecular dynamics simulation of β-D-glucose in 1,3-dimethylimidazolium chloride ([MMIM]Cl) also suggested the hydrogen bonding between chloride anions and hydroxyl groups.^{52,53}

As shown by our study in Table 2, *t*-butanol (**1**) and hydrophobic ILs (**2–4**) do not dissolve cellulose. [BMIM]Cl (**11**) dissolved about 10% (wt) Avicel® PH-101, but chloride-based ILs have higher melting-points (~70 °C for [BMIM]Cl (**11**)) than those of non-halides ones, and are usually very hygroscopic. Therefore, this IL (**11**) is not a suitable solvent for enzymatic reactions because most enzymes exhibit low activities above

Table 2 The cellulose solubility and lipase activity in ILs^a

Solvent	Avicel PH-101 Solubility at 110 °C (wt%)	Initial Rate at 60 °C/ $\mu\text{mol min}^{-1} \text{g}^{-1}$
1	<i>t</i> -BuOH	<i>n/d</i>
2	[EMIM][Tf ₂ N]	<i>n/d</i>
3	[BMIM][Tf ₂ N]	<0.5
4	[HMIM][Tf ₂ N]	<i>n/d</i>
5	[P66614][dca]	< 0.5
6	[BMIM][HCOO]	8
7	[Bu ₄ N][HCOO]	1.5
8	[Bu ₄ P][HCOO]	6
9	[Choline][Tf ₂ N]	<i>n/d</i>
10	[Choline][dca]	<i>n/d</i>
11	[BMIM]Cl	10
12	[BMIM][dca]	1
13	[EMIM][OAc]	15
14	[OMIM][OAc]	<1
15	[Amm110]Cl	0.5
16	[Amm110][Tf ₂ N]	<i>n/d</i>
17	[Amm110][dca]	<0.5
18	[Amm110][HCOO]	0.5
19	[Amm110][OAc]	0.5
20	[Me(OEt) ₂ -Et-Im]Cl	2
21	[Me(OEt) ₂ -Et-Im][OAc]	12
22	[Me(OEt) ₃ -Et-Im][OAc]	12
23	[Me(OEt) ₄ -Et-Im][OAc]	10
24	[Me(OEt) ₇ -Et-Im][OAc]	3
25	[Me(OEt) ₃ -MeOEtOMe-Im][OAc]	0.5
26	[H(OEt) ₂ -Me-Im][OAc]	5
27	[H(OEt) ₃ -Me-Im][OAc]	2
28	[H(OEt) ₂ -Me-Im]Cl	1
29	[Me(OPr) ₃ -Et-Im][OAc]	0.5
30	[Me(OEt) ₃ -Bu-Im][OAc]	<0.5
31	[Me(OEt) ₃ -Et ₃ N][OAc]	10
32	[Me(OEt) ₂ -Et ₃ N][OAc]	10
33	[MM(EtOH)NH][OAc]	<0.5
34	[(MeOEt) ₂ NH ₂][OAc]	<0.5
35	[MM(MeOEt)NH][OAc]	<0.5
36	[M(MeOEt) ₂ NH][OAc]	<0.5

^a *n/d* means 'not determined' (typically due to very low solubility); P66614 is trihexyl tetradecyl phosphonium. **24** was synthesized from PEG 350 methyl ether.

70 °C. In addition, although ¹³C NMR measurements did not reveal the degradation of cellulose dissolved in [BMIM]Cl (**11**) at ~80 °C (implying that this IL is a non-derivatizing solvent),¹⁵ the molar mass distribution of cellulose dissolved in the same IL at 100 °C suggested an excessive degradation of the polymer.³⁸

The dicyanamide-based ILs dissolve considerable amounts of sugars and other oligosaccharides (such as D-glucose, sucrose, lactose and β -cyclodextrin) (see Table 1), but these ILs do not dissolve much polysaccharides. For example, the solubility of amylose in [BMIM][dca] (**12**) was only 4 g L⁻¹ at 25 °C,¹³ and several dca⁻ based ILs were not able to dissolve cellulose.³⁸ Our data in Table 2 also indicate that the cellulose solubility is 1% (wt) in [BMIM][dca] (**12**), and <0.5% in [P66614][dca] (**5**) at 110 °C. In addition, [BMIM][dca] (**12**) is known as an enzyme-denaturing IL.²⁴

Formate-based ILs are able to dissolve above 20% (wt) cellulose, dextrin, inulin, amylose, and xylan at elevated temperatures.⁴⁷ Our data in Table 2 also indicate the relatively high solubilities of cellulose in [BMIM][HCOO] (**6**) (8%) and [Bu₄P][HCOO] (**8**) (6%), despite a low solubility (1.5%) in [Bu₄N][HCOO] (**7**). However, formate-based ILs generally have low thermal stability due to decarboxylation.⁴⁸ As shown in Table 3, formate IL (**6**) is less thermally stable than those

Table 3 Decomposition temperatures and viscosities of ILs

IL	<i>T</i> (onset) ^a / °C	η at 20 °C/mPa s ^b
3	[BMIM][Tf ₂ N]	256
11	[BMIM]Cl	240
6	[BMIM][HCOO]	156
37	[BMIM][OAc]	206
13	[EMIM][OAc]	210
21	[Me(OEt) ₂ -Et-Im][OAc]	186
22	[Me(OEt) ₃ -Et-Im][OAc]	188
23	[Me(OEt) ₄ -Et-Im][OAc]	188
32	[Me(OEt) ₂ -Et ₃ N][OAc]	155
31	[Me(OEt) ₃ -Et ₃ N][OAc]	153

^a The onset decomposition temperatures were measured in air with a Shimadzu DSC-60/TA-60WS thermal analyzer at a heating rate of 10 °C min⁻¹. ^b *n/d* means "not determined".

based on Tf₂N⁻ and Cl⁻. In addition, the formate-based ILs are quite basic and unsuitable for enzymes. On the other hand, acetate-based ILs are more thermally stable (Table 3) and could dissolve substantial amounts of carbohydrates. [EMIM][OAc] (**13**) could dissolve 15% (wt) cellulose at 110 °C (Table 2) and 60% (wt) D-glucose at 60 °C (Table 4). As commercial products, 5% Weyerhaeuser cellulose (DP 350–1100) solutions in [EMIM][OAc], known as the CellionicTM BCW series, are

Table 4 Solubility of sugars in ILs at 60 °C

	IL	Sugar	Solubility (wt%)
3	[BMIM][Tf ₂ N]	D-Glucose	<0.5
13	[EMIM][OAc]	D-Glucose	60
17	[Amm110][dca]	D-Glucose	4.5
		Sucrose	3.5
19	[Amm110][OAc]	D-Glucose	30
22	[Me(OEt) ₃ -Et-Im][OAc]	D-Glucose	80
24	[Me(OEt) ₃ -Et-Im][OAc]	D-Glucose	26
29	[Me(OPr) ₃ -Et-Im][OAc]	D-Glucose	45
31	[Me(OEt) ₃ -Et ₃ N][OAc]	D-Glucose	16
		Sucrose	16

provided by the BASF Corporation. Therefore, we chose the acetate anion for designing our new ILs.

Designing cations for enzyme stabilization and cellulose dissolution

Not surprisingly, as illustrated by initial reaction rates in Table 2, we observed low lipase activities in denaturing ILs based on dca⁻ (**5**, **10** and **12**), HCOO⁻ (**6–8**), and OAc⁻ (**13**), when comparing with those less-denaturing hydrophobic ILs (**2–4**, and **9**). The reaction was not performed in [BMIM]Cl (**11**) because the melting-point of this IL is about 70 °C while the reaction temperature was 60 °C. Meantime, a recent study has suggested that this IL is cellulase-denaturing.²³

Surprisingly, we observed that the immobilized CaLB was quite active (1.03 μmol min⁻¹ g⁻¹ enzyme as shown in Table 2) in a commercial IL (ionic mixtures, Scheme 1) known as AmmoengTM 110 ([Amm110]Cl, **15**). This activity is comparable with those observed in hydrophobic ILs (**2–4** and **9**). We further modified the anion (Cl⁻) of [Amm110]Cl into Tf₂N⁻ (**16**), dca⁻ (**17**), HCOO⁻ (**18**) and OAc⁻ (**19**) respectively through the anion-exchange method, and obtained high enzyme activities in all cases except in [Amm110][HCOO] (**18**). We found the aqueous solution of **18** is quite basic; the basic nature of this IL could be the main reason of enzyme inactivation. Meanwhile, we conducted the same reaction in [OMIM][OAc] (**14**), which has a lower anion molar concentration than [EMIM][OAc] (**13**). We obtained a high lipase activity (0.80 μmol min⁻¹ g⁻¹ enzyme, Table 2) although the cellulose solubility in this IL was less than 1%. Therefore, a low anion concentration (*i.e.* high molecular weight) is beneficial for the enzyme stabilization. However, all these ILs (**15–19**) barely dissolved 0.5% cellulose (Table 2), although they could dissolve some D-glucose (Table 4).

To lower the anion concentration for enzyme stabilization, simply lengthening the alkyl chain on imidazolium cation would dramatically increase the IL viscosity, since [EMIM][OAc] already has a viscosity of 162 mPa s (at 20 °C)⁵⁰ and [BMIM][OAc] has an even higher viscosity (646 mPa s at 20 °C⁵⁴). In addition to the anion type and concentration, we also noticed that the IL viscosity is another factor in limiting the cellulose dissolution: in many cases, the cellulose solutions in ILs are too viscous to dissolve more cellulose. Inspired by the data in the AmmoengTM 110 series, the incorporation of an oxygenated chain in cations could be a solution in lowering the melting-points and viscosities of ILs because poly(glycol) compounds are known to have low melting-points and low viscosities. Based on these guidelines, we designed a variety of ILs (**20–32**)

incorporating poly(ethylene glycol) and poly(propylene glycol) as substituents of cations (Scheme 2 and Table 2). These ILs are liquids at room temperature and are not very viscous (Table 3). Noticeably, both ILs **21** and **22** have low viscosities of 92 mPa s at 20 °C.

Through examining a homologous series of ILs (**21–24**) as shown in Table 2, the cellulose solubility in these ILs generally decreased with the increase of alkyloxyalkyl chain length, while the lipase activity increased. Therefore, an optimum chain-length is needed to dissolve enough cellulose, and to stabilize the enzyme at the same time. In this scenario, ILs **21–23** are all satisfactory for this purpose with **22** yielding the best overall performance. In addition, ILs **21** and **22** were prepared from diethylene glycol monomethyl ether and triethylene glycol monomethyl ether respectively, which are readily available and inexpensive. Acetate-based IL **21** dissolved much more cellulose than the chloride-based analogue **20** (12% vs. 2%). Meanwhile, the lipase was more active in **21** than in **20**, implying the chloride anion is more enzyme-denaturing.^{23,55} Therefore, choosing acetate over chloride as anions of our new ILs is advantageous for both cellulose dissolution and enzyme stabilization.

[OMIM][OAc] (**14**) has a similar molecular weight as **22** and **23**. However, the cellulose solubility in [OMIM][OAc] (<1%) is much lower than those in **22** and **23** (≥10%). Therefore, in addition to the anion's ability in forming hydrogen-bonds, the cations of **22** and **23** also played a critical role in the cellulose dissolution. A plausible explanation is that oxygen atoms in the alkyloxyalkyl chains of cations (**21–24**) act as Lewis-base/hydrogen-bond acceptors,⁵⁶ form hydrogen-bonds with cellulose, and promote the cellulose dissolution. Although a longer alkyloxyalkyl-chain is desirable for more cation-cellulose interactions, it also changes the hydrophobicity of the overall IL, which is another important factor in solvating cellulose molecules. Therefore, a suitable alkyloxyalkyl-chain length on cation is necessary for an optimum dissolution of carbohydrates.

We also made other modifications on side chains of imidazolium cations. Lengthening the other side-chain of imidazolium (**25** and **30**) induced a dramatic decrease in cellulose solubilities (0.5% or less) and lower enzyme activities. IL **29** was derived from tripropylene glycol monomethyl ether, which is a mixture of isomers (*n*-propyl and isopropyl segments). The cellulose solubility was also quite low in this IL. The low cellulose solubilities in ILs **25**, **29** and **30** are likely due to the high bulkiness of cations, which reduces the number of hydrogen-bonds between cellulose and cations. With a hydroxyl group at the end of side-chains, ILs (**26–28**) dissolved much less cellulose compared to their analogues (**21** and **22**), and inactivated the lipase. The hydroxyl group might compete with cellulose in forming hydrogen-bonds with anions (acetate or chloride). This speculation was confirmed by Bernson and Lindgren,⁵⁷ who dissolved lithium salts (LiX) in poly(propylene glycol) (MW = 3000) with hydroxy end-groups. Through IR spectroscopy, they observed that the shifts of –OH stretching band depend on the strength of hydrogen-bonds formed between the –OH group and the anion, as well as the coordination of cations with the –OH group. The low enzyme activities in hydroxyl containing ILs (**26–28**) could be due to the competition between these hydroxyl groups with the substrate (1-propanol) during the transesterification.

To emphasize the effect of anion concentration on lipase stabilization, we correlated the lipase activity data with anion molar concentrations for a series of homologous ILs (Fig 1). As a general trend, a higher lipase activity was observed in an IL with a lower acetate concentration. However, in addition to the anion concentration, the structures of cations and the overall IL properties also play important roles on enzyme stabilization as illustrated by Table 2. Therefore, the overall IL structure must be optimized to allow sufficient cellulose dissolution and also enable enzyme stabilization. Such an optimization may vary with specific applications.

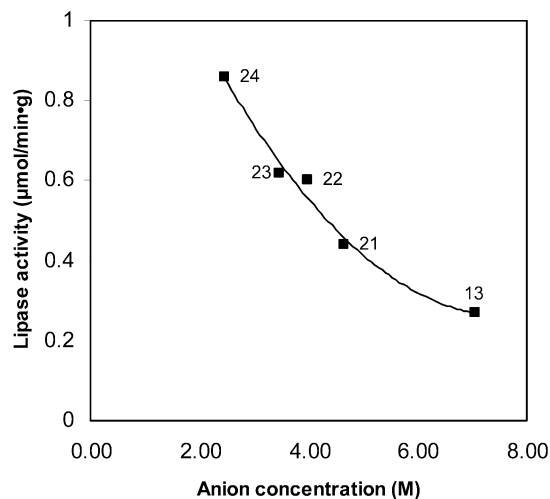


Fig. 1 Effect of anion (acetate) concentration on the lipase activity (plot from data in Table 2; the anion concentrations were calculated from molecular weights of ILs assuming their densities are $\sim 1.2 \text{ g mL}^{-1}$).

Based on the above guideline, we synthesized two ammonium based ILs (**31** and **32**) with glycol-substituted chains. Both ILs could dissolve 10% (wt) Avicel® PH-101 at 110°C . The lipase showed a very high activity in IL **31** ($0.83 \mu\text{mol min}^{-1} \text{ g}^{-1}$ enzyme), but a low activity in **32** probably due to its higher anion concentration (Table 2). In addition, these ILs have lower costs than imidazolium salts (**20–30**). For comparison purpose, we investigated several other commercial ammonium salts (**33–36** in Table 2) containing short alkoxy groups. Unfortunately, these ILs could neither dissolve much cellulose ($<0.5\%$) nor stabilize the lipase.

To further evaluate the CaLB stability, we incubated the lipase in $[\text{Me}(\text{OEt})_3\text{-Et}_3\text{N}][\text{OAc}]$ (**31**) in the presence of substrates at 60°C . The residual activity was measured by the spectrophotometric assay of 4-nitrophenyl acetate (Fig 2). It is surprising that the lipase lost almost 50% of its activity within 10 min of incubation in IL, but maintained the remaining activity quite well even after 1 h of incubation. In addition to the denaturing effect of IL, we also observed the loss of enzyme due to its dissolution in IL **31**. The Bradford reagent detected 0.60 mg mL^{-1} protein dissolved in IL after 20 min of incubation at 60°C , which corresponds to 15% enzyme loss (the immobilized enzyme contains 20% (wt) of CaLB⁵⁸). Since the residual activity was determined after the separation of immobilized lipase from IL, the dissolution of enzyme in IL contributed considerably to the activity loss within the first 10–20 min of incubation. However, the undissolved CaLB maintained most of its activity in IL **31**

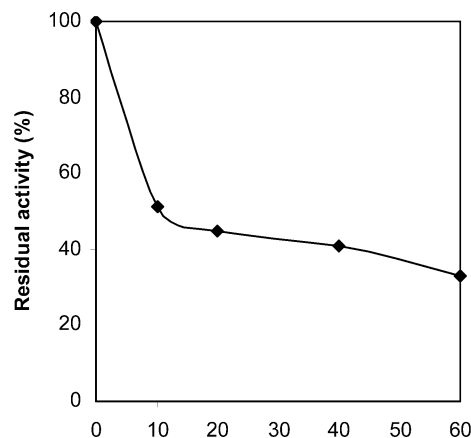


Fig. 2 Stability of immobilized CaLB in $[\text{Me}(\text{OEt})_3\text{-Et}_3\text{N}][\text{OAc}]$ (**31**) at 60°C (10 mg CaLB was incubated in 0.5 mL IL **31** in the presence of substrates for a certain time; after separating the enzyme from IL and washing, the residual activity was determined by the 4-nitrophenyl acetate assay).

(Fig 2), suggesting a high stability of CaLB in this IL and a high possibility of recycling this enzyme.

Enzymatic transesterification of D-glucose in ILs

ILs have been shown as useful solvents in the enzymatic transformation of D-glucose. Park and Kazlauskas⁴⁹ reported a high regioselectivity in CaLB-catalyzed acetylation of D-glucose with vinyl acetate in a number of ILs. Kim *et al.*⁵⁹ observed enhanced reactivity and regioselectivity during the selective enzymatic acylation of glycosides in ILs. The Bornscheuer's group⁶⁰ conducted the regioselective transesterification of D-glucose with fatty acid vinyl ester in biphasic systems consisting of $[\text{BMIM}][\text{BF}_4]$ (or $[\text{BMIM}][\text{PF}_6]$) and 40% *t*-BuOH, achieving conversions up to 60% when catalyzed by CaLB. The same reaction in the same solvent medium was further improved by using poly(ethylene glycol)-modified CaLB, producing conversions up to 90% and isolated yields up to 89%.⁶¹ On the other hand, the enzymatic glycosylation of D-glucose with other sugars was also successfully demonstrated in ILs.^{62,63}

In addition to their high dissolution power towards cellulose, acetate-based ILs also dissolve a significant amount of sugars including D-glucose and sucrose (Table 4). Hydrophobic ILs such as $[\text{BMIM}][\text{Tf}_2\text{N}]$ (**3**) dissolve little D-glucose. $[\text{Amm110}][\text{dca}]$ (**17**) could dissolve low concentrations of D-glucose and sucrose, while some acetate ILs dissolved up to 60–80% (wt) glucose (Table 4). A likely explanation is that acetate anions form strong hydrogen-bonds with sugars, enabling them to dissolve.^{52,53}

As mentioned in the Introduction, it is difficult to catalyze reactions on insoluble sugars such as D-glucose in organic solvents with insoluble enzymes. To illustrate the potential applications of our ILs in carbohydrate chemistry, we conducted the enzymatic transesterification of methyl methacrylate with D-glucose (both dissolved in ILs). As shown in Fig 3, the immobilized lipase exhibited moderate to high activities in several ionic media. The ^{13}C -NMR chemical shifts of D-glucose- $^{13}\text{C}_6$ and D-glucose- $^{13}\text{C}_6$ methacrylate suggested that only the C-6 position of D-glucose was regioselectively esterified by CaLB in ILs (see Table 5). This conclusion is consistent with previous reports on

Table 5 ^{13}C -NMR chemical shifts of D-glucose and its ester^a

Carbon	D-Glucose- $^{13}\text{C}_6$		D-Glucose- $^{13}\text{C}_6$ methacrylate	
	α	β	α	β
C-1	93.2	97.2	93.1	97.1
C-2	73.4	76.5	73.3	76.2
C-3	75.0	76.9	75.0	77.2
C-4	71.7	71.0	71.3	70.9
C-5	72.7	77.3	71.7 (up)	77.3
C-6	61.5	62.2	65.2 (down)	67.4 (down)

^a Assignments of carbon positions were based on the literature;⁶⁴ the reaction was conducted in [Amm110][dca].

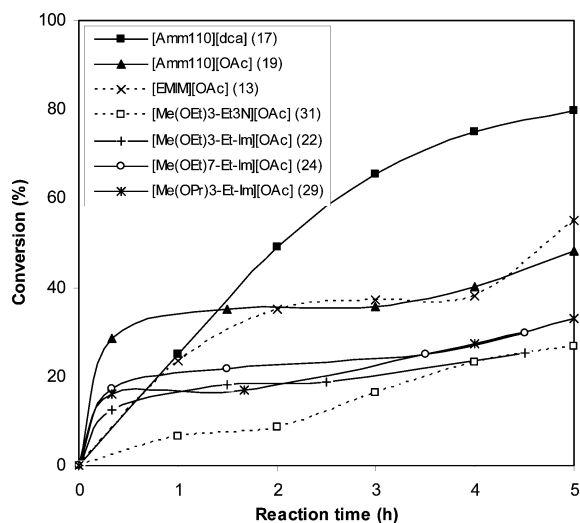


Fig. 3 Enzymatic transesterification of D-glucose (100 mM) and methyl methacrylate (100 mM) catalyzed by Novozyme 435 in various D-glucose-dissolving ILs.

the C-6 position of D-glucose being more regioselective during enzymatic acylations by lipases or proteases in both ILs and organic solvents.^{49,64,65}

However, the order of enzyme activity in these ILs (Fig 3) is different from that of the previous reaction (*N*-acetyl-L-phenylalanine ethyl ester with 1-propanol). The lipase showed the highest overall activity in [Amm110][dca] (17), which could only dissolve 4.5% (wt) D-glucose. On the hand, the enzyme showed lower activities in other ILs (Fig 3), which could dissolve much more D-glucose (16–80%) (Table 4). The high solubility of D-glucose (due to H-bonding) and the low solubility of the product ester (due to loss of the primary hydroxyl) in these ILs could induce substrate ground-state stabilization by ionic media, and shift the reaction equilibrium to the reactant side, resulting in lower enzymatic conversions of D-glucose.

Enzyme-catalyzed regioselective transesterification of cellulose dissolved in ILs

To demonstrate another application of these ILs in carbohydrate derivatization, we carried out the enzymatic transesterification of dissolved cellulose in ILs. Although enzymes can be made

Table 6 Enzyme-catalyzed transesterification of Avicel PH-101 cellulose with methyl methacrylate in different ILs (60 °C, 72 h)^a

IL	Conversion of methyl methacrylate (%)	Isolated product yield (%)
31 [Me(OEt) ₃ -Et ₃ N][OAc]	89	61
21 [Me(OEt) ₂ -Et-Im][OAc]	67	66
24 [Me(OEt) ₇ -Et-Im][OAc]	60	54

^a Reaction conditions: 0.04 g Avicel in 2.0 g IL, 150 mM methyl methacrylate, 30 mg Novozyme 435, and 60 °C.

soluble in organic solvents, cellulose is not soluble in most conventional solvents resulting in slow reaction rates and incomplete reactions. However, we can dissolve cellulose in ILs as homogeneous solutions, and then perform the transesterification reactions in these ILs (**31**, **21** and **24**) at 60 °C using Novozyme 435. As shown in Table 6, the conversions of acylating agent (*i.e.* methyl methacrylate) were determined by HPLC measurements, and the highest conversion (89%) at 72 h was obtained in IL **31**. Overall, the conversions and isolated yields are satisfactory. Since the cellulose was dissolved in ILs at 110 °C before reactions, residual moisture in cellulose and IL was removed. In addition, both methyl methacrylate and lipase were also dried. Therefore, the hydrolysis side-reaction was kept to a minimum. We observed that 72 h is sufficient for all reactions to reach maximum conversions. The formation of an ester group was confirmed by FT-IR spectra (Fig 4). The cellulose ester produced in IL **24** showed a characteristic peak at 1745 cm^{-1} (Fig. 4b). The ester synthesized in other two ILs (**21** and **31**) showed similar peaks (data not shown).

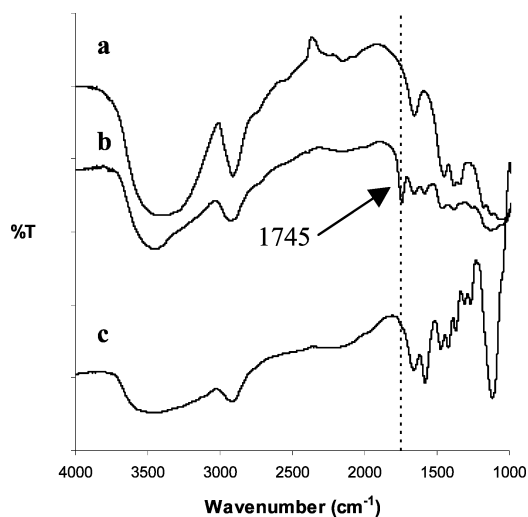


Fig. 4 FTIR-KBr spectra of Avicel PH-101 cellulose (a), and CaLB-catalyzed transesterifications on (b) cellulose with methyl methacrylate and (c) 6-*O*-trityl-cellulose with methyl methacrylate (reactions were carried out in [Me(OEt)₇-Et-Im][OAc] (**24**) at 60 °C for 72 h).

To examine the regioselectivity of this enzymatic transesterification, 6-*O*-trityl-cellulose was dissolved in IL **24** and subject to the same enzymatic reaction. Fig 4c suggests that no ester product was formed. Therefore, the transesterification did not occur on the two secondary hydroxyls (2,3-OH) of

cellulose, but on the primary hydroxyls (C-6 position). Such a regioselectivity was also observed in the subtilisin Carlsberg-catalyzed transesterification of cellulose,⁵ and enzyme-catalyzed transesterification of sugars and amylose.^{8,49,64-67}

Conclusions

We have synthesized new glycol-substituted ILs that are capable of dissolving carbohydrates but do not denature the lipase. The hydrogen-bond forming anions, oxygen-containing cations, and low cation bulkiness are beneficial to the carbohydrate dissolution, while the low anion concentration is necessary for enzyme stabilization. Therefore, an optimization could be achieved through the adjustment of IL parent ion structures. The length and steric hindrance of glycol-chains on cations could be designed to dissolve sufficient carbohydrates, and to stabilize the immobilized lipase B from *Candida antarctica* at the same time. These ILs are useful for enzymatic transformations of carbohydrates in homogeneous ionic solutions. As a demonstration of this concept, this study achieved the regioselective transesterifications of D-glucose and cellulose, respectively, both dissolved in ILs.

Acknowledgements

Acknowledgement is made to the Donors of the American Chemical Society Petroleum Research Fund (46776-GB1) for support of this research.

Notes and references

- J. A. Akkara, M. S. R. Ayyagari and F. F. Bruno, *Trends Biotechnol.*, 1999, **17**, 67–73.
- A. M. Klibanov, *Acc. Chem. Res.*, 1990, **23**, 114–120.
- L. Cao, U. T. Bornscheuer and R. D. Schmid, *J. Mol. Catal. B: Enzym.*, 1999, **6**, 279–285.
- V. Sereti, H. Stamatis, E. Koukios and F. N. Kolisis, *J. Biotechnol.*, 1998, **66**, 219–223.
- J. Xie and Y.-L. Hsieh, *J. Polym. Sci., Part A: Polym. Chem.*, 2001, **39**, 1931–1939.
- V. M. Paradkar and J. S. Dordick, *J. Am. Chem. Soc.*, 1994, **116**, 5009–5010.
- V. M. Paradkar and J. S. Dordick, *Biotechnol. Bioeng.*, 1994, **43**, 529–540.
- F. F. Bruno, J. A. Akkara, M. Ayyagari, D. L. Kaplan, R. Gross, G. Swift and J. S. Dordick, *Macromolecules*, 1995, **28**, 8881–8883.
- F. F. Bruno, J. S. Dordick, D. L. Kaplan and J. A. Akkara, in *Enzymes in Polymer Synthesis*, ed. R. Gross, D. L. Kaplan and G. Swift, *American Chemical Society*, Washington, DC, Edition edn, 1998, ch. 9, pp. 167–174.
- D. A. Fort, R. C. Remsing, R. P. Swatloski, P. Moyna, G. Moyna and R. D. Rogers, *Green Chem.*, 2007, **9**, 63–69.
- I. Kilpeläinen, H. Xie, A. King, M. Granstrom, S. Heikkinen, D. S. Argyropoulos and J. Agric, *Food Chem.*, 2007, **55**, 9142–9148.
- C. F. Liu, R. C. Sun, A. P. Zhang and J. L. Ren, *Carbohydr. Polym.*, 2007, **68**, 17–25.
- Q. Liu, M. H. A. Janssen, F. van Rantwijk and R. A. Sheldon, *Green Chem.*, 2005, **7**, 39–42.
- S. Köhler and T. Heinze, *Cellulose*, 2007, **14**, 489–495.
- T. Heinze, K. Schwikal and S. Barthel, *Macromol. Biosci.*, 2005, **5**, 520–525.
- K. Schlufte, H.-P. Schmauder, S. Dorn and T. Heinze, *Macromol. Rapid Commun.*, 2006, **27**, 1670–1676.
- S. Barthel and T. Heinze, *Green Chem.*, 2006, **8**, 301–306.
- A. Biswas, R. L. Shogren, D. G. Stevenson, J. L. Willett and P. K. Bhowmik, *Carbohydr. Polym.*, 2006, **66**, 546–550.
- A. P. Dadi, S. Varanasi and C. A. Schall, *Biotechnol. Bioeng.*, 2006, **95**, 904–910.
- H. Xie, S. Li and S. Zhang, *Green Chem.*, 2005, **7**, 606–608.
- M. B. Turner, S. K. Spear, J. D. Holbrey and R. D. Rogers, *Biomacromolecules*, 2004, **5**, 1379–1384.
- R. C. Remsing, R. P. Swatloski, R. D. Rogers and G. Moyna, *Chem. Commun.*, 2006, 1271–1273; N. P. Novoselov, E. S. Sashina, V. E. Petrenko and M. Zaborsky, *Fibre Chem.*, 2007, **39**, 152–158.
- M. B. Turner, S. K. Spear, J. G. Huddleston, J. D. Holbrey and R. D. Rogers, *Green Chem.*, 2003, **5**, 443–447.
- A. R. Toral, A. P. de los Ríos, F. J. Hernández, M. H. A. Janssen, R. Schoevaert, F. van Rantwijk and R. A. Sheldon, *Enzyme Microb. Technol.*, 2007, **40**, 1095–1099.
- A. P. De, Los Ríos, F. J. Hernández-Fernández, F. A. Martínez, M. Rubio and G. Villora, *Biocatal. Biotransform.*, 2007, **25**, 151–156.
- H. Ohno, *Bull. Chem. Soc. Jpn.*, 2006, **79**, 1665–1680.
- H. Ohno, *Electrochemical Aspects of Ionic Liquids*, John Wiley & Sons, Hoboken, NJ, 2005.
- H. Ohno, Y. Nakai and K. Ito, *Chem. Lett.*, 1998, **27**, 15–16.
- M. Yoshizawa and H. Ohno, *Chem. Lett.*, 1999, **28**, 889–890.
- M. Yoshizawa and H. Ohno, *Electrochim. Acta*, 2001, **46**, 1723–1728.
- J. Pernak, A. Czepukowicz and R. Pozniak, *Ind. Eng. Chem. Res.*, 2001, **40**, 2379–2383.
- L. C. Branco, J. N. Rosa, J. J. Moura, Ramos and C. A. M. Afonso, *Chem.–Eur. J.*, 2002, **8**, 3671–3677.
- J. Fraga-Dubreuil, M.-H. Famelart and J. P. Bazureau, *Org. Process Res. Dev.*, 2002, **6**, 374–378.
- J. Pernak, A. Olszówka and R. Olszewski, *Pol. J. Chem.*, 2003, **77**, 179–187.
- U. Domanska and A. Marciniak, *J. Chem. Thermodyn.*, 2005, **37**, 577–585.
- E. Kuhlmann, S. Himmler, H. Giebelhaus and P. Wasserscheid, *Green Chem.*, 2007, **9**, 233–242.
- M. Wang, X. Xiao, X. Zhou, X. Li and Y. Lin, *Sol. Energy Mater. Sol. Cells*, 2007, **91**, 785–790.
- G. Laus, G. Bentivoglio, H. Schottenberger, V. Kahlenberg, H. Kopacka, T. Röder and H. Sixta, *Lenzinger Ber.*, 2005, **84**, 71–85.
- A. M. Leone, S. C. Weatherly, M. E. Williams, H. H. Thorp and R. W. Murray, *J. Am. Chem. Soc.*, 2001, **123**, 218–222.
- J. Pernak and M. Branicka, *J. Surfact. Deterg.*, 2003, **6**, 119–123.
- J. A. Laszlo and D. L. Compton, *Biotechnol. Bioeng.*, 2001, **75**, 181–186.
- M. Eckstein, M. Sesing, U. Kragl and P. Adlercreutz, *Biotechnol. Lett.*, 2002, **24**, 867–872.
- R. P. Swatloski, S. K. Spear, J. D. Holbrey and R. D. Rogers, *J. Am. Chem. Soc.*, 2002, **124**, 4974–4975.
- B. Kosan, C. Michels and F. Meister, *Cellulose*, 2008, **15**, 59–66.
- H. Zhang, J. Wu, J. Zhang and J. He, *Macromolecules*, 2005, **38**, 8272–8277.
- J. Wu, J. Zhang, H. Zhang, J. He, Q. Ren and M. Guo, *Biomacromolecules*, 2004, **5**, 266–268.
- Y. Fukaya, A. Sugimoto and H. Ohno, *Biomacromolecules*, 2006, **7**, 3295–3297.
- Y. Fukaya, K. Hayashi, M. Wada and H. Ohno, *Green Chem.*, 2008, **10**, 44–46.
- S. Park and R. J. Kazlauskas, *J. Org. Chem.*, 2001, **66**, 8395–8401.
- P. Bonhote, A.-P. Dias, N. Papageorgiou, K. Kalyanasundaram and M. Gratzel, *Inorg. Chem.*, 1996, **35**, 1168–1178.
- T. Erdmenger, C. Haensch, R. Hoogenboom and U. S. Schubert, *Macromol. Biosci.*, 2007, **7**, 440–445.
- T. G. A. Youngs, C. Hardacre and J. D. Holbrey, *J. Phys. Chem. B*, 2007, **111**, 13765–13774.
- T. G. A. Youngs, J. D. Holbrey, M. Deetlefs, M. Nieuwenhuyzen, M. F. C. Gomes and C. Hardacre, *ChemPhysChem*, 2006, **7**, 2279–2281.
- J. M. Crosthwaite, M. J. Muldoon, J. K. Dixon, J. L. Anderson and J. F. Brennecke, *J. Chem. Thermodyn.*, 2005, **37**, 559–568.
- S. H. Lee, S. H. Ha, S. B. Lee and Y.-M. Koo, *Biotechnol. Lett.*, 2006, **28**, 1335–1339.
- Y. Ishida, D. Sasaki, H. Miyauchi and K. Saigo, *Tetrahedron Lett.*, 2004, **45**, 9455–9459.
- A. Bernson and J. Lindgren, *Polymer*, 1994, **35**, 4848–4851.
- Y. Mei, A. Kumar and R. Gross, *Macromolecules*, 2003, **36**, 5530–5536.

- 59 M.-J. Kim, M. Y. Choi, J. K. Lee and Y. Ahn, *J. Mol. Catal. B: Enzym.*, 2003, **26**, 115–118.
- 60 F. Ganske and U. T. Bornscheuer, *J. Mol. Catal. B: Enzym.*, 2005, **36**, 40–42.
- 61 F. Ganske and U. T. Bornscheuer, *Org. Lett.*, 2005, **7**, 3097–3098.
- 62 N. Kaftzik, P. Wasserscheid and U. Kragl, *Org. Process Res. Dev.*, 2002, **6**, 553–557.
- 63 N. Kaftzik, S. Neumann, M.-R. Kula and U. Kragl, in *Ionic Liquids as Green Solvents: Progress and Prospects*, ed. R. D. Rogers and K. R. Seddon, American Chemical Society, Washington D.C., Editon edn, 2003, pp. 206–211.
- 64 T. Maruyama, S.-I. Nagasawa and M. Goto, *J. Biosci. Bioeng.*, 2002, **94**, 357–361.
- 65 M. Therisod and A. M. Klibanov, *J. Am. Chem. Soc.*, 1986, **108**, 5638–5640.
- 66 S. Riva, J. Chopineau, A. P. G. Kieboom and A. M. Klibanov, *J. Am. Chem. Soc.*, 1988, **110**, 584–589.
- 67 J. O. Rich, B. A. Bedell and J. S. Dordick, *Biotechnol. Bioeng.*, 1995, **45**, 426–434.

Efficient synthesis of disulfides by air oxidation of thiols under sonication

José Luis García Ruano,* Alejandro Parra and José Alemán†

Received 15th January 2008, Accepted 8th April 2008

First published as an Advance Article on the web 9th May 2008

DOI: 10.1039/b800705e

Alkyl, aryl and heteroaryl symmetrical disulfides can be easily obtained by heating the corresponding thiols for several hours at 80 °C with Et₃N in DMF under atmospheric oxygen. These reactions are markedly accelerated by ultrasounds (few minutes at rt). Aromatic groups bearing electron donating and electron withdrawing groups, heteroaromatic, and alkyl thiols are analogously efficient affording disulfides in almost quantitative yields. Amino thiols and *L*-cysteine provide the corresponding disulfides without affecting the nitrogen function.

Introduction

Disulfides play interesting roles both in biological¹ (DNA-cleavage properties and stabilization of peptides in proteins) and chemical^{2,3} (protecting groups, vulcanizing agents, and oils for rubber and elastomers) processes. The easy interconversion between thiols and disulfides⁴ and the higher stability of the latter determines that disulfides are frequently used as a source for thiols.

Most of the methods used in the synthesis of disulfides involve the oxidation of thiols.^{5–21} Reagents such as permanganates,⁵ sodium perborate,⁶ ferric chloride,⁷ cerium(IV) salt,⁸ copper salt,⁹ rhenium-sulfoxide complex,¹⁰ chromate and dichromate compounds,¹¹ are the most used in the synthesis of disulfides. The limitations of these reagents derive from the toxicity and high price of some of them and the over-oxidation of the disulfide to thiosulfonates and derivatives. There are methods using oxygen as a co-oxidant (FeCl₃-NaI/air^{7b} and Cobalt(II) phthalocyanines/O₂ in ionic liquid¹²) that require additional oxidant or oxygen-gas bubbling, long reaction times, and laborious experimental procedures. Voelter *et al.*¹³ have recently reported that the CsF-Celite/air system is quite efficient to oxidize thiols into disulfides where the high price of the cesium fluoride¹⁴ is the main drawback of this method.

The non-metal oxidating reagents which include sodium chlorite,¹⁵ bromine supported on silica gel,¹⁶ nitric oxide or sodium nitrite,¹⁷ hydrogen peroxide in tetrafluoroethanol,¹⁸ hydantoin derivatives,¹⁹ and sulfuryl chloride and peroxy monosulfate,²⁰ among others, have also been used for oxidation of thiols to disulfides. However, the manipulation, the toxicity, the price and the work up of some of these reagents are not an easy task. Moreover, some of these reagents are environmentally non-friendly compounds. The Burgess reagent²¹ has also been used for obtaining disulfides from thiols, with the high cost of this reagent (it must be used in stoichiometric amount) being the main limitation of the method.

Thus, there is still an interest in developing clean, fast, inexpensive, environmentally harmless oxidative methods that would produce the desirable disulfides in high yields. In this sense, the oxidation of thiols into disulfides using molecular oxygen (air-oxygen or oxygen pressure)²² has drawn the attention of researchers for several decades because this reagent is inexpensive, easy to handle, and scarcely toxic. In the last years, our research group has been interested in the synthesis of *N*-sulfonylimines,²³ *N*-sulfonyloxaziridines,²⁴ and more recently *N*-sulfonamides.²⁵ In all these cases, disulfides are used as starting materials and therefore we were interested in developing a simple, environmentally friendly, and inexpensive multi-gram scale method to prepare them. In this work, we present our efforts obtained in the mild transformation of thiols to disulfides under sonication using the cheapest oxidant on earth (atmospheric oxygen). It can be used for preparing aromatic, heteroaromatic and aliphatic symmetrical disulfides.

Results and discussion

Synthesis of disulfides under thermal conditions

The role of polar-aprotic solvents having high dielectric constants, such as DMF (dimethylformamide) is known to increase the oxidation rate of the thiols with oxygen.²² Moreover, reaction times can be shortened by addition of bases able to form thiolates from thiols²⁶ and therefore good yields have been reported for reactions catalyzed by amines as tetramethylguanidine.²⁷ Inspired in both facts, we studied the behaviour of a solution of benzenethiol (1 equiv.), Et₃N (1 equiv.) in DMF heated at 80 °C in an open air flask.²⁸ We could check that after 24 h diphenyl disulfide **1** was obtained in 95% yield (entry 1, Table 1). Other aryldisulfides under the same conditions, containing electron donating (2, 3 and 4) and electron withdrawing groups (4 and 5), could also be obtained in high yields (entries 2–6, Table 1). The presence of substituents at the *ortho* position does not affect the reaction conditions required to obtain very good yields of the disulfide **7** significantly (entry 6). Finally, alkyldisulfide **8** is also obtained under the same conditions (entry 8, Table 1). It is noteworthy that all these reactions usually evolve with almost quantitative yields, the work-up procedure is very easy, and they can be made in a multigram scale as it was demonstrated for

Departamento de Química Orgánica, Universidad Autónoma de Madrid, Cantoblanco, 28049, Madrid, Spain.

E-mail: joseluis.garcia.ruano@uam.es; Fax: +34914973966

† Current Address: Center for Catalysis, Department of Chemistry, University of Aarhus, DK-8000, Aarhus C, Denmark.

Table 1 Synthesis of symmetrical disulfides under thermal conditions^a

R-SH		$\xrightarrow[\text{DMF, Et}_3\text{N}]{\text{Air}}$ $\xrightarrow[\text{T (}^\circ\text{C)}]{}$		R-S-S-R	
				1-8	
Entry	R	Product	T/°C	Time/h	Yield (%) ^c
1	Ph	1	80	24	95
2	4-MeC ₆ H ₄	2	80	24	99
3	4-MeOC ₆ H ₄	3	50	24	99
4	2-MeOC ₆ H ₄	4	100	48	98
5	4-CF ₃ C ₆ H ₄	5	80	48	90
6	4-ClC ₆ H ₄	6	100	48	80 ^b
7	2,6-DiMeC ₆ H ₃	7	100	24	94
8	CH ₃ CH ₂ CH ₂	8	100	24	97

^a All the reactions were carried out in 10 mmol scale (of the corresponding thiol) using 1 equiv. of Et₃N (10 mmol, 1.6 mL) and 8 mL of DMF.

^b This reaction has been performed in a 0.138 mol scale (20 g of thiol).

^c Isolate yield.

disulfide **5**, obtained from 20 g (0.13 mol) of the corresponding thiol (entry 6).

Synthesis of disulfides under sonication conditions

Despite the good features, this method has two important drawbacks that seriously restrict its usefulness to be used as the electing method in the large scale synthesis of disulfides: the reaction times (24–48 h) and the temperature (50–100 °C). For this reason, we explored external activation for the acceleration rate of this reaction. The use of sonication in organic chemistry for increasing chemical reactivity has found broad application in the last years.²⁹ Sonication has been shown to be more efficient for reactions involving free radicals.²⁹ The mechanism for the conversion of thiols into disulfides seems to involve these intermediates,^{29a} we decided to investigate the influence of the sonication on our reactions. The results obtained from thiophenol under different conditions are depicted in Table 2.

Under sonication conditions the reaction took place only in 5 min at 40 °C in quantitative yield (entry 1, Table 2) with identical proportions to those used in entry 1 of Table 1 (24 h at

80 °C). Therefore, it is shown that the reaction has been strongly accelerated. In order to optimize this reaction, we have studied the role of different factors. As expected, longer reaction times were required when decreasing the temperature (compare entries 1 and 2, Table 2) however the yield remains quantitative. The amount of solvent could be decreased, which simplifies the purification and decreases the cost of the process, up to 1.25 mL (entry 3), however slightly longer reaction times are needed to obtain similar yield (compare entries 1 and 2, Table 2). Additional decreases in the amount of solvent have a negative influence on reaction time and yield (see for example entry 4). The conversion was also strongly decreased when the amount of base was diminished, even if the reaction time was increased (compare entries 2 with 5 and 6, Table 2). This fact supports the conversion of thiol into thiolate as a previous step of its coupling into disulfide.²² We have carried out the reaction in 0.18 mol scale (20 grams) without significant loss of yield (entries 7 and 8) supporting this as a strong method for disulfide synthesis.

With the optimized conditions in hand we studied the scope of the reaction at 40 °C and room temperature (Table 3). Small significant differences in reaction times can be observed depending on the electronic character of the substituents at the aromatic rings. Thus, longer reaction times were necessary for electron donating groups (methyl and methoxy, entries 2–4, Table 3) and shorter reaction times for electron withdrawing groups (*p*-chloro, *p*-nitro and 2-naphthyl, entries 5–7, Table 3), which could be related to the influence of the substituents on the ease of formation of the thiophenolate ions.

The reactivity of thiophenols with 2-*i*Pr and 2,6-diMe phenyl groups is slightly lower with longer reaction times (entries 8 and 9, Table 3), probably due to the steric hindrance of the anions and radical involved in these reactions. Additionally, the reaction could be done with thiols derived from aromatic heterocycles in excellent yield (entry 10, Table 3). Alkylthiols also reacted under these conditions, proving the general scope of the methodology. Thus, the propanothiol, dodecanthiol, and cyclohexanethiol reacted in 15 min, giving the corresponding disulfides **8**, **14**, and **16** in excellent yields (entries 11–13, Table 3). Unexpectedly, *t*-butylthiol reacts more slowly (entry 14, Table 3), affording a 2 : 1 mixture of the disulfide (55% yield) and trisulfide (25% yield).

Table 2 Optimization of the reaction of thiophenol under sonication^a

Ph-SH		$\xrightarrow[\text{DMF, Et}_3\text{N}]{\text{Air}}$ $\xrightarrow[\text{T (}^\circ\text{C)}]{\text{sonication}}$		Ph-S-S-Ph		
				1		
Entry	mmol (g)	Solvent/mL	Base (equiv.)	T/°C	Time/min	Yield (%) ^b
1	10 (1.1)	8.0	1.0	40	5	98
2	10 (1.1)	8.0	1.0	rt	30	96
3	10 (1.1)	1.25	1.0	rt	40	97
4	10 (1.1)	0.8	1.0	rt	60	92
5	10 (1.1)	1.25	0.5	rt	45	40
6	10 (1.1)	1.25	0.5	rt	60	40
7	181 (20)	50	1.0	rt	15	89
8	181 (20)	23	1.0	rt	45	89

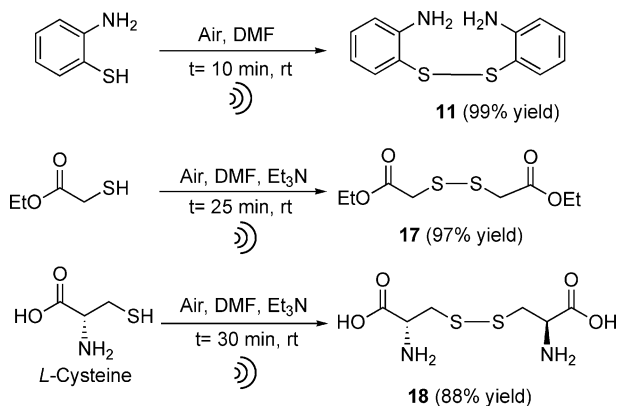
^a The reactions were carried out using 10–181 mmol scale (of the corresponding thiol) using 0.5–1.0 equiv. of Et₃N (10 mmol, 1.6 mL) and DMF as solvent. ^b Isolate yield.

Table 3 Synthesis of symmetrical disulfides under thermal conditions^a

Entry	R	Product	R-S-S-R 1-16			
			Temperature (rt)		Temperature (40 °C)	
			Time/min	Yield (%) ^c	Time/min	Yield (%) ^c
1	Ph	1	40	97	5	99
2	4-MeC ₆ H ₄	2	40	96	5	96
3	4-MeOC ₆ H ₄	3	45	96	10	97
4	2-MeOC ₆ H ₄	4	60	98	15	98
5	4-ClC ₆ H ₄	6	25	97	5	99
6	4-NO ₂ C ₆ H ₄	9	22	96	5	98
7	2-Naphthyl	10	25	98	5	97
8	2,6-DiMeC ₆ H ₃	7	80	93	20	92
9	2- <i>i</i> Pr-C ₆ H ₄	12	75	98	20	97
10	<i>N</i> -Phenyltetrazol	13	30	91	5	94
11	CH ₃ CH ₂ CH ₂	8	45	93	15	92
12	CH ₃ (CH ₂) ₁₁	14	45	96	15	99
13	(CH ₃) ₃ C	15	120	49	60	55 ^b
14	Cy	16	40	96	15	98

^a All the reactions were carried out in 3.0 mmol scale. ^b Obtained along with the trisulfide (2 : 1 mixture). ^c Isolate yield.

In order to know the compatibility of this method in the presence of other functional groups in the molecule, we explored the synthesis of disulfides **11**, **17** and **18** (Scheme 1). Thus, the 2-mercapto-aniline required 10 min to be quantitatively transformed into the corresponding disulfide **11** (eqn 1, Scheme 1). Interestingly, this reaction can be done without adding Et₃N, since the amine group of the starting material acts as a base to form the thiolate.



Ethyl 2-mercaptoacetate also gave disulfide **17** in 97% yield (eqn 2, Scheme 1), and the amino acid *L*-cysteine, which is involved in a huge number of biological processes,¹ is converted into disulfide **18** with 88% yield without observing modification or decomposition of the carboxylic and amino function (eqn 3, Scheme 1).

Conclusions

In conclusion, we have developed a new method to obtain disulfides from thiols that uses the cheapest and most environmentally friendly oxidant, the air, along with an inexpensive base such

as Et₃N (1.0 equiv.) and DMF (1.25 equiv.) as solvent. Under sonication, reactions are strongly accelerated and they can be made in short times (usually less than 1 h) at room temperature. The scope of the method is almost general since it is successful for aliphatic, aromatic (with electron-rich and electron-poor substituents), and heteroaromatic thiols. Additionally, it is compatible with the presence of other functional groups in the molecule. The yields are almost quantitative in most cases, and can be performed in multigram scale without losing the good features.

This work was supported by grants from the Ministerio de Educación y Ciencia (CTQ2006-06741/BQU). A. P. thanks "Ministerio de Educación y Ciencia" of Spain for the predoctoral fellowship.

Experimental

¹H-NMR spectra were acquired at 300 MHz and ¹³C-NMR were acquired at 75 MHz. Chemical shifts (δ) are reported in ppm relative to CDCl₃ (7.26 and 77.0 ppm). Melting points were determined in open capillary tubes. All thiols were purchased from Aldrich. For sonication an Elma (Model transonic-T460/H) was used, ultrasonic frequency 35 kHz and the internal temperature was controlled by an external thermometer in the water bath.

Representative procedure for the atmospheric oxidation of thiols using DMF reflux (procedure A) (Table 1)

To a flask charged with corresponding thiol (3.0 mmol) was added DMF (2.5 mL) and Et₃N (3.0 mmol). It was heated at the temperature indicated in Table 1. The reaction was followed by TLC. The reaction mixture was extracted with Et₂O (2 × 10 mL), and the organic phase was washed with H₂O (2 × 30 mL) to eliminate the DMF entirely. The solvent was removed

under vacuum to afford the corresponding disulfide pure. Yield is indicated in each case.

Representative procedure for the atmospheric oxidation of thiols using ultrasound (procedure B) (Table 3)

To a flask charged with corresponding thiol (3.0 mmol) was added DMF (2.5 mL) and Et₃N (3.0 mmol). It was placed in an ultrasonic bath at rt or 40 °C. The reaction was followed by TLC. The reaction mixture was extracted with Et₂O (2 × 10 mL), and the organic phase was washed with H₂O (2 × 30 mL) to eliminate the DMF entirely. The solvent was removed under vacuum to afford the corresponding disulfide pure. Yield is indicated in each case.

Phenyl disulfide (1) [CAS 882-33-7]³⁰

This disulfide was obtained following the general procedure A (reaction temperature: 80 °C; yield: 95%) or procedure B (yield: 97% at rt and 99% at 40 °C) using benzenethiol as starting material. White solid; mp: 57–59 °C [Lit.³⁰ mp: 58–60 °C]. ¹H-NMR (300 MHz, CDCl₃): δ 7.42–7.39 (m, 4H), 7.22–7.09 (m, 6H). ¹³C-NMR (300 MHz, CDCl₃): δ 137.0, 129.0, 127.5, 127.1.

p-Tolyl disulfide (2) [CAS 103-19-5]³¹

This disulfide was obtained following the general procedure A (reaction temperature: 80 °C; yield: 99%) or procedure B (yield: 96% at rt and 40 °C) using 4-methylbenzenethiol as starting material. White solid; mp: 47–49 °C [Lit.³¹ mp: 46–48 °C]. ¹H-NMR (300 MHz, CDCl₃): δ 7.40 (d, *J* = 8.3 Hz, 4H), 7.11 (d, *J* = 8.3 Hz, 4H), 2.33 (s, 6H). ¹³C-NMR (300 MHz, CDCl₃): δ 137.4, 133.9, 129.8, 128.5, 21.0.

p-Methoxyphenyl disulfide (3) [CAS 5335-87-5]³²

This disulfide was obtained following the general procedure A (reaction temperature: 50 °C; yield: 99%) or procedure B (yield: 96% at rt and 97% at 40 °C) using 4-methoxybenzenethiol as starting material. White solid; mp: 41–43 °C [Lit.³² mp: 42–44 °C]. ¹H-NMR (300 MHz, CDCl₃): δ 7.27 (d, *J* = 8.9 Hz, 4H), 6.70 (d, *J* = 8.9 Hz, 4H), 3.64 (s, 6H). ¹³C-NMR (300 MHz, CDCl₃): δ 159.8, 133.5, 128.2, 114.5, 55.2.

o-Methoxyphenyl disulfide (4) [CAS 1142-19-4]³³

This disulfide was obtained following the general procedure A (reaction temperature: 100 °C; yield: 98%) or procedure B (yield: 98% at rt and 40 °C) using 2-methoxybenzenethiol as starting material. Brown solid; mp: 118–119 °C. ¹H-NMR (300 MHz, CDCl₃): δ 7.54 (dd, *J* = 6.2, 1.5 Hz, 2H), 7.19 (t, *J* = 6.6 Hz, 2H), 6.94–6.84 (m, 4H), 3.90 (s, 6H). ¹³C-NMR (300 MHz, CDCl₃): δ 156.5, 127.7, 127.5, 124.5, 121.3, 110.4, 55.9.

p-Chlorophenyl disulfide (6) [CAS 1142-19-4]³⁴

This disulfide was obtained following the general procedure A (reaction temperature: 100 °C; yield: 80%) or procedure B (yield: 97% at rt and 99% at 40 °C) using 4-chlorobenzenethiol as starting material. White solid; mp: 72–74 °C [Lit.³⁴ mp: 72–73 °C]. ¹H-NMR (300 MHz, CDCl₃): δ 7.32 (d, *J* = 8.8 Hz,

4H), 7.20 (d, *J* = 8.8 Hz, 4H). ¹³C-NMR (300 MHz, CDCl₃): δ 135.1, 133.6, 129.3, 129.3.

2,6-Dimethylphenyl disulfide (7)

This disulfide was obtained following the general procedure A (reaction temperature: 100 °C; yield: 94%) or procedure B (yield: 93% at rt and 92% at 40 °C) using 2,6-dimethylbenzenethiol as starting material. White solid; mp: 57–58 °C. ¹H-NMR (300 MHz, CDCl₃): δ 7.19–7.03 (m, 6H), 2.29 (s, 6H). ¹³C-NMR (300 MHz, CDCl₃): δ 143.3, 134.7, 129.2, 127.9, 21.4.

n-Propyl disulfide (8) [CAS 629-19-6]³⁵

This disulfide was obtained following the general procedure A (reaction temperature: 100 °C; yield: 97%) or procedure B (yield: 93% at rt and 92% at 40 °C) using 1-propanethiol as starting material. Colorless oil. ¹H-NMR (300 MHz, CDCl₃): δ 2.63 (t, *J* = 7.1 Hz, 4H), 1.66 (sp, *J* = 7.5 Hz, 4H), 0.96 (t, *J* = 7.3 Hz, 6H). ¹³C-NMR (300 MHz, CDCl₃): δ 40.9, 22.4, 12.9.

p-Nitrophenyl disulfide (9) [CAS 100-32-3]³²

This disulfide was obtained following the general procedure B using 4-nitrobenzenethiol as starting material. Orange solid. Yield: 96% at rt and 98% at 40 °C; mp: 175–177 °C [Lit.³² mp: 177–178 °C]. ¹H-NMR (300 MHz, CDCl₃): δ 8.17 (d, *J* = 7.0 Hz, 4H), 7.61 (d, *J* = 7.0 Hz, 4H). ¹³C-NMR (300 MHz, CDCl₃): δ 144.0, 142.7, 126.4, 124.4.

2-Naphthalenyl disulfide (10) [CAS 5586-15-2]²¹

This disulfide was obtained following the general procedure B using 2-naphthalenethiol as starting material. White solid. Yield: 98% at rt and 97% at 40 °C; mp: 136–137 °C [Lit.³⁶ mp: 135–138 °C]. ¹H-NMR (300 MHz, CDCl₃): δ 7.99 (d, *J* = 0.9 Hz, 2H), 7.81–7.72 (m, 4H), 7.65–7.61 (m, 2H), 7.49–7.42 (m, 4H). ¹³C-NMR (300 MHz, CDCl₃): δ 134.0, 133.5, 132.5, 128.9, 127.8, 127.5, 126.7, 126.6, 126.2, 125.7.

2-Isopropylphenyl disulfide (12)³⁶

This disulfide was obtained following the general procedure B using 2-isopropylbenzenethiol as starting material. White solid. Yield: 98% at rt and 97% at 40 °C; mp: 43–45 °C. ¹H-NMR (300 MHz, CDCl₃): δ 7.70 (d, *J* = 7.7 Hz, 2H), 7.39–7.30 (m, 4H), 7.25–7.19 (m, 2H), 3.64 (sept, *J* = 6.6 Hz, 2H), 1.35 (d, *J* = 6.6 Hz, 12H). ¹³C-NMR (300 MHz, CDCl₃): δ 148.1, 134.6, 129.5, 127.8, 126.5, 125.6, 30.2, 23.4.

2,5,5'-Dithiobis(1-phenyl-1H-tetrazole) (13) [CAS 5117-07-7]³⁷

This disulfide was obtained following the general procedure B using 1-phenyl-1H-tetrazole-5-thiol as starting material. White solid. Yield: 91% at rt and 94% at 40 °C. mp: 144–146 °C. ¹H-NMR (300 MHz, CDCl₃): δ 7.59 (m, 10H). ¹³C-NMR (300 MHz, CDCl₃): δ 144.1, 133.1, 130.9, 130.0, 124.4.

Dodecyl disulfide (14) [CAS 2757-37-1]²¹

This disulfide was obtained following the general procedure B using dodecanethiol as starting material. Colorless oil. Yield:

96% at rt and 99% at 40 °C. ¹H-NMR (300 MHz, CDCl₃): δ 2.49 (t, *J* = 6.9 Hz, 4H), 1.64–1.54 (m, 4H), 1.35–1.25 (m, 36H), 0.86 (t, *J* = 6.3 Hz, 6H). ¹³C-NMR (300 MHz, CDCl₃): δ 34.0, 31.9, 29.6, 29.6, 29.5, 29.5, 29.3, 29.1, 28.4, 24.6, 22.6, 14.0.

tert-Butyl disulfide (15) [CAS 10-06-5]²¹

This disulfide was obtained following the general procedure B using 2-methyl-2-propanethiol as starting material. Colorless oil. Yield: 49% at rt and 55% at 40 °C. ¹H-NMR (300 MHz, CDCl₃): δ 1.26 (s, 18H) ¹³C-NMR (300 MHz, CDCl₃): δ 45.9, 30.5.

Cyclohexyl disulfide (16) [CAS 2550-40-5]³⁴

This disulfide was obtained following the general procedure B using cyclohexylthiol as starting material. Colorless oil. Yield: 96% at rt and 98% at 40 °C. ¹H-NMR (300 MHz, CDCl₃): δ 2.77–2.72 (m, 2H), 1.98–1.94 (m, 4H), 1.71–1.58 (m, 3H), 1.57–1.53 (m, 3H), 1.37–1.13 (m, 10H). ¹³C-NMR (300 MHz, CDCl₃): δ 38.3, 37.8, 26.2, 25.2.

2-Aminophenyl disulfide (11) [CAS 1141-88-4]³⁸

This disulfide was obtained following the general procedure B using 2-aminobenzenethiol as starting material. Yellow solid. mp: 93–94 °C [Lit.³⁸ mp: 91–92 °C]. Yield: 99% ¹H-NMR (300 MHz, CDCl₃): δ 7.18–7.13 (m, 4H), 6.72 (d, *J* = 4.1 Hz, 2H), 6.49 (t, *J* = 6.4 Hz, 2H), 4.33 (bs, 4H). ¹³C-NMR (300 MHz, CDCl₃): δ 148.6, 136.8, 131.7, 118.7, 118.2, 115.2.

Ethyl glycolate disulfide (17) [CAS 505-73-7]³⁹

This disulfide was obtained following the general procedure B using ethyl thioglycolate as starting material. Colorless oil. Yield: 97% ¹H-NMR (300 MHz, CDCl₃): δ 4.10 (q, *J* = 7.2 Hz, 4H), 3.48 (s, 4H), (m, 3H), 1.19 (t, *J* = 7.2 Hz, 6H). ¹³C-NMR (300 MHz, CDCl₃): δ 168.3, 61.3, 41.1, 13.9.

L-Cystine disulfide (18) [CAS 56-89-3]⁴⁰

This disulfide was obtained following the general procedure B using L-cysteine as starting material. Colorless solid. mp: 258–260 °C [Lit.⁴⁰ mp: 260–261 °C] Yield: 88%. ¹H-NMR (300 MHz, 3% NaOH-D₂O): δ 3.41 (dd, *J* = 4.2, 1.3 Hz, 2H), 3.95 (dd, *J* = 6.3, 4.3 Hz, 2H), 2.75 (dd, *J* = 6.2, 4.1 Hz, 2H). ¹³C-NMR (300 MHz, 3% NaOH-D₂O): δ 183.6, 57.6, 46.1.

Notes and references

- (a) M. Bodanszky, Principles of Peptide, *Synthesis*, 1984, 307; (b) P. C. Jocelyn, *Biochemistry of the Thiol Group*, American Press, New York, 1992; (c) Y. Kanda and T. Fukuyama, *J. Am. Chem. Soc.*, 1993, **115**, 8451; (d) B. D. Palmer, G. W. Newcastle, A. M. Thompson, M. Boyd, H. D. H. Showalter, A. D. Sercel, D. W. Fry, A. J. Kraker and W. A. Dennyrosine, *J. Med. Chem.*, 1995, **38**, 58; (e) B. Schmidt, S. Lindman, W. Tong, G. Lindeberg, A. Gogoll, Z. Lai, M. Thornwall, B. Synnergren, A. Nilson, C. J. Welch, M. Sohtell, C. Westerlund, F. Nyberg, A. Karlen and A. Hallberg, *J. Med. Chem.*, 1997, **40**, 903.
- (a) *Organic Sulfur Chemistry: Structure and Mechanism*, ed. S. Oae, CRS Press, Boca Raton FL, USA, 1991; (b) R. J. Cremlyn, *An Introduction to Organosulfur Chemistry*, Wiley & Sons, New York, 1996.
- (a) A. Leitao, C. Costa and A. Rodrigues, *Chem. Eng. Sci.*, 1987, **42**, 2291; (b) K. Ramadas and N. Srinivasan, *Synth. Commun.*, 1995, **25**, 227; (c) D. L. Holbrook, *Handbook of Petroleum Refining Processes*, ed. R. A. Meyers, McGraw-Hill, New York, 1996, ch. 11.3.
- S. N. Maiti, P. Spevak, M. P. Singh and R. G. Micetic, *Synth. Commun.*, 1988, **18**, 575.
- (a) M. Naderi, A. Sardarian and M. Vessal, *Synth. Commun.*, 1983, **13**, 611; (b) H. Firouzabadi, E. Mottaghinejad and M. Sed-dighi, *Synthesis*, 1989, 378; (c) N. A. Nouredin, M. Cadewell, J. Hendry and D. G. Lee, *Synthesis*, 1998, 1587; (d) A. Shaa-bani and D. G. Lee, *Tetrahedron Lett.*, 2001, **42**, 5833; (e) A. Shaabani, A. Bazgir and D. G. Lee, *Synth. Commun.*, 2004, **35**, 3595.
- (a) A. McKillop and D. Koyuncu, *Tetrahedron Lett.*, 1990, **31**, 5007; (b) M. Bagheri, N. Azizi and M. R. Saidi, *Can. J. Chem.*, 2005, **83**, 146.
- (a) A. R. Ramesha and S. Chamedarsekran, *J. Org. Chem.*, 1994, **59**, 1354; (b) N. Iranpoor and B. Zeynizadeh, *Synthesis*, 1999, 49.
- D. N. Dhar and A. K. Bag, *Ind. J. Chem.*, 1984, **23B**, 974.
- J. Choi and N. M. Yoon, *J. Org. Chem.*, 1995, **60**, 3266.
- J. B. Arterburm, M. C. Perry, S. L. Nelson, B. R. Dible and M. S. Holguin, *J. Am. Chem. Soc.*, 1997, **119**, 9309.
- (a) H. Firouzabadi, N. Iranpoor, H. Parham, A. Sardarian and J. Toofan, *Synth. Commun.*, 1984, **14**, 717; (b) S. Patel and B. K. Mishra, *Tetrahedron Lett.*, 2004, **45**, 1371; (c) M. Tajbakhsh, R. Hosseinzadeh and A. Sharoori, *Tetrahedron Lett.*, 2004, **45**, 1889; (d) S. Ghammany and M. Tajbakhsh, *J. Sulfur Chem.*, 2005, **26**, 145.
- S. M. S. Chauhan, A. Kumar and K. A. Srinivas, *Chem. Commun.*, 2003, 2348.
- A. S. Tasadaque, K. M. Shad, M. K. Khalid, M. Fecker and W. Voelter, *Tetrahedron Lett.*, 2003, **44**, 6789.
- The cost of the cesium fluoride reagent from Aldrich is \$176.8 per gram.
- (a) K. Ramadas and N. Srinivasan, *Synth. Commun.*, 1995, **25**, 227; (b) M. Hashemi, A. Rahimi and Z. Jaberi-Karimi, *Lett. Org. Chem.*, 2005, **2**, 485; (c) Synthesis of disulfides has recently published using sodium iodine and H₂O₂. M. Kiri-hara, Y. Asai, S. Ogawa, T. Noguchi, A. Hatano and Y. Hiraib, *Synthesis*, 2007, 3286.
- (a) W. L. Christesen and D. J. Heacock, *Synthesis*, 1978, 50; (b) D. L. deLeeuw, W. K. Musker and J. K. Doi, *J. Org. Chem.*, 1982, **47**, 4860; (c) J. Drabowicz and M. A. Mikolajczyk, *Synthesis*, 1980, 32; (d) X. Wu and R. D. Rieke, *Synth. Commun.*, 1996, **26**, 191; (e) V. Kevasan, D. Bonnet-Delpon and J. P. Begue, *Synthesis*, 2000, 223; (f) M. H. Ali and M. Mcdermott, *Tetrahedron Lett.*, 2002, **43**, 6271.
- (a) W. A. Pryor, D. F. Church and C. K. Govindan, *J. Org. Chem.*, 1982, **47**, 156; (b) M. A. Zolfigol, F. Shirini, A. G. Choghamarani and E. Ghofrani, *Phosphorus, Sulfur Silicon Relat. Elem.*, 2003, **178**, 1477; (c) M. A. Zolfigol, K. Zamani, E. Ghofrani and S. Ebrahimi, *Phosphorus, Sulfur Silicon Relat. Elem.*, 2004, **179**, 2177; (d) N. Iranpoor, H. Firouzabadi and A. R. Pournali, *Phosphorus, Sulfur Silicon Relat. Elem.*, 2006, **181**, 473.
- (a) V. Kevasan, D. Bonnet-Dulpon and J.-P. Bégue, *Synthesis*, 2000, 223; (b) S. R. Kabayadi, V. Kevasan, C. Benoit, D. Bonnet-Dulpon and J.-P. Bégue, *Org. Synth.*, 2003, **80**, 184.
- (a) A. Akdag, T. Webb and S. D. Worley, *Tetrahedron Lett.*, 2006, **47**, 3509; (b) A. Christoforou, G. Nicolaou and Y. Elemes, *Tetrahedron Lett.*, 2006, **47**, 9211.
- (a) R. Leino and J. Lonnqvist, *Tetrahedron Lett.*, 2004, **45**, 8489; (b) A. Hajipour, S. E. Mallakpour and H. Adibi, *J. Org. Chem.*, 2002, **67**, 8666.
- The cost of the Burgess reagent from Aldrich is \$50–60 per gram. S. C. Banfield, A. T. Omori, H. Leish and T. Hudlcky, *J. Org. Chem.*, 2007, **72**, 4989.
- G. Capozzi, G. Modena, in *The Chemistry of the Thiol Group*, ed. S. Patai, John & Sons, London, 1974, part 2, ch. 17, p. 801 and references cited therein.
- (a) J. L. García Ruano, J. Alemán, M. B. Cid and A. Parra, *Org. Lett.*, 2005, **7**, 179; (b) J. L. García Ruano, J. Alemán, A. Parra and M. B. Cid, *Org. Synth.*, 2007, **84**, 129.
- J. L. García Ruano, J. Alemán, C. Fajardo and A. Parra, *Org. Lett.*, 2005, **7**, 5493.
- J. L. García Ruano, A. Parra, F. Yuste and V. M. Mastranzo, *Synthesis*, 2008, 311.
- (a) T. J. Wallace and A. Schriesheim, *J. Org. Chem.*, 1962, **27**, 1514; (b) T. J. Wallace, A. Schriesheim and W. Bartok, *J. Org. Chem.*, 1963, **28**, 1311; (c) A. A. Oswald, T. J. Wallace, in *Organic Sulfur Compounds*, ed. N. Kharash, Pergamon Press, New York, 1964, vol. 2, ch. 8.

- 27 T. J. Wallace, N. Jacobson and A. Schriesheim, *Nature*, 1964, **201**, 609.
- 28 The reaction did not work in a close flash without air.
- 29 (a) *Sonochemistry: The uses of ultrasound in chemistry*, ed. T. J. Mason, Royal Society of Chemistry, Cambridge, 1990; (b) T. J. Mason, *Chem. Soc. Rev.*, 1997, **26**, 443; (c) P. D. Lickiss, Ultrasound in Chemical Synthesis, in *The New Chemistry*, ed. N. Hall, Cambridge University Press, Cambridge, UK, 2000, pp. 76–84; (d) W. Bonrath and R. A. P. Schmidt, *Adv. Org. Syn.*, 2005, **1**, 81; (e) G. Cravotto and P. Cintas, *Chem. Soc. Rev.*, 2006, **35**, 180; (f) M. Moroianu, *Rev. Fiz. Chim.*, 2007, **42**, 20.
- 30 G. De Martino, G. La Regina, A. Coluccia, M. C. Edler, M. C. Barbera, E. Wilcox, Hamel, M. Artico and R. Silvestre, *J. Med. Chem.*, 2004, **47**, 6120.
- 31 I. M. Baltork, A. R. Hajipour and H. Mohammadi, *Bull. Chem. Soc. Jpn.*, 1998, **71**, 1649.
- 32 A. S. Tasadaque, K. M. Shad, M. K. Khalid, M. Fecker and W. Voelter, *Tetrahedron Lett.*, 2003, **44**, 6789.
- 33 I. Yavari, A. A. Rounaqi and L. Moradi, *Phosphorus, Sulfur Silicon Relat. Elem.*, 2006, **181**, 2659.
- 34 A. R. Hajipour and A. E. Ruoho, *Phosphorus, Sulfur Silicon Relat. Elem.*, 2003, **178**, 1277.
- 35 M. M. Hossain, H. M. Lin, J. Zhu, Z. Lin and S.-G. Shyu, *Organometallics*, 2006, **25**, 440.
- 36 R. S. Atkinson, B. D. Judkins and B. J. Patwardhan, *J. Chem. Soc., Perkin Trans. 2*, 1979, 1490.
- 37 J. Lalevee, X. Allonas and J. P. Fouassier, *J. Org. Chem.*, 2006, **71**, 9723.
- 38 C. N. Yiannios and J. V. Karabinos, *J. Org. Chem.*, 1963, **28**, 3246.
- 39 B. P. Bandgar, L. S. Uppalla and V. S. Sadavarte, *Tetrahedron Lett.*, 2001, **42**, 6741.
- 40 M. Oba, H. Iwasaka, T. Ikegame, H. Banba, K. Ura, T. Takamura and K. Nishiyama, *Tetrahedron: Asymmetry*, 2006, **17**, 1890.

Synthesis of cyclic acetals (ketals) from oleochemicals using a solvent free method

Kenneth M. Doll* and Sevim Z. Erhan

Received 28th February 2008, Accepted 9th April 2008

First published as an Advance Article on the web 12th May 2008

DOI: 10.1039/b803513j

The reaction selectivities of acid catalyzed ring opening reactions of epoxidized methyl oleate (methyl 9,10-epoxy stearate; EMO), to form either ketal (acetal) or branched ester products have been studied. We have produced methyl 9-(2-butyl-2-methyl-5-octyl-1,3-dioxolan-4-yl) nonanoate (hexanone methyl stearate acetal, HMSA), an oleochemically based ketal (acetal), in 83% isolated yield; from epoxidized methyl oleate and 2-hexanone. Utilizing our reaction chemistry, we have also been able to demonstrate the relative selectivities, in competitive experiments, by reacting EMO with 2-pentanone and octanoic acid. Finally, by controlling temperature and acid concentration, we were able to control the product distribution of the reaction of EMO with the bi-functional levulinic acid. Either the ketal (acetal), or the branched ester product could be favored. This research may help lead to the formation of new hydrophobic molecules for the synthesis of new surfactants from oleochemicals.

Introduction

There are many different reasons why the use of bio-based products is favorable. They include federal regulations,¹ high petroleum prices,²⁻⁵ environmental concerns,⁶⁻⁸ or to support the United States agricultural industry. Soybean oil based products have entered the market in many industrial areas,⁹⁻¹³ often using oil that has been subjected to a variety of chemical modifications.¹²

One area of chemistry which we have studied is the synthesis of compounds based on epoxidized methyl oleate (methyl 9,10-epoxy stearate, EMO). This compound is readily available from the epoxidation of methyl oleate, or from a transesterification reaction on commercially available epoxidized soybean oil.¹⁴ A commercial source of the mixed epoxy esters is also available. In previous work we have studied the properties of EMO, and EMO derived compounds, relevant for their use as lubrication fluids,¹⁵ surfactants,¹⁶ or fuel additives.¹⁷⁻¹⁹ We have recently reported²⁰ the synthesis of a series of branched oleochemicals from EMO. The system utilizing levulinic acid as a reactant was particularly interesting. Although the expected ester structure was formed, an acetal (or ketal) was also produced as a minor product (Scheme 3). Our goal was to obtain product control of this reaction, thereby taking advantage of some of the properties

of oleochemically based ketals that have been reported in the open literature.^{21,22}

The acetal (ketal) structure has attracted interest in several areas of chemistry, including pharmaceutical synthesis, natural product derivatization, and extraction methodologies. In the synthesis of pH degradable molecules,²³⁻²⁵ acetals have shown promise as potential hydrophobes for surfactants. They can be adjusted to extract an analyte, then release it in a controlled manner. Because of its biobased nature and track record of success in our earlier work, EMO was used to synthesize these desirable hydrophobes.

The chemistry controlling the formation of acetal and ketals is well understood from organic chemistry protecting group literature.^{26,27} Using this methodology, the reaction product specificity could be controlled by use of an acid catalyst. Herein we report a reaction of EMO with 2-hexanone, to form a ketal product. We also report a competition reaction between ketal formation and ester formation. Finally, we study the levulinic acid system under different temperature and catalyst conditions.

Experimental

Materials

Epoxidized methyl oleate (methyl 9,10-epoxy stearate; EMO) was synthesized by the same method used in previous work.²⁰ Levulinic acid (Sigma-Aldrich, St. Louis, MO, 98%); octanoic acid (Sigma-Aldrich, St. Louis, MO, 98+%); 2-hexanone (Sigma-Aldrich, St. Louis, MO, 98%); 2-pentanone (Fluka, Buchs Switzerland, $\geq 99\%$); copper sulfate (Sigma-Aldrich, St. Louis, MO, Reagent Plus $\geq 99\%$); sulfuric acid (H_2SO_4 , Baker, Phillipsburg, NJ, ACS Reagent 96% assay); and (*o*-phosphoric acid (H_3PO_4 , Fisher, Pittsburgh, PA NF/FCC grade 85%); were used as received.

Food and Industrial Oil Research Unit, National Center for Agricultural Utilization Research, United States Department of Agriculture, Agricultural Research Service, 1815 N. University St., Peoria, IL, 61604, USA. E-mail: Kenneth.Doll@ars.usda.gov; Fax: 309-681-6340; Tel: 309-618-6103

† The use of trade, firm, or corporation names in this publication is for the information and convenience of the reader. Such use does not constitute an official endorsement or approval by the United States Department of Agriculture or the Agricultural Research Service of any product or service to the exclusion of others that may be suitable.

Instrumentation and equipment

FTIR spectra of the starting material and products were recorded, neat, on a Thermo Nicolet (Madison, WI) Nexus 470 FTIR with a Smart ARK accessory containing a 45° ZeSe trough running 64 scans. Data were collected and processed on a Windows 2000 equipped Dell Optiplex GX260 Pentium 4, 2.46 GHz computer running Omnic 6.2 software. Gas chromatography was performed on a Hewlett Packard (Loveland, CO) 5890 GC system equipped with a 6890 series injector and an FID detector. A J and W DB-1 column (15 m × 320 μm) was used with a helium flow rate of ~0.9 mL min⁻¹. The temperature program used started at 180 °C. The temperature was held for two min, then increased to 280 °C at 5 °C min⁻¹, then held for 5 min. NMR was performed on a Bruker (Boston, MA) Avance 500 NMR operating at 500 MHz for ¹H and 125 MHz for ¹³C. Bruker Icon NMR software was used running on an HP x1100 Pentium 4 workstation. Peaks were referenced to sodium 3-trimethylsilylpropionate-2,2,3,3-d₄ (TSP) at 0.0000 ppm. Simulations of ¹³C NMR spectra were performed using ACD/Labs 6.00 ACD/CNMR predictor software, running on a Gateway Pentium 4 CPU with a 2.53 GHz processor.

Reactions

The reactions were performed on a Pierce (Rockford, IL) Reacti-vap model 18780 or 18970. A 9 place B-1 aluminum heating block and 7.4 mL (2 dram) glass vials were used. The vials and reactions were kept under nitrogen by utilizing the Reacti-vap 18780 evaporating unit to flow nitrogen into the vials *via* 22 gauge needles that were inserted through the septa capped vials.

Typically, ~1.5 g of EMO and ~5 g of ketone were added to the vial. Next, the catalyst, ~0.01–0.1 g, was injected into the vials using a small volume syringe. The reaction progress was monitored by taking 20 μL aliquots of the reaction solution and analyzing by GC. To remove the residual catalyst, the compounds were washed 4 × with ~40 mL of Nanopure (Barnstead International, Dubuque, IA) water, then separated in a separatory funnel. The excess ketone and the residual water were removed under vacuum in a Kugelrohr at 50–70 °C. In the case where 2-hexanone was used as a ketone, the product, methyl 9-(2-butyl-2-methyl-5-octyl-1,3-dioxolan-4-yl) nonanoate (hexanone methyl stearate acetal, HMSA), was characterized by ¹³C NMR (Fig. 1) and FTIR (Fig. 2) spectroscopies. ¹³C NMR: (125 MHz, CDCl₃) δ 174.2 (carbonyl carbon), δ 129 (olefinic impurity), δ 109.4 (cyclic ketal carbon), δ 80.6–81.3 (oxygen bonded carbons at the 9 and 10 positions of the fatty chain), δ 51.4 (carbon of the methoxide group), δ 34.5–22.3 (multiple signals from fatty carbon chain), δ 25.6 (methyl group adjacent to ketal) δ 14.1 (end carbon of fatty chain and end of branched sidechain). The spectral peaks and assignments are close to the computed chemical shift and in order.

Larger scale synthesis

The synthesis of HMSA was performed at 4× the scale of the earlier reactions. In this synthesis, 6.0064 g of EMO was reacted with 20.0625 g of 2-hexanone with 0.40 mL of *o*-phosphoric acid catalyst. The reaction was run at 50 °C in a roundbottom flask for 4 h under nitrogen atmosphere and utilized magnetic stirring. The resulting product was washed three times with Nanopure (Barnstead International, Dubuque, IA) water and dried in a

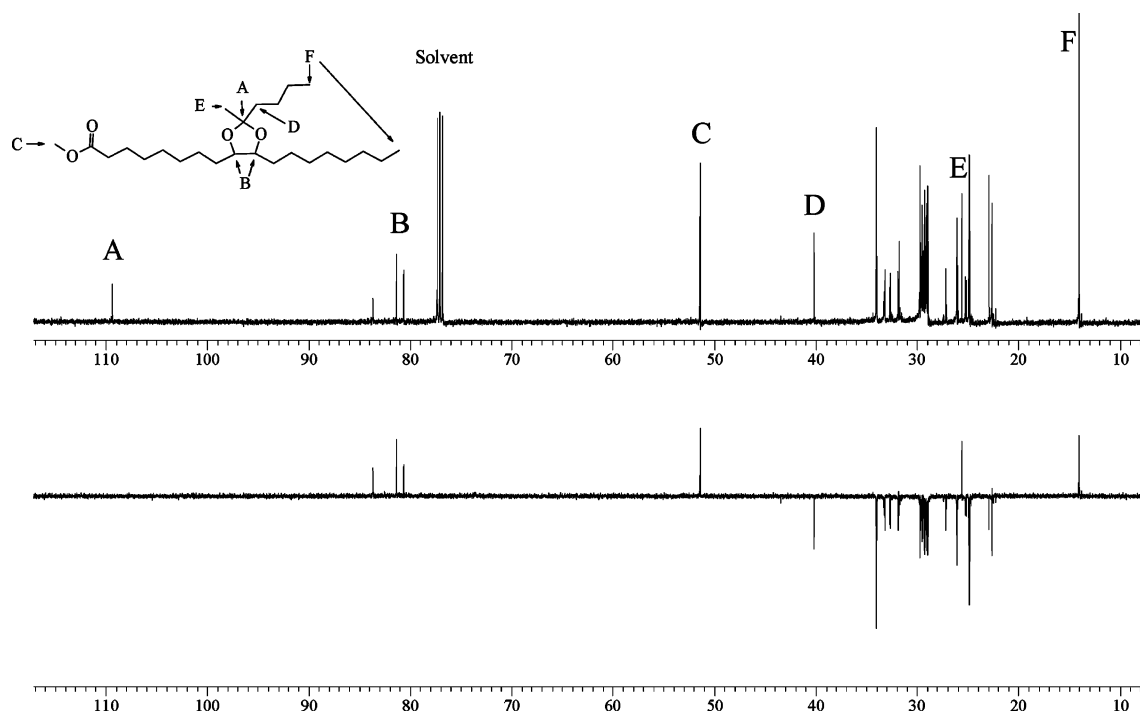


Fig. 1 The ¹³C NMR spectra of the ketal formed from 2-hexanone and EMO (HMSA) with phosphoric acid catalyst. The spectra were taken using normal proton decoupling (top) and a DEPT-135 pulse sequence (bottom). Using the spectra together, the peaks can be assigned to the carbons in the figure insert. Not shown are the carbonyl peak δ 174, and an olefinic impurity at δ ~129.

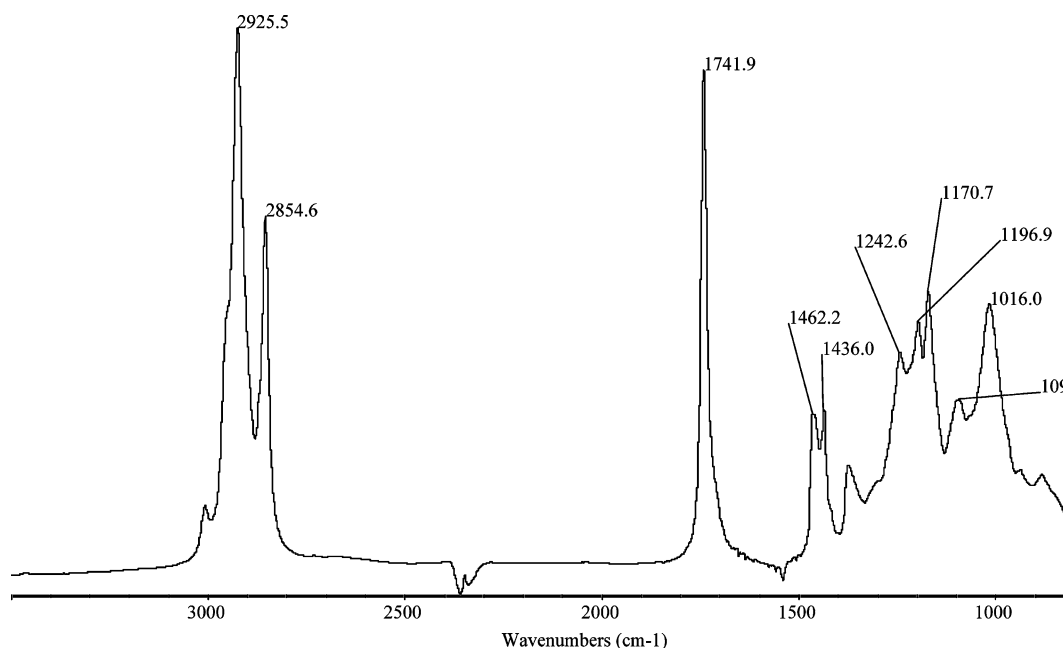


Fig. 2 FTIR spectrum of the acetal formed from 2-hexanone and EMO (HMSA) with phosphoric acid catalyst.

Kugelrohr under vacuum. The final yield was 6.60 g, an 83% isolated yield.

Results and discussion

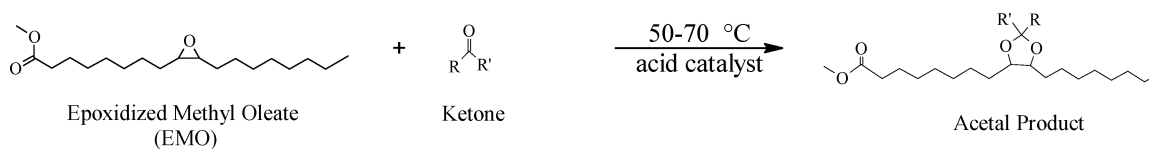
The epoxidation of methyl oleate was performed *via* a modified Swern epoxidation^{28,29} which has been extensively used by us^{15,16,20,30,31} and others.^{32,33} An alternative method for the production of a mixture of EMO and other epoxidized fatty esters, from commercially available epoxidized soybean oil, has been reported.¹⁴ It shows the feasibility of the use of this material, even on a commercial scale.

For our initial studies, we selected 2-hexanone as our ketone, due to its convenient properties. It is not as volatile as lower molecular weight ketones, and because the oxygen group is at position 2, the ketal product synthesized from 2-hexanone has unsymmetrical chains, enabling easier recognition of the reaction product using ¹³C NMR. We initially chose to study the systems at 50 °C, which was below the level of significant reaction observed in our earlier work, when EMO was reacted with carboxylic acids.²⁰ The reaction between EMO and 2-hexanone (Scheme 1) was performed using acid catalysts that have been effective in literature syntheses of both open and cyclic acetals and ketals.²⁶ Sulfuric acid, phosphoric acid, tosic acid, and copper sulfate were all tried. Both the tosic acid system and the copper sulfate system displayed very little reactivity, whereas the stronger acids, H₃PO₄ and H₂SO₄, gave a complete

reaction of the starting material in ~1 h at concentrations > 3 wt% (compared to EMO or 0.7 wt% compared to the entire solution). The overall conversion was dependent on the catalyst concentration (Table 1). Interestingly, in the phosphoric acid systems with lower catalyst loadings (0.7 and 1.3 wt%), the starting material reacted completely and rapidly, but GC analysis shows that two other unidentified compounds formed as well as a lower yield of the desired product. At higher concentrations of H₂SO₄ or CuSO₄, the loss of starting material is complete, but again complete formation of HMSA is not observed. In the H₂SO₄ case, the yield of HMSA was between 56–69% and the rest of the starting material formed an EMO decomposition product. Although this complete structure of the compound was not definitively determined, GC retention time showed that it did not incorporate the ketone and it appeared

Table 1 The yield of acetal (ketal) formed in solution, by reacting 2-hexanone and EMO (HMSA), at 50 °C for 4 h, with different catalysts and catalyst loadings

Catalyst loading (wt % compared to EMO)	H ₃ PO ₄	H ₂ SO ₄	Tosic acid	CuSO ₄
0	0	0	0	0
0.7	28	17	0	0
1.3	25	15	0	0
3.2	100	56	2	0
6.3	100	69	4	0



Scheme 1 The synthesis of an oleochemically based cyclic acetal from epoxidized methyl oleate and a ketone.

to have undergone a reaction of the methyl headgroup. In the CuSO_4 case, no HMSA formed, only the decomposition product was formed.

The structure of the HMSA product was confirmed by ^{13}C NMR (Fig. 1). Comparison of the proton decoupled NMR spectrum to the DEPT-135 analysis allows us to easily determine that the spiro carbon of the cyclic ketal appears at $\sim \delta$ 108, by noting that it gives no signal in the DEPT spectrum. Additionally, the spectra also allow us to pick out the CH_3 group on the 2-position of the cyclic ketal because its 3 protons cause it to be in the opposite phase as compared to the many carbon atoms with 2 protons. Its signal appears at $\sim \delta$ 26.

Next, we studied a mixed reaction system (Scheme 2) by reacting EMO with either a ketone or a carboxylic acid, in a competitive manner. Since the reaction between EMO and octanoic acid has previously been studied,²⁰ we revisited that reaction, but added 2-pentanone in the same amount (by mass) as the octanoic acid. We chose to run the reaction at 50 °C, a temperature which is too cold for rapid ring opening ester formation, demonstrated in the previous study. The reaction was also run under the same conditions with 3 wt% H_2SO_4 catalyst. In the catalyst free reaction, there was no detectable conversion, as expected. In the catalyzed reaction, the starting material was completely reacted in 1 h. There were 3 products observed, in

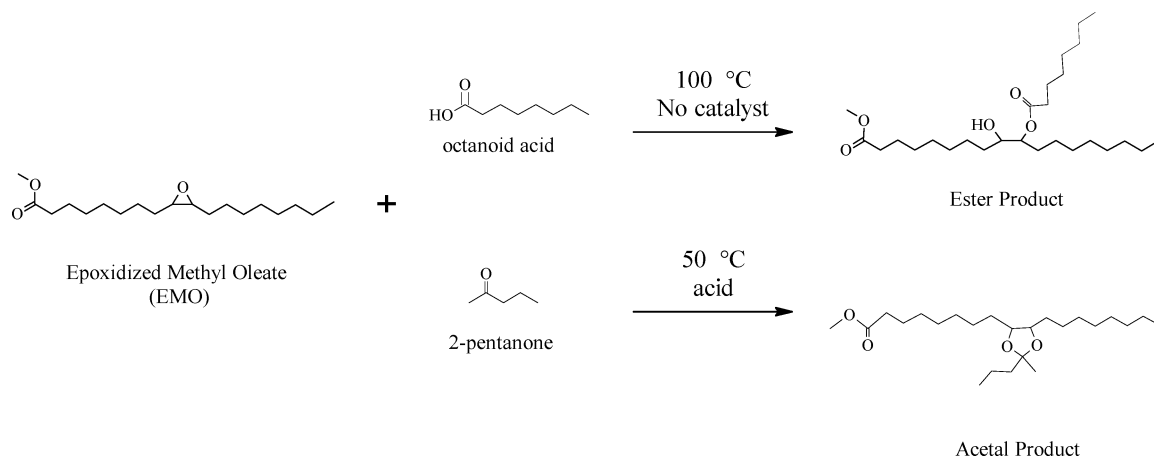
a $\sim 2:2:1$ ratio. The 1st was the EMO decomposition product which was also observed when H_2SO_4 was used in the EMO with 2-hexanone reactions. The balance between the two desired products (Table 2) showed strong favoring of the ketal product, indicating that the catalyst accelerates the ketone incorporation into the oleochemical, more than it accelerates the carboxylic acid incorporation.

In order to accomplish our goal of controlling the reaction of EMO with levulinic acid (Scheme 3), we decided to use the phosphoric acid system, since it did not form the EMO decomposition product. We ran the reactions utilizing molten levulinic acid as the reaction solvent, reducing the inputs required and increasing the efficiency of the process. The reactions were run and monitored by taking solution aliquots

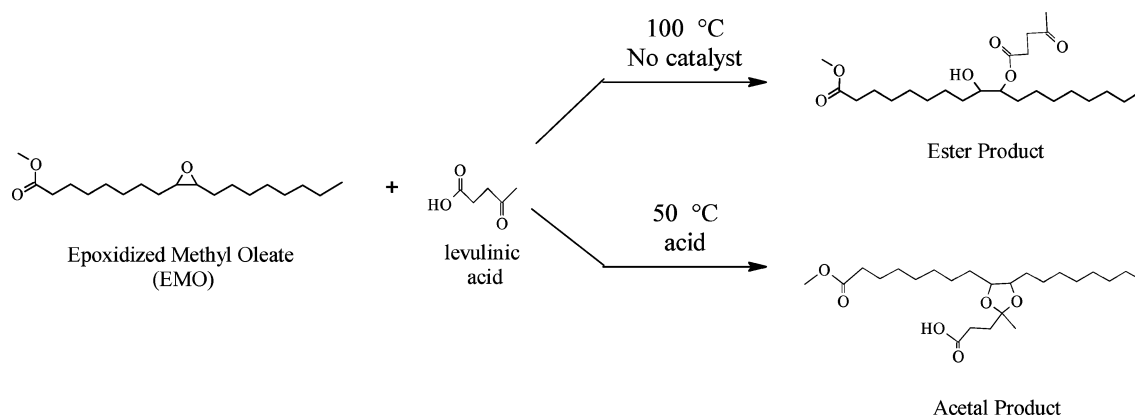
Table 2 The product distributions of the ketal product and the branched ester product from the competitive reactions of EMO with octanoic acid and 2-pentanone at 50 °C

Conditions	Acetal product (%)	Ester product (%)
No catalyst	No reaction	No reaction
3 wt% H_2SO_4 ^a	68	32

^a There was also a third product which was always produced when H_2SO_4 catalyst was used. It was in similar quantity to the acetal product.



Scheme 2 The competition reaction of EMO with octanoic acid and 2-pentanone. Depending on catalyst and reaction temperature, either the ester or the ketal (acetal) structure can be favored.



Scheme 3 Synthesis of branched oleochemicals from epoxidized methyl oleate (EMO). Depending on reaction temperature and catalyst, either the ester or the ketal (acetal) structure can be favored when levulinic acid is used as a reactant.

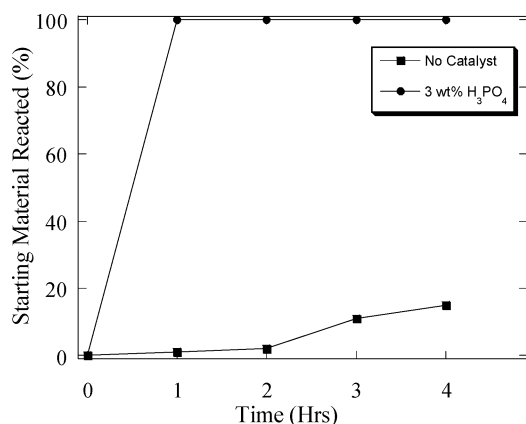


Fig. 3 A plot of the reaction progress of the EMO with 2-hexanone reaction, at 50 °C, with and without catalyst.

and analyzing them by GC (Fig. 3 and 4). Without catalyst, the reactions proceeded in a manner consistent with our earlier findings,²⁰ that is, complete reaction in less than 4 h at 100 °C, and little reaction at 50 °C. As expected, both of the reactions proceed more rapidly under H₃PO₄ catalysis, and were complete within 1 h at each temperature. However, the product distribution (Table 3) was dramatically different under the different conditions. The selectivities of the different reactions are opposite. This is probably because the increase in the rate of the ketal forming reaction is escalated dramatically leading to the HMSA product. Because the ester forming reaction is significantly faster at higher temperature, a lower selectivity of ketal was observed. This points to an even better selectivity at lower temperatures. However, levulinic acid has a melting point

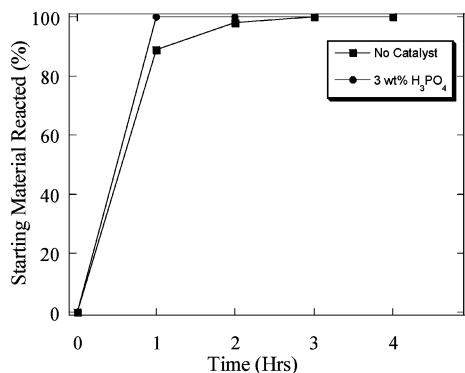


Fig. 4 A plot of reaction progress of the EMO with 2-hexanone reaction, at 100 °C, with and without catalyst.

Table 3 The product distributions of the ketal product and the branched ester product from reactions between EMO and levulinic acid

Conditions	Acetal product (%)	Ester product (%)
50 °C		
No catalyst ^a	13 ^a	87 ^a
3 wt% H ₃ PO ₄	64	36
100 °C		
No catalyst	17	83
3 wt% H ₃ PO ₄	56	44

^a In this reaction only 15% conversion was observed, so very little of either product was actually produced.

of 33–35 °C, so we could not run sub-ambient reactions in this system.

We have shown that by controlling the concentration of acidic catalyst and the reaction temperature, we can accomplish our goal and change the reaction products of our system. We have further demonstrated that this can be done, either in a competition reaction, or for multi-functional substrates like levulinic acid.

The chemistry of this system is straightforward, all the way from soybean oil to the surfactant precursor. Commercially common processes of epoxidation and transesterification can be used to produce EMO, or epoxidized methyl soyate. From that point, our synthesis utilized no organic solvent and a minimal amount of catalyst. It is also highly atom efficient. All of these factors make our system desirable from a green chemistry standpoint. Overall, our knowledge of this may help in the synthesis of new hydrophobes for surfactants, or lubricity additives with superior properties, all from a bio-based source.


Acknowledgements

We would like to acknowledge Ms Donna I. Thomas for synthesis and kinetic studies measurements. We would also like to thank Dr Karl E. Vermillion for NMR spectra and analysis.

References

- Guideline for designating biobased products for federal procurement, *Federal Register*, **70**, 1792–1812.
- R. Mullin, *Chem. Eng. News*, 2006, **84**, 34.
- P. Viswanathan, *Chem. Market Rep.*, 2005, **267**, 1.
- P. Van Arnum, *Chem. Market Rep.*, 2004, **266**, 1.
- P. Van Arnum, *Chem. Market Rep.*, 2004, **266**, 18.
- P. T. Anastas and M. M. Kirchhoff, *Acc. Chem. Res.*, 2002, **35**, 686.
- J. C. Warner, A. S. Cannon and K. M. Dye, *Env. Impact Assess. Rev.*, 2004, **24**, 775.
- N. Winterton, *Green Chem.*, 2001, **3**, G73.
- K. M. Doll, B. R. Moser, B. K. Sharma and S. Z. Erhan, *Chim. Oggi/Chem. Today*, 2006, **24**, 41.
- M. J. Rosen, *Surfactants and Interfacial Phenomena*, John Wiley and Sons, Inc., New York, 2004.
- G. Knothe, in *The history of vegetable oil-based diesel fuels*, ed. G. Knothe, AOCS Press, Champaign, IL, 2005.
- S. Z. Erhan, A. Adhvaryu, and B. K. Sharma, in *Chemically Functionalized vegetable oils*, ed. L. R. Rudnick, CRC Press, Boca Raton, FL, 2005.
- E. S. Stevens, *Green Plastics: An introduction to the new science of biodegradable plastics*, Princeton University Press, Princeton, NJ, 2002.
- R. A. Holser, *Ind. Crops Prod.*, 2008, **27**, 130.
- B. K. Sharma, K. M. Doll and S. Z. Erhan, *Green Chem.*, 2007, **9**, 469.
- K. M. Doll and S. Z. Erhan, *J. Surfact. Deterg.*, 2006, **9**, 377.
- K. M. Doll, B. R. Moser and S. Z. Erhan, *Energy Fuels*, 2007, **21**, 3044.
- B. R. Moser and S. Z. Erhan, *J. Am. Oil Chem. Soc.*, 2006, **83**, 959.
- B. R. Moser and S. Z. Erhan, *Eur. J. Lipid Sci. Technol.*, 2007, **109**, 206.
- K. M. Doll, B. K. Sharma and S. Z. Erhan, *Ind. Eng. Chem. Res.*, 2007, **46**, 3513.
- J. Filley, *Bioresour. Technol.*, 2005, **96**, 551.
- S. Selifonov, Adducts of Levulinic derivatives with epoxidized fatty acid esters and the uses thereof, WO 2007062158, May 31, 2007.
- D. A. Jaeger and S. G. G. Russell, *Tetrahedron Lett.*, 1993, **34**, 6985.
- D. A. Jaeger, J. Mohebalian and P. L. Rose, *Langmuir*, 1990, **6**, 547.
- M. Iyer, D. G. Hayes and J. M. Harris, *Langmuir*, 2001, **17**, 6816.

-
- 26 F. A. J. Meskens, *Synthesis*, 1981, **7**, 501.
27 K. Urata and N. Takaishi, *J. Surfact. Deterg.*, 1998, **1**, 73.
28 T. W. Findley, D. Swern and J. T. Scanlan, *J. Am. Chem. Soc.*, 1945, **67**, 412.
29 W. R. Schmits and J. G. Wallace, *J. Am. Oil Chem. Soc.*, 1954, **31**, 363.
30 K. M. Doll and S. Z. Erhan, *J. Agric. Food Chem.*, 2005, **53**, 9608.
31 B. R. Moser, B. K. Sharma, K. M. Doll and S. Z. Erhan, *J. Am. Oil Chem. Soc.*, 2007, **84**, 675.
32 S. P. Bunker and R. P. Wool, *J. Polym. Sci., Part A: Polym. Chem.*, 2002, **40**, 451.
33 J. La Scala and R. P. Wool, *J. Appl. Polym. Sci.*, 2005, **95**, 774.



2ND EUCHEMS CHEMISTRY CONGRESS

2008 SEPTEMBER 16 - 20
TORINO, ITALY

CHEMISTRY: THE GLOBAL SCIENCE

PLENARY LECTURES BY

Peter AGRE (Baltimore, USA)
Avelino CORMA (Valencia, Spain)
Jean M.J. FRÉCHET (Berkeley, USA)
Robert H. GRUBBS (Pasadena, USA)
Kyriacos C. NICOLAOU (La Jolla, USA)
Martyn POLIAKOFF (Nottingham, UK)
K. Barry SHARPLESS (La Jolla, USA)

KEYNOTE LECTURES BY

Varinder AGGARWAL (Bristol, UK)
Lucia BANJI (Florence, IT)
Matthias BELLER (Rostock, DE)
Richard CATLOW (London, UK)
Ken CAULTON (Bloomington, USA)
Fritz FRIMMEL (Karlsruhe, DE)
Dante GATTESCHI (Florence, IT)
Jana HAJLSLOVA (Prague, CZ)
Dino MORAS (Illkirch, FR)
Ulrich STIMMING (Munich, DE)
Philip TAYLOR (Geel, BE)
Jun-ichi YOSHIDA (Kyoto, JP)

SCIENTIFIC COMMITTEE

Chair **Hartmut MICHEL** (DE)
Co-chair **Igor TKATCHENKO** (FR)

ORGANISING COMMITTEE

Chair **Giovanni NATILE** (IT)
Co-chair **Francesco DE ANGELIS** (IT)

LOCAL ORGANISING COMMITTEE

Chair **Lorenza OPERTI** (IT)
Co-chair **Salvatore COLUCCIA** (IT)

Special topic symposia:

ADVANCES IN SYNTHESIS

- Organic Catalysis
- Radical Reactivity in Transition Metal Chemistry
- Reactions under Novel Conditions

ADVANCES IN UNDERSTANDING

- Chemical Measurement Quality: Societal Impact
- Cutting Edge Chemistry with Computers
- Food Analysis: Pushing Detection Limits down to Nothing

CHEMISTRY AND LIFE SCIENCES

- Biomolecular Interactions and Mechanisms
- Drug Targeting and Delivery
- Metal Homeostasis

ENERGY AND INDUSTRY

- Biorefineries and Biotechnologies
- Energy Production & Storage
- New Trends for Agrochemicals

ENVIRONMENT

- Greening Chemistry
- Greenhouse Gases
- Water Pollutants

MATERIALS AND DEVICES

- Branched Polymers - Smart Functional Materials
- Nanomaterials
- Porous Materials

cci ORGANISING SECRETARIAT

Centro Congressi Internazionale s.r.l. - Corso Bramante 58/9 10126 Torino - I
tel +39 011.2446911 fax +39 011.2446900/44 - info@euchems-torino2008.it

www.euchems-torino2008.it

*EuCheMS, the European Association for Chemical and Molecular Sciences incorporates
50 member societies which in total represent some
150.000 individual chemists in academia, industry and government in over
35 countries across Europe.



5th Green Chemistry and the Consumer Symposium

Greener Products

Plus pre-symposium Masterclass and evening event.
1st - 2nd July 2008
 Kings Manor, York



The fifth symposium, 'Greener Products', will explore recent advances in the field including case studies on successful methods developed by industry and challenges in practice.

The programme for the day will consist of a blend of both presentations and breakout sessions.

Speakers include:

- **Mary Kate Boggiano**, Research Scientist, Green Chemistry, Armstrong Floor Products - Innovation
- **Henk Vooijs**, Area Manager Benelux & UK, Novamont SpA
- **Jerker Ligthart**, Project Coordinator, International Chemical Secretariat

The event will be preceded by a one-day Masterclass and evening event on the 1st July, which will feature a plenary lecture from **Steve Johnson**, Sustainable Development Manager, Boots UK Ltd.

The symposium is open to all and will provide an invaluable opportunity to bring together representatives from throughout consumer product supply chains, as well as government, NGOs and trade associations, for mutual learning and technology transfer, as well as providing opportunities for networking.

For further information please contact:

Louise Summerton

Tel: +44 (0)1904 434546

Fax: +44 (0)1904 4352705

Email: ls25@york.ac.uk

or visit the GCN website at <http://www.chemsoc.org/networks/gcn/events.htm>

Faced with questions?

Can I search by structure to find articles?

Are there any related articles on this topic?

What groups and relationships are there for this compound?

Is there any Patent information?

Can I download files of these structures?

What's the definition of that term?

Looking for answers?

Use RSC Prospect enhanced HTML journal articles

Linking together related articles by subject ontologies and identified compounds, *RSC Prospect* enhanced HTML articles also provide you with definitions, synonyms, structures and RSS feeds. We've now introduced a structure and sub-structure searching function, widened the compound identifiers to include groups and relationships via the ChEBI (Chemical Entities of Biological Interest) ontology, and included additional features such as an Experimental Data Checker to allow downloading of data for analysis of results. Links to patent information and to compounds in PubChem have also been added.

Hailed as the future of publishing, we add computer readable meaning to our journal articles by applying internationally recognised labels and conventions. We are proud to be leading the way amongst scientific publishers.

RSC Prospect - winner of the 2007 ALPSP/Charlesworth Award for Publishing Innovation.



0208106

RSC Publishing

www.projectprospect.org

Registered Charity Number 207890